BONE MARROW DOSIMETY VIA MICROCT IMAGING AND STEM CELL SPATIAL MAPPING

By

KAYLA N. KIELAR

A DISSERTATION PRESENTED TO THE GRADUATE SCHOOL
OF THE UNIVERSITY OF FLORIDA IN PARTIAL FULFILLMENT
OF THE REQUIREMENTS FOR THE DEGREE OF
DOCTOR OF PHILOSOPHY

UNIVERSITY OF FLORIDA

2009

© 2009 Kayla N. Kielar

ACKNOWLEDGMENTS

I would like to express my gratitude first and foremost to Dr. Wesley Bolch for his guidance throughout my eight-year academic career at the University of Florida. His leadership, respect, and concern for both his students and the publications of the Bone Imaging Dosimetry group is unprecedented. The entire Nuclear and Radiological Engineering department has become like family to me, and I appreciate the guidance of all of the faculty and staff. I would also like to recognize the Warrington College of Business faculty and staff for their assistance in shaping me into a more professional being.

Several colleagues contributed to this work and I would like to thank them for their time, specifically Deanna Pafundi, Didier Rajon, Amish Shah, Chris Watchman, and Vince Bourke. Without your help this would not have been possible. I would also like to thank Dr. Edward Dugan and Dr. Sanford Berg for their wonderful recommendation letters and Dr. Amir Shahlaee, Dr. Parker Gibbs, and Dr. Bill Slayton for being part of my committee.

Thank you to the United States Department of Energy for funding me under the Health Physics Fellowship, as well as the American Nuclear Society for several need based scholarships. Without this, I truly would not have been able to achieve this dream, and I am forever grateful for your selflessness.

I am especially indebted to the previous students in the Bone Imaging and Dosimetry group for setting high standards for our work and the current students for their efforts in making this work possible. Finally, I am much obliged to my family for their support and my friends for their patience.

TABLE OF CONTENTS

page

ACKNOWLEDGMENTS 3

LIST OF TABLES 7

LIST OF FIGURES 10

ABSTRACT 16

CHAPTER

1 INTRODUCTION 18

2 BACKGROUND 26

Bone Structure and Physiology 26
Hematopoiesis and Target Cells 28
Lymphoma 30
Chemotherapy and Marrow Toxicity 31
Radionuclide Therapies 32
Internal Dosimetry Calculations 34
Previous Methods Detailed 35
Radiation Transport using Chord-based Methods 35
Radiation Transport using Voxel-based Methods 37
Stem Cell Distributions in Normal Marrow 38
Stem Cell Distribution in Diseased Marrow 40

3 REFERENCE SKELETAL DOSIMETRY MODEL FOR THE ADULT FEMALE 48

Introduction 48
Materials and Methods 52
Female Cadaver Selection 52
In-vivo Macrostructural Image Database 52
Ex-vivo Macrostructural Image Database 53
MicroCT Microstructural Image Database 54
Mass Calculations 56
Bone sites containing active marrow 56
Bone sites not containing active marrow 58
Transport Modeling 59
Absorbed Fractions 60
Results 60
Discussion 62
Spongiosa Volume and Percentages 62
Volume Fractions 63
Tissue Masses 63

Surface to Volume (S/V) Ratios....65
Surface Areas....65
Weighting Factors....66
Specific Absorbed Fractions (SAF)....68
SAF for individual bone sites containing active marrow....68
SAF for all bone sites containing active marrow....69
SAF for all bone sites not containing active marrow....70
Skeletal Averaged Absorbed Fractions (AF)....71
Effect of Update in Shallow Active Marrow Size....73
Conclusion....74

4 COMPARISON OF HUMAN STEM CELL MEASUREMENTS IN BIOPSIES VERSUS AUTOPSY SPECIMENS....109

Introduction....109
Materials and Methods....111
Autopsy Collection and Preparation....112
Digital Imaging and Processing....112
Measurement of Hematopoietic CD34+ Cells....113
Cellularity Measurement....114
Marrow Area Measurement....114
Results....116
Discussion....116
Full field Autopsy Measurements....116
Total Simulated Biopsy Measurements....117
Vertical Small Field Measurements....117
Horizontal Small Field Measurements....117
Statistical Analysis....118
Anisotropy....119
Dose Implications....120
Conclusion....121

5 EFFECT OF CHEMOTHERAPY ON THE SPATIAL DISTRIBTUION OF STEM CELLS IN HUMAN BONE MARROW....129

Introduction....129
Materials and Methods....129
Patient Selection and Slide Preparation....132
Digital Imaging and Processing....132
Measurement of Hematopoietic CD34+ Cells....133
Cellularity Measurement....133
Marrow Area Measurement....134
Results....134
Mean Cellular Concentration....136
Statistical Analysis....137
Spatial Gradient....137
Discussion....137

Comparison to Normal Marrow 138
Effect of Chemotherapy 138
Timing Effect....140
Effect on Cellularity 140
Dose Implications....141
Conclusion 141

6 CONCLUSIONS AND FUTURE WORK....150

Conclusions....150
Future Work....152
Improvements in Skeletal Database 152
Reference S Values for UFRF 153
Improvements in Cellular Measurements....153
Scalability and Clinical Applications 154

APPENDIX

A TABLES OF SPECIFIC ABSORBED FRACTION....155

B GRAPHS OF SPECIFIC ABORBED FRACTION 168

C SPECIFIC ABSORBED FRACTIONS FOR ALL BONE SITES....220

D SPECIFIC ABSORBED FRACTIONS FOR LONG BONES....225

E SKELETAL AVERAGED ABSORBED FRACTIONS....230

LIST OF REFERENCES....237

BIOGRAPHICAL SKETCH 245

LIST OF TABLES

Table		page
3-1	Ex-vivo CT data for all skeletal sites.	75
3-2	MicroCT data for the skeletal sites with active marrow.	76
3-3	Tissue compositions (% by mass) and mass densities used in skeletal mass calculations.	77
3-4	Percentage of spongiosa of reference female compared to a database of 20 cadavers.	77
3-5	Spongiosa volume and percentage of total for UF reference male and female.	78
3-6	Averaged marrow volume fractions, bone volume fractions and shallow marrow volume fractions by skeletal site for UFRF.	79
3-7	University of Florida Reference Female masses for the trabecular spongiosa, cortical bone, and mineral bone regions for all skeletal sites.	80
3-8	University of Florida Reference Female active marrow masses.	81
3-9	Shallow marrow masses for UFRF.	82
3-10	S/V Ratios.	83
3-11	Surface Areas for UFRF in both trabecular and cortical bone regions.	84
3-12	Weighting factors for marrow sources for each bone site for UFRF.	85
3-13	Weighting factors for bone surface and volume sources for UFRF.	86
4-1	Pertinent values for each patient in the simulated biopsy study.	122
4-2	Specimen fractional weight in total simulated biopsies or horizontal and vertical biopsies.	122
4-3	Cellular concentration for simulated biopsies versus autopsies in active and total marrow.	123
4-4	Cellular concentration for horizontal versus vertical biopsies in active and total marrow.	123
5-1	Pertinent data for all 12 patients, in both pre and post-chemotherapy biopsies	143
5-2	Mean cellular concentration and error for both normocellular and diseased marrow.	144
A-1	UFRF absorbed fraction for all sources irradiating the active marrow in the cranium.	155

A-2 UFRF absorbed fraction for all sources irradiating the shallow active marrow in the cranium. 155

A-3 UFRF absorbed fraction for all sources irradiating the active marrow in the clavicles. .156

A-4 UFRF absorbed fraction for all sources irradiating the shallow active marrow in the clavicles....156

A-5 UFRF absorbed fraction for all sources irradiating the active marrow in the mandible....157

A-6 UFRF absorbed fraction for all sources irradiating the shallow active marrow in the mandible....157

A-7 UFRF absorbed fraction for all sources irradiating the active marrow in the scapulae...158

A-8 UFRF absorbed fraction for all sources irradiating the shallow active marrow in the scapulae....158

A-9 UFRF absorbed fraction for all sources irradiating the active marrow in the sternum....159

A-10 UFRF absorbed fraction for all sources irradiating the shallow active marrow in the sternum....159

A-11 UFRF absorbed fraction for all sources irradiating the active marrow in the ribs. 160

A-12 UFRF absorbed fraction for all sources irradiating the shallow active marrow in the ribs....160

A-13 UFRF absorbed fraction for all sources irradiating the active marrow in the cervical vertebrae....161

A-14 UFRF absorbed fraction for all sources irradiating the shallow active marrow in the cervical vertebrae. 161

A-15 UFRF absorbed fraction for all sources irradiating the active marrow in the thoracic vertebrae....162

A-16 UFRF absorbed fraction for all sources irradiating the shallow active marrow in the thoracic vertebrae....162

A-17 UFRF absorbed fraction for all sources irradiating the active marrow in the lumbar vertebrae....163

A-18 UFRF absorbed fraction for all sources irradiating the shallow active marrow in the lumbar vertebrae. 163

A-19 UFRF absorbed fraction for all sources irradiating the active marrow in the sacrum. 164

A-20 UFRF absorbed fraction for all sources irradiating the shallow active marrow in the sacrum. 164

A-21 UFRF absorbed fraction for all sources irradiating the active marrow in the ossa coxae. 165

A-22 UFRF absorbed fraction for all sources irradiating the shallow active marrow in the ossa coxae. 165

A-23 UFRF absorbed fraction for all sources irradiating the active marrow in the proximal humeri. 166

A-24 UFRF absorbed fraction for all sources irradiating the shallow active marrow in the proximal humeri. 166

A-25 UFRF absorbed fraction for all sources irradiating the active marrow in the proximal femora. 167

A-26 UFRF absorbed fraction for all sources irradiating the shallow active marrow in the proximal femora. 167

D-1 Specific absorbed fractions in the shafts of the leg bones. 225

D-2 Specific absorbed fractions in the shafts of the arm bones. 226

E-1 UFRF skeletal averaged absorbed fraction (AF) for various sources irradiating the trabecular active marrow. 230

E-2 UFRF skeletal averaged absorbed fraction (AF) for various sources irradiating the shallow trabecular active marrow. 231

E-3 UFRF skeletal averaged specific absorbed fraction (SAF) for various sources irradiating the trabecular active marrow. 231

E-4 UFRF skeletal specific averaged absorbed fraction (SAF) for various sources irradiating the shallow trabecular active marrow. 232

LIST OF FIGURES

Figure		page
1-1	Sites of active marrow (red) and inactive marrow (yellow) in the adult.	24
1-2	Hematopoietic stem cell pathway	25
1-3	Marrow cavities showing bone surface sources	25
2-1	Human compact and spongy bone showing location of osteons and trabeculae	41
2-2	Bone remodeling and resoprtion are possible by osteoblasts and osteoclasts, respectively	41
2-3	Osteoporotic versus normal bone	42
2-4	Bone Mineral Density (BMD) changes with age and gender.	42
2-5	Stem cells may become either other stem cells (expansion) or further specialized cells (proliferation)	43
2-6	Hematopoietic stem cell differentiation pathways.	44
2-7	Lymphatic system and lymph circulation	45
2-8	Chord lengths across bone trabeculae (black) and marrow cavities (white) at scanning angle ϕ.	46
2-9	Paired Image Radiation Transport (PIRT)	47
2-10	Schema of future reference models at the University of Florida.	47
3-1	Top in-vivo scan of UF Reference Woman	87
3-2	In-vivo contoured image of the ribs	88
3-3	In-vivo contoured image of the cranium	89
3-4	In-vivo contoured image of the cranium showing the separated lobes:	90
3-5	CT images showing the abnormality of the right humerus.	90
3-6	Contoured ex-vivo image of the femur,	91
3-7	Contoured ex-vivo image of the lumbar vertebrae	91
3-8	Active marrow distribution as a function of age used as reference values in ICRP 70	92

3-9 Cellularity varies by bone site and decreases with age 93

3-10 Current ICRP 70 reference cellularities based on bone site and age 93

3-11 Microstructure of the frontal lobe (40% marrow) 94

3-12 Microstructure of the occipital lobe (11% marrow). 94

3-13 Microstructure of the femoral neck (87% marrow). 94

3-14 Microstructures of the femoral head (71% marrow 95

3-15 Microstructure of the sternum (99% marrow). 95

3-16 Microstructure of the 3rd cervical vertebrae (76% marrow). 95

3-17 Microstructure of the 5th lumbar vertebrae (91% marrow). 96

3-18 Specific absorbed fraction for the TAM irradiating the TAM for the lumbar vertebrae 97

3-19 Specific absorbed fraction for the TAM irradiating the TAM_{50} for the lumbar vertebrae 98

3-20 Specific absorbed fraction for all sources irradiating the TAM for the lumbar vertebrae 99

3-21 Specific absorbed fraction for all sources irradiating the TAM_{50} for the lumbar vertebrae 100

3-22 Specific absorbed fraction for the TAM irradiating the TAM for all bone sites. 101

3-23 Specific absorbed fraction for the TAM irradiating the TAM_{50} for all bone sites. 101

3-24 Specific absorbed fraction for the CIM irradiating the CIM_{50} in the shafts of all long bones. 102

3-25 Specific absorbed fraction for the CBS_{MC} irradiating the CIM_{50} in the shafts of all long bones. 103

3-26 Specific absorbed fraction for the CBV irradiating the CIM_{50} in the shafts of all long bones. 104

3-27 Skeletal averaged AF for marrow sources irradiating the TAM for both UFRF and Stabin and Siegel (2003). 105

3-28 Skeletal averaged AF for bone trabeculae sources irradiating the TAM for both UFRF and Stabin and Siegel (2003). 106

3-29 Skeletal averaged AF for marrow sources irradiating the TAM_{50} for both UFRF and Stabin and Siegel (2003). 107

3-30 Skeletal averaged AF for bone trabeculae sources irradiating the TAM_{50} for both UFRF and Stabin and Siegel (2003). 108

4-1 Limitations of cell count in biopsies 124

4-2 The lumbar vertebrae was chosen due to planar symmetry 124

4-3 Artificial biopsy sections 125

4-4 Independent cellularity measurements were made for each biopsy 125

4-5 Stained CD34+ cells in human bone marrow 125

4-6 Image processing to determine 50µm areal contours from surfaces of bone trabeculae 126

4-7 Spatial gradient of HSCs in the active marrow in simulated biopsies 127

4-8 Spatial gradient of HSCs in the active marrow for anisotropy 128

5-1 Co-stained biopsy 145

5-2 Binary digital images of total marrow and trabecula 146

5-3 CD34+ cell concentration as a function of depth into marrow cavities 147

5-4 Change in HSC concentration as a function of time between biopsies 148

B-1 Specific absorbed fraction for the TAM irradiating the TAM for the cranium. 168

B-2 Specific absorbed fraction for all sources irradiating the TAM for the cranium. 169

B-3 Specific absorbed fraction for the TAM irradiating the TAM_{50} for the cranium. 170

B-4 Specific absorbed fraction for all sources irradiating the TAM_{50} for the cranium. 171

B-5 Specific absorbed fraction for the TAM irradiating the TAM for the mandible. 172

B-6 Specific absorbed fraction for all sources irradiating the TAM for the mandible. 173

B-7 Specific absorbed fraction for the TAM irradiating the TAM_{50} for the mandible 174

B-8 Specific absorbed fraction for all sources irradiating the TAM_{50} for the mandible. 175

B-9 Specific absorbed fraction for the TAM irradiating the TAM for the scapulae. 176

B-10 Specific absorbed fraction for all sources irradiating the TAM for the scapulae. 177

B-11 Specific absorbed fraction for the TAM irradiating the TAM_{50} for the scapulae.....178

B-12 Specific absorbed fraction for all sources irradiating the TAM_{50} for the scapulae. 179

B-13 Specific absorbed fraction for the TAM irradiating the TAM for the clavicles. 180

B-14 Specific absorbed fraction for all sources irradiating the TAM for the clavicles. 181

B-15 Specific absorbed fraction for the TAM irradiating the TAM_{50} for the clavicles. 182

B-16 Specific absorbed fraction for all sources irradiating the TAM_{50} for the clavicles. 183

B-17 Specific absorbed fraction for the TAM irradiating the TAM for the sternum. 184

B-18 Specific absorbed fraction for all sources irradiating the TAM for the sternum. 185

B-19 Specific absorbed fraction for the TAM irradiating the TAM_{50} for the sternum.....186

B-20 Specific absorbed fraction for all sources irradiating the TAM_{50} for the sternum. 187

B-21 Specific absorbed fraction for the TAM irradiating the TAM for the ribs. 188

B-22 Specific absorbed fraction for all sources irradiating the TAM for the ribs. 189

B-23 Specific absorbed fraction for the TAM irradiating the TAM_{50} for the ribs. 190

B-24 Specific absorbed fraction for all sources irradiating the TAM_{50} for the ribs. 191

B-25 Specific absorbed fraction for the TAM irradiating the TAM for the cervical vertebrae.....192

B-26 Specific absorbed fraction for all sources irradiating the TAM for the cervical vertebrae.....193

B-27 Specific absorbed fraction for the TAM irradiating the TAM_{50} for the cervical vertebrae.....194

B-28 Specific absorbed fraction for all sources irradiating the TAM_{50} for the cervical vertebrae.....195

B-29 Specific absorbed fraction for the TAM irradiating the TAM for the thoracic vertebrae.....196

B-30 Specific absorbed fraction for all sources irradiating the TAM for the thoracic vertebrae.....197

B-31 Specific absorbed fraction for the TAM irradiating the TAM_{50} for the thoracic vertebrae.....198

B-32 Specific absorbed fraction for all sources irradiating the TAM_{50} for the thoracic vertebrae.....199

B-33 Specific absorbed fraction for the TAM irradiating the TAM for the lumbar vertebrae.....200

B-34 Specific absorbed fraction for all sources irradiating the TAM for the lumbar vertebrae.....201

B-35 Specific absorbed fraction for the TAM irradiating the TAM_{50} for the lumbar vertebrae.....202

B-36 Specific absorbed fraction for all sources irradiating the TAM_{50} for the lumbar vertebrae.....203

B-37 Specific absorbed fraction for the TAM irradiating the TAM for the sacrum.....204

B-38 Specific absorbed fraction for all sources irradiating the TAM for the sacrum. 205

B-39 Specific absorbed fraction for the TAM irradiating the TAM_{50} for the sacrum. 206

B-40 Specific absorbed fraction for all sources irradiating the TAM_{50} for the sacrum.....207

B-41 Specific absorbed fraction for the TAM irradiating the TAM for the os coxae. 208

B-42 Specific absorbed fraction for all sources irradiating the TAM for the os coxae. 209

B-43 Specific absorbed fraction for the TAM irradiating the TAM_{50} for the os coxae.....210

B-44 Specific absorbed fraction for all sources irradiating the TAM_{50} for the os coxae. 211

B-45 Specific absorbed fraction for the TAM irradiating the TAM for the proximal humeri. 212

B-46 Specific absorbed fraction for all sources irradiating the TAM for the proximal humeri. 213

B-47 Specific absorbed fraction for the TAM irradiating the TAM_{50} for the proximal humeri. 214

B-48 Specific absorbed fraction for all sources irradiating the TAM_{50} for the proximal humeri. 215

B-49 Specific absorbed fraction for the TAM irradiating the TAM for the proximal femora. 216

B-50 Specific absorbed fraction for all sources irradiating the TAM for the proximal femora. 217

B-51 Specific absorbed fraction for the TAM irradiating the TAM_{50} for the proximal femora. 218

B-52 Specific absorbed fraction for all sources irradiating the TAM_{50} for the proximal femora. 219

C-1 Specific absorbed fraction for the TAM irradiating the TAM for all bone sites. 220

C-2 Specific absorbed fraction for the TAM irradiating the TAM_{50} for all bone sites. 220

C-3 Specific absorbed fraction for the TBS irradiating the TAM for all bone sites. 221

C-4 Specific absorbed fraction for the TBS irradiating the TAM_{50} for all bone sites. 221

C-5 Specific absorbed fraction for the TBV irradiating the TAM for all bone sites. 222

C-6 Specific absorbed fraction for the TBV irradiating the TAM_{50} for all bone sites. 222

C-7 Specific absorbed fraction for the CBV irradiating the TAM for all bone sites. 223

C-8 Specific absorbed fraction for the CBV irradiating the TAM_{50} for all bone sites. 223

C-9 Specific absorbed fraction for the TIM irradiating the TAM for all bone sites. 224

C-10 Specific absorbed fraction for the TIM irradiating the TAM_{50} for all bone sites. 224

D-1 Specific absorbed fraction for the CIM irradiating the CIM_{50} in the shafts of all long bones. 227

D-2 Specific absorbed fraction for the CBS_{MC} irradiating the CIM_{50} in the shafts of all long bones. 228

D-3 Specific absorbed fraction for the CBV irradiating the CIM_{50} in the shafts of all long bones. 229

E-1 Skeletal averaged AF for marrow sources irradiating the TAM for both UFRF and Stabin and Siegel (2003). 233

E-2 Skeletal averaged AF for trabecular bone sources irradiating the TAM for both UFRF and Stabin and Siegel (2003). 234

E-3 Skeletal averaged AF for marrow sources irradiating the TAM_{50} for both UFRF and Stabin and Siegel (2003). 235

E-4 Skeletal averaged AF for trabecular bone sources irradiating the TAM_{50} for both UFRF and Stabin and Siegel (2003). 236

Abstract of Dissertation Presented to the Graduate School
of the University of Florida in Partial Fulfillment of the
Requirements for the Degree of Doctor of Philosophy

BONE MARROW DOSIMETRY VIA MICROCT IMAGING AND STEM CELL SPATIAL MAPPING

By

Kayla N. Kielar

August 2009

Chair: Wesley E. Bolch
Major: Nuclear Engineering Sciences

In order to make predictions of radiation dose in patients undergoing targeted radionuclide therapy of cancer, an accurate model of skeletal tissues is necessary. Concerning these tissues, the dose-limiting factor in these therapies is the toxicity of the hematopoietically active bone marrow. In addition to acute effects, one must be concerned as well with long-term stochastic effects such as radiation-induced leukemia. Particular cells of interest for both toxicity and cancer risk are the hematopoietic stem cells (HSC), found within the active marrow regions of the skeleton. At present, cellular-level dosimetry models are complex, and thus we cannot model individual stem cells in an anatomic model of the patient. As a result, one reverts to looking at larger tissue regions where these cell populations may reside.

To provide a more accurate marrow dose assessment, the skeletal dosimetry model must also be patient-specific. That is, it should be designed to match as closely as possible to the patient undergoing treatment. Absorbed dose estimates then can be tailored based on the skeletal size and trabecular microstructure of an individual for an accurate prediction of marrow toxicity. Thus, not only is it important to accurately model the target tissues of interest in a normal patient, it is important to do so for differing levels of marrow health.

A skeletal dosimetry model for the adult female was provided for better predictions of marrow toxicity in patients undergoing radionuclide therapy. This work is the first fully established gender specific model for these applications, and supersedes previous models in scalability of the skeleton and radiation transport methods. Furthermore, the applicability of using bone marrow biopsies was deemed sufficient in prediction of bone marrow health, specifically for the hematopoietic stem cell population. The location and concentration of the HSC in bone marrow was found to follow a spatial gradient from the bone trabeculae in lymphoma patients. Interestingly, chemotherapy was not found to effect the HSC population in concentration or gradient. Together, this work will provide more realistic and accurate dosimetry in internal radiation therapy of cancer patients.

CHAPTER 1
INTRODUCTION

The importance of assessing radiation dose was noted within one month of Wilhelm Roentgen's discovery of x-rays, when he reported radiation burns following x-ray exposure. Marie Curie also reported similar burns while working with radium, and as early as 1900, the need for precautions when working with radiation were well understood (Lombardi, 2006*).* Since then, dose assessment has become an important factor for not only health concerns, but for use in accurately treating medical conditions. All types of radiation therapy with energies high enough to pass through the outer layer of bone will provide some complication to the bone marrow, especially to those tissues that are hypersensitive to radiation (Lim *et al.*, 1997a). In particular, internal radiation therapy requires special dosimetry concerns since radiation is now completely encompassed within bone marrow itself.

In order to predict the risk of bone cancer, an accurate assessment of absorbed dose to skeletal tissues is necessary. Concerning these tissues, the limiting factor in radiation protection is the toxicity of hematopoietically active bone marrow *(*Sgouros *et al.,* 1993*;* Siegel *et al.,* 1990b*)*. Bone marrow is made up of red (active) marrow including stem cells, progenitors, precursors, and mature blood cells, and yellow (inactive) fatty marrow. Active marrow, fat, and trabecular bone comprise the spongiosa, which is encased by dense, cortical bone (Marieb, 2006). In adults, hematopoiesis occurs only within the bone marrow of the axial skeleton consisting of the skull, vertebral column, sternum, ribs, and the proximal ends of the femur and humerus, shown in Figure 1-1 (Vogler, 1988).

All blood cells develop from pluripotential stem cells, which are stimulated by hematopoietic growth factors into committed pathways depicted in Figure 1-2 (DOH, 2006). It is these hematopoietic stem cells that are the radiosensitive cell population and the basis for

acute toxicity and cancer risk. In particular, hematopoietic stem cells and osteoprogenitor cells are the primary cells of interest for the risk of inducing leukemia or bone cancer, respectively. The endosteum is defined as the connective tissue lining of all trabecular and cortical bone surfaces within bone, and is a radiosensitive organ because it is the site of OPC production (Gossner *et al*., 2000; Gossner, 2003). In all forms of radiation therapy, it is important to know the concentration and location of these cells, as well as their response to radiation in order to optimize cancer treatment with the risk of inducing new cancers.

To assess radiation dose, the Medical Internal Radiation Dose (MIRD) Committee is responsible for providing fundamental quantities and standard models for radiation protection, risk assessment, and treatment planning (Loevinger *et al.*, 1991; Sgouros *et al.*, 2009). MIRD methodologies of absorbed dose requires separate knowledge of the cumulated activity within the source and the radionuclide S value (absorbed dose per unit cumulated activity). Much research has been done to asses the cumulated activity within the source, while little has been done to make patient-specific assessments of absorbed dose per unit cumulated activity (Juweid *et al.*, 1995; Macey *et al.*, 1995; Sgouros, 1993; Sgouros *et al.*, 1996b; Siegel *et al.*, 1990a). Furthermore, these dose calculations require known reference values such as the fraction of energy deposited in a target tissue and the mass of those target tissues. This inherently requires the proper modeling of source and target tissues, including the radiosensitive cell populations within bone marrow.

In internal radioimmunotherapy, radiolabeled antibodies guide the radioactive element to a specific site of interest. Since these radionuclides localize in bone, they will cause a greater damage to endosteal tissues than would conventional radiation therapy (Gossner *et al.*, 2000). Bone marrow is continuously in contact with radiation while these particles circulate through the

patient's blood, causing dose to the hematopoietic stem cell population. Furthermore, the endosteum and trabecular bone regions receive a high dose, possibly damaging the osteoprogenitor cell population. This increases the risk for marrow toxicity, leukemia, and bone cancer in radioimmunotherapy patients (Lim *et al.*, 1997b). The spatial distribution of the stem cells is now an important factor in yielding a dose estimate that is predictive of marrow toxicity, especially if the antibody is a bone surface seeker, shown in Figure 1-3.

Current radioimmunotherapy procedures used for the treatment of blood cancers such as lymphoma may result in a large dose to the bone marrow, especially if there is some amount of marrow involvement. Lymphoma is a cancer of the white blood cells, which circulate through the bloodstream and lymphatic system via gravity and muscle compression. Lymphomas may arise in lymph nodes, bone marrow, or other organs such as the spleen, tonsils, appendix, thymus and the intestinal Peyer's patch, and may continue to circulate or may lodge themselves within that organ. Like other cancers, lymphomas divide continuously and do not undergo normal cell death. Consequently, nonfunctional white blood cells build up within affected organs and crowd out other functioning normal cells that are meant to nurture the bone marrow environment. This provides the basis for immunosuppresion in marrow-involved lymphomas (Harris *et al.*, 1994; Kuppers *et al.*, 1999).

Radionuclide therapies currently used to treat non-Hodgkin's lymphoma include Tositumomab and Iodine 131 (Bexxar) and Ibritumomab tiuxetan and Yttrium 90 (Zevalin). Both of these therapies rely on man-made antibodies designed to bind to the CD20 antigen on both malignant and nonmalignant mature B-lymphocytes, while carrying a radiation component. Thus, this targeted therapy delivers radiation to a specific cell for cell killing. Apoptosis is induced through gamma and beta radiation for Bexxar (Iodine 131) and beta radiation only with Zevalin

(Yttrium 90). Many of these patients will also undergo chemotherapy before, during, or after radiation treatment. The stem cell population may be disturbed to some degree by the radiation and chemotherapy and measurement of marrow dosimetry should be adjusted in these cases (Siegel *et al.*, 1993). Accordingly, not only is it important to accurately model the target tissues of interest in a normal patient, it is important to do so for differing levels of marrow health.

Previous analysis has shown that absorbed dose is an accurate measure of hematological toxicity, but only if the absorbed dose estimates is specific to the particular patient. At present, the vast majority of skeletal reference models (SRMs) used for these purposes are based on studies in the late 1960s and early 1970s at the University of Leeds in which a novel optical scanning method was used to obtain linear chord-length distributions across several skeletal sites of a single 44-year male subject. These data form an essential component of the ICRP's SRM published in ICRP Publications 30, 70, and 89.

Recent work has been done at the University of Florida Bone Imaging and Dosimetry Group to more accurately determine the fractional energy deposition in bone for alpha emitters and beta emitters as a function of bone site. Also, complete sets of skeletal macrostructural and microstructural data, in a format sufficient for radiation transport simulations, have been established for an image-based skeletal reference model for the adult male at an age representative of cancer patients undergoing radionuclide therapy (66-year). Relevant tissues of the microstructure, such as the bone trabeculae, bone endosteum, and marrow cavities were accounted for through image-based techniques. Skeletal tissue masses, which are important in determining radionuclide S values, have been reported to update those summarized in ICRP Publications 70 and 89 (ICRP, 1995, 2002).

At present, we cannot model the actual cell populations on the scale of the entire human skeleton, and so we revert to using the larger tissue regions instead. Along with being patient specific, dose estimates should properly model the tissue of interest. Radiosensitive tissues, particularly the stem cells within the red bone marrow, should be accurately known and modeled. The concentration and distribution of stem and progenitor cells within the hematopoietically active marrow thus needs to be characterized. This should be known for both normal and diseased states as the stem cell population can change drastically. A patient specific model is of no use if target or source tissues are poorly modeled. When incorporated into radiation transport techniques, an accurate, patient specific, absorbed fraction can be found and used in the S value calculation.

It is currently assumed by the International Commission on Radiological Protection (ICRP) that target cells of interest for bone marrow dosimetry are uniformly distributed throughout the marrow cavities, based on previous studies (Charlton *et al.*, 1996). Absorbed dose is averaged through all regions of bone marrow accordingly. Also, the number of target cells is considered to be proportional to the volume of red bone marrow as proposed by the ICRP due to a lack of data. However, recent studies have shown that a spatial gradient in the mouse femur may exist (Cui *et al.*, 1996; Frassoni *et al.*, 1982; Lord and Hendry, 1972). Moreover, studies have also shown a similar spatial gradient in hematopoietic stem and progenitor cells in the human iliac crest (Watchman *et al.*, 2007). It is proposed that the hematopoietic stem and progenitor cells are preferentially located closer to the bone trabecular surfaces, and decrease in concentration further into the bone marrow cavities. This could cause significant error in calculating the dose estimates using the current dose-response models for internal radionuclide therapy since the tissue surrogate (the entire red bone marrow) no longer matches the radiosensitive cells of interest.

In order to provide an accurate dose assessment in radiation protection, the reference skeletal dosimetry model must be patient-specific. That is, it should be designed to match as closely as possible to the individual for both radiation protection and medical treatment. The skeletal tissue doses are then to be used only to establish dose limits based upon an acceptable risk or radiation induced effects (stochastic or non-stochastic). Also, the location of radiosensitive cells must be characterized, as well as their relationship in diseased marrow. Background information regarding these aspects is provided in chapter two.

Previous work has been done to give mass estimated for the male model, however, work had not been done to assess differences based on gender. To date, there is no skeletal reference female model and the third chapter serves to present a companion skeletal reference model to the adult male. This reference model will be fully scalable for both skeletal size (macrostructure) and marrow health (microstructure) due to osteoporotic concerns in the current female population.

The fourth and fifth chapters serve to better understand the concentration and spatial gradient of the hematopoietic stem cell in both normal and diseased patients. Furthermore, current methods rely on using patient biopsies as a surrogate for the entire patient marrow, and the usefulness of small samples will be discussed. Finally, the sixth chapter provides insight into improvements needed in patient specific models for internal dosimetry.

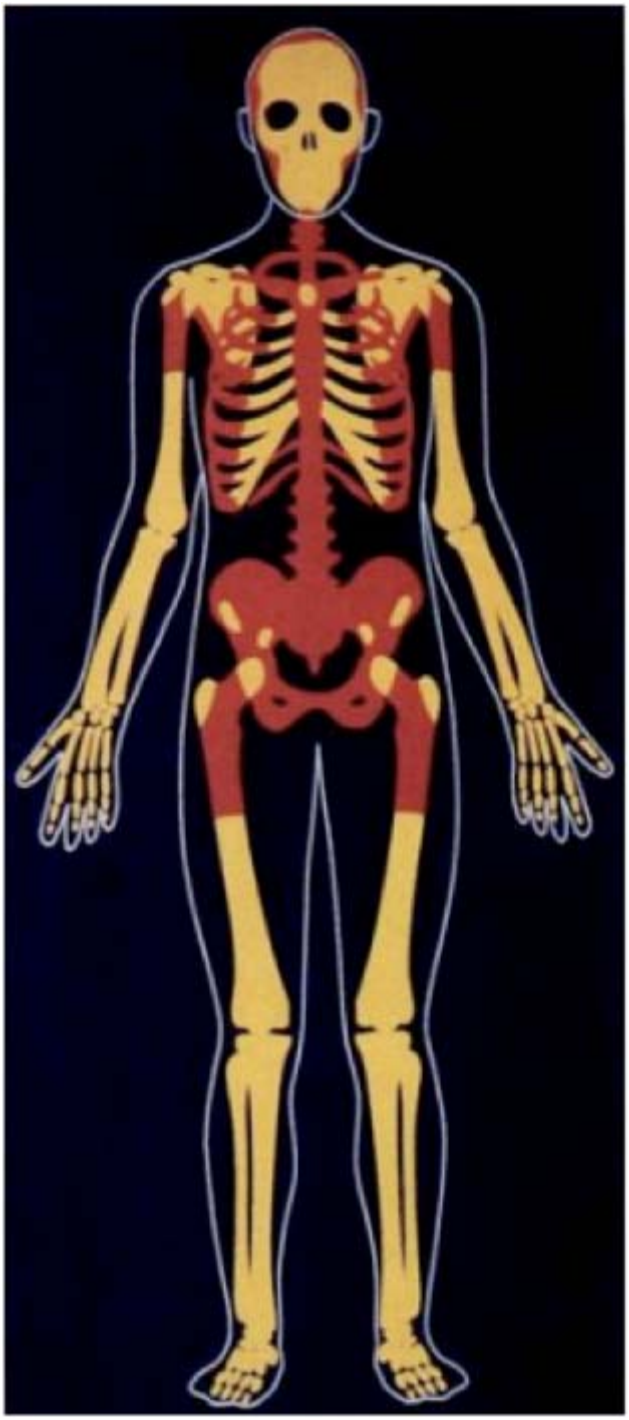

Figure 1-1. Sites of active marrow (red) and inactive marrow (yellow) in the adult (Vogler, 1988).

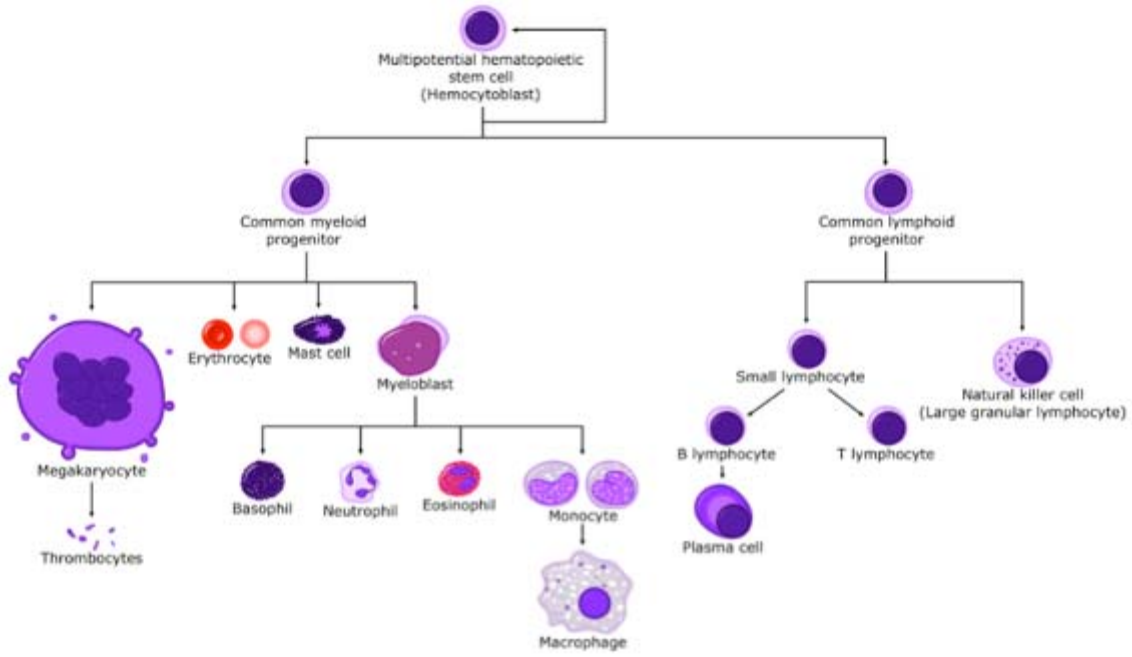

Figure 1-2. Hematopoietic stem cell pathway (DOH, 2006).

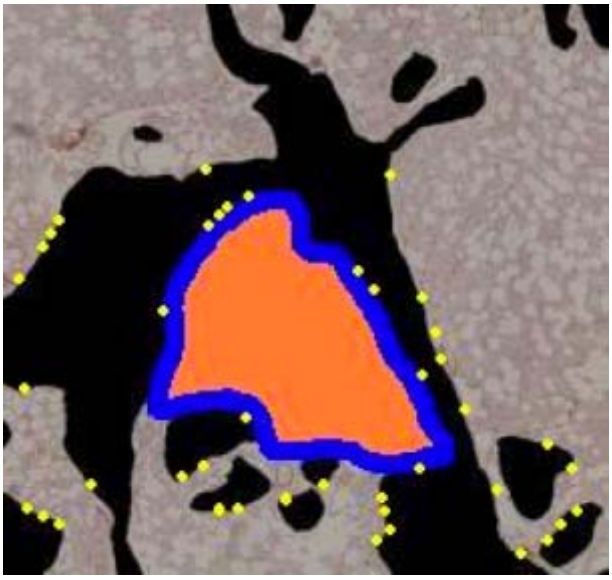

Figure 1-3. The marrow cavity encompasses both the orange (deep) and blue (shallow) marrow. Bone surface seekers (yellow) provide a higher dose to the radiosensitive stem cell population.

CHAPTER 2
BACKGROUND

Bone Structure and Physiology

Bone is a living, growing organ made up of two types of tissue: compact (cortical) and spongy (Spongiosa) bone, which differ by density and cellular function. The entire skeletal system consists mainly of bones, but also includes joints, ligaments and cartilage which together account for 20% of total body mass. Cortical bone consists of a central osteonic (haversian) canal surrounded by concentric rings (lamellae) of bone matrix, which make up the entire Haversian system. It is within the lamellae that mature bone cells called osteocytes reside, although they travel throughout the skeletal system through blood vessels in the canaliculi or small channels between the bone matrix (Marieb, 2006). Cortical bone makes up 80% of total bone mass.

Within the cortical bone and contained within the lining of the periosteum, is the spongy, cancellous bone whose lattice structure resembles that of a honeycomb. Thin bone structures called trabeculae are interwoven throughout the spongiosa, housing small, irregular cavities for bone marrow. Although the honeycomb structure may seem random, it is purposefully created based on the weight bearing requirements of the particular bone site. Because it contains the bone marrow, the spongy bone is the site of hematopoiesis or development of blood cells from hematopoietic stem cells. The compact and spongy bone regions are shown in Figure 2-1.

Both the lining of the trabeculae and the lining of the Haversian canals make up the endosteum. Along with the periosteum, this delicate tissue contains osteoblasts and osteoclasts, which are the cells responsible for creating and destroying bone, respectively (Figure 2-2). This is the also the location of the osteoprogenitor cell population which mature into osteoblasts. Traditional definitions of the endosteum are proposed in ICRP Publication 26, and assume a

layer of osteoprogenitor cells located 10 μm from all bone surfaces (ICRP, 1977). Thus, all new bone production starts from the lining of the cortical (periosteum) and trabecular (endosteum) bone.

It is well known that the trabecular bone varies by age (Atkinson, 1965; Snyder *et al.*, 1993) and bone site (Eckerman *et al.*, 1985; Patton, 2000). There have also been studies indicating that trabecular structure may vary with gender (Patton, 2000; Mosekilde, 1989). Since trabecular structure varies, the location and amount of endosteal tissue does as well. These studies have led to revisions in the current ICRP definition of the endosteum due to its relevance in bone cancer induction. It has been proposed that the cells of concern may reach beyond 10 μm from both trabecular and cortical bone, and as deep as 50 μm into the marrow cavity.

Bone is constantly remodeled in order to maintain constant levels of Ca^{2+} and PO_4^{3-}, and as a result of mechanical stress the particular bone site endures. At birth, osteoclasts are highly dominated by osteoblasts, leading to more bone growth than resoption. However, well into adult life, osteoclasts begin to outnumber osteoblasts, leading to less bone production (Calvi *et al.*, 2003; Zhang *et al.*, 2003). Osteoporosis is the most common bone disease in the United States and is a disorder that causes bone resorption to become much greater than bone formation. Thus, marrow cavities seem to get larger as trabeculae have unfilled cavities (Figure 2-3).

Women have a higher predisposition to osteoporosis, measured through bone mineral density (BMD). A low BMD corresponds to a low mineral content (grams of calcium and other bone minerals), which leads to less dense, weaker bones. Individuals with a t-score (bone mineral density compared to average 30 year old) less than 1.0 are considered to have normal bone health. A BMD of 1.0 to 2.5 would indicate an oteopenic individual, and a BMD of greater than 2.5 would show one with osteoporosis.

Osteoporosis affects women, and its onset and progression depends on both menopausal status and skeletal site, among other things. Studies have shown that women have bone changes that vary depending on whether that bone site was axial or appendicular. It seems that appendicular bone mass always decreased, whereas axial bones go through a five phase change of (1) buildup of BMD from 20-29 years old, (2) maintenance from 35 until 44 years old, (3) mild bone decrease from 40 until 49 years old, (4) rapid bone decrease at 50-54 years old, and (5) decelerated bone decrease after 55-59 (Yao *et al.*, 2001). This five-phase change is shown in Figure 2-4.

It was also found that BMD values are consistently higher for men in appendicular bones, but the same for both sexes in axial bones until about 50 years old. After 50 years old, BMD for women decreases greatly. This rapid bone decrease around 50 years old seems to be due to a decreased estrogen level postmenopausal and is also shown in Figure 2-4 (Yao *et al.*, 2001). Clearly, bone mass and bone mass changes are different by gender, and thus reference individuals of both male and female gender need to be established.

The mass of a skeletal site is strongly affected by Marrow Volume Fraction (MVF), or amount of marrow compared to the total skeletal mass. Osteoporosis changes the MVF, thus changing bone mass. Thus, for patient specific estimates of absorbed dose, marrow masses must be made as specific as possible and must include osteoporotic state. Currently, work is being done at the University of Florida to relate the measured BMD in a bone site of a patient to an estimate of the MVF of the bone site. It is hoped to build a dataset of reference individuals with varying microstructure that is scalable to a particular patient.

Hematopoiesis and Target Cells

All types of blood cells are generated through hematopoiesis in a self-regulated system set by demand. When the need for a particular type of cell increases, cytokines are released that

stimulate hematopoietic stem cells to generate new mature blood cells (Sugiyama *et al.*, 2006). Stem cells are unspecialized cells that can differentiate (turn into other cells) or self-regenerate (produce more stem cells) as shown in Figure 2-5. Therefore, under normal proliferation, some daughter cells remain allowing for an abundant supply of stem cells. Other daughter cells are myeloid or lymphoid progenitor cells, which commit to becoming a specific type of blood cell through various differentiation pathways (Figure 2-6). The only cells not generated by demand are lymphocytes, which are continually generated and destroyed. Therefore, lymphopoiesis is inefficient when compared to all other forms of hematopoiesis (DOH, 2001).

Blood cells are divided into three categories: erythroid, myeloid, and lymphoid. Erythroid cells are the oxygen carrying red blood cells, myeloid cells are varied cells such as granulocytes, megakaryocytes and macrophages, and lymphoid cells are T-cells and B-cells responsible for the body's immune system. Prenatally, hematopoiesis occurs in the yolk sack, liver, spleen, and bone marrow, but only occurs in the bone marrow in normal adults. Stem cells are rare in adults (<1% of all blood cells); however, a single HSC is capable of regenerating the entire hematopoietic system (Zhang *et al.*, 2003). The entire bone marrow microenvironment and hematopoiesis is shown in Figure 2-6.

Because they are the most primitive and least differentiated cells, hematopoietic stem cells are the most radiosensitive (Lim *et al.*, 1997a). Radiation sensitivity is characterized by DNA mutations (as opposed to cell death) that occur during the more vulnerable forms of the molecule seen during DNA replication in the cell cycle as induced by ionizing radiation or other mutagens. The more differentiated a cell is, the less sensitive it is to radiation because the cell is less likely to undergo mitosis during periods of potential radiation exposure. Currently it is assumed that HSCs are uniformly distributed throughout the active marrow, which resides in the axial skeleton

(skull, vertebral column, sternum, ribs, and the proximal ends of the femur and humerus) of adults (ICRP, 1977).

HSCs are found in bone marrow through markers present on their cell surface that are recognized by specific sets of antibodies. Methods to identify cell type and stage of differentiation were first proposed by the 1st International Workshop and Conference on Human Leukocyte Differentiation Antigens (HLDA) (Heddy and Swart, 2005). Through that body, the cluster of differentiation (CD) was established in 1982 and is the current protocol used to allow cells to be defined based on the molecules present on their surface. To date, CD34+/CD31- (indicating expression of CD34 antigen and suppression of CD31 antigen) is the most well known method to immunohistochemically stain CD34 antigen sites present on hematopoietic stem and progenitor cells, as well as endothelia cells, while excluding CD31 antigen sites present only on the vascular endothelium (Foucar, 2001; Rafii *et al.*, 1994; Kuznetsov *et al.*, 2001).

Lymphoma

Lymphoma is a disease of the bone marrow, whereby non-functional lymphocytes (a type of white blood cell), originally meant to protect from illness, build up and crowd out other nurturing cells. Many lymphomas arise within the lymph node, but some may originate in the spleen, thymus, Peyer's patches of the intestine, or from within the bone marrow itself. These cancerous cells then circulate in the blood and lymphatic system or reside in those organs, as shown in Figure 2-7. It is believed that these specific leukocytes undergo a malignant change sometime during cell division or maturation during circulation. Because of this, the separation between lymphoma and leukemia is becoming an outmoded idea, as both diseases are different manifestations of the same malignant cell as reflected in the Revised European American Lymphoma (REAL) classification system (Swerdlow *et al.*, 2008; Armitage, 2005).

There are two types of lymphomas, differentiated by the presence of *Reed-Sternberg cells* found only in Hodgkin's lymphoma. All other lymphomas are termed non-Hodgkin's lymphoma (NHL) and are separated into either B-cell or T-cell lymphoma, dependent upon whether the B-lymphocytes or T lymphocytes, respectively are infected. These cells were named via the organ responsible for their maturation, which is the bone marrow for B-cells and the thymus for T-cells. Lymphomas are then classified using the World Health Organization (WHO) system, which includes categories based on the appearance and chromosomal features of the cells (Swerdlow *et al.*, 2008). B-cell lymphomas make up 85% of NHL in the United States and are commonly Diffuse Large B-cell lymphoma, Follicular Lymphoma or Mantle Cell Lymphoma. Bone marrow involvement is assessed by the amount of malignant lymphocytes found in the bone marrow and is usually higher for leukemias than lymphomas (Muller *et al.*, 2005).

Chemotherapy and Marrow Toxicity

Chemotherapy is often used in conjunction with radiation therapy to provide systemic treatment of cancer cells (Forero and Lobuglio, 2003). Chemotherapy targets cells that divide rapidly, however, normal cells may divide just as fast as cancer cells, leading to less healthy tissue sparing. A common from of chemotherapy for non-Hodgkin's lymphoma is CHOP-R, a mixture of the drugs Cyclophosphamide, Doxorubicin, Vincristine, Prednisone, and an anti CD20 monoclonal antibody – Rituximab. While the drugs help disrupt abnormal growth by causing apoptosis, Rituximab targets B cell lymphocytes, through the CD20 antigen which is present on their cell surface. However, these proteins are also found on both normal and malignant cells, leading to ill side effects resulting from healthy tissue damage.

In all therapeutic regimes for hematological malignancies, some amount of depression in the immune system is guaranteed. Myelosupression is a well-known side effect of cancer treatment, whereby the bone marrow activity is severely decreased. This results in a reduction in

the number of red and white blood cells, as well as platelets. As radiation or chemicals produce lesions in DNA such as single/double strand breaks or base alterations, mutagenesis or cell killing can occur. Strictly speaking, cell killing is preferred to mutagenesis, as these aberrations cannot be passed on to progeny.

In radioimmunotherapy, as the antibody travels to the tumor, it will come into contact with all marrow and cause radiation damage to normal cells. There is also some amount of radiation that will cause hematopoietic toxicity in a specific patient. High "marrow involvement", that is, marrow that has a large amount of abnormal cells within, greatly affects radiation dosimetry levels (Martinez-Jaramillo *et al.*, 2004; Madrigal-Velazquez *et al.*, 2006). As the antibody travels to the tumor, a higher concentration will stay in the marrow and the crossfire from cancerous cells to normal cells will be high.

Treatments are performed in cycles to allow for increases cell sensitivity with re-oxygenation, and also to all for recovery from the side effects of marrow toxicity including fatigue and infection. In severe cases, a bone marrow cell transplant may be required to restore the depleted blood cell population. Some diseases that affect the bone marrow itself can also result in myelosupression. Bone marrow failures in hematological diseases including leukemia and lymphoma may be the result of inherent defects of the hematopoietic stem and progenitor cells or due to damage caused by ionizing radiation, viruses or chemical toxins. The increasing importance of HSCs in marrow health during therapies has brought attention to the stem cell niche, specifically the spatial codependence between stem cells and marrow vasculature (Taichman, 2005).

Radionuclide Therapies

Radiation may be delivered either externally or internally to treat malignant tumors or bone marrow cancers. DNA damage is induced by directly or indirectly ionizing individual atoms. In

external beam radiotherapy, the bone marrow as a whole is at risk and thus it is important to consider the entire tissue as a radiosensitive target. Radiation beams are shaped to conform as best as possible to the tumor in order to keep radiation dose extremely low in the healthy tissue. In internal radiotherapy, or radioimmunotherapy (RIT) radiolabeled antibodies guide the radioactive element to a specific site of interest. If the antibody is a bone surface seeker, such as radiopharmaceuticals used for bone pain palliation, the distribution of the stem cells is now important in estimating the radiation toxicity level (Kvinnsland *et al.*, 2001).

For treatment of non-Hodgkin's lymphoma, both Bexxar and Zevalin use beta sources to deliver radiation to abnormal cells throughout the bone marrow and tumor site. Monoclonal antibodies intended to bind to the CD20 antigen on lymphocytes are conjugated to radioisotopes and injected into the bloodstream. Tumor cells are then killed either by the antibody itself or by the crossfire from the radiation. In Bexxar, Tositumomab is tagged to Iodine 131, which emits gamma and beta radiation at approximately 0.6 MeV. Zevalin uses Ibritumomab Tiuxetan with Yttrium 90 which only emits beta radiation at a higher (maximum) energy of 2.3 MeV. Beta particle emission should eliminate tumor cells within 1000-5000 μm from their deposition. Gamma particles, if present, allow for more accurate dosimetry through monitoring radiation uptake in targeted sites.

Since February 2002, Zevalin has been approved by the FDA for treatment of relapsed, low grade, follicular B-cell NHL that is refractory to Rituximab. Similarly, Bexxar has been approved by the FDA for the treatment of CD20 positive, follicular B-cell, non-Hodgkin's lymphoma (NHL) patients whose disease in unmanageable by Rituximab and who have relapsed following chemotherapy since June 2003. However, Zevalin has been approved for use concurrently with therapeutic regimes involving Rituximab.

There has been much debate over whether these RIT procedures should be used in conjunction with chemotherapy, as well as their use as frontline treatment (Wiseman *et al.*, 2001). Compared to chemotherapy, RIT has the ability to induce apoptosis through radiation damage, as well as drugs aimed at targeting the CD20 antigen present on lymphocytes. This may provide a less toxic marrow environment than the untargeted concoction administered in chemotherapy. Clinical trials have shown good prognosis in the use of RIT as primary treatment (Kaminski *et al.*, 2005). The low use of Bexxar and Zevalin may be due to lack of awareness, insurance coverage, and unintended conflicts of interest among the range of therapies in local practice. Furthermore, lack of knowledge by referring oncologist unfamiliar with radionuclide therapy lends to it lack as frontline therapy.

Internal Dosimetry Calculations

Internal radiation dose is calculated according to methods determined by the Medical Internal Radiation Dose (MIRD) Committee. Dose to an organ *k* is defined as:

$$D_k = \sum_h \widetilde{A}_h S_{\{k \leftarrow h)} , \tag{2-1}$$

where *h* is the source organ, A_h is the cumulated activity or total disintegrations per unit time of the radionuclide in the source organ during irradiation, and $S_{(k \leftarrow h)}$ is the radionuclide S value as defined below. Much work has been done to quantify the cumulated activity but little effort has been afforded correct calculation of the radionuclide S value.

Radionuclide S values are defined for specific source rs and target rt region by:

$$S_{(r_T \leftarrow r_S)} = \sum_i \Delta_i \frac{\phi_i (r_T \leftarrow r_S)}{m_T} , \tag{2-2}$$

where m_T is the mass of the target region, Δ_i is the mean energy emitted per nuclear transition, and φ is the absorbed fraction (AF) of energy in the target region for the ith radiation type that

originated in the source region. AFs are the fraction of energy that reaches the target organ from which originated in the source organ.

Dividing the AF by the mass of the target yields the Specific Absorbed Fraction (SAF), and now the size of the organ is reflected in the fraction of energy retained. Regarding the radionuclide S value, the SAF is the critical component as it depends on the geometry and composition of the two organs, as well as any organs between the two in concern. The purpose of our modeling is to provide better approximation to the AF and mass of the target for more accurate clinical dosimetry.

Previous Methods Detailed

Radiation Transport using Chord-based Methods

Current absorbed fraction values used in clinical dosimetry, such as those implemented in the MIRDOSE program (Stabin, 1994), are acquired from AFs reported in ICRP Publication 30 (1979). These values are outdated for given current technological enhancements, as they are energy independent and based on chord length distributions from the Spiers and Whitwell studies (Spiers *et al.*, 1978; Whitwell, 1973; Whitwell and Spiers, 1976). As early as 1960 at the University of Leeds in England, Spiers and his students used an optical scanning device to measure chord-length distributions of bone marrow spaces from 5 to 7 skeletal sites from 1.7, 9 and 44 year old males (Beddoe *et al.*, 1976). Incorporating the path length through anisotropic bone or marrow and the frequency of occurrence allows for calculation of the fraction of the particles energy deposited in each tissue. Coupling these chord length distribution frequencies with range-energy relationships and providing dose conversion values, trabecular bone dosimetry models such as Reference Man were born.

Radionuclides studied in the Spiers era were 14C, 18F, 22Na, 32P, 45Ca, 90Sr, and 90Y, because of their application to radiation protection as the role of radiation for medical use was

not fully understood. Thus, the Spiers data included limited values of absorbed fraction for beta particles both for energy and location. For example, any beta particle originating in the bone volume would receive a single value regardless of energy, whereas one originating on the bone surface would receive either a high or low AF depending on whether it's energy was less than or grater than 0.2 MeV. Furthermore, the AF was given a value of unity when the source is the same as the target (such as marrow to marrow dose) with no response based on energy of the source.

While fitting for the time, chord based models are outdated for current use. First, chord models are only two-dimensional and do not reflect real trabecular microstructure. Along with that, the possibility for radiation sources to deposit their energy in the outer cortical bone is not included, hence the term infinite spongiosa transport model. Other assumptions made in chord-based models are that beta particles travel in straight paths (which they do not) and that bone and marrow distributions are independent of one another. An example of bone and marrow chords achieved through random chord length sampling is shown in Figure 2-8.

Spiers data has been updated by to include the role of adipocytes in the marrow (Watchman *et al.*, 2005). Furthermore, dose to the endosteum has been considered for monoenergetic electrons emitted within the bone marrow microenvironment (Eckerman, 1985; Eckerman *et al.*, 1985; Eckerman and Stabin, 2000). Moreover, the importance of 3D modeling to account for electron backscatter at bone-marrow interfaces have been addressed (Bouchet and Bolch, 1999; Bouchet *et al.*, 2000). However, these models still implicitly assume straight line path lengths for beta particles. Newer clinical models such as OLINDA have allowed for energy variations, but still rely on the Whitwell chord length data (Stabin, 2004). Overestimations in dose due to infinite spongiosa exist in all chord-based models.

Radiation Transport using Voxel-based Methods

To limit the deviation from accurate trabecular bone modeling and overestimations found in infinite spongiosa transport, Nuclear Magnetic Resonance (NMR) images have been used to provide 3D measurements. Studies have provided chord-length measurements of voxelized images and discussed the difficulty in calculating measurements and the dependency methods have in removing voxel effects (Rajon *et al.*, 2000). Later, EGS-nrc was used to transport particles in actual marrow cavities from 3D NMR images (Patton *et al.*, 2002a; Bolch *et al.*, 1998; Jokisch, 1999). Significant improvements over assuming an infinite trabecular region were made, and this voxel based approach served as a benchmark for future bone dosimetry models.

The work by Shah et al superseded previous models by accounting for radionuclide deposition in cortical bone as opposed to an infinite transport model. Furthermore, mathematical models are no longer needed as in previous stylized models because actual patient images are used. This technique also allows for reference data, as these models are fully scalable for patient specific absorbed fractions and S values. In the first part of this work, the first full image-based reference skeletal model was presented for an adult male radionuclide therapy patient including masses of the trabecular spongiosa and cortical bone for all skeletal sites. Moreover, absorbed fractions and S values were obtained for several radionuclides used in therapeutic regimes (Shah, 2004).

Paired-Image Radiation Transport (PIRT) significantly improves previous skeletal modeling approaches by incorporating both the ex-vivo CT image of the skeletal site with the microstructure from MicroCT images (Shah *et al.*, 2005b). The digital macrostructure (CT image) contains the mass of both the spongiosa and the cortical bone, which was digitally segmented. The microstructure contains the interior of the spongiosa, including the fraction of

trabeculae and marrow within. Using the novel PIRT model, these two images can be combined and radiation particles can be tracked. This is the first voxel model to encompass both macrostructure and microstructure to obtain absorbed fractions and is shown in Figure 2-9. The PIRT model developed by Shah et al was used for several skeletal sites containing active marrow and S values were calculated and compared to infinite transport models.

Stem Cell Distributions in Normal Marrow

The assumption that the stem and progenitor cells within bone marrow is uniformly distributed leads to the averaging of dose across marrow cavities. To address these concerns, Charlton et al studied the distribution of CD34+ and CD38+ cells to adipocytes. He postulated that if adipocytes are randomly distributed in bone marrow cavities, and stem cells are uniformly distributed from adipocytes, then stem cells should be randomly located in marrow. These studies found that there was a uniform distribution of adipocytes and an assumed uniform distribution of stem cells (Charlton *et al.*, 1996). However, studies by Shah et showed a weak or no spatial gradient in adipocytes to bone trabeculae in human bone marrow, leading to inconclusive evidence of the spatial extent of the hematopoietic stem and progenitor cells (Shah *et al.*, 2003). Charlton did not explicitly study the spatial distribution of stem cells to bone trabeculae.

The first studies to quantify the spatial distribution of stem and progenitor cells to trabecular bone were performed by Lord et al. In this murine model, a definitive spatial concentration gradient was noted, where stem and progenitor cells, identified by cytokine expression, were found to decrease as a function of depth in the marrow cavity in the marine femoral shaft (Lord and Hendry, 1972). These were the first results indicating that primitive cells are preferentially located closer to bone trabeculae, while mature cells tend to extent further into marrow cavities. Thus, using a uniform assumption to assess dose will be incorrect.

However, the trabecular microstructure of the mouse is known to be different than the structure of human bone, so applications are limited.

Studies to directly measure the spatial distribution of HSCs to bone trabeculae were then made on human marrow (Watchman *et al.*, 2007). CD34 and CD31 immunohistochemical staining was performed on subsequent slides from core biopsy samples of the iliac crest from disease-free normocellular human bone marrow. After slide preparation and imaging on the Morphometric microscope, distances to the nearest bone trabecular surface was measured for both hematopoietic CD34+ cells and blood vessels. Also, distances between nearest pairs of hematopoietic CD34+ cells and vessel fragments were determined and normalized to marrow area. The data fully supported the hypothesis by Lord that CD34+ HSCs and their progenitors follow a spatial gradient with respect to bone trabeculae within human bone marrow. Also, blood vessels seem to follow the same gradient indicating a shared spatial niche with stem cells. Distance-dependent weighting factors are provided as an update to the MIRD schema.

The most current work at the University of Florida used autopsy methods rather than biopsies to assess spatial distributions in larger samples and for several skeletal sites because of potential field of view limits (Bourke *et al.*, in press). CD34 and CD117 immunohistochemical staining was performed on autopsy sections from the iliac crest, lumbar vertebrae, and rib of disease free, normocellular patients. Moreover, cellularity was assessed via digital methods to provide normalization to hematopoietically active marrow only. This data shows the same trend found in previous studies, that the CD34+ cells decrease as a function of marrow depth. Although the same trend was found, differences in the concentrations of cells were found to be dependent upon bone site. Also, the method used to stain tissue was shown to alter the concentration of cells while preserving spatial gradient.

Stem Cell Distribution in Diseased Marrow

Recent studies have considered the composition and function of progenitor cells during treatment for malignancies specifically diffuse large cell non-Hodgkin's lymphoma (Martinez-Jaramillo *et al.*, 2004; Huerta-Zepeda *et al.*, 2000; Madrigal-Velazquez *et al.*, 2006). Patients were identified as being in remission following chemotherapy treatment by hematological parameters in blood. It was shown that lymphoma patients had a 35% reduction in progenitor cell concentration when compared to normal. Interestingly, this reduction in cell population was even noted after the patient was in clinical remission. This study thus proved deficiencies in the progenitor population in lymphoma patients during active disease and at the time of complete clinical remission.

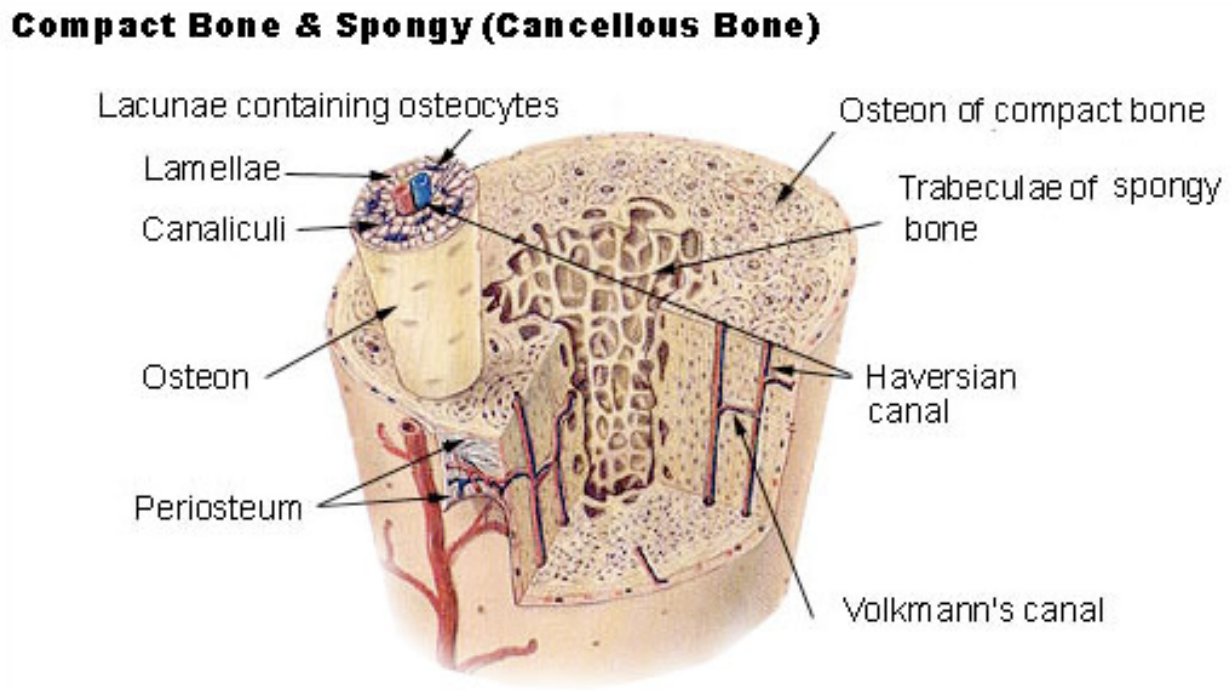

Figure 2-1. Human compact and spongy bone showing location of osteons and trabeculae (U. S. National Institutes of Health).

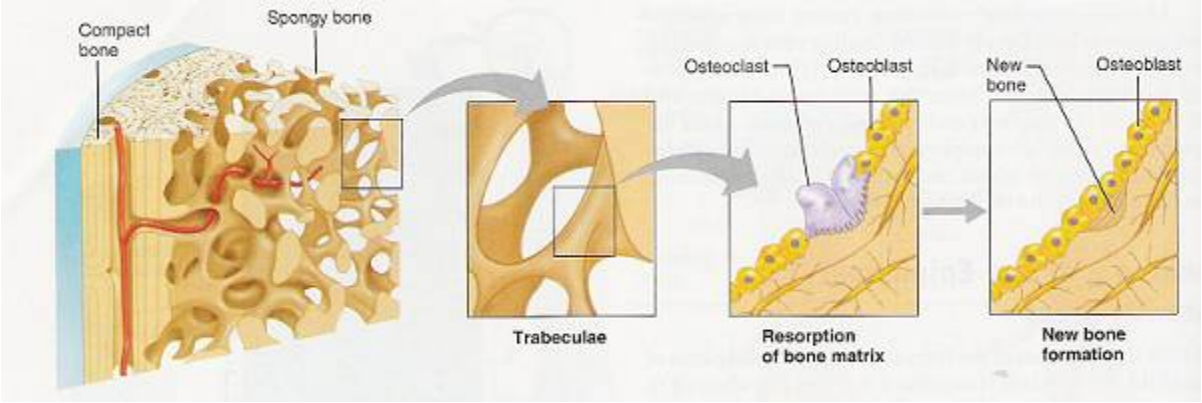

Figure 2-2. Bone remodeling and resoprtion are possible by osteoblasts and osteoclasts, respectively (Marieb, 2006).

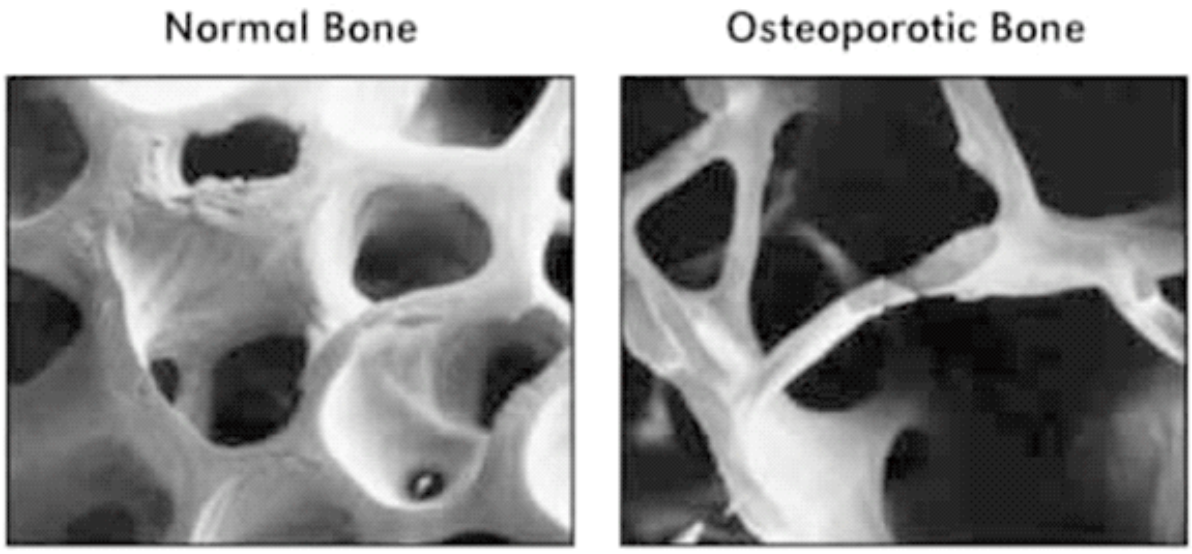

Figure 2-3. Osteoporotic versus normal bone (US Department of Health and Human Services).

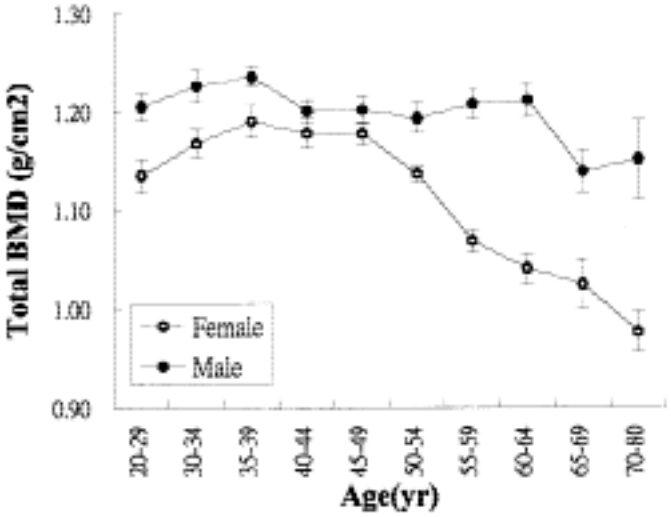

Figure 2-4. Bone Mineral Density (BMD) changes with age and gender (Yao *et al.*, 2001).

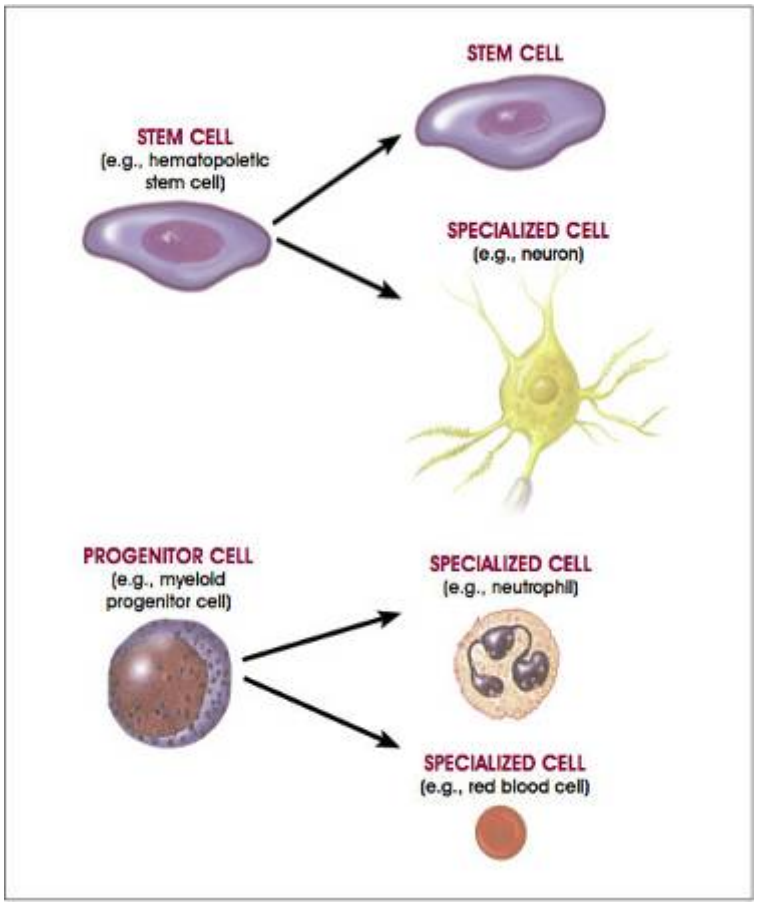

Figure 2-5. Stem cells may become either other stem cells (expansion) or further specialized cells (proliferation) (DOH, 2001).

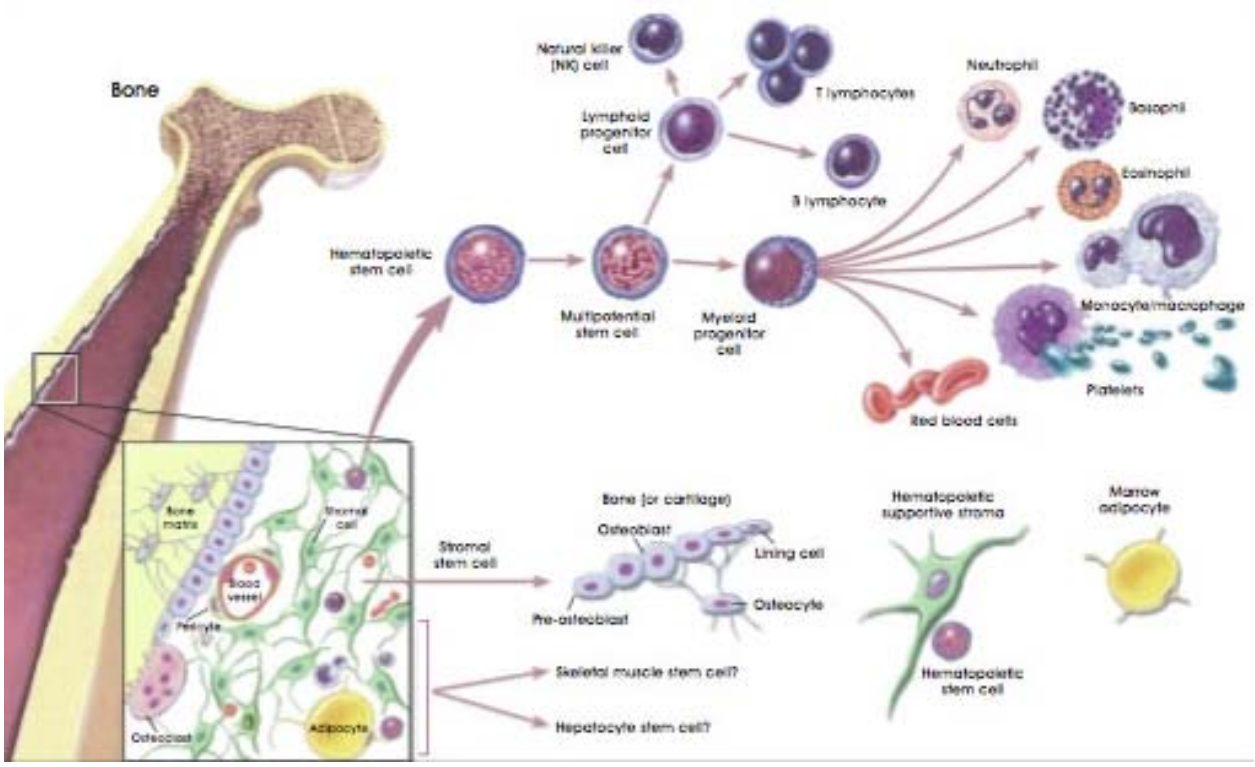

Figure 2-6. Hematopoietic stem cell differentiation pathways (DOH, 2001).

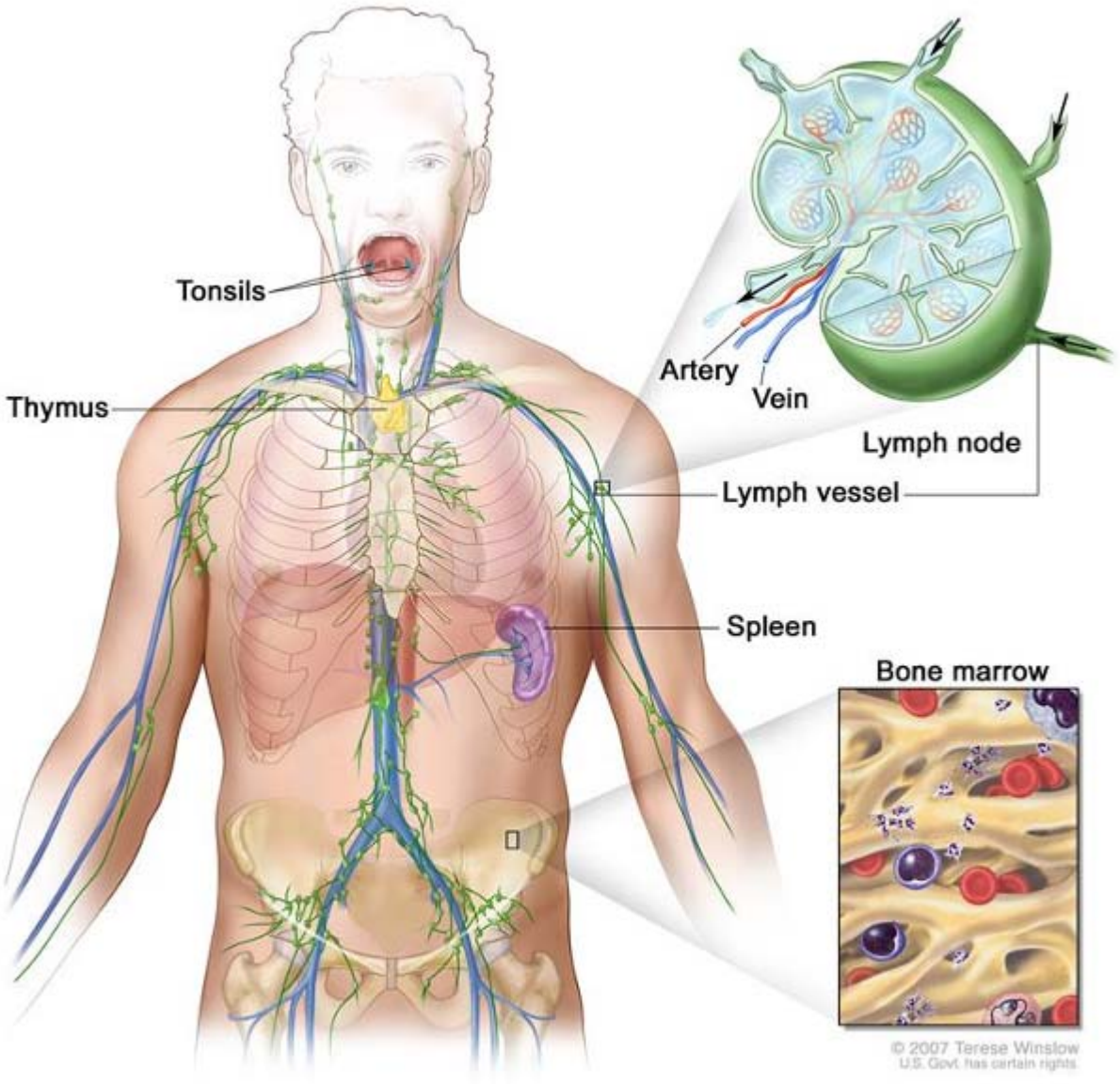

Figure 2-7. Lymphatic system and lymph circulation (Yoffey and Courtice, 1970)

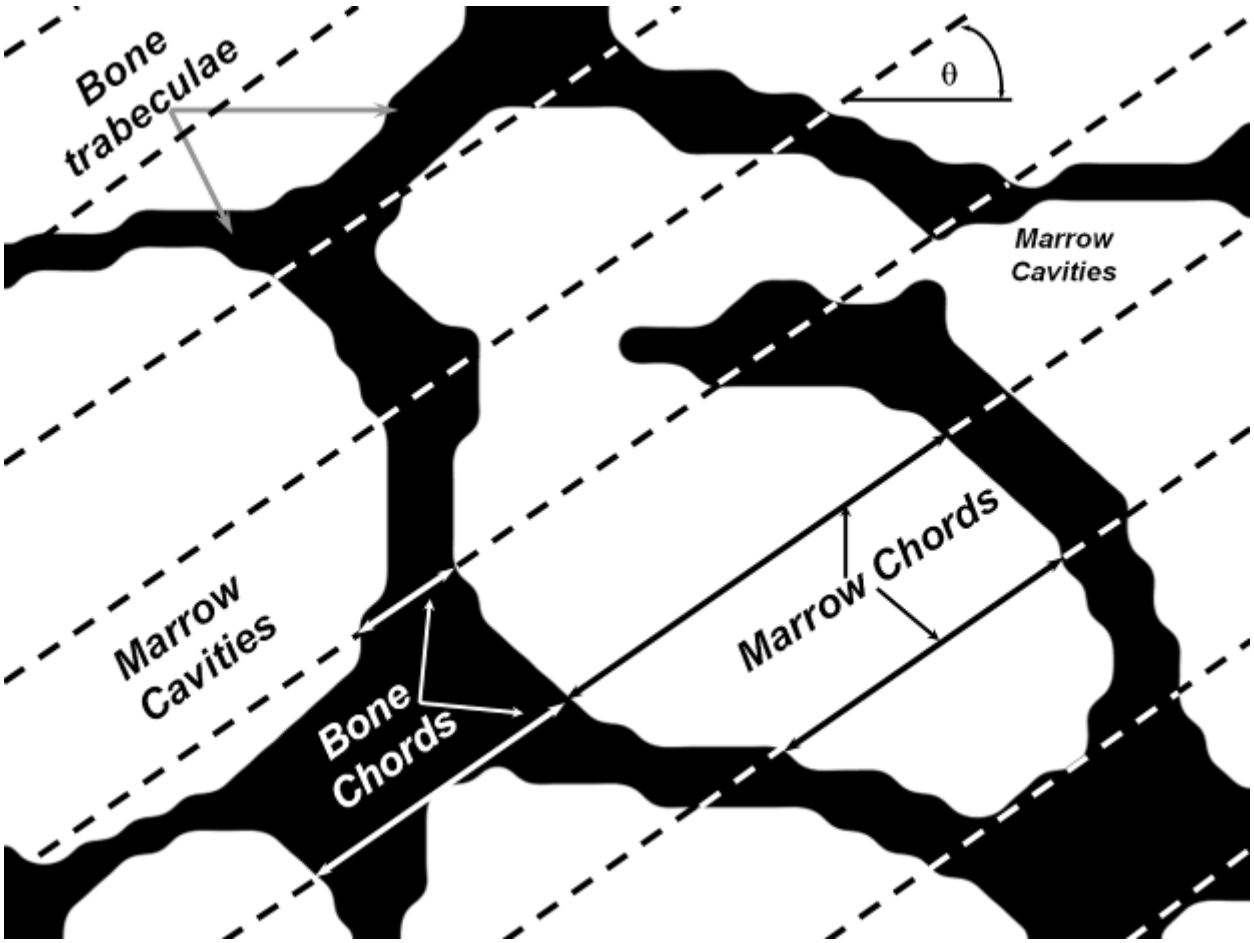

Figure 2-8. Chord lengths across bone trabeculae (black) and marrow cavities (white) at scanning angle ϕ (Shah *et al.*, 2005a).

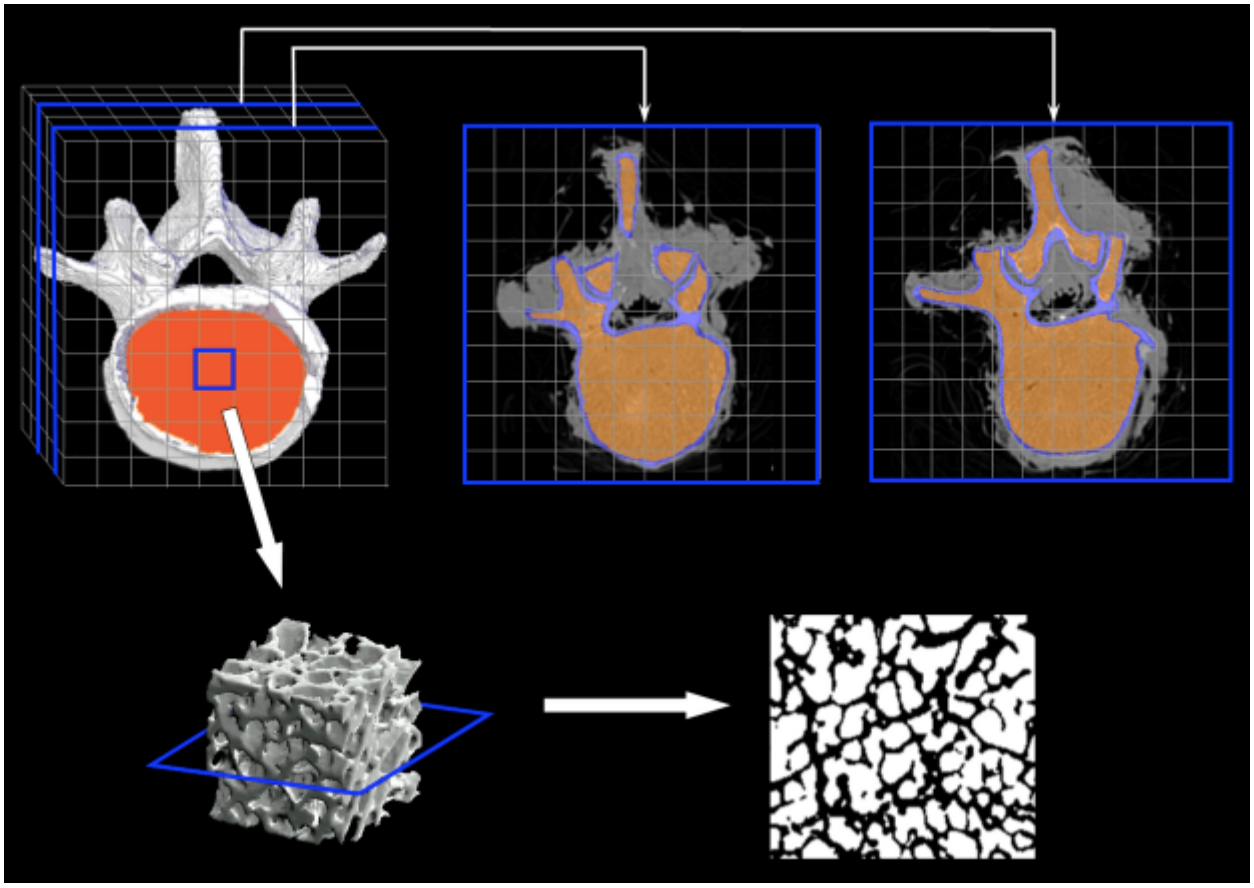

Figure 2-9. Paired Image Radiation Transport (PIRT) combines macrostructure (skeletal size) with microstructure (trabecular structure) for 3D radiation transport.

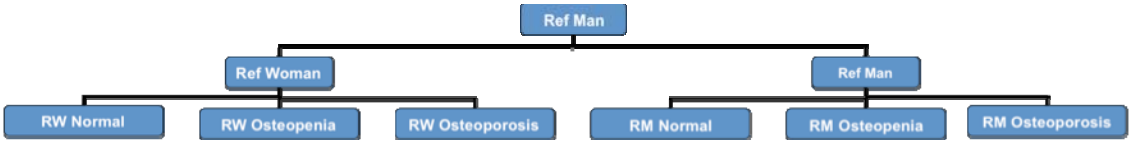

Figure 2-10. Schema of future reference models at the University of Florida.

CHAPTER 3
REFERENCE SKELETAL DOSIMETRY MODEL FOR THE ADULT FEMALE

Introduction

In order to predict the risk of bone cancer, an accurate assessment of absorbed dose to skeletal tissues is necessary. Concerning these tissues, the limiting factor in radiation protection is the toxicity of hematopoietically active bone marrow (Sgouros, 1993; Siegel *et al.*, 2003; Siegel *et al.*, 1990b). Bone marrow is made up of red bone marrow (RBM), which includes the hematopoietically active elements, and yellow (inactive) fatty bone marrow (YBM). In the adult, all axial bones contain both active RBM and inactive YBM to a certain degree dependent upon the cellularity factor (CF). The CF is the fraction of active marrow (1-fat fraction) and is 100% at birth and decreasing with age. The RBM and YBM, along with trabecular bone (TB) make up the spongiosa. The outer cortex of all skeletal sites is the cortical bone (CB), and together with the TB, the entire mineral bone (MB) is formed.

In this paper the RBM within spongiosa will be defined as trabecular active marrow (TAM) and the YBM will be defined as trabecular inactive marrow (TIM), where all bone marrow (TAM + TIM) in regions of spongiosa will be the trabecular marrow (TM). In the adult, the appendicular skeleton (long bones) contains only YBM without trabeculae and has a corresponding cellularity of zero. Thus, in the medullary cavities, hematopoietically active or inactive marrow will be termed cortical active marrow (CAM) or cortical inactive marrow (CIM), which together make up the entire cortical marrow (CM).

Particular tissues of interest for cancer risks are the hematopoietic stem cells (leukemia) and osteoprogenitor cells (bone cancer) of the trabecular endosteum within the red active marrow (Kuznetsov *et al.*, 2004; Charlton *et al.*, 1996). The hematopoietic stem cells (HSC) are assumed to be uniformly distributed throughout the TAM , whereas the osteoprogenitor cells (OPC) are

thought to be localized to 50 μm regions from the trabecular bone surface (TBS) within the spongiosa (Bolch *et al.*, 2007). This lends itself well to subcategorizing bone marrow by depth. Thus, TAM_{50} and TIM_{50} are the trabecular shallow active and inactive marrow, respectively, and comprise the soft tissues 50 μm from bone surfaces. All bone marrow ($TAM_{50} + TIM_{50}$) within 50 μm from the surfaces of bone trabeculae then are trabecular shallow marrow (TM_{50}).

In the adult, the medullary cavities of long bones contain only YBM and have a cellularity of zero. However, OPCs still exist, requiring a separate 50 μm region to denote the radiosensitive cell population within the CB. The cortical shallow active marrow (CAM_{50}) and the cortical shallow inactive marrow (CIM_{50}) then include all of the soft tissues from 50 μm from CB, and make up the entire cortical shallow marrow (CM_{50}). The cortical bone in the medullary cavities of the long bones is termed CB_{MC}, whereas the cortical bone in the sites containing active marrow is termed CB_{HC}, where HC denotes Haversian canals.

Previous analysis has shown that absorbed dose is an accurate measure of hematological toxicity, but only if the absorbed dose estimate is specific to the particular patient (Liu *et al.*, 1997; Shen *et al.*, 2002; Juweid *et al.*, 1999; O'Donoghue *et al.*, 2002; Sgouros *et al.*, 1997; Sgouros *et al.*, 1996a). At present, the vast majority of skeletal reference models (SRMs) used for these purposes are based on studies in the late 1960s and early 1970s at the University of Leeds in which a novel optical scanning method was used to obtain linear chord-length distributions across several skeletal sites of a single 44-year male subject. These data form an essential component of the ICRP's SRM published in ICRP Publications 30, 70, and 89 as well as clinical dosimetry codes such as MIRDOSE 3.0 and OLINDA 1.0 (Stabin, 1996; Stabin *et al.*, 2005).

MIRD methodologies of absorbed dose, requires separate knowledge of the cumulated activity within the source (marrow or bone), and the radionuclide S value (absorbed dose per unit cumulated activity). Much research has been done to asses the cumulated activity within the source, while little has been done to make patient-specific assessments of absorbed dose per unit cumulated activity (Juweid *et al.*, 1995; Macey *et al.*, 1995; Sgouros *et al.*, 1993; Sgouros *et al.*, 1996b; Siegel *et al.*, 1990a). Furthermore, these dose calculations requires known reference values such as the fraction of energy deposited in a target tissue and the mass of those target tissues.

While the Leeds data did report chord-length distributions to estimate the fraction of energy deposited, the methods used are far outdated given the technological improvements in the past few years. Most importantly, chord models are only two-dimensional and do not reflect real trabecular microstructure. These models also assume that beta particles travel in straight paths, which is known to be untrue. Furthermore, radiation sources cannot deposit their energy in the outer cortical bone and instead rely on infinite spongiosa transport. This causes overestimations in dose assessment to active marrow and an unrealistic estimate of marrow toxicity (Patton *et al.*, 2002b; Shah *et al.*, 2005a) .

Skeletal tissue masses were not given for the Leeds 44 year male subject, and thus ICRP Publications used a variety of studies to make up for this data (ICRP, 1995, 2002). Such studies include separate databases for total marrow mass (Mechanik, 1926) and bone marrow masses (Mechanik, 1926; Trotter and Hixon, 1974) as well as reference marrow cellularities (Custer, 1974). Furthermore, bone trabeculae surface to volume ratios are from other disjointed studies (Beddoe *et al.*, 1976). While novel at the time, these methods and values are outdated, and lead to an unrealistic ICRP Reference Man. Not only do the anatomical sources of absorbed fraction

data not match the tissue masses, there are biased variations due to a compilation of many independent knowledge bases.

Recent work has been done at the University of Florida Bone Imaging and Dosimetry Group to more accurately determine the fractional energy deposition in bone for alpha emitters and beta emitters as a function of bone site (Watchman, 2005). Also, complete sets of skeletal macrostructural and microstructural data, in a format sufficient for radiation transport simulations, have been established for an image-based skeletal reference model for the adult male at an age representative of cancer patients undergoing radionuclide therapy (Shah *et al.*, 2005b). Relevant tissues of the microstructure, such as the bone trabeculae, bone endosteum, and marrow cavities were accounted for through image-based techniques. Skeletal tissue masses, which are important in determining radionuclide S values, have been reported to update those summarized in ICRP Publications 70 and 89.

These reference skeletal dosimetry models can be used for dose assessment in radiation protection or therapeutic medicine. To provide an accurate dose assessment in, the reference skeletal dosimetry model must be patient-specific. That is, it should be designed to match as closely as possible to the average individual in the worker population for radiation protection. If used in therapeutic radionuclide planning, the reference model should match the patient being treated, including tissue masses and marrow cellularities. The skeletal tissue doses are then to be used only to establish dose limits based upon an acceptable risk of cancer induction or radiation induced effects (stochastic or non-stochastic).

There are current studies underway to estimate marrow cellularity in patients, including non-invasive bone scanning and magnetic resonance imaging techniques (Schick *et al.*, 1995). Methods for estimating patient skeletal spongiosa volume and active marrow masses, as well as

scaling models have also been provided (Brindle *et al.*, 2006a; Brindle *et al.*, 2006b; Brindle *et al.*, 2006c; Pichardo *et al.*, 2007). Previous studies have updated ICRP Reference Man with tissue masses and absorbed fraction data for the male model, however, work had not been done to assess differences based on gender. To date, there is no skeletal reference female model and this paper serves to present a companion skeletal reference model to the adult male.

Materials and Methods

Female Cadaver Selection

A female cadaver was selected through the State of Florida Anatomical Board located on the University of Florida campus. The cadaver was selected in order to represent an average, healthy female for use in therapeutic medical dosimetry. Selection criteria included (1) an age between 50 -75 years to be representative of a cancer patient, (2) a body-mass index between 18.5 – 25 kg m-2 (CDC recommended healthy range), and (3) a cause of death presenting a low probability of skeletal deterioration. The subject selected was a 64 year old female, 63 inches tall and 135 pounds. The subject thus had a body-mass index of 23.83 kg m^{-3} and died of respiratory complications.

In-vivo Macrostructural Image Database

Several imaging modalities and image processing techniques were required in order to provide a complete skeletal database for the reference female model. First, two whole body in-vivo images were acquired using a Siemens Sensation 16 multi-slice helical CT in the Department of Radiology at Shands Hospital at 1mm slice thickness, shown in Figure 3-1. In order to capture the whole body, the top of the body was imaged first, then the bottom. These in-vivo images were used to construct three-dimensional anatomical models of those skeletal sites that could not be completely harvested such as the entire rib cage or fully intact cranium.

Manual image segmentation of trabecular spongiosa and cortical bone was performed on CT_Contours, a program based upon Interactive Data Language (IDL) version 5.5. Using this program, patient anatomy was overlaid with a contour containing volume measurements based on the number of voxels manually selected. These contours provide the basis for the tomographic models used in radiation transport codes, as well as the tissue masses. The total voxels of marrow in the digital image of bone site j is the spongiosa volume $(SV)_j$, whereas all other bone voxels in that bone site are cortical bone volume $(CBV)_j$.

An image of the contoured in-vivo ribs is shown in Figure 3-2 and contoured in-vivo images of the cranium showing the separation of the left parietal, right parietal, occipital, frontal, facial bones, and other bones (sphenoid, ethmoid, temporal) are show in Figures 3-3 and 3-4. Furthermore, the images will provide a basis for planning the harvest of skeletal sites. The images were reconstructed using a B80 bone filter at the best possible resolution to capture the entire body. The CT images were stored within the UF Department of Nuclear and Radiological Engineering for data storage and image processing.

The right humeral head was found to be abnormal, possibly due to some sort of accident, and was not included in mass estimates. As shown in Figure 3-5, the cortical bone in the shaft seems to extend through to the proximal humeral head. This deformation did not lead to a doubt in the skeletal health of the individual, but merely some sort of injury at some point in the subject's life. To be safe, the macrostructural and microstructural data from the left (normal) humeral head was used in both the right and left volume and mass estimates.

Ex-vivo Macrostructural Image Database

Next, skeletal harvesting of those 13 skeletal sites containing the highest percentages of active marrow was performed. These included the cranial cap (parietal, occipital, and frontal lobes), clavicles (2), scapulae (2), entire vertebral column (cervical, lumbar, thoracic, and

sacrum), ribs (3 from each side), os coxae, proximal humeri (2), proximal femora (2), mandible, and sternum. These sites were cleaned, labeled, bagged, and stored in a freezer until ex-vivo micro imaging could be performed.

High-resolution ex-vivo CT images were acquired from the harvested skeletal sites at 1.0 mm slice thickness, with the best possible in-plane resolution (limited by sample size). The field of view (FOV) ranged from about 5.0 cm for the ribs and 33.2 cm for the os coxae. CT data for all skeletal sites is given in Table 3-1. These higher resolution CT images were used to determine volumes of both cortical bone and trabecular spongiosa for each skeletal site through the program CT_Contours based upon Interactive Data Language (IDL) version 6.0.

Samples of the ex-vivo contoured images are shown for the femur and lumbar vertebrae in Figures 3-6 and 3-7, respectively. Spongiosa volume, cortical bone volume, and null space are signified by red, blue and green, respectively. The separation of the femoral head and neck is shown, and were used distinctly because of known differences in trabecular microstructure as a result of weight loading. These images will also be used to determine the best location in that particular bone site to extract a sample for micro imaging. Eventually, they will provide the 3D anatomic macrostructural model for paired-image radiation transport (PIRT) simulations. Using this system, particles can start within the cortical bone (blue) and the fraction of radiation entering the spongiosa (red) or escaping (green) will be known.

MicroCT Microstructural Image Database

After all ex-vivo CT images were acquired and volumes were determined, physical sections of marrow intact trabecular spongiosa were cored from each bone site and imaged via microCT. There were limitations on sample size due to bone shape, cost, and the microCT imaging system. The maximum size of each bone cube was used to take advantage of microCTs large bore size compared to Nuclear Magnetic Resonance (NMR) imaging. Thus, only one

single sample was taken from each bone, at best representing 80% of the total spongiosa in that bone site (vertebral body samples). This is a clear advantage over the representative 25% spongiosa acquired using NMR techniques (Shah *et al.*, 2005b). Micro CT of the 35 cuboidal samples from the 13 major skeletal sites was performed on a desktop cone beam μCT80 scanner (Scanco Medical AG, Bassersdorf, Switzerland) at a 30 micron resolution. This resolution is relatively much higher than the previously 60 micron resolution used in the UF reference male skeletal database.

Post-acquisition image processing steps were then performed using gradient assisted manual segmentation to determine marrow volume fraction (MVF), and trabecular bone volume fraction (TBVF). Steps to determine the MVF included (1) extraction of a region of interest (ROI) to remove cortical bone from the image; (2) applying a median filter to improve the signal-to-noise ratio (SNR); (3) determining a threshold to best classify the voxels as either bone or marrow; and (4) segmentation of the ROI into a binary image based on the threshold gray-level value that was chosen. The thresholding of trabecular spongiosa was performed using gradient magnitude techniques (Rajon *et al.*, 2006). Visual inspection of the image gradient magnitude demonstrates the ability to retrieve sample volumes with 1% accuracy at 30-μm voxel resolution. Data for the 35 microCT images are given in Table 3-2.

Once filtered and segmented, the MVF and TBVF were determined by the ratio of marrow voxels to total voxels and bone voxels to total voxels (or 1-MVF), respectively. Next, MVFs were averaged dependent upon bone site and used to report trabecular active and inactive marrow masses. To determine shallow marrow masses in trabecular bone, the shallow marrow volume fraction (SMVF) was found by processing the microCT image and summing (1) marrow voxels that are adjacent to a bone voxel and (2) 2/3 of the volume of the next bone voxel, divided

by the total voxels in the digital image. Since microCT images are 30 μm in resolution, this leads to the best estimate of the amount of tissue 50 μm from bone surfaces. MVFs were weighted by SV (when available) in each respective site of acquisition to report total bone mass. An entire skeletal mass database was established for a female reference dosimetry model, including percentages of active marrow for those bone sites that contain active marrow. Reference percentages of active marrow by bone site are shown in Figure 3-8.

Mass Calculations

Mass estimates required both the macrostructural volume information (contoured ex-vivo CT images), microstructural volume information (filtered and segmented microCT spongiosa images), and the volume percentage of hematopoietically active versus inactive bone marrow for each skeletal site (marrow cellularity). Marrow cellularity can vary anywhere from 10% to 100% (no adipose tissue) with age, shown in Figure 3-9. Therefore, this reference individual does not have one single value of total active marrow mass, but a range of potential masses dependent upon the marrow cellularity chosen. The reported masses use those cellularities provided by ICRP Publication 70, purely as a comparison purpose only. Current ICRP reference cellularities based on bone site and age are shown in Figure 3-10.

Bone sites containing active marrow

Masses were calculated for the 13 major bone sites containing active marrow. Densities for all skeletal regions were taken from ICRU 46 (1992) and are in Table 3-3. For those sites where multiple cuboidal samples were taken, the marrow volume fractions were volume averaged. The mass of trabecular active marrow (TAM), trabecular inactive marrow (TIM), trabecular marrow (TM), shallow active marrow (TAM_{50}), shallow inactive marrow (TIM_{50}), trabecular shallow marrow (TM_{50}), trabecular bone (TB), and cortical bone (CB) at each skeletal site are calculated as:

$$(m_{TAM}) = (SV)(MVF)(CF)(\rho_{RBM}), \quad (3\text{-}1)$$

$$(m_{TIM}) = (SV)(MVF)(1-CF)(\rho_{YBM}), \quad (3\text{-}2)$$

$$(m_{TM}) = (m_{TAM}) + (m_{TIM}), \quad (3\text{-}3)$$

$$(m_{TAM_{50}}) = (SV)(SMVF)(CF)(\rho_{RBM}), \quad (3\text{-}4)$$

$$(m_{TIM_{50}}) = (SV)(SMVF)(1-CF)(\rho_{YBM}), \quad (3\text{-}5)$$

$$(m_{TM_{50}}) = (m_{TAM_{50}}) + (m_{TIM_{50}}), \quad (3\text{-}6)$$

$$(m_{TB}) = (SV)(TBVF)(CF)(\rho_{MB}), \quad (3\text{-}7)$$

$$(m_{CB}) = (CBV)(\rho_{MB}), \quad (3\text{-}8)$$

where SV is the spongiosa volume, CBV is the cortical bone volume, MVF is the marrow volume fraction, TBVF is the trabecular bone volume fraction (1-MVF), SMVF is the shallow marrow volume fraction, ρ_{RBM} is the density of RBM, ρ_{YBM} is the density of YBM, ρ_{MB} is the density of mineral bone, and CF is the cellularity factor for skeletal site j. As noted above, in most sites the SV came from the high resolution ex-vivo image, whereas others came from the in-vivo image. Marrow volume fractions were averaged in cases where there were more than one MicroCT sample acquired for the same bone site.

Marrow volume fractions were not available for the extremities as these bone sites were not harvested and microstructural data were used from a similar bone site. The marrow volume fraction of the humerus was used for the proximal and distal ends of the lower arm bones. For the lower leg bones, the marrow volume fraction of the femoral neck was used.

Bone sites not containing active marrow

The shafts of the long bones in adult (femur, tibia, fibula, humerus, radius, and ulna) do not contain active marrow or trabeculae and masses were calculated only for cortical inactive marrow (CIM), shallow inactive cortical bone (CIM_{50}). Volumes of the CIM and entire cortical bone were reported through direct image segmentation. ICRP 70 and 89 report marrow cellularity in the "upper half" and "lower half" and not for the entire femur and humerus, so in some cases the upper and lower halves were reported individually.

Masses of the shallow inactive cortical marrow (CIM_{50}) in the shafts of long bones were mathematically derived. Concentric cylinder models were used to stylistically model bone site j, with a cortical marrow radius and cortical marrow volume (CMV) defined as:

$$(CMV)_j = \pi (R_{MC})^2 (L_{MC})_j, \tag{3-10}$$

$$(R_{MC})_j = \sqrt{\frac{(CMV)_j}{\pi (L_{MC})_j}}, \tag{3-11}$$

where R_{MC} is the medullary cavity radius, L_{MC} is the medullary cavity length, and CMV is the segmented medullary volume from the contour.

The shallow marrow volume fraction in the medullary cavities ($SMVF_{shaft}$) is the ratio of the volume of the cortical shallow marrow (CMV_{50}) to the volume of the total medullary marrow (CMV). CM_{50} is defined as a 50 μm thick cylindrical shell of marrow at the outermost region of the medullary cavity, which includes only and cortical inactive marrow (CIM_{50}) in the adult. The $SMVF_{shaft}$) is calculated as follows:

$$\left(SMVF_{shaft}\right)_j = \frac{(CMV_{50})}{(CMV)_j} = 1 - \frac{(R_{MC} - 50\mu m)_j^2}{(R_{MC})_j^2}, \tag{3-12}$$

The mass of the CIM, CIM_{50}, and CB for the medullary cavity is then:

$$(m_{CIM}) = (CMV)(\rho_{YBM}), \tag{3-13}$$

$$(m_{CIM_{50}}) = (CMV)(SMVF_{shaft})(\rho_{YBM}), \tag{3-14}$$

$$(m_{CB}) = (CBV)(\rho_{MB}), \tag{3-15}$$

where the definitions are the same as above. Note that long bones may be further divided into upper and lower halves by dividing the mass by two. Again, volume fractions were weighted by SV (when available) for each respective site of acquisition to report total bone mass.

Transport Modeling

Both sets of images (ex-vivo CT and ex-vivo microCT) were combined under Paired-Image Radiation Transport (PIRT) via methods described previously by Shah et al (2005). Using PIRT, the 3D model of trabecular spongiosa was paired with the patient CT anatomy and beta particles were transported via EGSnrc. Possible tissue sources were the trabecular active marrow (TAM), trabecular inactive marrow (TIM), trabecular bone volume (TBV), trabecular bone surface (TBS), and cortical bone volume (CBV). These sources could irradiate tissue targets including TAM and the shallow trabecular active marrow (TAM_{50}). Cellularity was varied from 10% to 100% and energy from 0.01 MeV to 10 MeV. Particles were transported until the kinetic energy is zero, and until coefficients of variation in the absorbed fraction are less than 1%.

For the shafts of the long bones, a stylistic model was created in MCNP given the volume and lengths acquired from the segmented CT patient data. Tissue sources can be cortical inactive marrow (CIM), cortical bone surface in the medullary cavities (CBS_{MC}) and the CBV. Particles were transported until the source was evenly distributed throughout the bone site volume. The tissue target in the bones not containing active marrow was the cortical shallow inactive marrow (CIM_{50}) and Tally 2 identified the energy (MeV) deposited in this region.

Absorbed Fractions

Both the PIRT and MCNP techniques for radiation transport produced absorbed fractions using various source to target tissues for each bone site, and are fully dependent upon cellularity and energy. When divided by the mass of the target (and cellularity), the specific absorbed fraction (SAF) is determined. In bone sites where more than one MVF existed, particles were transported several times to combine each MVF with the corresponding SV. These values were then weighted by the MVF for each individual AF for one energy-dependent absorbed fraction per bone site j as shown below:

$$\phi(TAM \leftarrow TAM)_j = \frac{\sum_x (MVF)_x \phi(TAM \leftarrow TAM)_x}{\sum_x (MVF)_x}, \quad (3\text{-}16)$$

where ϕ(TAM←TAM) is the fraction of energy deposited in the TAM from a particle emitting radiation from the TAM, and MVF_x is the MVF for bone site x. For bone sources, TBVF was used in place of MVF.

Results

The University of Florida Reference Female (UFRF) was first matched to a database of cadavers to assess whether the cadaver used was similar to the average in terms of spongiosa volume, shown in Table 3-4. Next, the volume of spongiosa and percentage of total was compared to the University of Florida Reference Male (UFRF) in Table 3-5. Volume fractions are given in Table 3-6, which were then used to determine bone masses. Table 3-7 shows the percentage of trabecular bone and cortical bone to mineral bone, and is compared among UFRF, UFRM and ICRP 89 reference male. Since no ICRP female model exists, a comparison to the ICRP Reference Male must be made. To make such a comparison, cellularities were assigned to be the reference value, although any value of cellularity can be used.

The ratio of total UFRF trabecular bone mass and total cortical bone mass to ICRP 89 total masses is used as a method of fair comparison since there is too much variation in specific skeletal sites. Both total marrow masses and shallow marrow masses for active and inactive marrow are given for UFRF in Tables 3-8 and 3-9. Total marrow masses were compared to ICRP 89 and UFRM, however, since ICRP does not report shallow marrow masses, UFRF was only compared to UFRM for this case. Table 3-10 lists surface-to-volume (S/V) ratios for UFRF, URFM, and ICRP 70 as well as other studies by Beddoe et al and Lloyd et al. Surface areas for trabecular bone regions and all cortical bone regions including both Haversian canals and medullary cavities is provided in Table 3-11.

Fractional mass weights for each source and target region in UFRF are listed in Tables 3-12 and 3-13. These values were used to determine skeletal averaged SAFs. UFRF used reference cellularities from ICRP Publication 70 (1995), whereas the ICRP model used cellularities from Eckerman & Stabin (2000). Specific absorbed fraction data for UFRF is given in the appendices for any combination of source (TAM, TBS, TBV, TAM_{50}, TIM) and target (TAM, TAM_{50}) regions in the entire skeleton containing active marrow for a range of cellularities (10% to 100%). Tables and graphs of SAF for each bone site, given all source-target combinations, are given in Appendix A and B, respectively. Appendix C then contains SAF and graphs of all source-target combinations comparing all bone sites independently. In bone sites not containing active marrow (shafts of the long bones), absorbed fraction data is given for combinations of sources (CBV, CIM, CBS_{MC}) and target (CIM_{50}) and SAF are tabulated graphed in Appendix D. Finally, Appendix E contains tables and graphs of skeletal averaged SAFs and comparisons to models from Stabin and Siegel (2003).

Discussion

Spongiosa Volume and Percentages

The spongiosa volume and percentage of total for UFRF was first compared to a population of database of 20 cadavers, 10 male and 10 female, provided by Brindle et al (2006). This database included the UF Reference Male subject. The spongiosa volumes were averaged by skeletal site for female cadavers, male cadavers, and then an average of all cadavers of either sex. Table 3-4 shows the percentage of spongiosa volumes for the skeletal sites containing active marrow for UFRF, the average female, the average male, and the average of either sex.

UF Reference Female seems to match well to the average female with respect to total spongiosa volume and percentages of total. The total spongiosa volume (1535 cm^3) is remarkably close to the average female (1521 cm^3) with a difference less than 1%. UFRF has less spongiosa in the os coxae and more in the sacrum, but overall matches well to the average female. These differences are noted in many bone sites due to normal patient variation. When compared to the average male, total spongiosa volumes are greater in the average male population (2221 cm^3) and there seems to be more inherent variation in male spongiosa volume. In particular, the percentage of spongiosa in the ribs and scapulae vary greatly. Again, one would expect these differences due to natural skeletal variation.

A comparison of spongiosa volume and percentage of total for UF Reference Male and Female are given in Table 3-5. Although the spongiosa varied, as expected due to patient size, the percentage of spongiosa volume for both reference individuals was comparable. A higher percentage of spongiosa volume was seen in the os coxae of UFRF compared to UFRM, and lower percentages of spongiosa volume in the femora and humeri. ICRP 89 does not report spongiosa volume explicitly, thus no comparison can be made.

Volume Fractions

Averaged marrow volume fraction (MVF), bone volume fraction (BVF) and shallow marrow volume fraction (SMVF) by skeletal site are shown in Table 3-6. It is noted that the MVF are similar for a single bone site except in the cranium and femora. The cranium has MVF variation from 11% marrow in the occipital lobe to about 39% - 43% marrow in the frontal and occipital lobes. An image of the microstructure of the frontal and occipital lobes are given in Figure 3-11 and 3-12, respectively. The femoral neck is 87% marrow, whereas the femoral head is 71% marrow. An image of the microstructure showing the differences between the femoral neck and head is given in Figure 3-13 and 3-14, respectively. Since the microstructure varied greatly in these skeletal sites, volume averaging seemed best.

For completeness, an image of that bone site with the highest percent of marrow is given. The sternum is shown in Figure 3-15, having 99% marrow. Also, to show the changes in microstructure throughout the vertebral column, an image of the 3rd cervical vertebrae (76% marrow) and the 5th lumbar vertebrae (91% marrow) are shown in Figure 3-16 and 3-17. The marrow volume fraction increases as you move down the vertebral column.

Tissue Masses

Masses for the trabecular spongiosa region, cortical bone region and total mineral bone for all skeletal sites (both active and inactive marrow) are in given in Table 3-7. ICRP reference cellularity was used for each bones site. UFRF has a trabecular bone mass of 968 g, cortical bone mass of 4723 g and total mineral bone mass of 5691 g. Thus, mineral bone is 17% trabecular bone and 83% cortical bone. A comparison to ICRP 89 Reference Male model reveals that reference values yield 20% trabecular bone (1100 g) and 80% cortical bone (4400 g). Furthermore, trabecular bone makes up 17% of total mineral bone and cortical bone makes up the remaining 83% and overestimates trabecular bone mass compared to UFRF (ratio of 0.88).

UFRM was 22% trabecular bone (1267 g) and 78% cortical bone (4388 g). Total mineral bone mass was similar in both UFRM (5656 g) and UFRF (5691 g), which is slightly higher than the ICRP value (5500 g).

Compared to both UFRM and ICRP 89, the female model was found to be much lower in trabecular bone mass. Interestingly, the ICRP 89 value is in the middle at 20%, and perhaps represents an average for the two. The percentage of total cortical bone to mineral bone was found to be slightly higher for UFRF compared to both male models with a ratio to ICRP of 1.07. Thus, the female model seems to have less trabecular bone and more cortical bone when compared to males. This could be a result of the differences in bone resorption by gender and the effect of osteoporosis, or simply patient variation in skeletal bone mass.

Active marrow masses for UFRF are provided in Table 3-8. UFRF has 1984 g in inactive marrow, 686 g in active marrow, for a total marrow mass of 2670 g. Thus, marrow is 26% active and 74% inactive. It is emphasized again that the mass of UFRF is not bound by cellularity, and is given at ICRP 70/89 reference values only for comparison. Compared to ICRP 89, both the active marrow mass (1170 g) and inactive marrow mass (2480 g) yielding 32% active marrow and 68% inactive marrow. Thus, ICRP 89 active and inactive marrow masses are severely overestimated for the UFRF with ratios of 0.59 and 0.80, respectively. UFRM had an active marrow mass of 2406 g and an inactive marrow mass of 1170 g. Thus, this overestimation in marrow mass was also noted in the URFM data, although not as significantly (ratio of 0.91 and 0.97). This is due to the much lower total marrow mass of 2670 g found in UFRF, compared to 3650 g in ICRP 89 and 3469 g in UFRM. Since the active marrow is the region for hematopoiesis, this is a red flag for marrow toxicity and cancer risk when using ICRP 89 reference values to estimate radiation dose in females.

UFRF has a shallow marrow mass of 240.8 g, which is 20% shallow active marrow (48 g) and 80% shallow inactive marrow (193 g). These are shown in Table 3-9. ICRP does not report this data, therefore only a comparison to UFRM can be made. Again, these were calculated at reference cellularity, although any cellularity could be chosen. Shallow active marrow was only 100 g in UFRM, with 226 g of shallow inactive marrow. Accordingly, UFRM has 31% of active shallow marrow and 69% of inactive shallow marrow, with a total shallow mass of 326.3 g. Total shallow active marrow was less in UFRF due to a lower overall active marrow region. However, UFRF had a 10% higher inactive component of shallow marrow, leading to dosimetry concerns. This could be simply patient variation, or could signify heightened osteoporosis in females due to lower volume of active elements in general.

Surface to Volume (S/V) Ratios

Table 3-10 lists S/V ratios of the trabecular microstructure in all skeletal sites in UFRF, along with a comparison to UFRM and data from the University of Leeds studies, which provide the basis for the ICRP Reference Man model. The mean S/V ratio was found to be 21.2 mm^2/mm^3 across 13 skeletal sites with a standard deviation of 7.2 mm^2/mm^3. This value is slightly higher than the UFRM model (18.5 mm^2/mm^3), but within the standard deviation of 4.2 mm^2/mm^3. The Leeds data indicated a smaller ratio of 16.1 ± 4.8 mm^2/mm^3, while other studies in ICRP cited even lower values of 11.2 ± 5.0 mm^2/mm^3 (Lloyd and Hodges et al). ICRP 70 uses a single value of 18 for all bone sites, whereas this data lists S/V ratios for 13 separate skeletal sites allowing for a better estimate of the shallow marrow masses.

Surface Areas

Table 3-11 lists surface areas in all skeletal sites for both trabecular and cortical bone regions. UFRF was found to have 8.23 m^2 of trabecular bone surfaces, 7.38 m^2 of cortical bone surfaces within regions containing haversian canals, and 0.06 m^2 of cortical bone surfaces in the

medullary cavities. This leads to 47% of the total surface area being cortical bone within Haversian canal tissues, 0.4% of cortical bone surface in the medullary cavities and 53% of bone surface in the trabecular regions. ICRP does not list bone surface area in the cortical bone of medullary cavities, but does list 6.50 m^2 of cortical bone surfaces (38%) and 10.50 m^2 of trabecular bone surfaces (62%). UFRM had similar values to ICRP with 6.86 m^2 of cortical bone surfaces in the Haversian canal tissues (37%) and 11.74 m^2 of trabecular bone surfaces (63%). In the medullary cavities, UFRM had a surface area of 0.17 m^2 (0.9%).

It seems that the surface areas and S/V ratios reveal that UFRF has a higher surface to volume ratio and a lower overall trabecular bone surface. Compared to ICRP, UFRF has a much lower (0.78) ratio of trabecular surface area and more cortical bone surface area (1.14). UFRM also had a higher cortical bone surface area than ICRP, but had higher trabecular surface area as well. This could be an inherent difference in the cadaver selected, or a real difference among female bone anatomy. It seems that there is similar cortical bone volume but less trabecular spongiosa (both bone and marrow). Due to overall size differences, this difference must be thicker cortical bone and smaller trabeculae and marrow cavities.

Weighting Factors

The fractional distribution of tissue masses at reference cellularities for each skeletal site is given in Tables 3-12 and 3-13. Bone site weighting factors are provided for the fraction of total active marrow (TAM+CAM), total inactive marrow (TIM+CIM), total shallow active marrow (TAM_{50}+CAM_{50}) and total inactive shallow marrow (TIM_{50}+CIM_{50}). For surface sources, the fractional distribution of tissue masses are given for the TBS, CBS and total bone surface (TBS+CBS). For volume sources, weighting factors are provided for the TBV, CBV, and total bone volume (TBV+CBV).

UFRF had 68.9% of total active marrow ($f_{TAM}+f_{CAM}$) concentrated in the os coxae (26%), thoracic vertebrae (16.2%), lumbar vertebrae (14.5%) and ribs (12.2%). The same bone sites within the ICRP accounted for 79.7% of total active marrow (f_{TAM}): os coxae (33.3%), thoracic vertebra (17.4%), lumbar vertebrae (9.8%), and ribs (19.2%). The largest fraction of bone trabecular surfaces in the UFRF (f_{TBS}) is from the distal femora (23.9%), proximal tibiae (19.1%), os coxae (11.6%), and proximal femora (8.2%). In ICRP, the TBS mass was most concentrated in the thoracic vertebrae (28.2%), lower femora (16.9%), proximal femora (16.7%), and the cervical vertebrae (11%). The fraction of trabecular bone surface in the os coxae was only 1.8% in the ICRP values. A great deviation in the os coxae was also found in UFRM, when comparing to current ICRP fractions.

The largest fraction of bone trabeculae mass in the UFRF (f_{TBV}) is found in the distal femora (23%), proximal tibiae (18.4%), cranium (16.8%) and proximal femora (7.9%). In the ICRP model, most of the TBV mass is found in the thoracic vertebrae (27.6%), with the rest located in the lower femora (16.5%), proximal femora (16.3%) and cervical vertebrae (10.7%). These values seem to differ greatly in the cranium, with only 2.6% noted in ICRP values.

Finally, the fraction of cortical bone volume in UFRF was found to be highest in the cranium (10.7%), distal femora (9.3%), os coxae (8.7%) and the proximal tibiae (8%). ICRP values of f_{CBV} were found to be highest in the lower femora (20.7%), proximal femora (14%), cranium (12.8%), and ribs (12%). These bone sites comprise 36.7% of the UFRF cortical bone volume, and 59.5% of the ICRP cortical bone. The low fractional mass in UFRF is due to the cortical bone being distributed over more regions in the extremities.

Specific Absorbed Fractions (SAF)

SAF for individual bone sites containing active marrow

SAFs for each individual bone site is provided for two targets - TAM and TAM_{50} and all five sources in Appendix A (tables) and B (graphs). For this discussion, a single bone site will be used since all bone sites followed the same general trend with slight differences in SAF value. The SAF for the TAM irradiating either the TAM or the TAM_{50} for the lumbar vertebrae is shown in Figure 3-18 and 3-19, respectively. Both source target combinations followed the same decrease in SAF with energy. SAF decreases with higher energy since higher energy particles will have enough energy to escape the TAM and deposit energy elsewhere. At low energies and at high cellularity (no fatty marrow), the absorbed fraction is at a maximum because all of the particles are absorbed in the active marrow. Conversely, at low energies and low cellularity (fatty marrow), the particles are absorbed in the fat and there is a low absorbed fraction to the active marrow. Calculating the SAF requires a division of the mass of the target which depends on the cellularity, thus, cellularity trends are switched. There is a point of convergence where cellularity no longer causes dose implication at an intermediate energy (<1 MeV).

Figure 3-20 and 3-21 shows the SAF for each source irradiating either the TAM or TAM_{50} for the lumbar vertebrae. While trends are similar, there is a difference in the overall value of each source-target combination depending on the target. When the target is the entire active marrow, the SAF is highest in the TAM for all energies. However, when the target is the shallow active marrow, the SAF is now highest for the TBS, as this source would cause more dose implications to the voxels directly adjacent. If this is the true location of radiosensitive cells, dose would be incorrectly assessed if averaging over the entire marrow cavity.

The ϕ(TAM←TBS) followed the same trend as an active marrow source, but was slightly lower in value, shown in Figure 3-20. This is because there would be less energy deposited in

the active marrow for a particle starting in the trabecular bone surface than there would be for actually starting in the active marrow. The ϕ(TAM←TIM) slightly increases with increasing energy and levels off to the same value as active marrow and trabecular bone surface values. A particle would need to have enough energy to leave the inactive marrow in order to deposit energy into the active marrow regions. The ϕ(TAM←TBV) is the second lowest value and follows the same trend as an inactive marrow source. The lowest SAF is found for a cortical bone volume source where the ϕ(TAM←CBV) increases with increasing energy and then decreases at very high energies. This is because a particle needs to have a significant amount of energy to leave the cortical bone volume and deposit energy into the active marrow. At very high energies, the particle leaves the active marrow to deposit dose elsewhere.

The SAF for all sources to a TAM_{50} target follows the same trends with differences only in values (Figure 3-21). For a TAM_{50} target, the highest SAF is for a TBS source at all energies or a TBV source at intermediate energies. This is because this is closest in proximity to the TAM_{50} since, by definition, this region is 50 microns from the surface of all trabecular bone regions. The SAF is also large for the TAM source, and this is expected as well. SAF for either a TIM or CBV is very low for the shallow active marrow, as most particles cannot escape the adipose tissue or cortical bone to deposit energy into the bone trabeculae which are well within marrow cavities.

SAF for all bone sites containing active marrow

Appendix C lists the SAF data comparing all source-target combinations for all bone sites containing active marrow independently. Figures 3-22 and 3-23 graph the ϕ(TAM←TAM) and ϕ(TAM← TAM_{50}) for all bone sites, respectively. The TAM_{50} target followed the same trends as the TAM target. At low energies, the ϕ(TAM←TAM) was highest for those bone sites with

small marrow cavities (e.g. mandible, cervical vertebrae, sternum, cranium). At higher energies, the same trend was followed except for the mandible. The ϕ(TAM←TAM) is decreasing over energy because at higher energies more particles leave the marrow regions. The bone site with the lowest ϕ(TAM←TAM) was the os coxae, where there is a large amount of active marrow and large cavities.

The ϕ(TAM←TAM_{50}) was also high for bone sites with low marrow volume fractions and more bone volume fractions (e.g. mandible, cranium, cervical vertebrae, scapulae) at low energies. The same trend was followed except for the cranium, which does not decrease as much as other bone sites at high energies. The ϕ(TAM←TAM_{50}) is decreasing over energy because at higher energies more particles leave the shallow marrow regions. Again, the bone site with the lowest ϕ(TAM←TAM) was the os coxae, where there is a large amount of active marrow and large cavities.

SAF for all bone sites not containing active marrow

SAF tables and graphs for all source-target combinations in the shafts of long bones are given in Appendix D. The SAF for the CIM irradiating the CIM_{50}, CBS_{MC}, and CBV for all skeletal sites, are given in Figures 3-24 through 3-26, respectively. As expected, ϕ(CIM_{50}←CIM) decreases with energy, as particles can escape the shallow inactive marrow, as shown in Figure 3-24. This seems to become more drastic after 1MeV. The long bones of the arms (radius, ulna) have the largest SAF, with the smallest being the humerus and femur. This seems plausible since these bone sites are larger and contain more marrow space to absorb particles, with less being deposited in the shallow regions. The ϕ(CBS_{MC}←CIM) also decreases with energy, and is shown in Figure 3-25. As particles gain energy they can escape the cortical

bone surface and deposit energy into the shallow cortical marrow. For this case the ulna and radius also had the largest SAF, with the smallest again being the humerus and femur.

Figure 3-26 plots ϕ(CBV←CIM), which decreases with energy drastically from 0.1 MeV to 1 MeV and then tapers off until 10 MeV. Due to the low count of particles escaping the cortical bone volume, good statistics are not as realizable for this source. Again the long bones of the arms had the largest SAF (radius, ulna), with the humerus and femur having the lowest SAF. SAF from sources emitting from the bone surfaces provide less radiation dose to the shallow cortical marrow than would a source starting within the cortical inactive marrow itself. This is due to the high density of the cortical bone which is difficult for particles to traverse, and those that do will be significantly reduced in energy.

Skeletal Averaged Absorbed Fractions (AF)

Current models for marrow dose estimates do not provide specific absorbed fractions by bone site, and instead use one value that is averaged over all skeletal sites. These include models used in MIRDOSE 3.0 (Eckerman & Stabin 1994) and OLINDA 1.0 (Stabin and Siegel 2003). Furthermore, these models do not use Paired Image Radiation Transport to take advantage of true trabecular microstructure, nor do the tissue masses come from the same patient anatomy. To provide a fair comparison, absorbed fractions for each bone site have been averaged over the entire skeleton. To facilitate this, UFRF bone site weighting factors (Table 3-12 and 3-13) were used, along with ICRP reference cellularities (Figure 3-10). Appendix E gives all tables and graphs for skeletal averaged UFRF AFs, as well as comparisons to the Stabin and Siegel models (2003).

The skeletal averaged SAF for UFRF compared to Stabin and Siegel (SS) for a marrow source irradiating the total active marrow and for bone sources irradiating the total active marrow

are shown in Figures 3-27 and 3-28, respectively. Under current ICRP assumptions, the total active marrow is the surrogate tissue for the hematopoietic stem cell (HSC) population, so this will be the estimated dose to that radiosensitive population. When the marrow itself is a source, the UFRF model matches well with the SS model at energies less than 1 MeV. However, beyond this point, SS converges to 0.431, whereas AF continues to decrease until 0.103 for UFRF. This discrepancy has been noted to be due to energy independent modeling approaches in the SS model (Shah *et al.*, 2005a). Also shown in Figure 3-27 is the AF for a TIM source, which is not provided in the SS models. Here it is noted that the decrease in AF for the TAM source follows the TIM source past 1 MeV only in the UFRF model, which is to be expected. Discrepancies in bone source models irradiating the total marrow are shown in Figure 3-28. Both the TBS and TBV sources seem to be a reasonably accurate when comparing UFRF and SS models at low energies. Differences in values are due to tissue definitions, which are described below. The SS model continues to overestimate dose at energies beyond 1 MeV, as explained above. Also shown in Figure 3-28 is the AF to the total marrow from a CBV source for UFRF. This was not provided for comparison in the SS models.

The skeletal averaged SAF for UFRF compared to Stabin and Siegel (SS) for a marrow source irradiating the shallow trabecular marrow and for bone sources irradiating the shallow trabecular marrow are shown in Figures 3-29 and 3-30, respectively. Under current ICRP assumptions, the shallow trabecular marrow is the surrogate tissue for the osteoprogenitor cell (OPC) population, so this will be the estimated dose to that radiosensitive population. It is noted that this region was once termed the endosteum, which was updated from a 10μm region adjacent to bone surfaces in the SS model to a 50μm region adjacent to bone surfaces in the UFRF modeling approach. Figure 3-29 shows marrow sources irradiating the shallow active

marrow for the UFRF and SS model. In this case, differences are noted at low energies, whereby the UFRF has a higher fraction of energy being deposited in the shallow active marrow. This is due to the updated definition of the endosteum, with a higher volume encompassing a higher AF. The same divergence at high energies is again prevalent, as discussed previously. Again, a TIM source for the UFRF is provided. Bone trabeculae sources irradiating the shallow active marrow are shown in Figure 3-30. Here, similar results are found between UFRF and SS modeling approaches for both the TBS and TBV sources as described above. Differences at low energies are explained by the updated tissue definitions that confirm the OPC population. The SS model has a much higher value of AF for a CBV source when compared to the UFRF model.

Discrepancies between the SAFs include differences in modeling approach (voxel based versus chord based), imaging technique (3D MicroCT versus 2D optical scanning), and gender differences in macrostructure and microstructure (64y female versus 44y male). Perhaps one of the main differences is the tissue region definition used for both trabecular active marrow and shallow trabecular active marrow as described in Shah et al (2003). This also lends to differences in fractional mass weighting factors used in the determination of skeletal averaged AFs.

Effect of Update in Shallow Active Marrow Size

This reference female model is the first to use the newly proposed definition of the endosteum (50 μm from 10 μm), which leads to a larger volume of shallow trabecular active marrow. This should cause a greater number of particles depositing dose into the $TAM_{50,}$ when compared to previous models. However, the mass of the target will be larger, as there are more voxels, thus the dose implications may be spread out for a similar SAF. It was shown that for bone sources irradiating the shallow active marrow, the updated definition of the endosteum

allows for a much higher dose to the OPC population. Due to these discrepancies, the new definition of shallow active marrow should be used to predict marrow toxicity, as current models do not provide an accurate measure of dose to the radiosensitive cell population.

Conclusion

A complete skeletal mass database has been given for a reference female model to be used to provide a patient specific scalable model for accurate dose assessment in radiation protection and medical applications. No model for a female subject has previously been given, and this paper serves to provide a companion skeletal reference model to the adult male. The mass database comes from actual macrostructural patient data (ex-vivo CT) as well as accurate trabecular structure (microCT). Specific absorbed fractions are provided using Paired Image Radiation Transport, where the macrostructure and microstructure of the actual, same patient is combined. It is hoped that this model will be used to better assess dose estimates of the female population.

Table 3-1. Ex-vivo CT data for all skeletal sites.

Skeletal Site	Filter	kV	mAs	thick (mm)	FOV (cm)	In-Plane Res (microns)	# slices (z-direction)
Os Coxae	B80	140	250	1	33.2	648.44	241
Cervical Vertebrae	B80	140	250	1	16.5	322.27	128
Thoracic Vertebrae	B80	140	250	1	16.5	322.27	272
Lumbar Vertebrae	B80	140	250	1	16.5	322.27	172
Sacrum	B80	140	250	1	16.5	322.27	128
Upper Right Rib	B80	140	250	1	7.4	144.53	126
Middle Right Rib	B80	140	250	1	10.9	212.89	241
Lower Right Rib	B80	140	250	1	5.6	109.38	158
Upper Left Rib	B80	140	250	1	5	97.66	105
Middle Left Rib	B80	140	250	1	12.4	242.19	251
Lower Left Rib	B80	140	250	1	6	117.19	188
Clavicle Right	B80	140	250	1	5	97.66	163
Clavicle Left	B80	140	250	1	5	97.66	161
Femur Right	B80	140	250	1	9.8	191.41	171
Femur Left	B80	140	250	1	9.8	191.41	187
Humerus Right	B80	140	250	1	5.8	113.28	138
Humerus Left	B80	140	250	1	5.8	113.28	151
Sternum	B80	140	250	1	10.8	210.94	218
Scapula Right	B80	140	250	1	12.6	246.09	207
Scapula Left	B80	140	250	1	12.6	246.09	200
Mandible	B80	140	250	1	17.2	335.94	131
Cranium	B80	140	250	1	21.2	414.06	200

Table 3-2. MicroCT data for the skeletal sites with active marrow.

microCT Data	Voxel Dimensions			Voxel Resolution			Threshold	MVF
	I	J	K	X (cm)	Y (cm)	Z (cm)		(%)
Right Femur Head	722	732	801	0.003	0.003	0.003	160	0.70
Left Femur Head	869	554	752	0.003	0.003	0.003	160	0.72
Right Femur Neck	554	572	744	0.003	0.003	0.003	159	0.87
Left Femur Neck	599	543	621	0.003	0.003	0.003	159	0.87
Left Parietal Bone	492	798	49	0.003	0.003	0.003	165	0.39
Right Parietal Bone	618	869	60	0.003	0.003	0.003	166	0.43
Frontal Bone	873	828	127	0.003	0.003	0.003	165	0.40
Occipital Bone	643	512	63	0.003	0.003	0.003	169	0.11
Mandible	1020	137	203	0.003	0.003	0.003	156	0.89
Pelvis Pubis	1114	160	204	0.003	0.003	0.003	160	0.82
Pelvis Ischium	1245	84	354	0.003	0.003	0.003	157	0.92
Pelvis Ilium	797	875	255	0.003	0.003	0.003	158	0.88
C3 Vertebra	365	646	180	0.003	0.003	0.003	158	0.76
C6 Vertebra	233	286	438	0.003	0.003	0.003	158	0.81
T3 Vertebra	388	335	585	0.003	0.003	0.003	158	0.87
T6 Vertebra	455	374	658	0.003	0.003	0.003	161	0.92
T11 Vertebra	438	512	614	0.003	0.003	0.003	158	0.91
L1 Vertebra	643	357	662	0.003	0.003	0.003	158	0.90
L2 Vertebra	629	415	617	0.003	0.003	0.003	158	0.90
L3 Vertebra	652	367	628	0.003	0.003	0.003	159	0.90
L4 Vertebra	722	305	870	0.003	0.003	0.003	159	0.92
L5 Vertebra	647	361	746	0.003	0.003	0.003	159	0.91
Sacrum	390	244	126	0.003	0.003	0.003	159	0.96
Sternum	1203	142	651	0.003	0.003	0.003	158	0.99
Left Humerus	748	702	531	0.003	0.003	0.003	157	0.95
Right Humerus	*	*	*	*	*	*	*	*
Right Scapula	748	91	238	0.003	0.003	0.003	160	0.87
Left Scapula	655	188	217	0.003	0.003	0.003	164	0.68
Right Clavicle	630	273	343	0.003	0.003	0.003	155	0.96
Left Clavicle	968	156	264	0.003	0.003	0.003	158	0.96
Upper Right Rib	626	69	190	0.003	0.003	0.003	157	0.94
Middle Right Rib	1326	81	173	0.003	0.003	0.003	157	0.93
Lower Right Rib	771	37	181	0.003	0.003	0.003	160	0.85
Upper Left Rib	586	53	311	0.003	0.003	0.003	157	0.94
Middle Left Rib	1344	76	178	0.003	0.003	0.003	157	0.95
Lower Left Rib	875	37	175	0.003	0.003	0.003	164	0.81

Table 3-3. Tissue compositions (% by mass) and mass densities used in skeletal mass calculations.

Tissue	H	C	N	O	Trace	Mass Density
Red Bone Marrow (RBM)	10.5	41.4	3.4	43.9	0.1 P, 0.2 S, 0.2 Cl, 0.2 K, 0.1 Fe	1.03
Yellow Bone Marrow (YBM)	11.5	64.4	0.7	23.1	0.1 Na, 0.1 S, 0.1 Cl	0.98
Trabecular Bone Endosteum (TBE)	10.5	25.6	2.7	60.2	0.1 Na, 0.2 P, 0.3 S, 0.2 Cl, 0.2 K	1.03
Trabecular Bone Volume (TBV)	3.4	15.5	4.2	43.5	0.1 Na, 0.2 Mg, 10.3 P, 0.3 S, 22.5 Ca	1.92
Cortical Bone Volume (CBV)	3.4	15.5	4.2	43.5	0.1 Na, 0.2 Mg, 10.3 P, 0.3 S, 22.5 Ca	1.92
Surrounding tissues	10.5	25.6	2.7	60.2	0.1 Na, 0.2 P, 0.3 S, 0.2 Cl, 0.2 K	1.03

Table 3-4. Percentage of spongiosa of reference female compared to a database of 20 cadavers.

Skeletal Site	**Spongiosa Volume Percentages**			
with active marrow	**Ref Woman**	**Avg Either Sex**	**Avg Male**	**Avg Female**
Os Coxae	26.56%	22.69%	23.08%	22.12%
Cervical Vertebrae	2.06%	2.45%	2.42%	2.51%
Thoracic Vertebrae	11.17%	11.94%	11.98%	11.88%
Lumbar Vertebrae	9.87%	10.14%	10.41%	9.75%
Sacrum	5.42%	7.36%	6.77%	8.24%
Clavicles	1.69%	1.56%	1.68%	1.39%
Right	0.89%	0.78%	0.84%	0.69%
Left	0.80%	0.78%	0.84%	0.69%
Femora, proximal	13.36%	12.85%	13.04%	12.58%
Right	6.88%	6.43%	6.52%	6.29%
Left	6.48%	6.43%	6.52%	6.29%
Humeri, proximal	6.03%	5.50%	5.77%	5.12%
Right	3.02%	2.75%	2.89%	2.56%
Left	3.02%	2.75%	2.89%	2.56%
Scapulae	3.70%	4.06%	4.52%	3.39%
Right	1.86%	2.03%	2.26%	1.69%
Left	1.84%	2.03%	2.26%	1.69%
Sternum	1.99%	2.12%	2.21%	1.99%
Mandible	1.00%	0.98%	0.91%	1.08%
Ribs	8.37%	9.55%	10.21%	8.58%
Cranium	8.64%	8.79%	7.00%	11.38%
	99.88%	100.00%	100.00%	100.00%

Table 3-5. Spongiosa volume and percentage of total for UF reference male and female.

Skeletal Site (w/active marrow)	Spongiosa Volume		Percent of Total	
	Female	Male	Female	Male
Os Coxae	407.65	558.40	21.81%	23.08%
Cervical Vertebrae	31.67	57.30	1.69%	2.37%
Thoracic Vertebrae	171.51	292.10	9.18%	12.07%
Lumbar Vertebrae	151.47	237.30	8.10%	9.81%
Sacrum	83.25	159.50	4.45%	6.59%
Clavicles	25.94	25.90	1.39%	1.07%
Right	13.63	*	0.73%	*
Left	12.32	*	0.66%	*
Femora, proximal	205.05	430.80	10.97%	17.81%
Right	105.55	*	5.65%	*
Left	99.50	*	5.32%	*
Humeri, proximal	92.60	173.10	4.96%	7.16%
Left	46.30	*	2.48%	*
Scapulae	56.73	115.30	3.04%	4.77%
Right	28.48	*	1.52%	*
Left	28.25	*	1.51%	*
Sternum	30.59	33.90	1.64%	1.40%
Mandible	15.42	17.90	0.83%	0.74%
Ribs	128.44	194.40	6.87%	8.04%
Cranium	132.63	117.50	7.10%	4.86%
Facial bones	1.86	5.80	0.10%	0.24%
Total	1868.83	2419.20	100.00%	100.00%

Table 3-6. Averaged marrow volume fractions, bone volume fractions and shallow marrow volume fractions by skeletal site for UFRF.

	Trabecular Spongiosa Regions		
Skeletal Sites	***Bone Volume Fraction*** *(BVF)*	***Marrow Volume Fraction*** *(MVF)*	***Shallow Marrow Volume Fraction*** *(SMVF)*
Cranium			
Frontal	0.602	0.398	0.138
Occipital	0.893	0.107	0.081
Right Parietal	0.572	0.428	0.157
Left Parietal	0.605	0.395	0.172
Mandible	0.111	0.889	0.622
Scapulae			
Right	0.127	0.873	0.064
Left	0.324	0.676	0.107
Clavicles			
Right	0.038	0.962	0.023
Left	0.043	0.957	0.024
Sternum	0.012	0.988	0.010
Ribs			
Upper Right	0.056	0.944	0.037
Middle Right	0.067	0.933	0.042
Lower Right	0.151	0.849	0.075
Upper Left	0.058	0.942	0.027
Middle Left	0.045	0.955	0.033
Lower Left	0.190	0.810	0.079
Cervical Vertebra			
C3	0.245	0.755	0.096
C6	0.189	0.811	0.098
Thoracic Vertebra			
T3	0.129	0.871	0.074
T6	0.083	0.917	0.052
T11	0.085	0.915	0.052
Lumbar Vertebra			
L2	0.100	0.900	0.056
L4	0.084	0.916	0.049
Sacrum	0.035	0.965	0.022
Os Coxae			
Ilium	0.116	0.884	0.058
Ischium	0.081	0.919	0.054
Pubis	0.180	0.820	0.059
Humeri, proximal			
Right	0.049	0.951	0.030
Left			
Femora, proximal			
Right Head	0.295	0.705	0.110
Right Neck	0.133	0.867	0.068
Left Head	0.279	0.721	0.107
Left Neck	0.132	0.868	0.070

Table 3-7. University of Florida Reference Female masses for the trabecular spongiosa, cortical bone, and mineral bone regions for all skeletal sites.

	Trabecular Spongiosa Regions			*Cortical Bone Regions*		
Skeletal Sites	**Spongiosa**[a] *Volume (cm^3)*	**BVF**[b] *(% of SV)*	**Trabecular Bone**[c] *Mass (g)*	**Cortical Bone**[a] *Volume (cm^3)*	**Cortical Bone**[c] *Mass (g)*	**Total Mineral Bone** *Mass (g)*
Cranium[a]	132.6	63.8%	162.3	262.4	503.8	666.2
Facial Bones[d,e]	1.9	11.1%	0.4	24.9	47.8	48.2
Mandible	15.4	11.1%	3.3	22.1	42.4	45.7
Scapulae	56.7	22.6%	24.6	55.1	105.7	130.3
Clavicles	25.9	4.1%	2.0	20.0	38.3	40.4
Sternum	30.6	1.2%	0.7	16.2	31.2	31.9
Ribs[e]	128.4	9.5%	23.3	180.8	347.2	370.5
Cervical Vertebra	31.7	21.7%	13.2	34.1	65.5	78.7
Thoracic Vertebra	171.5	9.9%	32.6	79.7	153.1	185.7
Lumbar Vertebra	151.5	9.2%	26.8	68.0	130.6	157.3
Sacrum	83.2	3.5%	5.6	40.8	78.4	84.0
Os Coxae	407.6	11.5%	90.3	213.0	408.9	499.3
Humeri, proximal	92.6	4.9%	8.7	20.6	39.6	48.3
Femora, proximal	205.1	19.4%	76.5	66.7	128.0	204.5
Totals:	*1534.8* [f]		*470.3*	*1104.4*	*2120.5*	*2590.8*
	Spongiosa[e]	**BVF**[g]	**Trabecular Bone**[c]	**Cortical Bone**[e]	**Cortical Bone**[c]	**Total Mineral Bone**
	Volume (cm^3)	*(% of SV)*	*Mass (g)*	*Volume (cm^3)*	*Mass (g)*	*Mass (g)*
Humeri, shaft				91.5	175.6	175.6
Humeri, distal	53.64	4.9%	5.0	54.8	105.3	110.3
Ulnae, proximal	20.92	4.9%	2.0	25.3	48.6	50.6
Ulnae, shaft				40.6	77.9	77.9
Ulnae, distal	5.9	4.9%	0.6	10.6	20.4	20.9
Radii, proximal	16.84	4.9%	1.6	18.6	35.7	37.3
Radii, shaft				41.7	80.1	80.1
Radii, distal	29.74	4.9%	2.8	28.1	53.9	56.7
Hands	*	4.9%	*	*	*	*
Femora, shaft				280.2	538.0	538.0
Femora, distal	596.18	19.4%	222.4	228.3	438.4	660.8
Tibiae, proximal	477.24	19.4%	178.0	197.6	379.4	557.4
Tibiae, shaft				112.7	216.5	216.5
Tibiae, distal	173.28	19.4%	64.6	109.8	210.8	275.4
Fibulae, proximal	29.5	19.4%	11.0	16.0	30.7	41.7
Fibulae, shaft				74.6	143.2	143.2
Fibulae, distal	26.68	19.4%	10.0	24.9	47.9	57.8
Feet	*	19.4%	*	*	*	*
Totals:	*1430.0*		*498.0*	*1355.4*	*2602.4*	*3100.4*
Totals for UFRF Model:	*2964.8*		**968**		**4723**	**5691**
% mineral bone			*17%*		*83%*	
Totals for UFRM Model:	*3874.0*		1267		4388	5656
% mineral bone			22%		78%	
ICRP 89 Ref Male:			**1100**		**4400**	**5500**
% mineral bone			*20%*		*80%*	
Ratio (UFRF / ICRP):			**0.88**		**1.07**	**1.03**
Ratio (UFRM / ICRP):			1.15		1.00	1.03

[a] *Indicates values determined from ex-vivo CT segmentation (PIRT macroimage)*
[b] *Indicates values determined from image processing of microCT data (PIRT microimage)*
[c] *Mass density of 1.92 g cm^{-3} is assumed for both cortical bone and bone trabeculae as given in ICRU Report 46.*
[d] *Facial bones - maxilla, nasal, zygomatic, lacrimal, palatine, vomer. Volume fractions taken from mandible*
[e] *Indicates values determined from in-vivo CT segmentation (whole-body cadaver images)*
[f] *Corresponding to TSSV (total skeletal spongiosa volume) as defined in Brindle et al. (2006).*
[g] *Volume fractions taken as those of the proximal humerii for arm bones and proximal femora for leg bones.*

Table 3-8. University of Florida Reference Female active marrow masses.

	UF Reference Model (64-Year Female)							ICRP Ref Male
Skeletal Sites	**Spongiosa**[a] *Volume (cm^3)*	**MVF**[b] *(% of SV)*	**Total Marrow** *Volume (cm^3)*	**Marrow Cellularity**[c] *(% of MV)*	**Inactive Marrow**[d] *Mass (g)*	**Active Marrow**[d] *Mass (g)*	**Active Marrow** *% of total*	**Active Marrow** *% of total*
Cranium	132.6	36.2%	48.1	38%	29.2	18.8	2.7%	7.6%
Facial Bones[a]	1.9	88.9%	1.7	38%	1.0	0.6	0.1%	
Mandible	15.4	88.9%	13.7	38%	8.3	5.4	0.8%	0.8%
Scapulae	56.7	77.5%	43.9	38%	26.7	17.2	2.5%	2.8%
Clavicles	25.9	96.0%	24.9	33%	16.3	8.5	1.2%	0.8%
Sternum	30.6	98.8%	30.2	70%	8.9	21.8	3.2%	3.1%
Ribs[a]	128.4	90.6%	116.3	70%	34.2	83.8	12.2%	16.1%
Cervical Vertebra	31.7	78.3%	24.8	70%	7.3	17.9	2.6%	3.9%
Thoracic Vertebra	171.5	90.1%	154.5	70%	45.4	111.4	16.2%	16.1%
Lumbar Vertebra	151.5	90.8%	137.5	70%	40.4	99.2	14.5%	12.3%
Sacrum	83.2	96.5%	80.3	70%	23.6	57.9	8.4%	9.9%
Os Coxae	407.6	88.5%	360.6	48%	183.8	178.3	26.0%	17.5%
Humeri, proximal	92.6	95.1%	88.1	25%	64.7	22.7	3.3%	2.3%
Femora, proximal	205.1	80.6%	165.2	25%	121.4	42.5	6.2%	6.7%
Totals:	*1534.8*[f]		*1289.8*		*611.4*	*686.0*	*100.0%*	*99.9%*
	Spongiosa[e] *Volume (cm^3)*	**MVF**[g] *(% of SV)*	**Total Marrow** *Volume (cm^3)*	**Marrow Cellularity**[c] *(% of MV)*	**Inactive Marrow**[d] *Mass (g)*	**Active Marrow**[d] *Mass (g)*	**Active Marrow** *% of total*	
Humeri, shaft (upper 1/2)			26.73	0%	26.2	0	0%	
Humeri, shaft (lower 1/2)			26.73	0%	26.2	0	0%	
Humeri, distal	53.6	95.1%	51.0	0%	50.0	0	0%	
Ulnae, proximal	20.9	95.1%	19.9	0%	19.5	0	0%	
Ulnae, shaft			11.7	0%	11.5	0	0%	
Ulnae, distal	5.9	95.1%	5.6	0%	5.5	0	0%	
Radii, proximal	16.8	95.1%	16.0	0%	15.7	0	0%	
Radii, shaft			8.0	0%	7.8	0	0%	
Radii, distal	29.7	95.1%	28.3	0%	27.7	0	0%	
Hands	*	95.1%	*	0%	*	*	*	
Femora, shaft (upper 1/2)			42.8	0%	42.0	0	0%	
Femora, shaft (lower 1/2)			42.8	0%	42.0	0	0%	
Femora, distal	596.2	80.6%	480.3	0%	470.7	0	0%	
Tibiae, proximal	477.2	80.6%	384.5	0%	376.8	0	0%	
Tibiae, shaft			36.62	0%	35.9	0	0%	
Tibiae, distal	173.3	80.6%	139.6	0%	136.8	0	0%	
Fibulae, proximal	29.5	80.6%	23.8	0%	23.3	0	0%	
Fibulae, shaft			34.1	0%	33.4	0	0%	
Fibulae, distal	26.7	80.6%	21.5	0%	21.1	0	0%	
Feet	*	80.6%	*	0%	*	*	*	**Total Marrow**
Totals:	*1430.0*		*1400.2*		*1372.2*	*0.0*	*0.0%*	*Mass (g)*
Totals for UFRF Model:	**2964.8**		**2690.0**		**1,984**	**686**		**2,670**
% total marrow					*74%*	*26%*		
Totals for UFRM Model:	3874.0		3487.6		2,406	1,063		3,469
% total marrow					*69%*	*31%*		
ICRP 89 Ref Male:					**2,480**	**1,170**		**3,650**
% total marrow					*68%*	*32%*		
Ratio (UFRF / ICRP):					**0.80**	**0.59**		**0.73**
Ratio (UFRM / ICRP):					0.97	0.91		0.95

[a] *Indicates values determined from ex-vivo CT segmentation (PIRT macroimage)*
[b] *Indicates values determined from image processing of microCT data (PIRT microimage)*
[c] *Marrow cellularity given in ICRP Publication 70 for the 40-year adult*
[d] *Mass density of 0.98 and 1.03 g cm^{-3} is assumed for inactive (yellow) and active (red) bone marrow, respectively, as given in ICRU Report 46.*
[e] *Indicates values determined from in-vivo CT segmentation (whole-body cadaver images)*
[f] *Corresponding to TSSV (total skeletal spongiosa volume) as defined in Brindle et al. (2006).*
[g] *Volume fractions taken as those of the proximal humerii for arm bones and proximal femora for leg bones.*

Table 3-9. Shallow marrow masses for UFRF.

Skeletal Sites	Spongiosa Volume (cm^3)	Shallow Marrow SMVF (% of SV)	Shallow Marrow (% of MV)	Shallow Marrow Volume (cm^3)	Marrow Cellularity (% of MV)	Shallow Inactive Marrow Mass (g)	Shallow Active Marrow Mass (g)	Shallow Total Marrow Mass (g)
Cranium	132.6	14.5%	40.1%	19.3	38%	11.7	7.5	19.3
Facial Bones	1.9	62.2%	70.0%	1.2	38%	0.7	0.5	1.2
Mandible	15.4	62.2%	70.0%	9.6	38%	5.8	3.8	9.6
Scapulae	56.7	8.6%	11.0%	4.9	38%	2.9	1.9	4.8
Clavicles	25.9	2.4%	2.4%	0.6	33%	0.4	0.2	0.6
Sternum	30.6	1.0%	1.0%	0.3	70%	0.1	0.2	0.3
Ribs	128.4	4.9%	5.4%	6.3	70%	1.8	4.5	6.4
Cervical Vertebra	31.7	9.7%	12.4%	3.1	70%	0.9	2.2	3.1
Thoracic Vertebra	171.5	5.9%	6.6%	10.2	70%	3.0	7.3	10.3
Lumbar Vertebra	151.5	5.3%	5.8%	8.0	70%	2.3	5.7	8.1
Sacrum	83.2	2.2%	2.3%	1.8	70%	0.5	1.3	1.9
Os Coxae	407.6	5.7%	6.5%	23.4	48%	11.9	11.5	23.5
Humeri, proximal	92.6	3.0%	3.2%	2.8	25%	2.0	0.7	2.8
Femora, proximal	205.1	8.5%	10.5%	17.4	25%	12.8	4.5	17.3
Totals:	*1534.8*	9.2%		*108.6*		*57.0*	*51.9*	*109.0*
Humeri, Distal	53.64	3.2%	3.3%	1.7	0%	1.7	0.0	1.7
Ulnae, proximal	20.92	3.2%	3.3%	0.7	0%	0.6	0.0	0.6
Ulnae, Distal	5.94	3.2%	3.3%	0.2	0%	0.2	0.0	0.2
Radii, proximal	16.84	3.2%	3.3%	0.5	0%	0.5	0.0	0.5
Radii, Distal	29.74	3.2%	3.3%	0.9	0%	0.9	0.0	0.9
Hands	*	3.2%	0.0%	*	0%	*	0.0	*
Femora, Distal	596.18	10.5%	13.1%	62.7	0%	61.5	0.0	61.5
Tibiae, proximal	477.24	10.5%	13.1%	50.2	0%	49.2	0.0	49.2
Tibiae, Distal	173.28	10.5%	13.1%	18.2	0%	17.9	0.0	17.9
Fibulae, proximal	29.5	10.5%	13.1%	3.1	0%	3.0	0.0	3.0
Fibulae, Distal	26.68	10.5%	13.1%	2.8	0%	2.8	0.0	2.8
Feet	*	10.5%	0.0%	*	0%	*	0.0	*
Totals:	*1430.0*			*141.1*		*138.3*	*0.0*	*138.3*
	Shaft Marrow Volume (cm^3)	**Shaft Length** (cm)						
Humeri, shaft (upper 1/2)	26.7	6	1.2%	0.3	0%	0.3	0.0	0.3
Humeri, shaft (lower 1/2)	26.7	6	1.2%	0.3	0%	0.3	0.0	0.3
Ulnae, shaft	11.7	13	2.6%	0.3	0%	0.3	0.0	0.3
Radii, shaft	8.0	10	2.8%	0.2	0%	0.2	0.0	0.2
Femora, shaft (upper 1/2)	42.8	8	1.1%	0.5	0%	0.4	0.0	0.4
Femora, shaft (lower 1/2)	42.8	8	1.1%	0.5	0%	0.4	0.0	0.4
Tibiae, shaft	36.6	9	1.3%	0.5	0%	0.5	0.0	0.5
Fibulae, shaft	34.1	23	2.0%	0.7	0%	0.7	0.0	0.7
Totals:	*229.6*			*3.2*		*3.2*	-	*3.2*
Totals for UFRF Model:						**199**	**52**	**250.5**
% total shallow marrow						*79%*	*21%*	
Totals for UFRM Model:						226	100	326.3
% total shallow marrow						*69%*	*31%*	

Table 3-10. S/V Ratios.

Skeletal Sites	S/V Ratio (mm^2 / mm^3) *(UFRF - Present Study)*	S/V Ratio (mm^2 / mm^3) *(UFRM)*	S/V Ratio (mm^2 / mm^3) *Beddoe et al. (1976) (44y M)*	S/V Ratio (mm^2 / mm^3) *Lloyd et al. (1968) (1 Adult)*	S/V Ratio (mm^3 / mm^3) *Lloyd & Hodges (1971) (1 Adult)*	S/V Ratio (mm^2 / mm^3)	ICRP Publication 70 *References*
Cranium	6.9	11.4	7.8		4.1		
Mandible	21.9	12.8					
Ribs	21.9	17.8	18.5	11.5			
Sternum	39.0	23.9					
Cervical Vertebra	17.0	24.5		11.5			
Thoracic Vertebra	23.6	22.7			12.0		
Lumbar Vertebra	22.1	21.7	19.7	11.4	12.0	14.6	*Amstutz & Sission (1969) (1 adult)*
						23.0	*Arnold & Wei (1972) (39-50y)*
						23.9	*Beddoe et al. (1976) (39-55y)*
						14.0	*Bromley et al. (1966) (30-60y)*
						21.0	*Dyson et al. (1970) (1 adult)*
Sacrum	26.8	24.2					
Os Coxae	20.3	21.8	17.2		18.0	17.4	*Merk & Schenk (1970) (30-60y)*
						20.2	*Shulz & Delling (1976) (31-40y)*
						21.4	*Shulz & Delling (1976) (41-50y)*
						18.6	*Shulz & Delling (1976) (51-60y)*
						21.6	*Shulz & Delling (1976) (61-70y)*
Femora, proximal			17.3	9.5	10.0		
Right	16.6	16.0					
Left	17.4	17.0					
Humeri, proximal							
Right		18.3					
Left	24.6	17.0					
Clavicles							
Right	27.2	13.4					
Left	23.3	20.6					
Scapulae							
Right	19.5	13.8					
Left	11.2	18.2					
Mean ± 1 SD	21.2 ± 7.2	18.5 ± 4.2	16.1 ± 4.8	11.0 ± 1.0	11.2 ± 5.0	19.3 ± 4.7	Lumbar Vertebrae
						19.8 ± 1.8	Os Coxae (Illiac Crest)
ICRP Publication 70	18.0						

Table 3-11. Surface Areas for UFRF in both trabecular and cortical bone regions.

	Trabecular Spongiosa Regions					*Cortical Bone Regions - Harversian Canals*			*Cortical Bone Regions - Medullary Cavities*		
Skeletal Sites	**Spongiosa** *Volume (cm^3)*	**BVF** *(% of SV)*	**Trabecular Bone** *Volume (cm^3)*	**Surface:Volume** *(cm^2/cm^3)*	**Trab Surfaces** *Area (m^2)*	**Cortical Bone** *Volume (cm^3)*	**Surface:Volume** *(cm^2/cm^3)*	**Cortical Surfaces** *Area (m^2)*	**Effective Shaft Radius** *(cm)*	**Shaft Length** *(cm)*	**Cortical Surfaces** *Area (m^2)*
Cranium	132.6	63.8%	84.6	69	0.58	262.4	30	0.79			
Facial Bones	1.9	11.1%	0.2	219	0.00	24.9	30	0.07			
Mandible	15.4	11.1%	1.7	219	0.04	22.1	30	0.07			
Scapulae	56.7	22.6%	12.8	154	0.20	55.1	30	0.17			
Clavicles	25.9	4.1%	1.1	252	0.03	20.0	30	0.06			
Sternum	30.6	1.2%	0.4	390	0.01	16.2	30	0.05			
Ribs	128.4	9.5%	12.1	219	0.27	180.8	30	0.54			
Cervical Vertebra	31.7	21.7%	6.9	170	0.12	34.1	30	0.10			
Thoracic Vertebra	171.5	9.9%	17.0	236	0.40	79.7	30	0.24			
Lumbar Vertebra	151.5	9.2%	13.9	221	0.31	68.0	30	0.20			
Sacrum	83.2	3.5%	2.9	268	0.08	40.8	30	0.12			
Os Coxae	407.6	11.5%	47.0	203	0.95	213.0	30	0.64			
Humeri, proximal	92.6	4.9%	4.5	246	0.11	20.6	30	0.06			
Femora, proximal	205.1	19.4%	39.8	170	0.68	66.7	30	0.20			
Totals:	*1534.8*		*244.9*		*3.8*	*1104.4*		*3.3*			
Humeri, shaft						91.5	30	0.27	0.849	11.8	**0.013**
Humeri, distal	53.64	4.9%	2.6	246	0.06	54.8	30	0.16			
Ulnae, proximal	20.92	4.9%	1.0	246	0.03	25.3	30	0.08			
Ulnae, shaft						40.6	30	0.12	0.379	13.0	**0.006**
Ulnae, distal	5.94	4.9%	0.3	246	0.01	10.6	30	0.03			
Radii, proximal	16.84	4.9%	0.8	246	0.02	18.6	30	0.06			
Radii, shaft						41.7	30	0.13	0.352	10.2	**0.005**
Radii, distal	29.74	4.9%	1.5	246	0.04	28.1	30	0.08			
Hands	*	4.9%	*	246	*	*	30	*			
Femora, shaft						280.2	30	0.84	0.935	15.6	**0.018**
Femora, distal	596.18	19.4%	115.8	170	1.97	228.3	30	0.69			
Tibiae, proximal	477.24	19.4%	92.7	170	1.58	197.6	30	0.59			
Tibiae, shaft						112.7	30	0.34	0.787	9.4	**0.009**
Tibiae, distal	173.28	19.4%	33.7	170	0.57	109.8	30	0.33			
Fibulae, proximal	29.52	19.4%	5.7	170	0.10	16.0	30	0.05			
Fibulae, shaft						74.6	30	0.22	0.488	22.8	**0.014**
Fibulae, distal	26.68	19.4%	5.2	170	0.09	24.9	30	0.07			
Feet	*	19.4%	*	170	*	*	30	*			
Totals:	*1430.0*		*259.4*		*4.46*	*1355.4*		*4.07*			*0.065*
Totals for UFRF Model:	*2965*		*504*		**8.23**	*2460*		**7.38**			**0.06**
% total surface area					*53%*			*47%*			*0.4%*
Totals for UFRM Model:	*3874*		*660*		*11.74*	*2286*		6.86			*0.17*
% total surface area					*63%*			*37%*			*0.9%*
ICRP 89 Ref Male:			*580*		**10.50**	*2130*		**6.50**			
% total surface area					*62%*			38%			
Ratio (UFRF / ICRP):			*0.87*		***0.78***	*1.15*		***1.14***			
Ratio (UFRM / ICRP):			*1.14*		*1.12*	*1.07*		*1.05*			

Table 3-12. Weighting factors for marrow sources for each bone site for UFRF.

Skeletal Sites	Cellularity (% of MV)	$f_{TAM + CAM}$	$f_{TIM + CIM}$	$f_{TAM50 + CAM50}$	$f_{TM50 + CM50}$
Cranium	38%	0.027	0.015	0.157	0.061
Facial Bones	38%	0.001	0.001	0.001	0.000
Mandible	38%	0.008	0.004	0.008	0.003
Scapulae	38%	0.025	0.013	0.039	0.015
Clavicles	33%	0.012	0.008	0.004	0.002
Sternum	70%	0.032	0.004	0.005	0.000
Ribs	70%	0.122	0.017	0.094	0.010
Cervical Vertebra	70%	0.026	0.004	0.046	0.005
Thoracic Vertebra	70%	0.162	0.023	0.152	0.016
Lumbar Vertebra	70%	0.145	0.020	0.119	0.012
Sacrum	70%	0.084	0.012	0.027	0.003
Os Coxae	48%	0.260	0.093	0.240	0.062
Humeri, proximal	25%	0.033	0.033	0.015	0.011
Femora, proximal	25%	0.062	0.061	0.093	0.066
Subtotals:		***1.000***	***0.308***	***1.000***	***0.265***
Humeri, shaft (upper 1/2)	*0%*		0.013		0.002
Humeri, shaft (lower 1/2)	0%		0.013		0.002
Humeri, distal	0%		0.025		0.009
Ulnae, proximal	0%		0.010		0.003
Ulnae, shaft	0%		0.006		0.002
Ulnae, distal	0%		0.003		0.001
Radii, proximal	0%		0.008		0.003
Radii, shaft	0%		0.004		0.001
Radii, distal	0%		0.014		0.005
Hands	0%		*		*
Femora, shaft (upper 1/2)	0%		0.021		0.002
Femora, shaft (lower 1/2)	0%		0.021		0.002
Femora, distal	0%		0.237		0.319
Tibiae, proximal	0%		0.190		0.256
Tibiae, shaft	0%		0.018		0.002
Tibiae, distal	0%		0.069		0.093
Fibulae, proximal	0%		0.012		0.016
Fibulae, shaft	0%		0.017		0.004
Fibulae, distal	0%		0.011		0.014
Feet	0%		*		*
Subtotals:			***0.692***		***0.735***
Totals:		**1.000**	**1.000**	**1.000**	**1.000**

Table 3-13. Weighting factors for bone surface and volume sources for UFRF.

Skeletal Sites	Surface Sources			Volume Sources		
	f_{TBS}	f_{CBS}	$f_{TBS+CBS}$	f_{TBV}	f_{CBV}	$f_{TBV+CBV}$
Cranium	0.071	0.106	0.087	0.168	0.107	0.117
Facial Bones	0.001	0.010	0.005	0.000	0.010	0.008
Mandible	0.005	0.009	0.007	0.003	0.009	0.008
Scapulae	0.024	0.022	0.023	0.025	0.022	0.023
Clavicles	0.003	0.008	0.006	0.002	0.008	0.007
Sternum	0.002	0.007	0.004	0.001	0.007	0.006
Ribs	0.032	0.073	0.052	0.024	0.074	0.065
Cervical Vertebra	0.014	0.014	0.014	0.014	0.014	0.014
Thoracic Vertebra	0.049	0.032	0.041	0.034	0.032	0.033
Lumbar Vertebra	0.037	0.027	0.033	0.028	0.028	0.028
Sacrum	0.009	0.016	0.013	0.006	0.017	0.015
Os Coxae	0.116	0.086	0.102	0.093	0.087	0.088
Humeri, proximal	0.014	0.008	0.011	0.009	0.008	0.008
Femora, proximal	0.082	0.027	0.056	0.079	0.027	0.036
Subtotals:	***0.459***	***0.445***	***0.452***	***0.486***	***0.449***	***0.455***
Humeri, shaft (upper 1/2)		0.019	0.009		0.019	0.015
Humeri, shaft (lower 1/2)		0.019	0.009		0.019	0.015
Humeri, distal	0.008	0.022	0.015	0.005	0.022	0.019
Ulnae, proximal	0.003	0.010	0.006	0.002	0.010	0.009
Ulnae, shaft		0.017	0.008		0.016	0.014
Ulnae, distal	0.001	0.004	0.002	0.001	0.004	0.004
Radii, proximal	0.002	0.007	0.005	0.002	0.008	0.007
Radii, shaft		0.017	0.008		0.017	0.014
Radii, distal	0.004	0.011	0.008	0.003	0.011	0.010
Hands	*	*	0.000	*	*	*
Femora, shaft (upper 1/2)		0.058	0.027		0.057	0.047
Femora, shaft (lower 1/2)		0.058	0.027		0.057	0.047
Femora, distal	0.239	0.092	0.169	0.230	0.093	0.116
Tibiae, proximal	0.191	0.080	0.138	0.184	0.080	0.098
Tibiae, shaft		0.047	0.022	0.000	0.046	0.038
Tibiae, distal	0.070	0.044	0.058	0.067	0.045	0.048
Fibulae, proximal	0.012	0.006	0.009	0.011	0.007	0.007
Fibulae, shaft		0.032	0.015	0.000	0.030	0.025
Fibulae, distal	0.011	0.010	0.010	0.010	0.010	0.010
Feet	*	*	0.000	*	*	*
Subtotals:	***0.541***	***0.555***	***0.548***	***0.514***	***0.551***	***0.545***
Totals:	**1.000**	**1.000**	**1.000**	**1.000**	**1.000**	**1.000**

Figure 3-1. Top in-vivo scan of UF Reference Woman

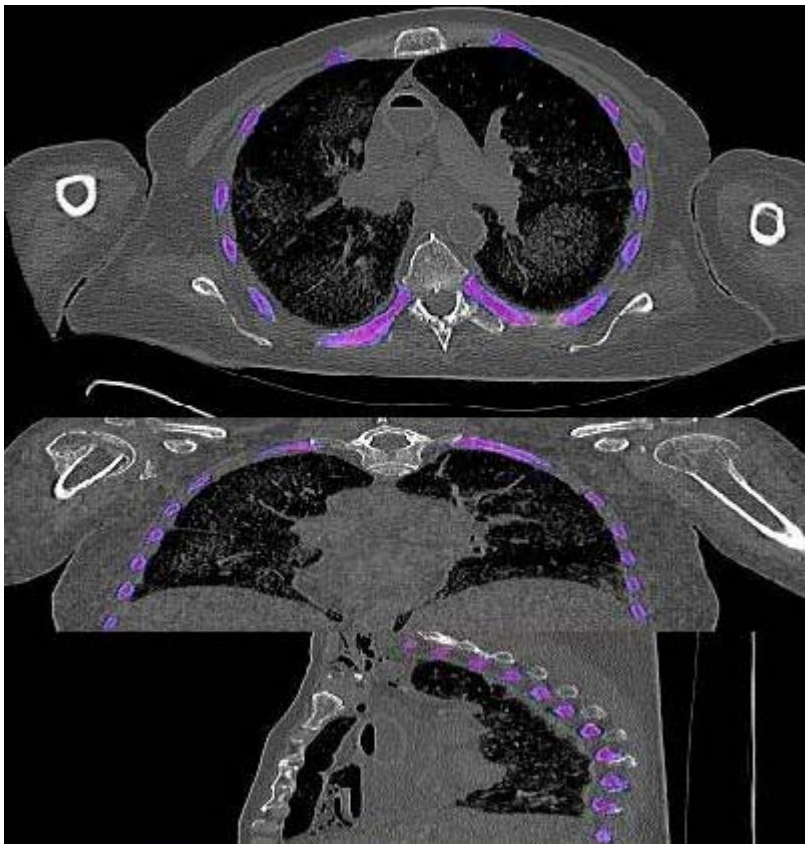

Figure 3-2. In-vivo contoured image of the ribs in transverse (top), coronal (middle) and sagittal (bottom) planes.

Figure 3-3. In-vivo contoured image of the cranium, showing the separation of the lobes: left parietal (orange), right parietal (yellow), occipital (green), facial bones (pink), cortical bone (blue) and other bones (red).

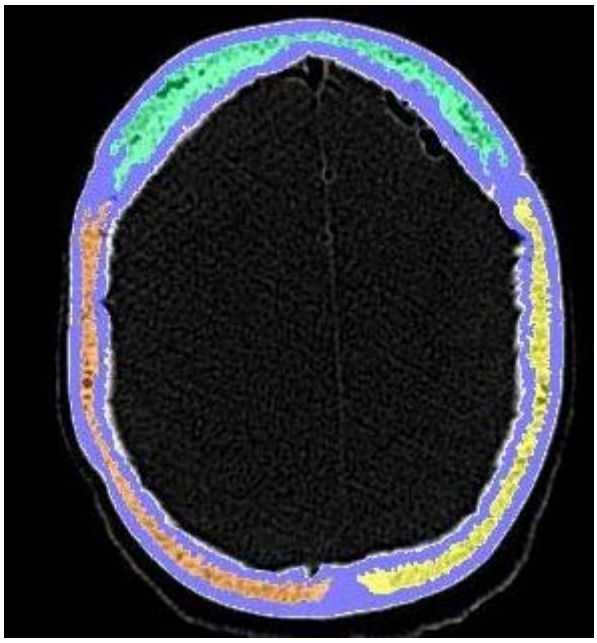

Figure 3-4. In-vivo contoured image of the cranium showing the separated lobes: left parietal (orange), right parietal (yellow), and frontal (green).

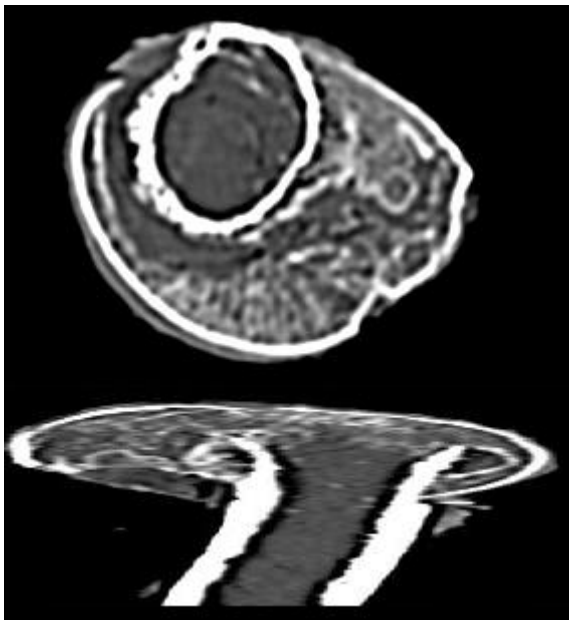

Figure 3-5. Transverse (top) and coronal (bottom) CT images showing the abnormality of the right humerus. The cortical shell of the shaft extends through to the proximal humeral head.

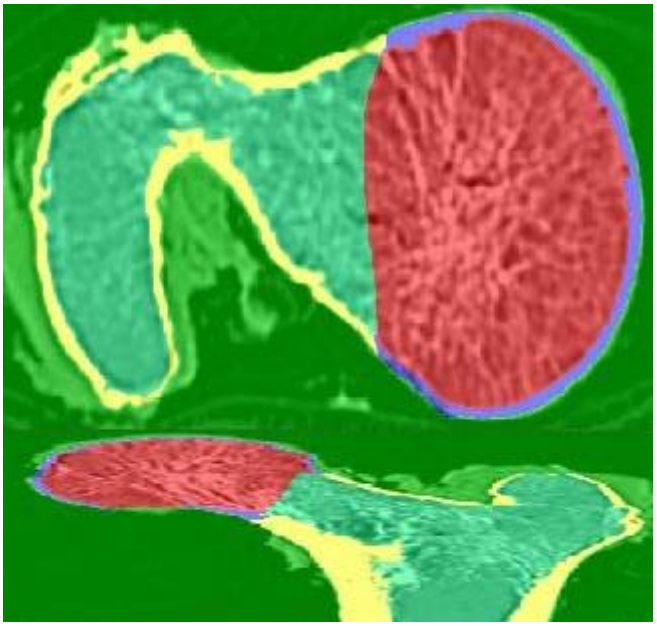

Figure 3-6. Transverse (top) and Coronal (bottom) Contoured ex-vivo image of the femur, showing the separation of the femoral head and neck

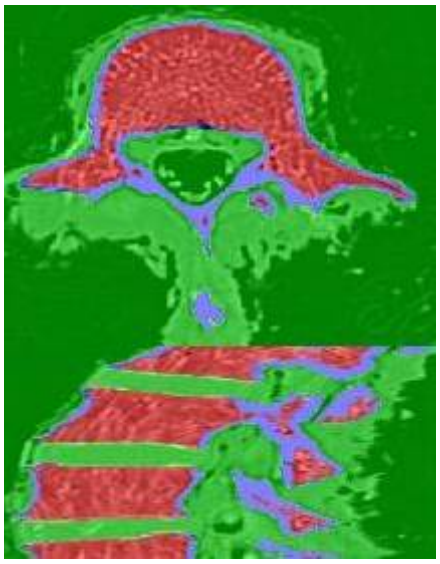

Figure 3-7. Transverse (top) and sagital (bottom) contoured ex-vivo image of the lumbar vertebrae with cortical bone in blue and spongiosa in red.

Bone	Percentage of active marrow at various ages (y)						
	0	1	5	10	15	25	40
Cranium	27.0	25.1	15.9	11.6	9.2	7.7	7.6
Mandible	2.5	2.4	1.6	1.1	0.9	0.8	0.8
Scapulae	2.7	2.7	2.7	2.9	3.3	2.9	2.8
Clavicles	0.8	0.8	0.9	0.9	1.0	0.8	0.8
Sternum	0	0.8	1.7	2.1	2.7	3.0	3.1
Ribs	9.2	8.9	8.8	10.9	13.6	15.2	16.1
Cervical vertebrae	3.4	2.8	2.2	2.7	3.3	3.7	3.9
Thoracic vertebrae	8.3	8.4	8.9	10.9	13.7	15.3	16.1
Lumbar vertebrae	2.4	4.3	6.8	8.4	10.5	11.7	12.3
Sacrum	0.1	2.4	5.5	6.7	8.4	9.4	9.9
Os coxae	9.2	11.1	13.1	15.6	18.5	19.5	17.5
Femora, upper half	3.7	4.1	6.8	9.4	9.2	7.4	6.7
Femora, lower half	3.7	3.9	6.3	6.1	2.0	0	0
Tibiae, fibulae, patellae	8.0	8.7	9.0	5.5	0	0	0
Ankle and foot bones	8.3	4.7	2.5	0	0	0	0
Humeri, upper half	2.3	2.4	2.4	2.5	3.1	2.5	2.3
Humeri, lower half	2.3	2.3	2.2	1.6	0.7	0	0
Ulnae and radii	2.5	2.5	2.0	1.1	0	0	0
Wrist and hand bones	3.6	1.9	0.9	0	0	0	0

From Cristy (1981).

Figure 3-8. Active marrow distribution as a function of age used as reference values in ICRP 70 (Cristy, 1981).

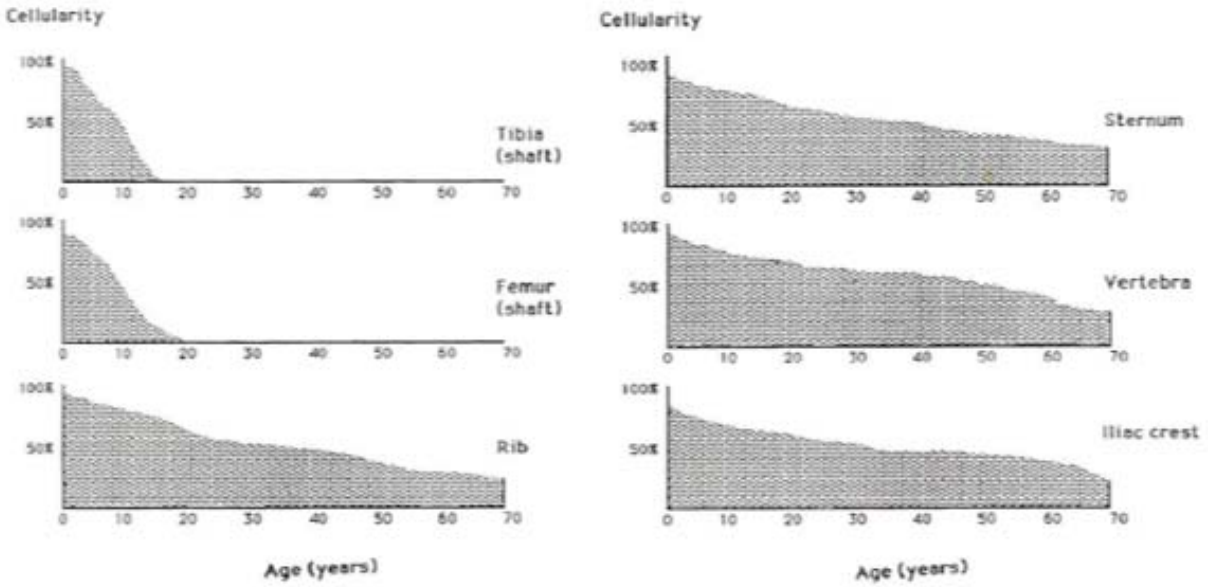

Figure 3-9. Cellularity varies by bone site and decreases with age (Custer, 1974)

Table 41. Age-specific bone marrow cellularity

Bone	Cellularity factor at various ages (y)							Source of cellularity values
	0	1	5	10	15	25	40	
Vertebrae, sternum, ribs	1.00	0.95	0.85	0.80	0.75	0.72	0.70	Age 40 values taken from Hashimoto and Yamada (1964); age patterns based on shapes of cellularity against age curves for vertebrae, sternum and ribs given by Custer (1949, 1974) and for anterior iliac crest given by Hartsock *et al.* (1965)
Skull, scapulae	1.00	0.95	0.80	0.65	0.55	0.42	0.38	
Clavicles	1.00	0.95	0.79	0.63	0.52	0.37	0.33	
Upper half of femora and humeri	1.00	0.95	0.77	0.60	0.45	0.30	0.25	
Lower half of femora and humeri	1.00	0.89	0.71	0.39	0.10	0	0	Femur shaft data of Custer (1974)
Tibiae, fibulae, patellae, ulni, radii	1.00	0.89	0.57	0.23	0	0	0	Tibia shaft data of Custer (1974)
Ankle, foot, wrist, and hand bones	1.00	0.50	0.20	0	0	0	0	Rough estimate, based on information given by Emery and Follett (1964) and Piney (1922)
Os coxae	1.00	0.95	0.79	0.72	0.64	0.58	0.48	Anterior iliac crest data of Hartsock *et al.* (1965)

From Cristy (1981).

Figure 3-10. Current ICRP 70 reference cellularities based on bone site and age (Cristy, 1981).

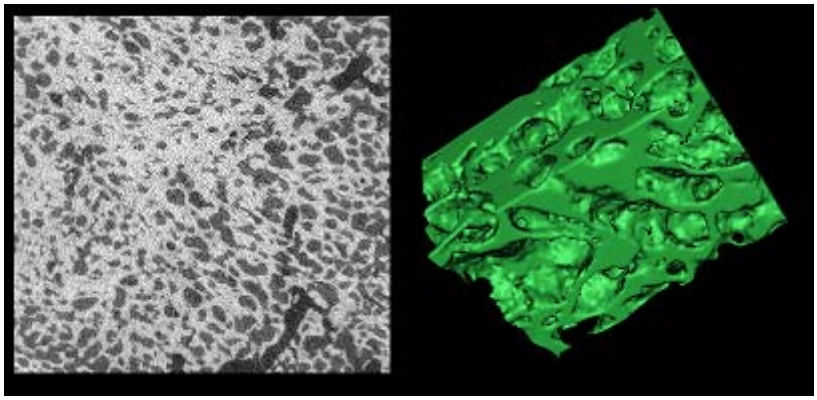

Figure 3-11. Microstructure of the frontal lobe (40% marrow).

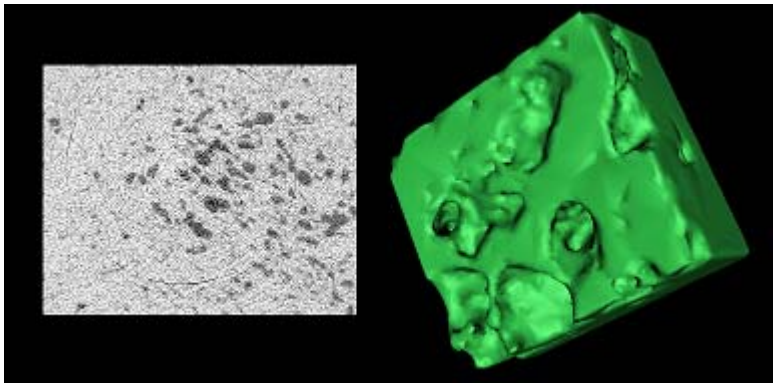

Figure 3-12. Microstructure of the occipital lobe (11% marrow).

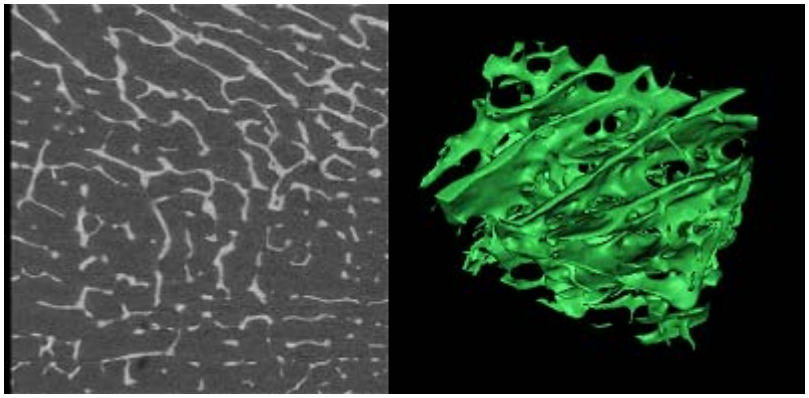

Figure 3-13. Microstructure of the femoral neck (87% marrow).

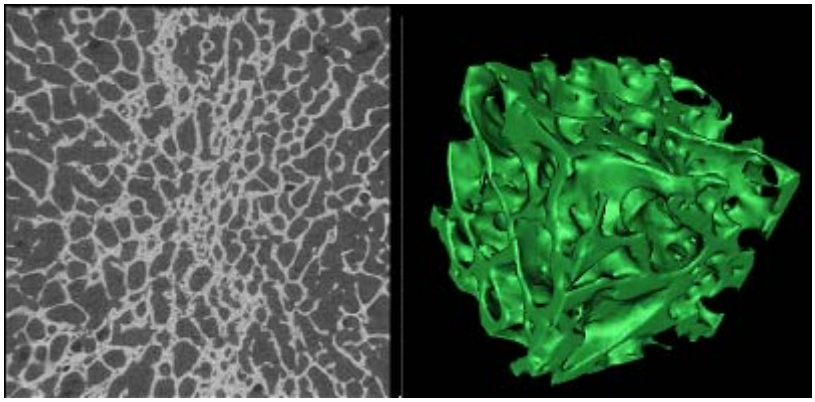

Figure 3-14. Microstructures of the femoral head (71% marrow).

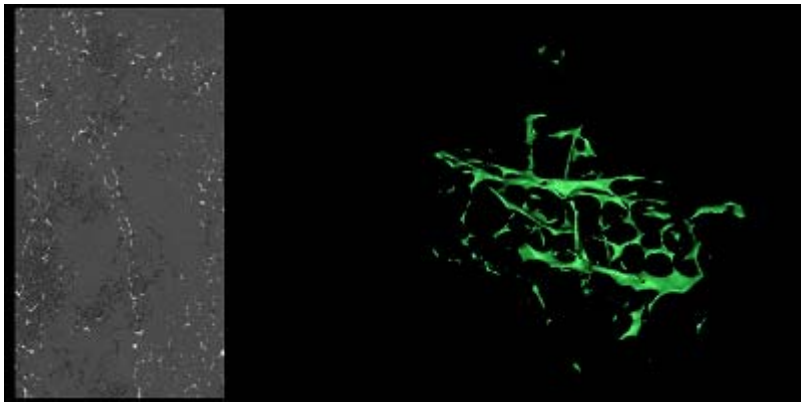

Figure 3-15. Microstructure of the sternum (99% marrow).

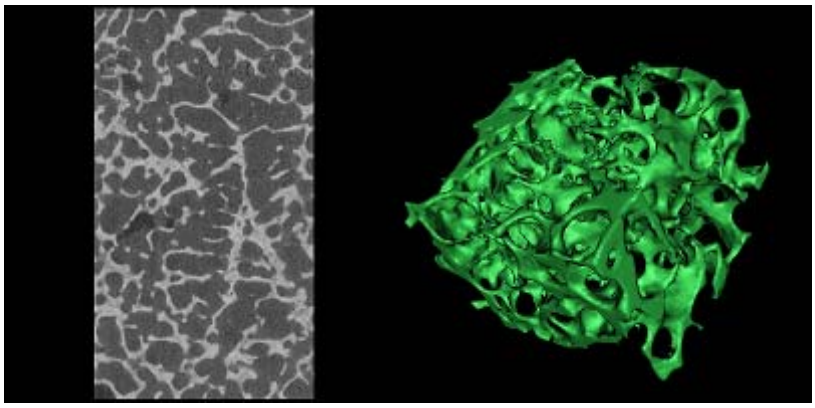

Figure 3-16. Microstructure of the 3rd cervical vertebrae (76% marrow).

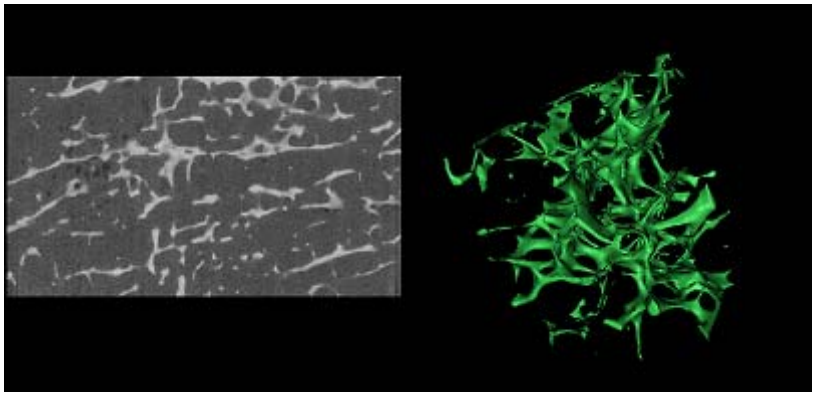

Figure 3-17. Microstructure of the 5th lumbar vertebrae (91% marrow).

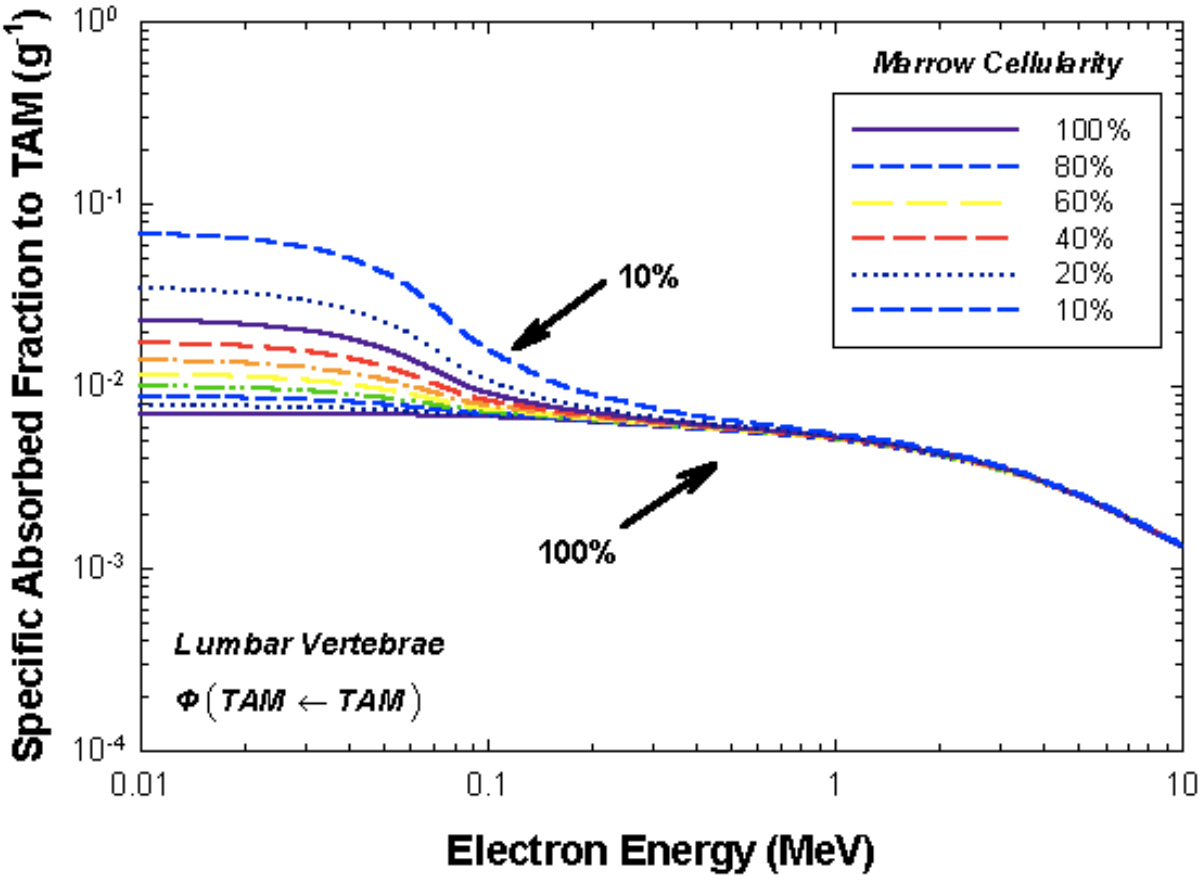

Figure 3-18. Specific absorbed fraction for the TAM irradiating the TAM for the lumbar vertebrae.

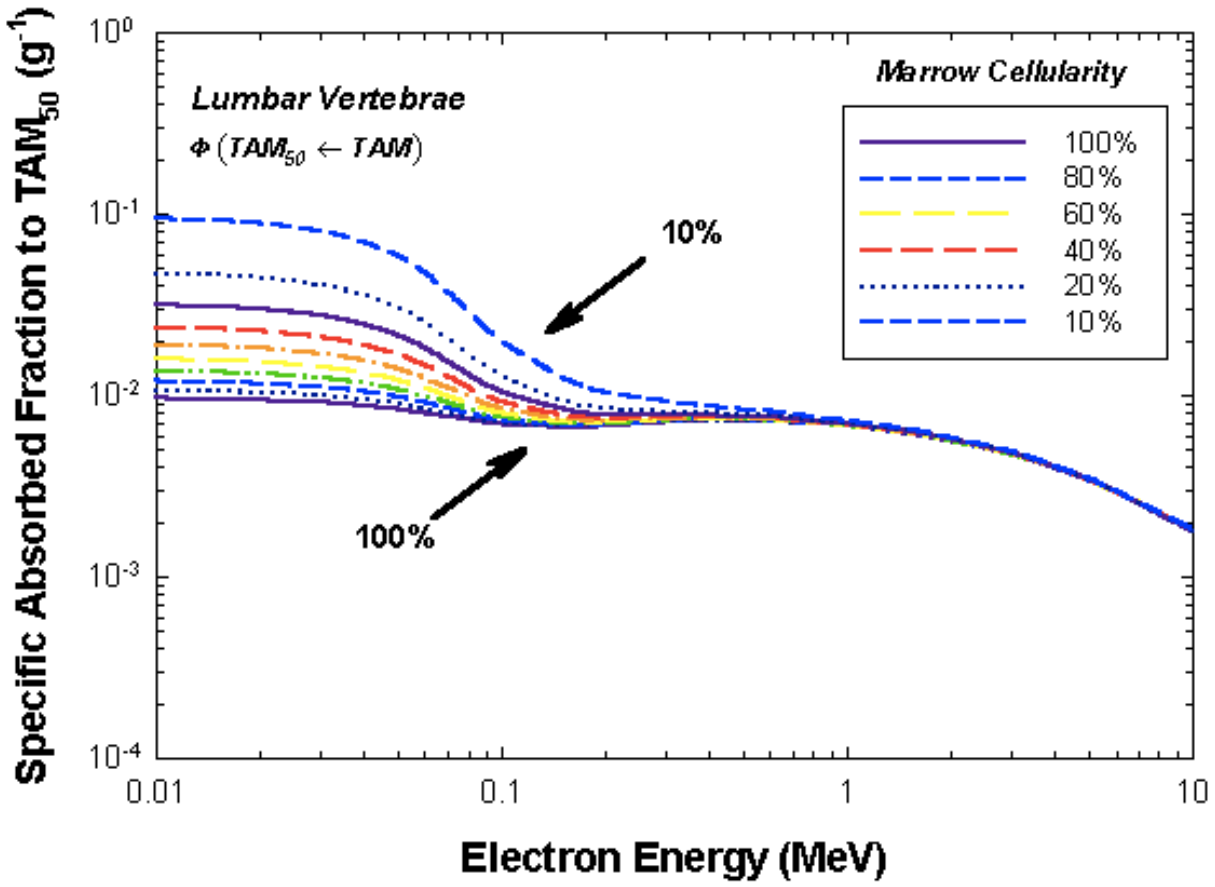

Figure 3-19. Specific absorbed fraction for the TAM irradiating the TAM_{50} for the lumbar vertebrae.

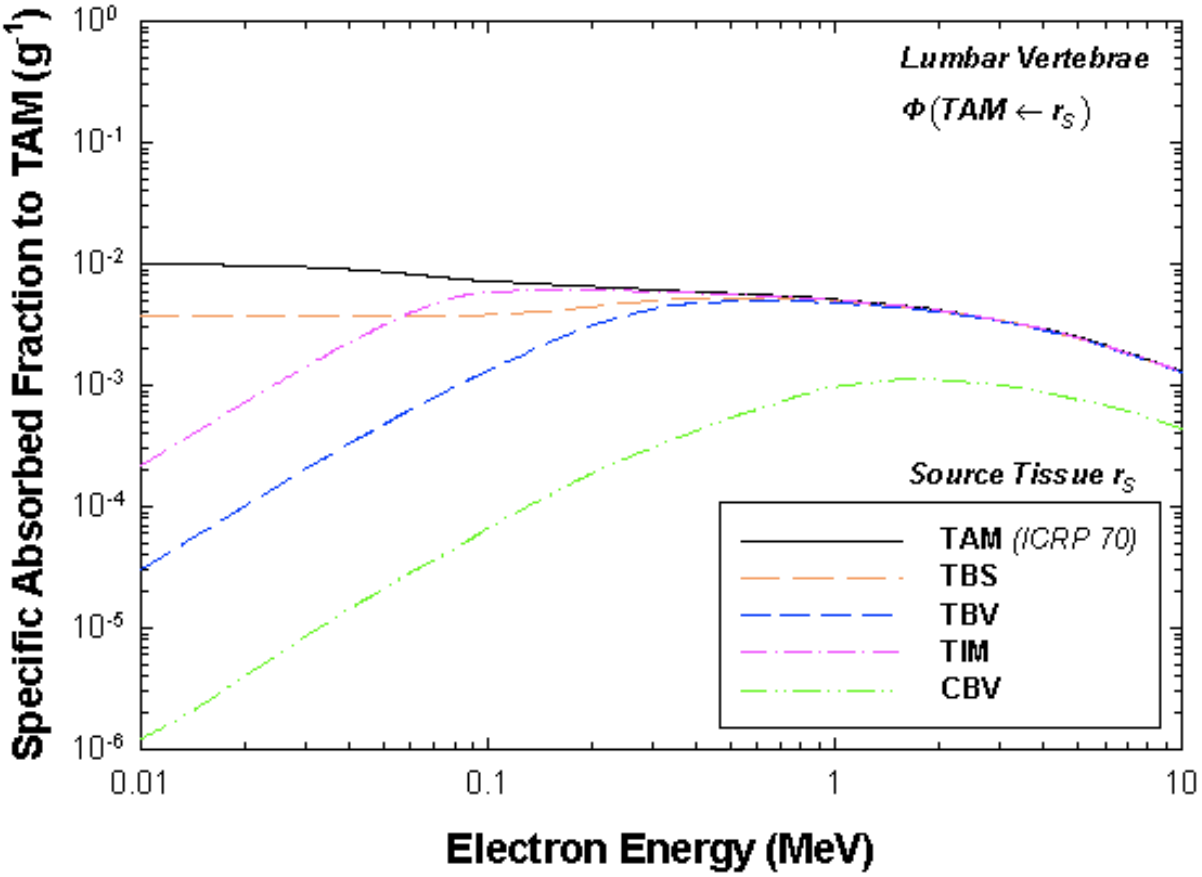

Figure 3-20. Specific absorbed fraction for all sources irradiating the TAM for the lumbar vertebrae.

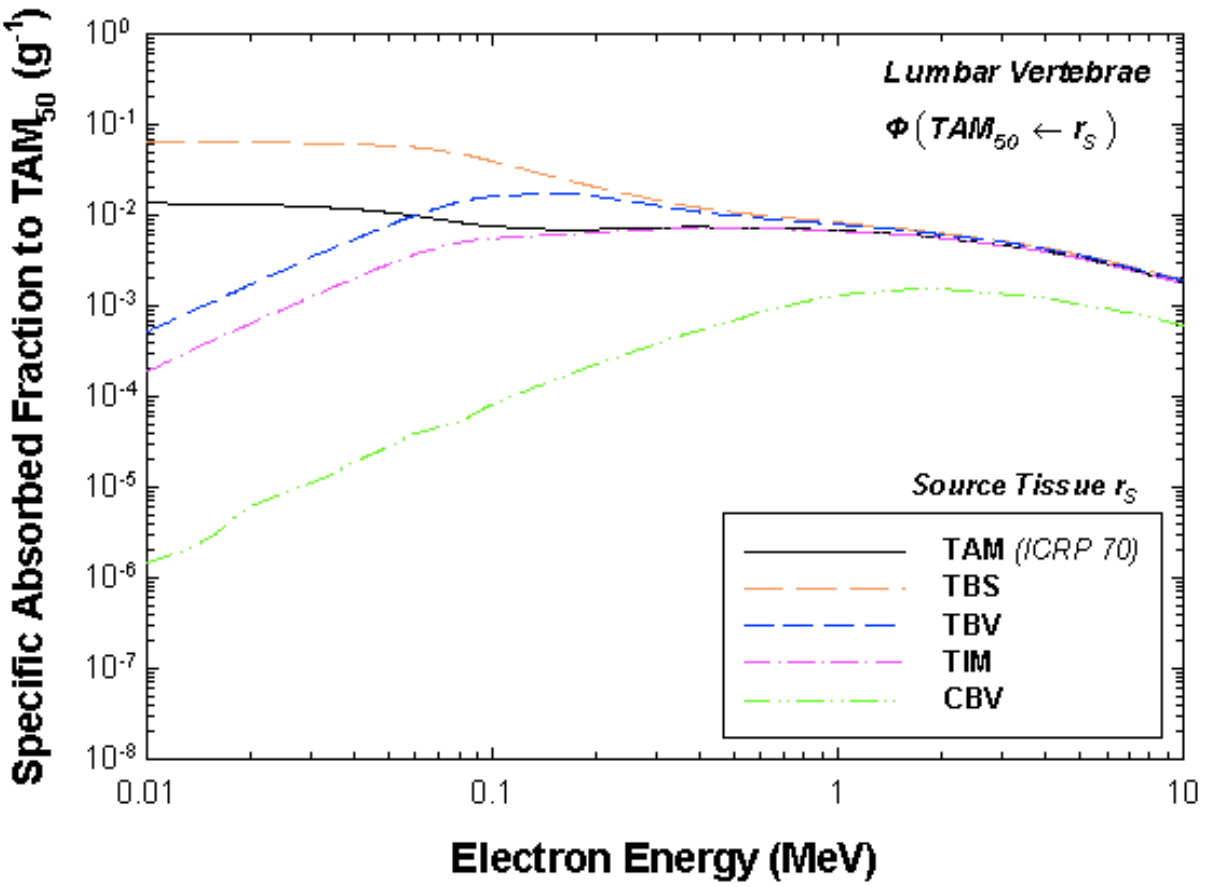

Figure 3-21. Specific absorbed fraction for all sources irradiating the TAM_{50} for the lumbar vertebrae.

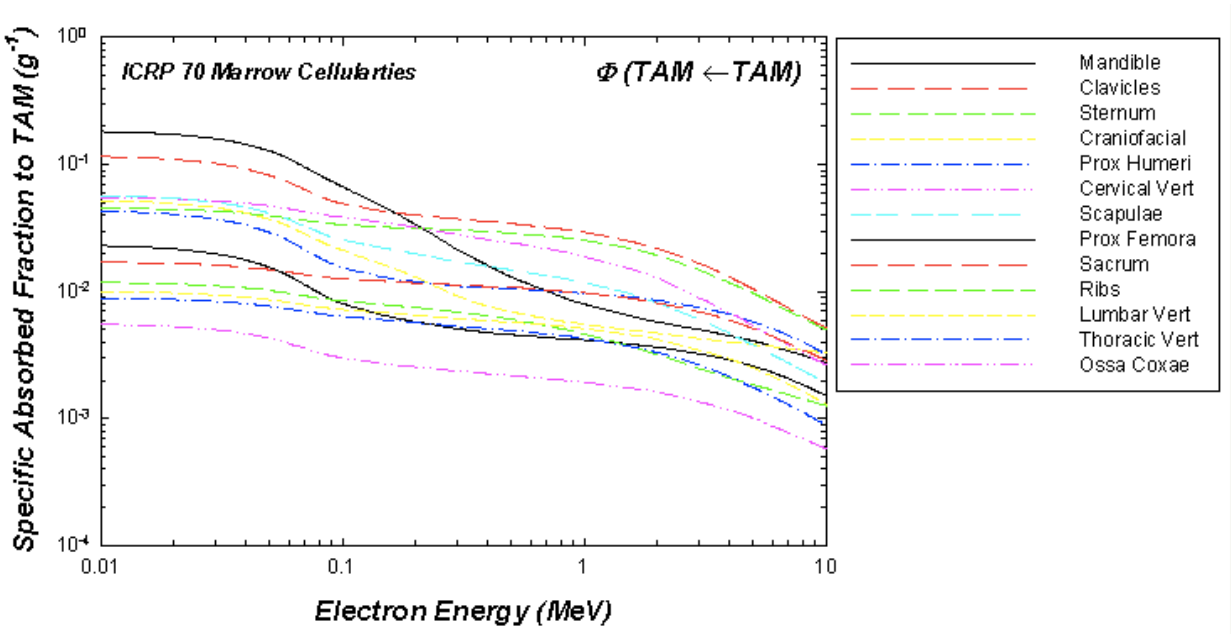

Figure 3-22. Specific absorbed fraction for the TAM irradiating the TAM for all bone sites.

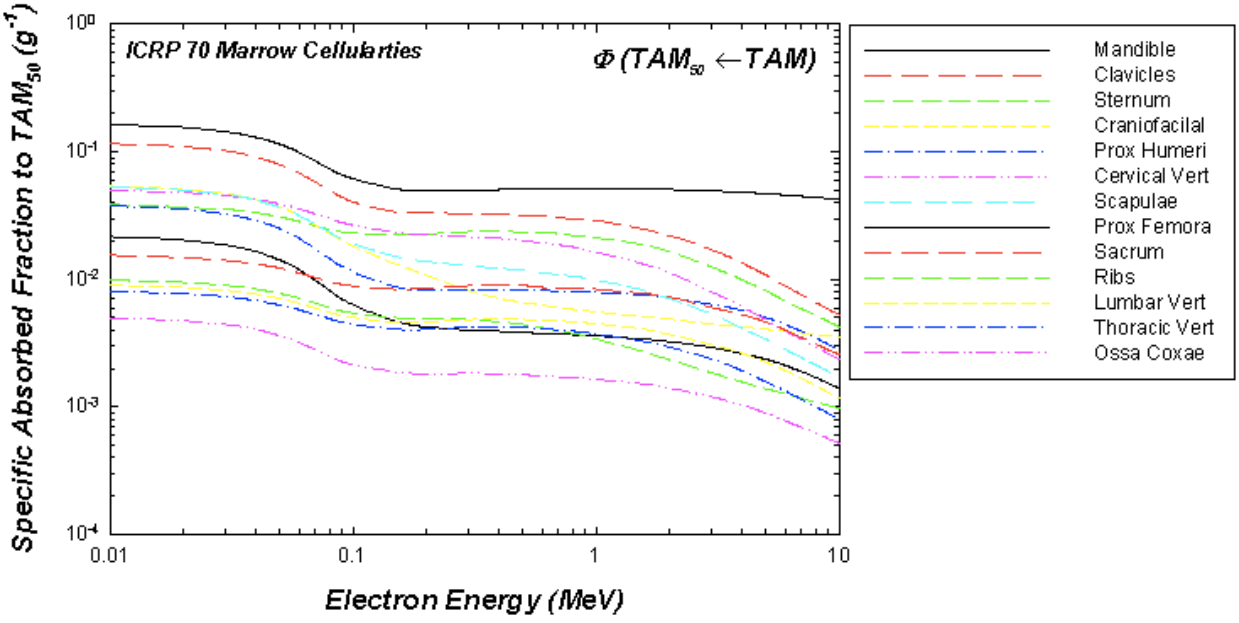

Figure 3-23. Specific absorbed fraction for the TAM irradiating the TAM_{50} for all bone sites.

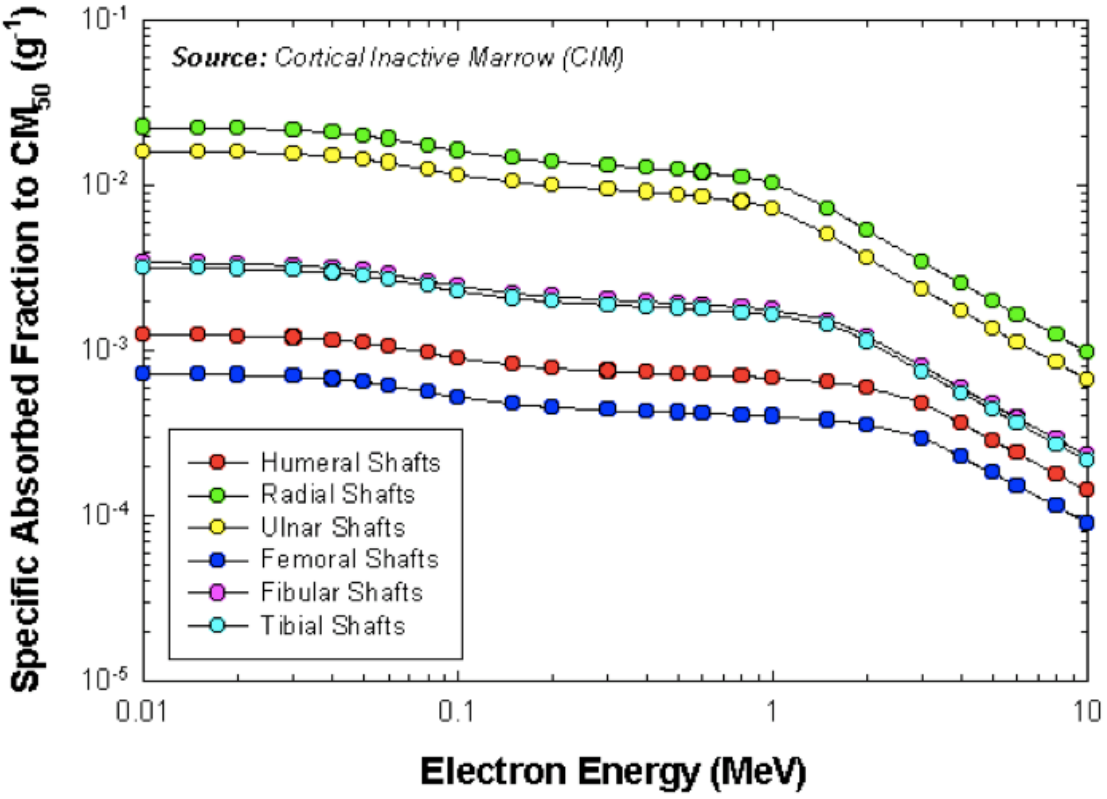

Figure 3-24. Specific absorbed fraction for the CIM irradiating the CIM_{50} in the shafts of all long bones.

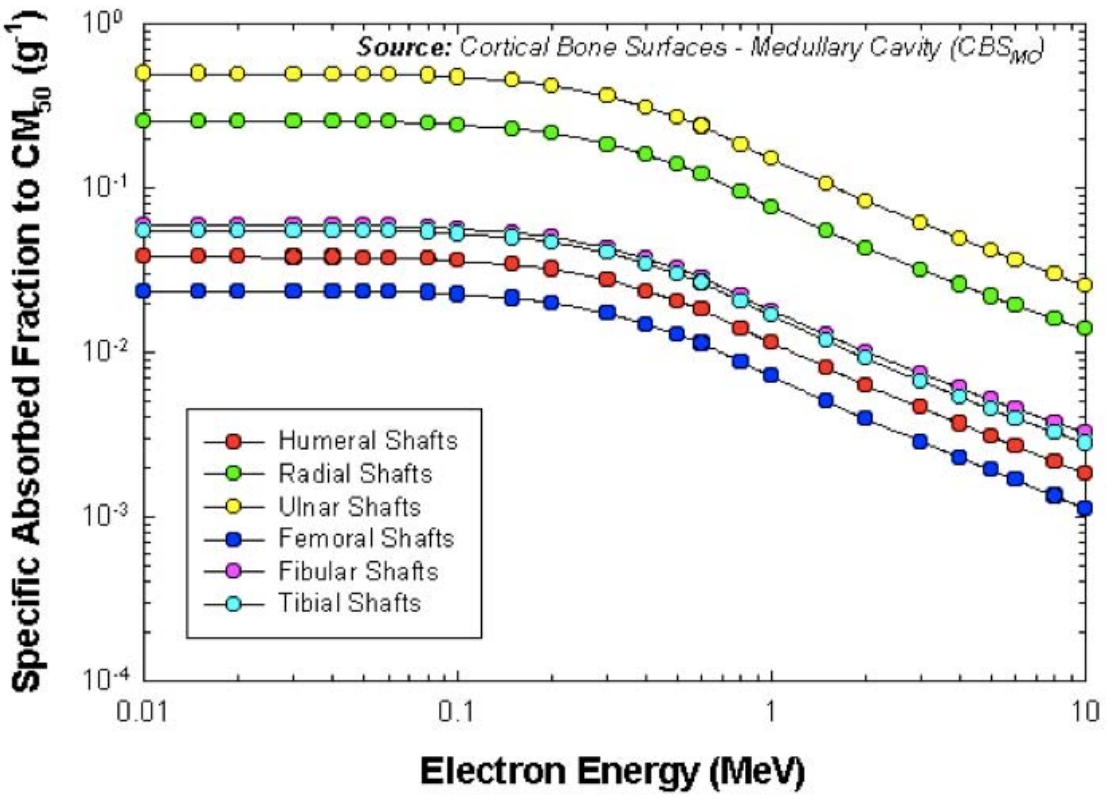

Figure 3-25. Specific absorbed fraction for the CBS_{MC} irradiating the CIM_{50} in the shafts of all long bones.

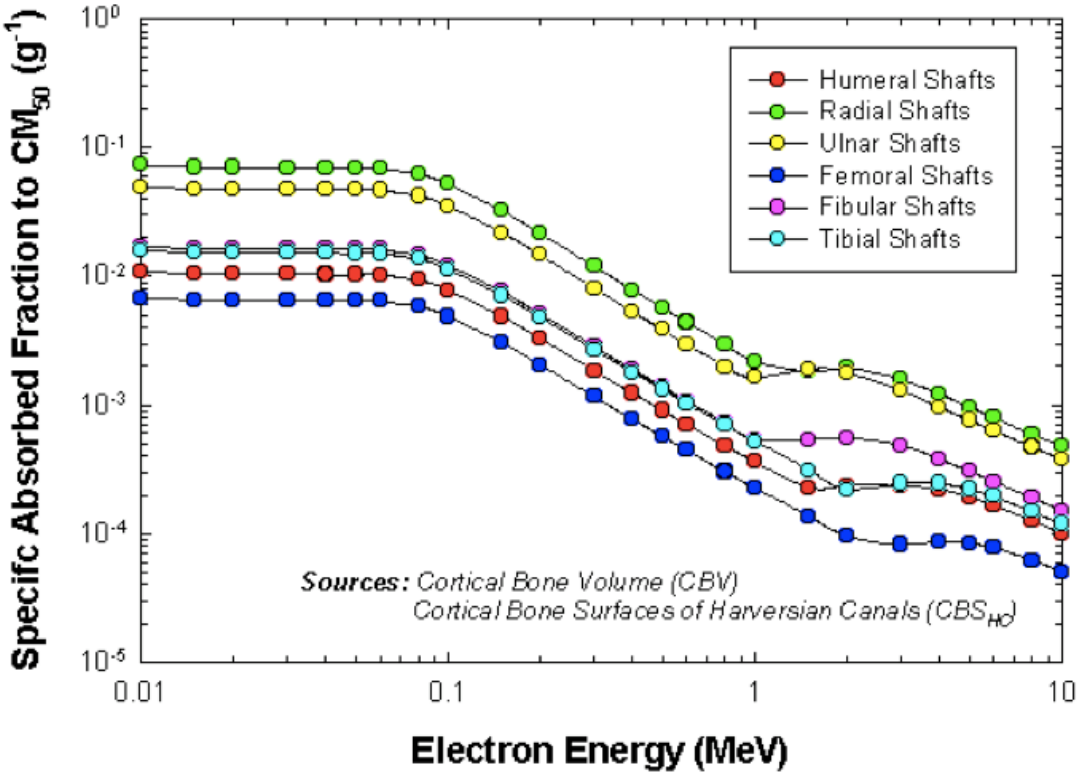

Figure 3-26. Specific absorbed fraction for the CBV irradiating the CIM_{50} in the shafts of all long bones.

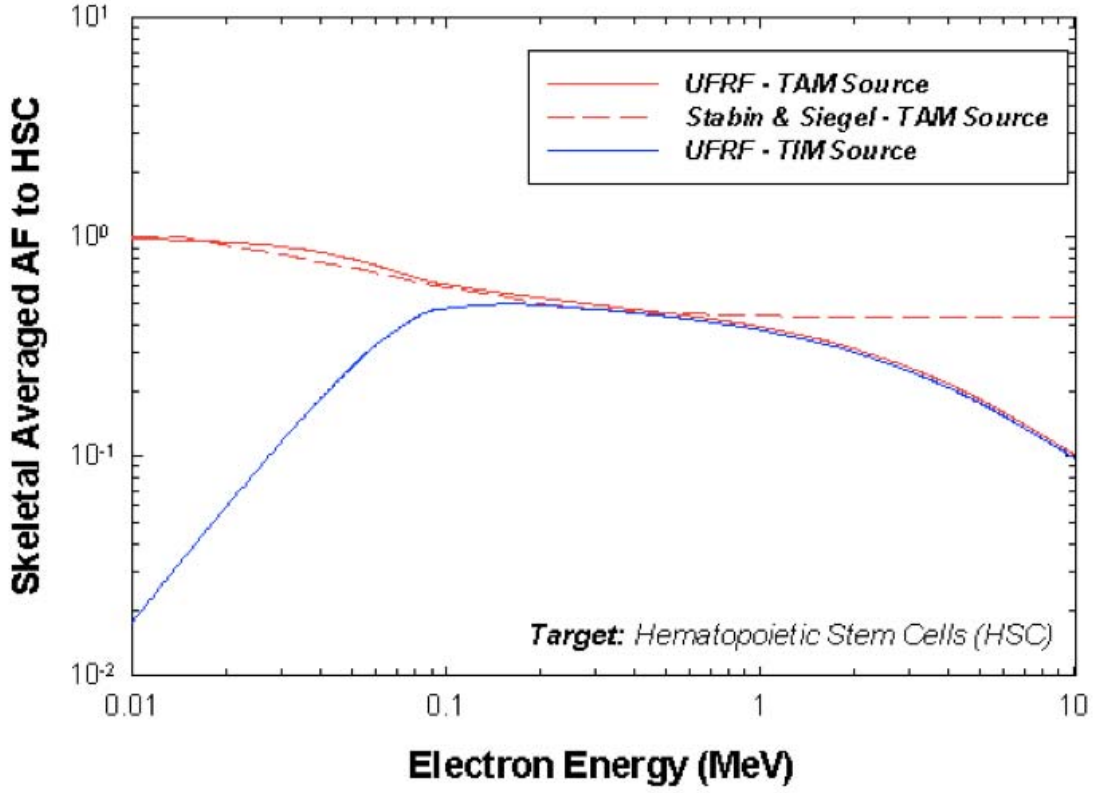

Figure 3-27. Skeletal averaged AF for marrow sources irradiating the TAM for both UFRF and Stabin and Siegel (2003).

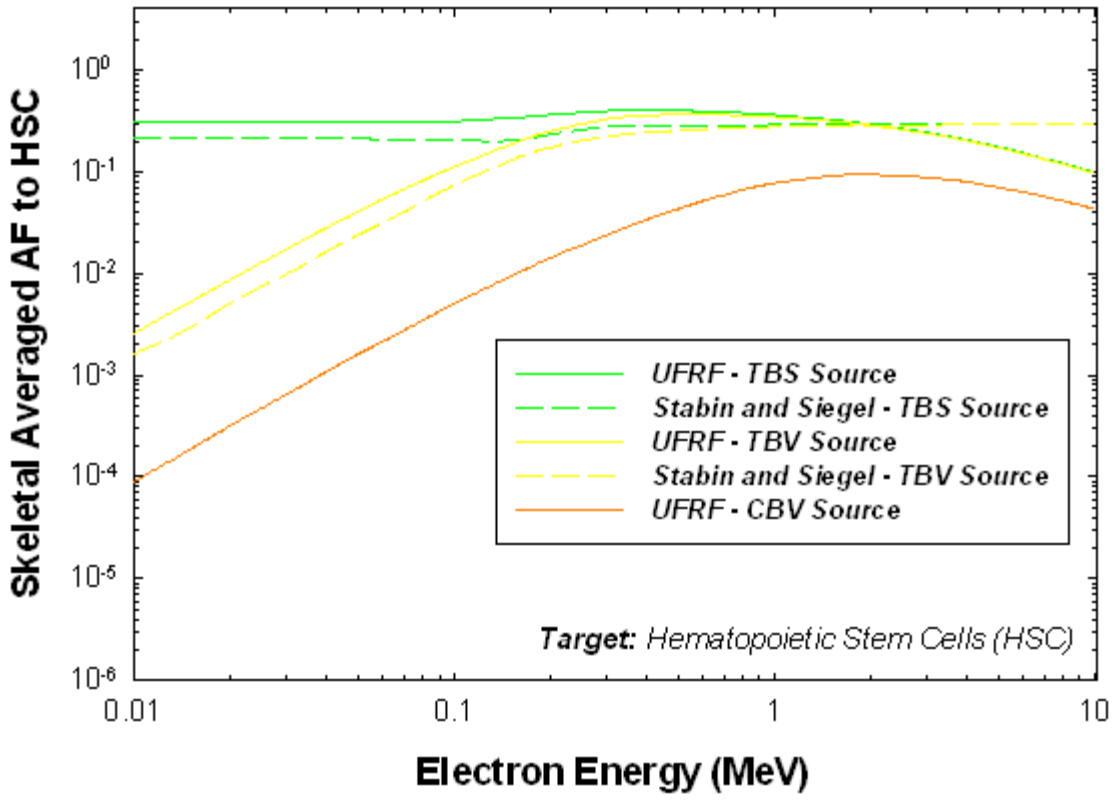

Figure 3-28. Skeletal averaged AF for bone trabeculae sources irradiating the TAM for both UFRF and Stabin and Siegel (2003).

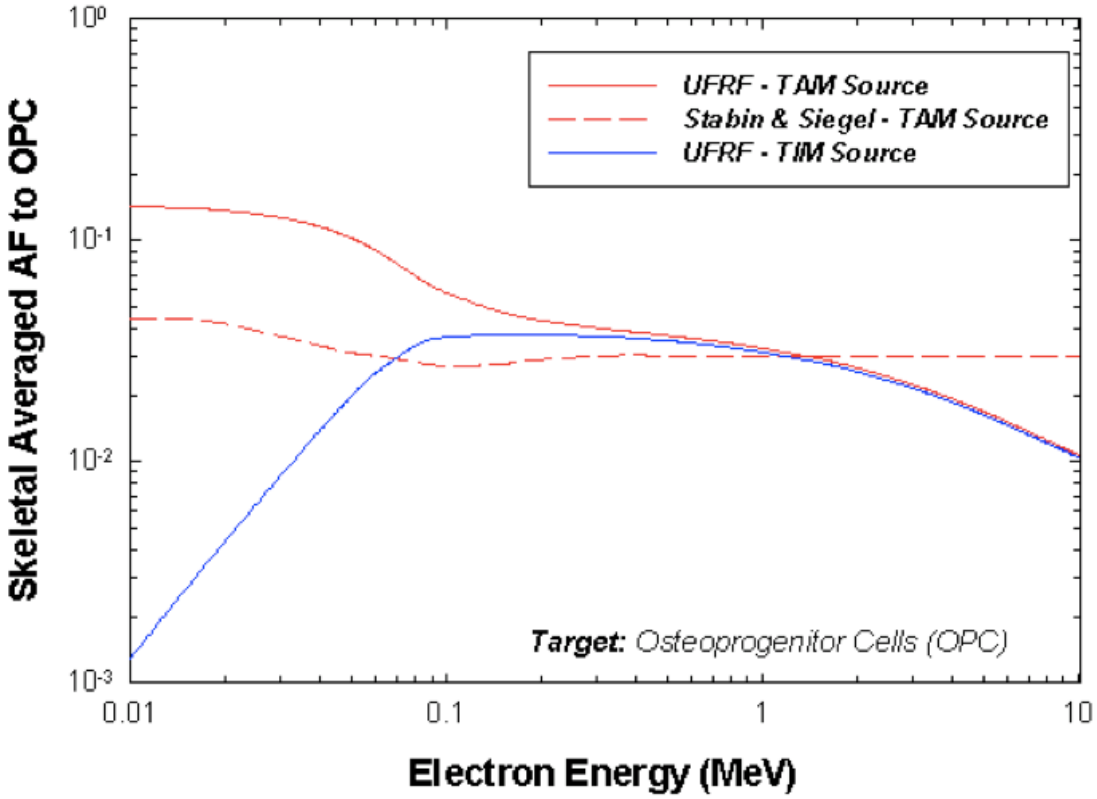

Figure 3-29. Skeletal averaged AF for marrow sources irradiating the TAM_{50} for both UFRF and Stabin and Siegel (2003).

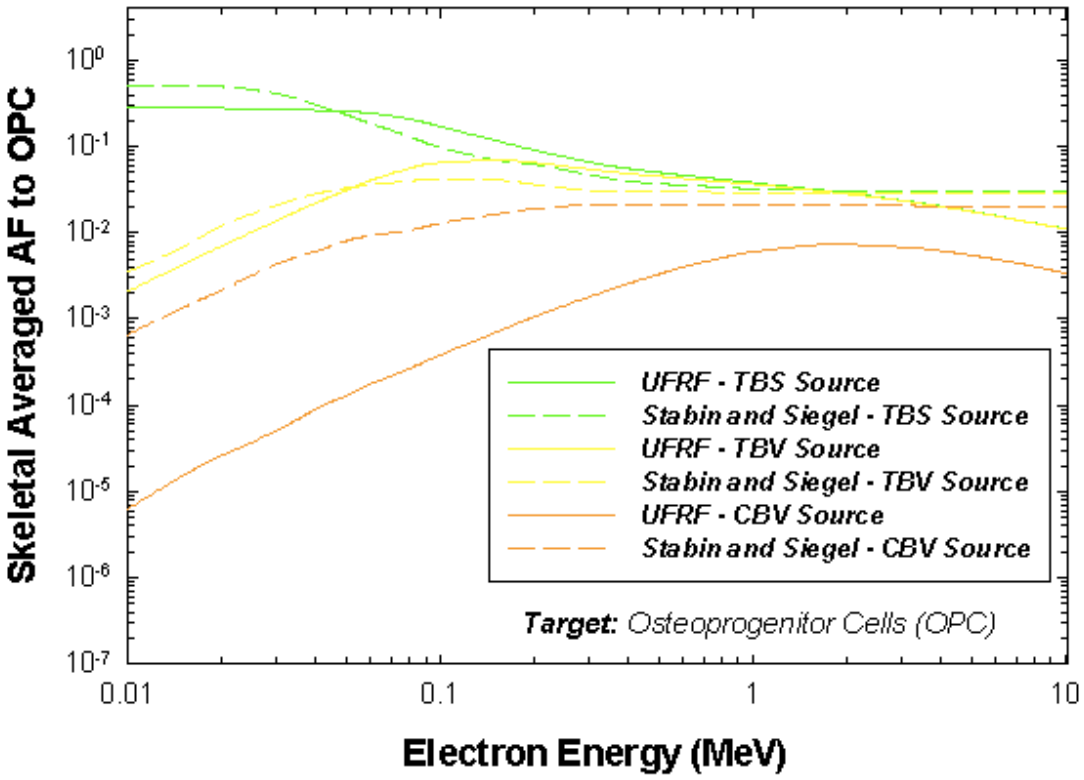

Figure 3-30. Skeletal averaged AF for bone trabeculae sources irradiating the TAM_{50} for both UFRF and Stabin and Siegel (2003).

CHAPTER 4
COMPARISON OF HUMAN STEM CELL MEASUREMENTS IN BIOPSIES VERSUS AUTOPSY SPECIMENS

Introduction

Bone marrow biopsies are widely used to assess the health of bone marrow and prediction of disease. Advances in the understanding of blood disorders and their ties to cellular elements in bone marrow have vastly increased the use of biopsies in the past decade. Consequently, bone marrow biopsies are taken frequently in both normal and abnormal patients as a part of routine diagnosis for conditions in hematology, internal medicine, and oncology. Bone biopsies are valuable not only for diagnosis of cytopenia, myelo- and lymphoproliferative disorders, but also for vast problems relating to immunology and hematopoietic regulatory mechanisms (Hoffman *et al.*, 1991).

Typical bone marrow biopsies are taken from either the anterior or posterior iliac crest, with core sizes ranging from 4-8 mm x 10-22 mm depending on the acquisition site and procedure followed. Hematopoietic tissue and trabecular bone account for 40% and 26% by volume of the biopsy, respectively, assuming 28% fatty tissue. The remaining bone marrow biopsy is osteoid, sinuses, and edema. Disease specific processing techniques are applied to the biopsy to quantify the degree of hematological disorder through a cellular count such as red blood cell quantity in the case of potential anemia or Reed-Sternberg cells in the case of Hodgkin's lymphoma (McPherson and Pincus, 2007).

In radioimmunotherapy, the dose limiting organ is the hematopoietically active (red) bone marrow and estimates of the absorbed dose require knowledge of the marrow health. Moreover, the red marrow is in reality a surrogate for the underlying radiosensitive cell populations, namely that of the hematopoietic stem cells. Thus, a measure of marrow health is related to the quantity of hematopoietic stem cells. In particular, the concentration of CD34+

stem and progenitor cells has been shown to be directly related to the prognosis of therapeutic outcome following marrow ablation (Sgouros, 1993). Recent studies have shown that a spatial gradient exists for this stem cell population in human bone marrow, with a higher concentration of cells localized near the trabecular bone and decreasing further into the marrow cavities (Watchman *et al.*, 2007). This relationship is seemingly found to exist in both large field specimens (autopsies) as well as smaller fields (biopsies). The spatial distribution itself does not prove to have any particular bone site dependence, and thus any bone site should yield the same linearly decreasing trend (Bourke *et al.*, in press).

The first studies to directly measure the spatial distribution of HSCs to bone trabeculae were performed at the University of Florida by Watchman et al (2007). In that study, CD34 and CD31 immunohistochemical staining was performed on subsequent slides from core biopsy samples of the iliac crest from disease-free normocellular human bone marrow. The data fully supported the hypothesis that CD34+ HSCs and their progenitors follow a spatial gradient with respect to bone trabeculae within human bone marrow. Also, blood vessels seem to follow the same gradient indicating a shared spatial niche with stem cells. Distance-dependent weighting factors are provided as an update to the MIRD schema.

The most current work at the University of Florida by Bourke et al (2009) used autopsy methods rather than biopsies to assess spatial distributions in larger samples and for several skeletal sites because of potential field of view limits. CD34 and CD117 immunohistochemical staining was performed on autopsy sections from the iliac crest, lumbar vertebrae, and rib of disease free, normocellular patients. This data shows the same trend found in previous studies, that the CD34+ cells decrease as a function of marrow depth. Also, the method used to stain tissue was shown to alter the concentration of cells while preserving spatial gradient.

Cellular measurements are often made in small biopsy samples, with hopes that the sample is representative of the entire marrow. Accuracy may be limited by the field of view in a biopsy, when compared to a full field autopsy specimen. Shown in Figure 4-1, a biopsy may only show the white portion of the marrow, leading to cell distances being measured to the nearest trabeculae in view for total distances of 331, 287, 404, and 365 pixels. If, however, the full field was seen and the pink region of marrow was included, cellular measurements would now correctly be 331, 287, 241, and 271 pixels. This brings to question the validity of using limited field biopsy specimens as a surrogate for the entire marrow cavity.

Artificial cell-to-bone distances by trabeculae lying just outside the processed specimen's field-of-view has been termed a potential 'edge effect', and is postulated as a potential limitation of the use of biopsies to assess marrow health (Watchman *et al.*, 2007). This has implications not only for cellular distributions, but could lend to inaccuracies in any cell count expressed as a percentage of total marrow. Biopsies are widely used to assess blood disease, but their usefulness is solely dependent upon the accuracy of such a measurement technique. The objective of the present study is to directly quantify the difference in hematopoietic stem cells concentration and distribution due to areal effects. The objective is thus to determine whether hematopoietic cellular distributions found in biopsy specimens will yield the same result that would have been found had a larger tissue field-of-view been used. Furthermore, any directional dependence (anisotropy) in HSC concentration will be discussed through use of simulated biopsies taken in vertical or horizontal planes.

Materials and Methods

Artificial biopsy sections were taken from previously collected and stained autopsy specimens from the L1 vertebrae. The skeletal site of the autopsy specimen was chosen due to its planar symmetry. Unlike the Iliac crest, autopsies from the L1 vertebrae are 5000μm on end

and allows for identical sized masks in both two dimensional planes (Figure 4-2). This is advantageous for assessing anisotropy within bone sites. Six artificial sections were taken, three in the horizontal and three in the vertical plane (Figure 4-3). Horizontal and vertical planes were chosen to study any anisotropy or directional dependence. Each "simulated biopsy" specimen was treated independently, i.e. each was looked at as if there was no other information other than what was in that view. Accordingly, cellularity was measured for each biopsy section separately (Figure 4-4).

Autopsy Collection and Preparation

Previously acquired post-mortem bone samples from Bourke et al (2009), sectioned and fixed in paraffin from the L_1 vertebrae of nine recently deceased patients were assembled. All samples were collected within 24 hours of death and were determined to be absent of marrow disease under a HIPAA-compliant and IRB-approved protocol. Autopsy blocks were decalcified and embedded in paraffin for preservation. Sequential sections were collected from each specimen at a thickness of 5 mm, and the most intact section was kept. Table 4-1 summarizes the age, gender, and cause of death for each subject in the study. These sections were then manually stained using mouse anti-CD34 (dilution 1:25, QBEND10, DAKOCytomation; Carpinteria,CA). CD34 staining of endothelial cells served as an internal control.

Digital Imaging and Processing

After staining, the autopsy specimens were imaged at the Optical Microscopy (OM) facility of the University of Florida McKnight Brain Institute (MBI). Image resolution was verified via a caliper slide giving a calibration factor of 1.2 pixels/mm. Using these digital images, bone trabeculae were digitally segmented using Adobe Photoshop. Following the acquisition of digital autopsy specimens, masks the average width of a clinical biopsy were overlaid to achieve a "simulated biopsy" within the full field autopsy specimen.

Using 16 previously collected biopsy samples from Watchman et al (2007), the width of a typical clinical biopsy was found to be 1.24 mm with a standard deviation of 0.46 mm, or 1489 ± 550 pixels. This large variation in biopsy width is to be expected and based on the individual procedure used to collect biopsies. Three sample width measurements were averaged per biopsy slide, for a total sample size of 48. Six "simulated biopsy" masks were overlaid in non-overlapping regions of each autopsy slide, three in the horizontal plane and three in the vertical plane. In the horizontal plane, sections were in the upper, middle, and lower regions, whereas sections were in the left, middle, and right regions in the vertical plane. An example of both the horizontal (yellow) and vertical (purple) middle simulated biopsy sections are shown in Figure 4-2.

Measurement of Hematopoietic CD34+ Cells

Cells were optically identified using an OM36LED contour microscope (Microscope Store, Rock Mount, VA) with a 20X objective as a compromise between field of view and image resolution. SPOT Advanced imaging software (Diagnostic Instruments Inc, Sterling Heights, MI) was used to make distance measurements in pixel units. A CD34+ cell was found in the slide under the microscope, and the distance from that corresponding cell to the nearest bone trabeculae was measured on the digital image. Pixel values were then transformed to micrometers using a calibration factor of 1.2 pixels/mm. Histological distance measurements were determined for each of the six simulated biopsy, and compared to the cell count and concentration in the total autopsy specimen. Also, the average concentration of the horizontal masks and the average of the vertical masks were compared to the total to explore anisotropy.

Cells were not considered CD34+ unless they exhibited visible membrane expression of the antigen, in addition to small, primitive morphology consistent with a HSC. This is shown in Figure 4-5. When bone trabeculae were obviously missing or were partially separated from the

tissue during the sectioning process, distance measurements and trabeculae segmenting were made to the boundary of its original anatomical space. No boundary masks were used, and only those cells within each simulated biopsy were counted and compared to the total cellular count in the autopsy as a whole. Sample measurements from cells to nearest bone trabeculae are found in Figure 4-1.

Cellularity Measurement

Regions of active bone marrow were determined via manual segmentation of adipocytes using Adobe Photoshop. For each simulated biopsy, a 500 mm x 500 mm location within each bone site, deemed visually to be representative of the entire marrow space was confirmed. Three sample locations were averaged, when possible. At the very least, two cellularity measurements were sampled for more accurate determination of fat percentage (Figure 4-4). The resulting color image was converted to grayscale, filtered, and converted to a binary black and white image, and then pixel counted. The ratio of the final non-zero pixel count to the original image pixel count was used as the precise digital estimate of the amount of total marrow area contributed by the adipocytes population, and is termed the marrow cellularity factor (CF).

Marrow Area Measurement

In order to determine cellular concentration, the area of marrow must be known. First, bone trabeculae was segmented using Adobe Photoshop. Shown in Figure 4-6, each specimen's digital image was converted to grayscale, filtered, and then converted to binary black and white image. In this image, white and black signify marrow regions and trabecular regions, respectively. Trabecular surfaces were then expanded in 50 μm increments using an in-house edge dilation algorithm developed for use with ImageJ (NIH, Bathesda, MD). Using this data, binned areal measurements were determined for each simulated biopsy through pixel counting of the merged dilated trabecular bone image with the total marrow image. These binned cell counts

were normalized to the amount of marrow contributed by each region, yielding cells/mm^2 in 50 μm increments from the bone surface. For each simulated biopsy s, the average cellular concentration is simply the ratio of total number of CD34+ hematopoietic stem and progenitor cells (HSPC) to marrow area for that site:

$$\rho_s^{HSPC} = \frac{N_s^{HSPC}}{A_s}, \tag{4-1}$$

where N is the number of cells and A is the area. This was performed for each 50 μm bin, substituting the cell count and subsequent area for that bin. For example, ρ for the first 50 μm bin would the number of cells in the first 50 μm from all bone trabeculae, divided by the marrow area 50 μm from all bone trabeculae in the simulated biopsy.

Cellular concentration of hematopoietically active (red) bone marrow regions were obtained by multiplying total marrow area contributed by each region by its cellularity factor (CF) within the specimen:

$$\rho_{s-active}^{HSPC} = \frac{N_s^{HSPC}}{CF \times A_s}, \tag{4-2}$$

Each specimen's cellular concentration gradient was weighted by its fractional contribution (f_s) to the total marrow area measured in that bone site across all specimens. This leads to two fractional contributions dependent upon the measurement made. For the case of total simulated biopsies, f_s was weighted to the total marrow of all specimens. If horizontal and vertical biopsies are assessed separately, f_s was weighted to the amount of marrow in either all horizontal or all vertical biopsies, respectively. The fractional weights for each case are shown in Table 4-2. Specimen-weighted mean cell concentrations and weighted standard deviations of the mean cell concentration were also calculated and plotted at each distance interval, in each bone site. Specifically,

$$\overline{\rho}^{HSPC} = \sum_{x} f_s \rho_s^{HSPC} \quad , \tag{4-3}$$

where the fractional weight and areal density are decribed above.

The weighted standard deviation is then given as:

$$\sigma_{\overline{\rho}_x}^{HSPC} = \sqrt{\frac{\sum_{x} f_s \left(\rho_s^{HSPC} - \overline{\rho}_x^{HSPC}\right)^2}{n_x - 1}} \quad , \tag{4-4}$$

where *n* is the number of samples.

Results

The simulated biopsy cellular concentrations were compared to the entire autopsy from which they came. Cellularity, specimen fractional weight for total biopsies, total marrow area, active marrow area, and cell counts for each patient are given in Table 4-1. Specimen fractional weights are shown in Table 4-2. The mean cellular concentration and standard error for both simulated biopsies and autopsies in the total and active marrow among all patients are provided in Table 4-3. Mean cellular concentration and standard error for vertical and horizontal biopsies in both total and active marrow if given in Table 4-4. Figure 4-7 shows the concentration of cells for the simulated biopsies versus autopsies. In this case, simulated biopsies are all six simulated biopsy cases separately weighted and added together to provide a comparison to the autopsy cell count. Finally, Figure 4-8 is a comparison between the cellular concentration in vertical biopsies, horizontal biopsies, and the autopsies.

Discussion

Full field Autopsy Measurements

Mean average CD34+ cell concentration in the total marrow was found to be 12.55 $\pm$ 2.84 cells per mm^2 among all patients in the total vertebrae autopsy. In the active marrow, cellular concentration was 7.62 $\pm$ 1.38 cells per mm^2. The cellular concentration was best modeled by a

linear curve fit, and was found to have an R^2 of 0.848. Most HSCs were found between found between 0 and 250 μm from the bone surfaces (80.4%), and this region contained most of the active marrow area (71.3%). The cellular concentration was essentially equal to the mean up to 250 μm, and diminished rapidly after this point with no cells found beyond 700 μm.

Total Simulated Biopsy Measurements

Each of the six simulated biopsy measurements were compared independently, and the mean cellular concentration in both total and active marrow was found to be 7.04 $\pm$ 0.98 cells per mm^2 and 10.97 $\pm$ 1.58 cells per mm^2 , respectively. A linear fit provided an R^2 of 0.939. Again, most cells were found in the first 250 μm from the bone surfaces (79.6%), comprising 70.4% of the active marrow area. HSCs dropped off quite rapidly after 300 μm, with no cells past 700 μm.

Vertical Small Field Measurements

CD34+ mean cell concentration in the vertical fields was found to be 7.30 $\pm$ 1.22 cells per mm^2 in the total marrow and 11.37 $\pm$ 1.99 cells per mm^2 in the active marrow. A linear fit was performed, with an R^2 of 0.911. As in the previous case, most cells and active marrow were within the first 250 μm, with 80.8% and 70.7% respectively. A drastic linear decrease was noted after 300 μm, with no cells past 700 μm.

Horizontal Small Field Measurements

Mean cell concentration of HSCs in the horizontal fields were 6.81 $\pm$ 1.17 cells per mm^2 and 10.45 $\pm$ 1.88 cells per mm^2 in the total and active marrow, respectively. A linear fit provided an R^2 of 0.920. In this study, 78.3% of the cells were within the first 250 μm from bone trabecular surfaces, and this region accounted for 70% of the active marrow. The cellular concentration was found to be near the mean until 250 μm, where the concentration of cells decreased until no cells were found as far as 700 μm into the marrow cavities.

Statistical Analysis

A student's t-test reveals that there is no statistically significant difference between mean cell concentrations in the simulated biopsies and the autopsies in the total marrow (t=1.21, p=.24) or in the active marrow (t=1.63, p=0.14) with a 95% confidence level. There is also no difference between the vertical biopsy and the autopsy in the total marrow (t=0.62, p=0.55) or active marrow (t=1.16, p=.29). Furthermore, there was no difference between the mean cell concentration in the horizontal biopsy and autopsy in the total marrow (t=1.58, p=0.06) or active marrow (t=2.07, p=0.07) with a 95% confidence level. Lastly, there was no statistically significant difference found between the vertical and horizontal biopsies in the total (t=1.51, p=0.14) and active marrow (t=0.96, p=0.09).

Field of View

The possibility of artifacts when assessing the spatial distribution of stem cells in bone marrow is greater at smaller fields of view. The less marrow viewed in the field of view, the greater the chance of inducing an edge effect, and artificially skewing measurements to longer distances. In this study, small field of views are the simulated biopsies, with large views of views comprising the full autopsy specimen. The mean spatial concentration of simulated biopsies was compared to the mean cellular concentration of the autopsy from which it came to assess the degree of artifact induction.

Comparing the average spatial concentration of each simulated biopsy to the autopsy from which it came yields the same linear decrease as depth into the marrow cavity increases. In the active marrow, mean cellular concentration is somewhat lower in small fields (10.97 cells per mm^2) than in large fields (12.55 cells per mm^2), but are within one standard deviation from the mean (1.58 cells per mm^2). The same trend in cellular concentration is noted in the active marrow, with small and large fields yielding 7.62 cells per mm^2 and 7.04 cells per mm^2 ,

respectively. Again, both are within the error bars (0.98 cells per mm^2), deeming no difference between the two. Identical mean concentrations are not noted since the simulated biopsies did not cover the entire autopsy error and were instead measured to have the same average width of an actual patient biopsy.

Although the simulated biopsy yields a slightly smaller mean cellular concentration when compared to the autopsy, there is no difference given the error in counts. It would be expected that a smaller area would reveal lower cell counts, however, this data is relative to the amount of area in the viewing area. Because of this normalization to area, cellular concentration is the same regardless of field of view. Furthermore, the same decreasing spatial gradient is noted in both cases. Thus, the small field simulated biopsy can be used to predict the spatial concentration within the larger field of view. This is noted when accounting for both total and active marrow. This lends itself well to determining the accuracy of using biopsies as a surrogate of the entire marrow cavity to assess marrow health in both normal and diseased patients.

Anisotropy

One concern in using biopsies to determine marrow health is the proper location of insertion. To determine whether there is any directional dependence (anisotropy) in cellular concentration measurements, vertical and horizontal simulated biopsies were compared independently. Vertical biopsies in the total marrow provided a mean cellular concentration of 7.30 cells per mm^2, whereas vertical biopsies in the total marrow showed a mean of 6.45 cells per mm^2. Both are within one standard deviation of the mean: 1.22 cells per mm^2 and 1.10 cells per mm^2 in the vertical and horizontal biopsies, respectively. In the active marrow, mean spatial concentration was 11.37 cells per mm^2 in the vertical biopsies and 9.97 cells per mm^2 in the

horizontal biopsies. Again, these are within both vertical biopsy error (1.99 cells per $mm^{2)}$ and horizontal biopsy error (1.80 cells per mm^2).

Both the vertical and horizontal mean cellular concentrations matched the autopsy from which they came, and did not vary amongst each other. This was noted in both active and total marrow. Moreover, the same decrease in spatial gradient as depth into the marrow cavity increases was seen. This proves that there is no directional dependence among specimens. It can be assumed that a bone marrow biopsy in one direction will yield a similar cellular concentration as any other direction and an accurate assessment of marrow health.

Dose Implications

The inclusion of artifacts such as those caused by edge effects would have great implications in proper assessment of dose to the red bone marrow. As proposed by Watchman et al (2007), the MIRD dose equation should be modified to include a distance-dependent weighting factor as follows:

$$D(RBM \leftarrow r_s) = \widetilde{A}_s \sum_x \overline{\omega}_x S(RBM_x \leftarrow r_s), \tag{4-5}$$

where A is the cumulated activity with the source, S is the radionuclide S value for marrow depth x, and ω is a distance-dependent weighting factor which is the mean fractional mass of red bone marrow at marrow depth x. Had a biopsy not correctly measured the concentration and spatial gradient in the red bone marrow, the weighting factor would have been incorrectly measured, and the dose to the red bone marrow would be incorrectly assessed. This can be significant for radioimmunotherapy, as low energy particles with short ranges now irradiate a large portion of the radiosensitive cell population, leading to increase marrow toxicity.

Conclusion

In this study, the mean cellular concentration and spatial gradient of HSCs were compared in simulated biopsies and the autopsies from which they came. Six small field simulated biopsies were superimposed on each full field autopsy, and CD34+ measurements were made. These were normalized to the area of either total or active marrow. The mean concentration of HSCs was found to be the same in both simulated biopsies and autopsies, signifying the accuracy in using small fields to measure cellular concentration as a surrogate for larger field of views. Furthermore, horizontal and vertical simulated biopsies were compared independently to assess anisotropy in cellular measurements. Again, no difference was found in both mean and spatial concentration and thus we conclude that there is no directional dependence. This study has shown that a biopsy should provide an accurate assessment of marrow health.

Table 4-1. Pertinent values for each patient in the simulated biopsy study.

Specimen No.			1	2	3	4	5	6	7	8	9	Totals
Age			13	26	47	48	49	55	59	67	75	
Gender			Male	Female	Female	Male	Female	Female	Female	Male	Female	
Cause of Death			Heart Failure	Pulmonary Hypertension	Pulmonary Fibrosis	Blood Clot	Unknown -Suspected Heart Failure	Organ Transplant Failure	Stroke	Renal Failure	Cerebral Hemorrage	
Cellularity (%)	Vertical	Left	68.4%	59.1%	54.1%	90.4%	48.3%	80.7%	82.6%	70.2%	65.5%	n/a
		Middle	70.1%	54.6%	67.1%	86.1%	51.8%	71.3%	88.9%	83.6%	56.1%	n/a
		Right	75.9%	58.6%	61.7%	87.5%	48.3%	67.7%	81.9%	84.3%	40.8%	n/a
	Horizontal	Top	72.1%	51.9%	56.6%	86.3%	55.2%	80.2%	90.3%	73.5%	57.0%	n/a
		Middle	64.8%	59.2%	65.1%	89.5%	45.5%	67.5%	90.2%	78.2%	62.7%	n/a
		Bottom	71.6%	61.5%	58.9%	91.7%	47.2%	67.2%	85.5%	82.8%	58.2%	n/a
Specimen Fractional Weight	Vertical	Left	0.01	0.02	0.02	0.02	0.02	0.02	0.02	0.02	0.02	0.16
		Middle	0.02	0.02	0.02	0.02	0.02	0.02	0.02	0.02	0.02	0.17
		Right	0.01	0.02	0.02	0.02	0.02	0.02	0.02	0.02	0.02	0.17
	Horizontal	Top	0.01	0.02	0.02	0.02	0.02	0.02	0.02	0.02	0.02	0.17
		Middle	0.01	0.02	0.02	0.02	0.02	0.02	0.02	0.02	0.02	0.16
		Bottom	0.01	0.02	0.02	0.02	0.02	0.02	0.02	0.02	0.02	0.17
Total Marrow Area (mm^2)	Vertical	Left	2.31	4.06	3.99	4.13	4.43	3.76	4.04	4.56	3.56	35.27
		Middle	3.33	4.23	4.66	3.84	4.05	3.91	4.37	4.36	3.72	36.46
		Right	2.75	4.19	4.39	4.21	4.48	3.34	4.21	4.07	4.20	35.84
	Horizontal	Top	2.51	4.57	4.27	4.14	4.25	4.52	4.51	4.49	3.89	37.25
		Middle	2.34	4.02	4.08	3.96	4.35	3.50	4.09	4.36	3.54	34.74
		Bottom	2.28	4.13	4.62	4.23	4.47	3.77	3.97	4.43	4.18	36.08
Active Marrow Area (mm^2)	Vertical	Left	1.32	2.40	2.16	3.73	2.14	3.03	3.33	3.20	2.29	24.27
		Middle	2.33	2.31	3.13	3.30	2.10	2.79	3.89	3.64	2.08	25.57
		Right	2.09	2.46	2.71	3.68	2.17	2.27	3.45	3.43	1.71	23.95
	Horizontal	Top	1.38	2.37	2.42	3.59	2.35	3.62	4.07	3.30	2.22	25.82
		Middle	1.34	2.38	2.66	3.55	1.98	2.36	3.69	3.40	2.22	24.08
		Bottom	1.54	2.54	2.72	3.87	2.11	2.54	3.39	3.67	2.43	24.97
Total Cell Count	Vertical	Left	47	69	37	15	35	36	19	33	11	302
		Middle	54	57	25	14	21	22	17	30	6	246
		Right	42	47	12	12	47	26	27	21	9	237
	Horizontal	Top	38	42	14	12	31	21	27	34	6	219
		Middle	65	60	23	7	36	17	14	16	5	253
		Bottom	31	56	38	24	33	26	14	28	11	261

Table 4-2. Specimen fractional weight in total simulated biopsies or horizontal and vertical biopsies.

Specimen No.			1	2	3	4	5	6	7	8	9	Totals
Age			13	26	47	48	49	55	59	67	75	
Gender			Male	Female	Female	Male	Female	Female	Female	Male	Female	
Cause of Death			Heart Failure	Pulmonary Hypertension	Pulmonary Fibrosis	Blood Clot	Unknown -Suspected Heart Failure	Organ Transplant Failure	Stroke	Renal Failure	Cerebral Hemorrage	
Specimen Fractional Weight for Total Simulated Biopsies	Vertical	Left	0.01	0.02	0.02	0.02	0.02	0.02	0.02	0.02	0.02	0.16
		Middle	0.02	0.02	0.02	0.02	0.02	0.02	0.02	0.02	0.02	0.17
		Right	0.01	0.02	0.02	0.02	0.02	0.02	0.02	0.02	0.02	0.17
	Horizontal	Top	0.01	0.02	0.02	0.02	0.02	0.02	0.02	0.02	0.02	0.17
		Middle	0.01	0.02	0.02	0.02	0.02	0.02	0.02	0.02	0.02	0.16
		Bottom	0.01	0.02	0.02	0.02	0.02	0.02	0.02	0.02	0.02	0.17
Specimen Fractional Weight for Horizontal or Vertical Biopsies	Vertical	Left	0.03	0.04	0.04	0.04	0.04	0.03	0.04	0.04	0.03	0.33
		Middle	0.03	0.04	0.04	0.04	0.04	0.04	0.04	0.04	0.03	0.34
		Right	0.03	0.04	0.04	0.04	0.04	0.03	0.04	0.04	0.04	0.33
	Horizontal	Top	0.02	0.04	0.04	0.12	0.04	0.04	0.04	0.04	0.03	0.40
		Middle	0.02	0.03	0.03	0.03	0.04	0.03	0.03	0.04	0.03	0.29
		Bottom	0.02	0.03	0.04	0.04	0.04	0.03	0.03	0.04	0.04	0.31

Table 4-3. Cellular concentration for simulated biopsies versus autopsies in active and total marrow.

		Simulated Biopsy	Autopsy
Cellular Concentration ($cells/mm^2$) Total Marrow	Mean	7.04	7.62
	Error	0.98	1.38
	# Samples	54	9
Cellular Concentration ($cells/mm^2$) Active Marrow	Mean	10.97	12.55
	Error	1.58	2.84
	# Samples	54	9

Table 4-4. Cellular concentration for horizontal versus vertical biopsies in active and total marrow.

		Vertical Biopsy	Horizontal Biopsy	Autopsy
Cellular Concentration ($cells/mm^2$) Total Marrow	Mean	7.30	6.81	7.62
	Error	1.22	1.17	1.38
	# Samples	27	27	9
Cellular Concentration ($cells/mm^2$) Active Marrow	Mean	11.37	10.45	12.55
	Error	1.99	1.88	2.84
	# Samples	27	27	9

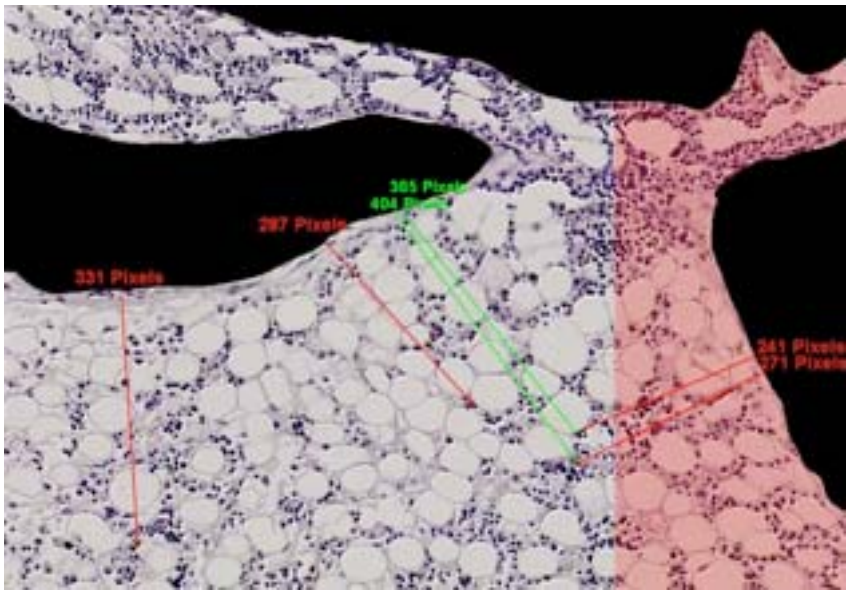

Figure 4-1. Limitations of cell count in biopsies: A biopsy may only show the white portion of the marrow, leading to cell distances being measured incorrectly.

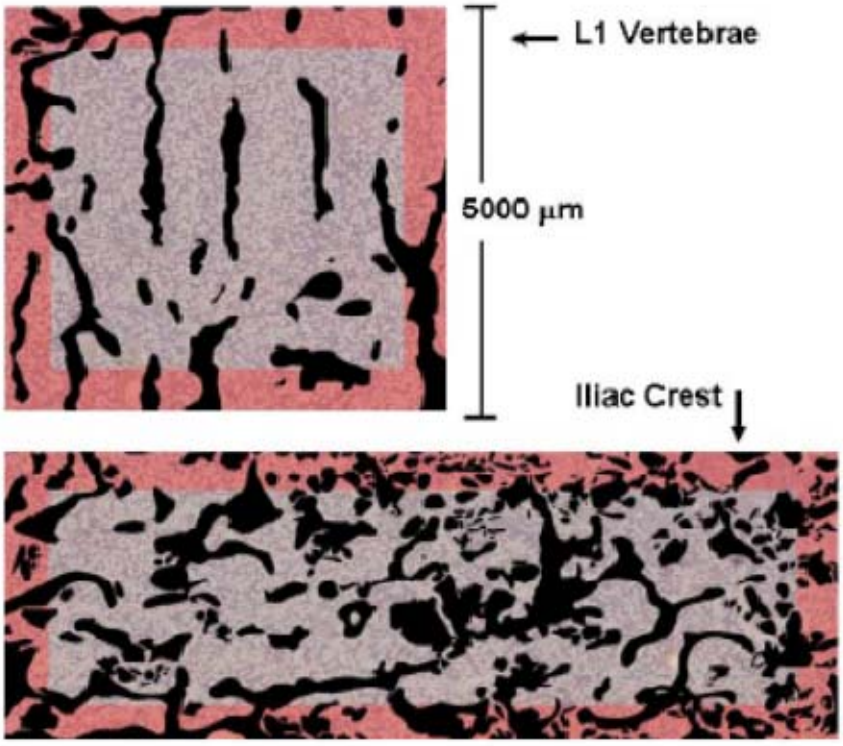

Figure 4-2. The lumbar vertebrae was chosen due to planar symmetry as compared to the illiac crest (Bourke *et al.*, in press).

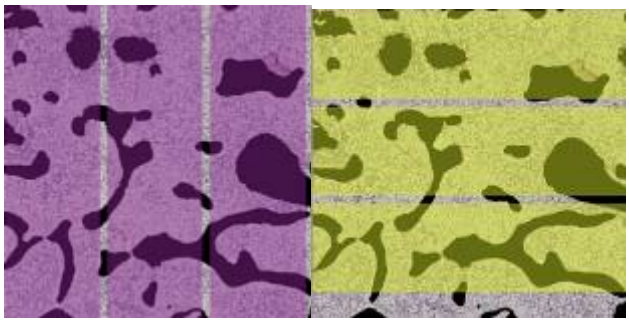

Figure 4-3. Artificial biopsy sections, 3 in the horizonal plane (yellow) and 3 in the vertical plane (purple).

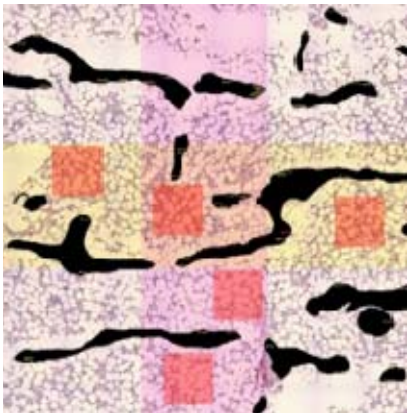

Figure 4-4. Independent cellularity measurements were made for each biopsy (red squares).

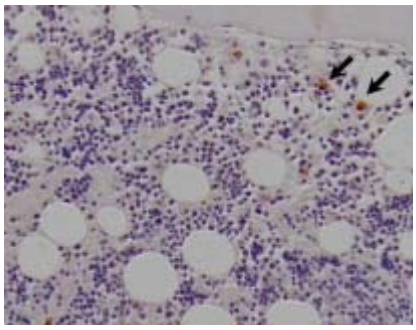

Figure 4-5. Stained CD34+ cells in human bone marrow (Bourke *et al.*, in press).

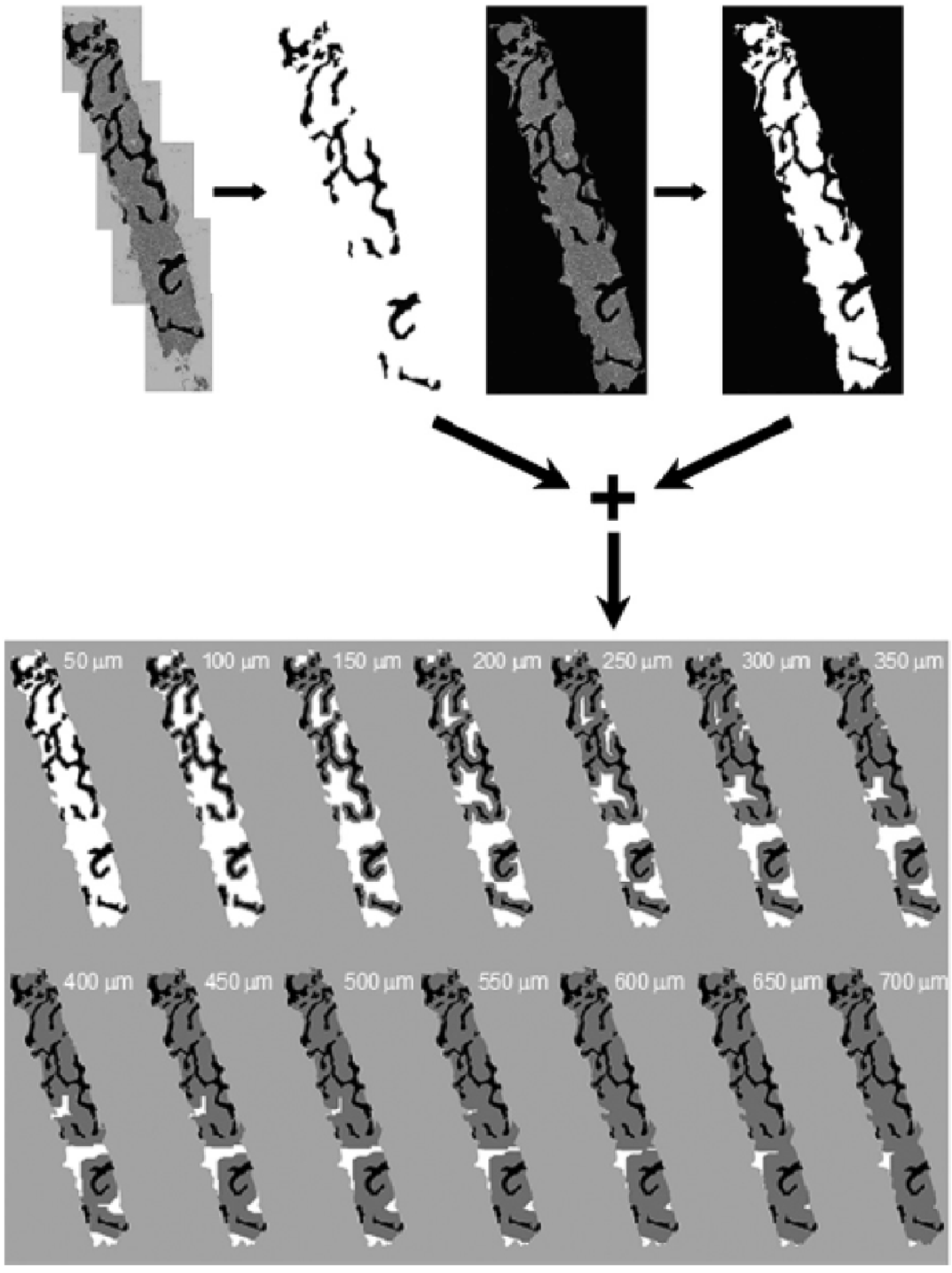

Figure 4-6. Image processing to determine 50µm areal contours from surfaces of bone trabeculae (Watchman *et al.*, 2007).

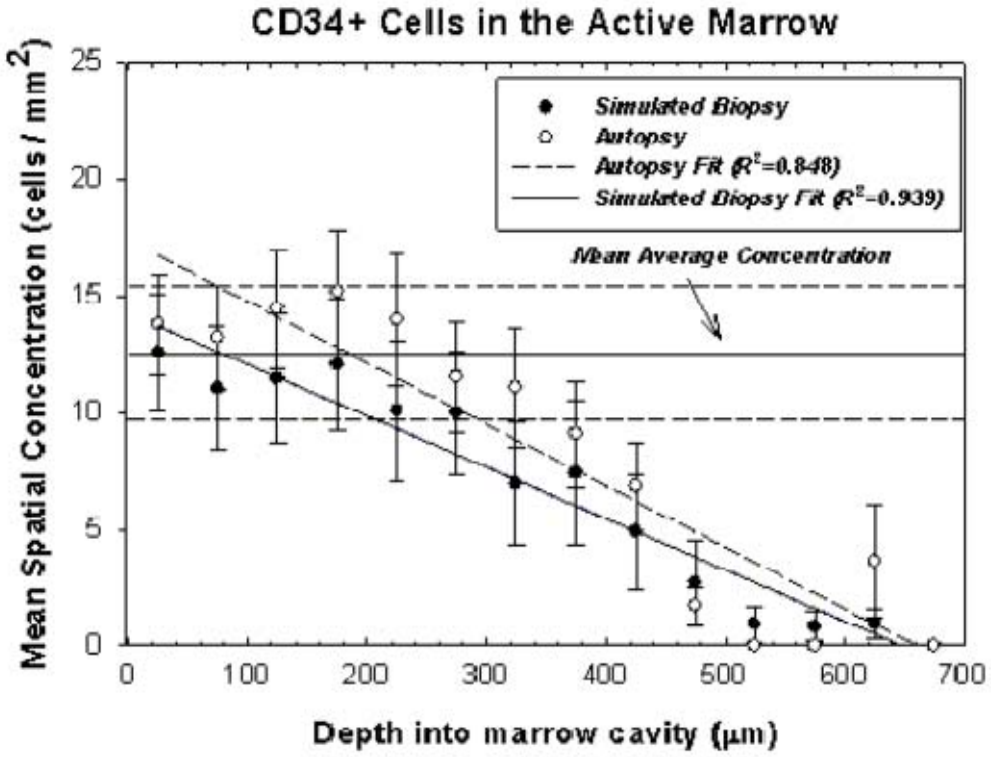

Figure 4-7. Spatial gradient of HSCs in the active marrow in simulated biopsies versus autopsies

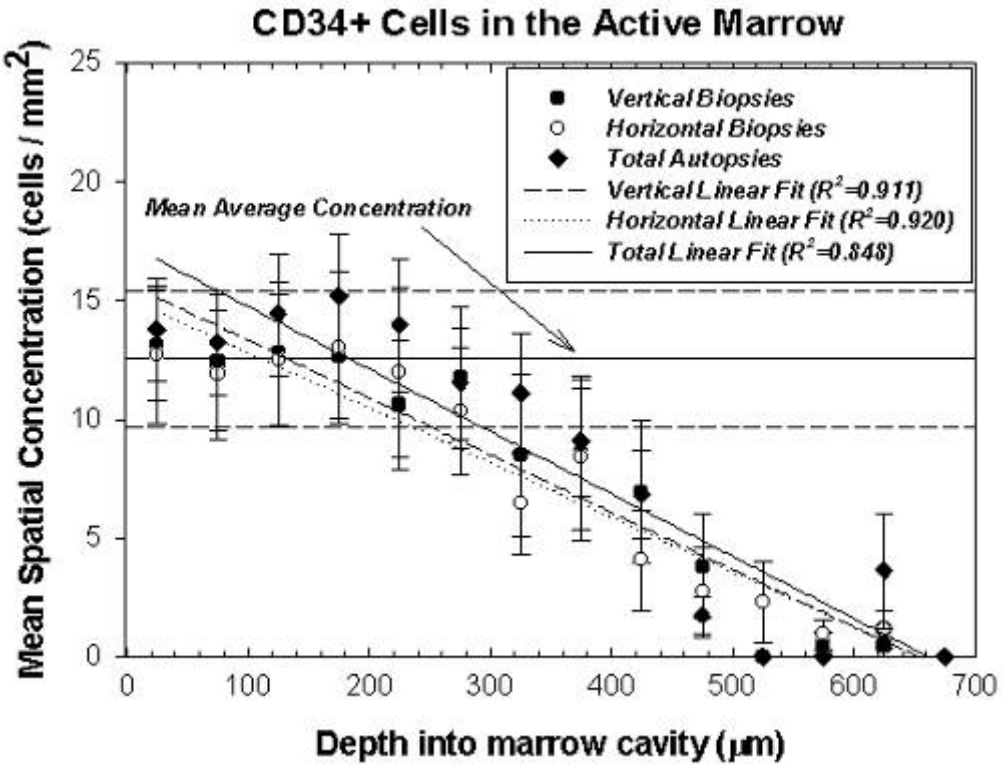

Figure 4-8. Spatial gradient of HSCs in the active marrow for vertical and horizontal biopsies versus autopsies.

CHAPTER 5
EFFECT OF CHEMOTHERAPY ON THE SPATIAL DISTRIBTUION OF STEM CELLS IN HUMAN BONE MARROW

Introduction

To make predictions of radiation dose in patients undergoing targeted radionuclide therapy for cancer, an accurate model of skeletal tissues is necessary. Concerning these tissues, the dose-limiting factor in these therapies is toxicity of the hematopoietically active bone marrow (Sgouros, 1993; Siegel *et al.*, 1990). In addition to acute effects, one must also be concerned with long-term stochastic effects such as radiation-induced leukemia. Cells of particular interest for both toxicity and cancer risk are the hematopoietic stem cells (HSC), found within the active marrow regions of the skeleton (Lim *et al.*, 1997). At present, cellular-level dosimetry models are complex, and thus we cannot model individual stem cells in an anatomic model of the patient. As a result, one reverts to looking at larger tissue regions where these cell populations may reside. Regions of bone marrow exclusive of marrow adipocytes thus serve as surrogate target tissue for underlying radiosensitive cell populations.

The current assumption made in internal radiation dosimetry is that the HSC population is uniformly distributed throughout the marrow cavities of all skeletal sites (ICRP, 1977). Absorbed dose is then averaged through all regions of bone marrow accordingly. Also, the number of target cells is considered to be proportional to the volume of active bone marrow due to a lack of measured data. However, recent studies have shown that a spatial gradient of HSCs may exist in human bone marrow (Watchman *et al.*, 2007). It is proposed that the hematopoietic stem and progenitor cells are preferentially located closer to the bone trabecular surfaces, and decrease in concentration further into the bone marrow cavities. This may cause significant errors in calculating the marrow dose estimates using the current dose-response models for

internal radionuclide therapy since the tissue surrogate (the entire active bone marrow) no longer matches the spatial location of the radiosensitive cells of interest.

In radioimmunotherapy (RIT), radiolabeled antibodies guide the radioactive element to a specific site of interest. For treatment of Non-Hodgkin's lymphoma (NHL), beta sources are used to deliver radiation to abnormal cells in affected body sites. In the process of targeting tumor cells, radiolabeled antibodies come in contact with marrow elements causing radiation damage to diseased and normal cells. All radiolabeled antibodies cause some amount of bone marrow suppression, however the degree of marrow toxicity is difficult to ascertain using current methodology. The inability to predict and modify the degree of marrow toxicity adds significant clinical complexity to utilizing these agents. As a general rule however higher "marrow involvement" with lymphoma, greatly affects radiation dosimetry levels (Martinez-Jaramillo *et al.*, 2004). As the antibody travels to the tumor, a higher concentration will stay in the marrow and the crossfire from cancerous cells to normal cells will be high. Severe myelotoxicity cases as a result of radioimmunotherapy can affect much of the hematopoietic stem cell population. A bone marrow transplant may be required to restore the depleted population in extreme cases.

Systemic therapy, consisting of traditional cytotoxic agents and more recently immunotherapeutic agents such as Rituximab, is the corner stone of front line therapy for non-Hodgkin's lymphoma. External beam radiation therapy is sometimes used in select histological variants and clinical presentations with radioimmunotherapy commonly used in the setting of relapsed or refractory disease. The most commonly used chemotherapeutic regimen for NHL is R-CHOP consisting of Cyclophosphamide, Doxorubicin, Vincristin, and Prednisone, along with the anti CD 20 monoclonal antibody, Rituximab. Rituximab targets B lymphocytes, including abnormal lymphocytes, through the CD20 antigen that is present on their cell surface. While the

traditional cytotoxic agents target all rapidly growing cells including the cancerous cells, Rituximab more specifically targets cells expressing CD20 such as the NHL cells. Some degree of toxicity to normal marrow cells including stem cells is anticipated in all systemic therapies including cytotoxic agents, therapeutic antibodies and RIT.

To provide a more accurate marrow radiation dose assessment, the skeletal dosimetry model must also be patient-specific. That is, it should be designed to match as closely as possible to the patient undergoing treatment. Patients with relapsed NHL, depending on the degree of bone marrow disease involvement and previous therapy, may have variable amounts of marrow reserve including numbers of HSC. Studies have shown hematopoietic alterations in patients with diffuse large-cell lymphoma, with as much as a 35% reduction in progenitor cell numbers (Huerta-Zepeda *et al.*, 2000; Chavez-Gonzalez *et al.*, 2004). Current radioimmunotherapy procedures used for the treatment of lymphoma may result in a large dose to the bone marrow, and will result in increased marrow toxicity if the stem cell population is lower than normal. Additionally, the ability to accurately estimate marrow toxicity from RIT will improve our ability to include these agents in clinical protocols utilizing cytotoxic agents also.

There has been much debate over whether RIT procedures should be used in conjunction with chemotherapy, as well as their use as frontline treatment (Wiseman *et al.*, 2001; Kaminski *et al.*, 2005). Compared to chemotherapy, RIT has the ability to induce apoptosis through radiation damage, a strategy that may prove more effective than current approaches to targeting the CD20 antigen present on lymphocytes. Unfortunately, current internal dosimetry models do not account for any difference in stem cell population due to hematopoietic alterations known to exist in diseased patients during treatment, increasing the difficulty of predicting marrow

toxicity. While it is known that HSC will be disrupted to some degree in all therapeutic regimes, finding the optimal timing based on marrow health is key to successful incorporation of these agents treatment regimens. Thus, not only is it important to accurately model the target tissues of interest in a normal patient, it is important to do so for differing levels of marrow health and among treatment regimes. This study serves to better define the HSC population in NHL patients at diagnosis and after standard chemotherapy and will help establish a more accurate assessment of dose estimates for patients who are candidates for RIT.

Materials and Methods

The overall concentration and spatial distribution of CD34+/CD31- hematopoietic stem and progenitor cells from pre- and post-chemotherapy lymphoma patients was compared to that seen in non-NHL patients. Patients were screened and confirmed to have had CHOP-R or similar treatments, have low or no marrow involvement at diagnosis and in follow up. Twelve patient biopsies pairs - both pre-chemotherapy and post-chemotherapy, were collected, stained for CD34/CD31, mapped and compared to previously acquired measurements provided by Watchman et al (2007). Pathology reports of patients in that study included positive screens for Hodgkin's lymphoma, HIV+, seminoma, CNS lymphoma, ITP, and abdominal mass. Those slides were cleared to have no marrow involvement and were all negative for NHL.

Patient Selection and Slide Preparation

Twelve previously treated B-cell non-Hodgkin's lymphoma patients were identified from the University of Florida Hematological pathology archives under an approved institutional review board protocol. Eight females and four males were enrolled in the study, with ages ranging from 14 to 75 years and confirmed to meet the requirements stated above. Two bone marrow samples, one pre-chemotherapy and one post-chemotherapy, from samples collected as part of their routine were masked of identity and evaluated. All patients were screened for low

marrow involvement, similar chemotherapy regimes, disease status and degree of hematological toxicity after therapy. Most patients received CHOP or CHOP-R or other similar regimens as specified in Table 5-1. Post-chemotherapy biopsies were collected when the patient was determined to be in complete remission, with the timing since pre-chemotherapy biopsy noted. Thus, a total of 24 biopsies were collected: 12 pre-chemotherapy biopsy samples and 12 post-chemotherapy samples (two per patient). Patient data is shown in Table 5-1.

Paraffin blocks were stained for CD34/CD31 using methodology defined in Watchman, et al (2007). As noted, 4mm sections were cut and placed on slides to be dried and freed of all paraffin. Co-staining was preformed, using CD34 antibody (QBend/10 clone prediluted from Ventana) and CD31 antibody (Dako Corp) at a dilution of 1:20. Antigen presence was visually determined using detection kits. Slides were then dehydrated and permanently mounted for further use.

Digital Imaging and Processing

After CD34/CD31 staining, slides were imaged at the University of Florida Molecular Pathology Core using an Aperio ScanScope CS system to provide a digital image of each specimen. Slides were submitted with all identifying marks masked, and viewed via Spectrum software. Using Aperio ImageScope, a region of interest was defined and resolution was verified. Digital images were then stored locally and adjusted based on memory and field of view limitations. A sample co-stained biopsy is shown in Figure 5-1.

Measurement of Hematopoietic CD34+ Cells

Cells were optically identified using an OM36LED contour microscope (Microscope Store, Rock Mount, VA) with a 20x objective as a compromise between field of view and image resolution. SPOT Advanced imaging software (Diagnostic Instruments Inc, Sterling Heights, MI) was used to make distance measurements in pixel units. A CD34+/CD31- (red) cell was

found in the slide under the microscope, and the distance from that corresponding cell to the nearest bone trabeculae was measured on the digital image. Pixel values were then transformed to micrometers using a calibration factor of 1.2 pixels/mm. Histological distance measurements were determined for each patient both before and after chemotherapy and compared to the mean cell count and concentration gradient in previously acquired non-NHL marrow.

Cellularity Measurement

Regions of active bone marrow were determined via manual segmentation of adipocytes using Adobe Photoshop. For each biopsy, a 500 mm x 500 mm location within each bone site deemed visually to be representative of the entire marrow space was confirmed. Three sample locations were averaged for each biopsy. The resulting color image was converted to grayscale, filtered, converted to a binary black and white image, and then pixel counted. The ratio of the final non-zero pixel count to the original image pixel count was used as the precise digital estimate of the amount of total marrow area contributed by the adipocytes population, and is termed the marrow cellularity factor (CF).

Marrow Area Measurement

In order to determine cellular concentration, the area of marrow must be known. First, bone trabeculae was segmented using Adobe Photoshop. Shown in Figure 5-2, each specimen's digital image was converted to grayscale, filtered, and then converted to a binary black and white image. In this image, white and black signify marrow regions and trabecular regions, respectively. Trabecular surfaces were then expanded in 50 mm increments using an in-house edge dilation algorithm developed for use with ImageJ (NIH, Bethesda, MD). Using this data, binned areal measurements were determined for each simulated biopsy through pixel counting of the merged dilated trabecular bone image with the total marrow image. These binned cell counts were normalized to the amount of marrow contributed by each region, yielding cells/mm^2 in 50

μm increments from the bone surface. For each biopsy s, the average cellular concentration is simply the ratio of total number of CD34+ hematopoietic stem and progenitor cells (HSPC) to marrow area for that site:

$$\rho_s^{HSPC} = \frac{N_s^{HSPC}}{A_s}, \tag{5-1}$$

where N is the number of cells and A is the area. This was performed for each 50μm bin, substituting the cell count and subsequent area for that bin. For example, ρ for the first 50μm bin would the number of cells in the first 50μm from all bone trabeculae, divided by the marrow area 50μm from all bone trabeculae in the simulated biopsy.

Cellular concentration of hematopoietically active (red) bone marrow regions were obtained by multiplying total marrow area contributed by each region by its cellularity factor (CF) within the specimen:

$$\rho_{s-active}^{HSPC} = \frac{N_s^{HSPC}}{CF \times A_s}, \tag{5-2}$$

Each specimen's cellular concentration gradient was weighted by its fractional contribution (f_s) to the total marrow area measured in that bone site across all specimens. Specimen-weighted mean cell concentrations and weighted standard deviations of the mean cell concentration were also calculated and plotted at each distance interval, in each bone site. Specifically,

$$\overline{\rho}^{HSPC} = \sum_x f_s \rho_s^{HSPC}, \tag{5-3}$$

The weighted standard deviation is then given as:

$$\sigma_{\overline{\rho}_x}^{HSPC} = \sqrt{\frac{\sum_x f_s \left(\rho_s^{HSPC} - \overline{\rho}_x^{HSPC}\right)^2}{n_x - 1}}, \tag{5-4}$$

where n is the number of samples.

Results

Table 5-1 lists the cellularity, specimen fractional weight, total and active marrow areas, and total cell count for each patient both pre and post-chemotherapy. Mean cellular concentrations are given in Table 5-2, along data used in the statistical analysis. Figure 5-3 plots the spatial gradient of HSCs to compare chemotherapy regime and disease states to non-NHL marrow provided in Watchman et al. Figure 5-4 shows the percent change in HSPC concentration depending on the time between biopsies, and Figure 5-5 shows the cellularity changes for each patient.

Mean Cellular Concentration

In the pre-chemotherapy total marrow, HSPC concentration ranged from 0.46 cells per mm^2 in patient 2 to 16.05 cells per mm^2 in patient 11. Post-chemotherapy showed similar variation, with 1.25 cells per mm^2 in patient 4 and 13.76 cells per mm^2 in patient 12. In the active marrow, pre-chemotherapy HSPC concentration ranged from 0.99 cells per mm^2 in patient 2 to 41.47 cells per mm^2 in patient 11. Cellular concentrations in the active marrow for post-chemotherapy biopsies ranged from 1.48 cells per mm^2 in patient 4 and 26.61 cells per mm^2 in patient 12.

The mean concentration of HSCs in the total marrow among all 12 patients was found to be 5.08 ± 1.13 cells per mm^2 pre-chemotherapy and 5.72 ± 0.93 cells per mm^2 post-chemotherapy. Non-NHL marrow using similar slide preparation and staining methods reports 9.03 ± 1.47 cells per mm^2. In the active marrow, pre-chemotherapy specimens yield 10.18 ± 2.81 cells per mm^2 and post-chemotherapy specimens yield 11.37 ± 2.28 cells per mm^2. There is no reported cell concentration in active marrow for the non-NHL marrow.

Statistical Analysis

A student's t-test reveals that there is a statistically significant difference between both non-NHL marrow and pre-chemotherapy marrow (t=7.38, p=0) and post-chemotherapy marrow (t=6.592, p=0) with a 95% confidence level. However, there is no statistically significant difference between pre and post-chemotherapy marrow for both total marrow (t=1.515, p=0.1372) and active marrow (t=0.1342, p=0.2686).

Spatial Gradient

As shown in Figure 5-3, the CD34+/CD31- cells decreased in concentration as depth into the marrow cavity increased. Specifically, the first 50 μm of diseased marrow comprised 17% of the total bone marrow, and this region contained 42.6% of the HSC population in pre-chemotherapy patients and 46.6% of the HSC population in post-chemotherapy patients. Nearly all cells (88.4% pre-chemotherapy and 87.08% post-chemotherapy) were found within the first 200 μm of total marrow. No CD34+/CD31- cells were found beyond 600 μm of bone trabeculae in diseased marrow. Previously documented non-NHL marrow was best fit to a linearly decreasing trend (R^2=0.935). Both pre and post-chemotherapy data were best fit to an exponentially decreasing model (R^2=0.988 and R^2=0.990, respectively).

Discussion

The data presented in Figure 5-3 confirms previous findings of a spatial gradient in human bone marrow for NHL patients. In both pre and post-chemotherapy lymphoma patients, a higher concentration of cells is seen close to the bone trabeculae, which decreases with depth into the marrow cavities. Thus, a larger proportion of cells are prudentially located in the first 50 μm from bone surfaces, and a more specialized surrogate for marrow toxicity would be to assume a spatial gradient instead of a single value. Furthermore, red bone marrow dose should not be simply averaged over marrow cavities as is currently assumed, and should instead be weighted

by the fractional weight of HSPC present as noted by Watchman et al (2007). This would provide a more accurate prediction of marrow toxicity than is currently performed.

Comparison to non-NHL Marrow

The mean cellular concentration of the 12 pre-chemotherapy lymphoma patients in this study was found to be less than the non-NHL marrow (5.08 versus 9.03 cells per mm^2, respectively). This result was statistically significant with 95% confidence, signifying a real decrease in the average HSC population in NHL patients when compared to non-NHL. The same spatial gradient was seen in non-NHL, however more pronounced and following an exponential instead of linear fit. It seems there may be a higher population of stem cells in post-chemotherapy diseased marrow within the first 50μm from bone surfaces when compared to non-NHL, although the reason for this is not fully understood. It is speculated that this may be HSC translocation and repopulation of the bone marrow niche during hematopoietic recovery.

Possible decreases in progenitor cell counts due to malignant lymphoma has been confirmed in studies as far back as 2000 (Huerta-Zepeda *et al.*, 2000). In that study, the composition and function of the hematopoietic microenvironment was found to be compromised in the presence of diffuse large-cell lymphoma. Specifically, a 35% reduction in progenitor cell numbers was found. In the present study, a 44% reduction in hematopoietic stem and progenitor cells is noted. While the presence of deficiencies in the hematopoietic system is noted in lymphoma patients, the reason for this is still not fully understood.

Further studies were made to determine whether the alterations in the hematopoietic microenvironment were due to an intrinsic defect in the progenitor cell compartment of lymphoma patients, or to an altered microenvironment altogether. It was found that the expansion ability of the hematopoietic progenitor cells to produce new cells capable of forming hematopoietic colonies was limited in lymphoma patients (Martinez-Jaramillo *et al.*, 2004).

Interestingly, most patients showed normal hematological parameters even though they had reduced progenitor cell numbers. It is speculated that while the expansion process is deficient, proliferation is not and normal numbers of mature blood cells can be maintained. This may suggest an intrinsic deficiency in the hematopoietic stem cells themselves in lymphoma or possibly the presence of a paraneoplastic mechanism causing depression of HSC during the development of lymphoma. Moreover, recent studies have also indicated that molecular alterations are present in hematopoietic precursers, mature cells, as well as primitive HSCs, some of which may be morphologically recognizable (Madrigal-Velazquez *et al.*, 2006; Chavez-Gonzalez *et al.*, 2004). Still other studies have shown a possible microenvironment defect as well as the well established inherent flaw in expansion potential (Soligo *et al.*, 1998).

Effect of Chemotherapy

Chemotherapy was found to have no affect on the mean concentration of HSCs, and there was no statistical difference when comparing pre and post-chemotherapy biopsies among the 12 patients. Thus, it is believed that chemotherapy regime did not affect the stem cell population when averaged over all patients. Previous studies by Huerta et al (2000) also found that hematopoietic alterations were still present in patients at complete clinical remission after chemotherapy.

It has been shown that a large heterogeneity exists in the response of progenitor cell growth after chemotherapy. In studies by Martinez-Jaramillo et al (2004), of 24 patients, 8 patients had reduced progenitor cell numbers, 11 showed an increase in progenitor cells, and 5 showed no difference. There was no correlation found, however, between the change in progenitor cell number and clinical outcome. In the present study, a decrease in the HSC population post-chemotherapy occurred only in patients 4, 6, 9, and 11. All 8 other patients had higher HSC counts after chemotherapy, thus a similar heterogeneity was found. It has also been

noted that after 18 months of chemotherapy and clinical remission, normal progenitor cell proliferation and expansion is expected leading to an indication of normal hematopoietic function (Yao *et al.*, 2000).

Timing Effect

The percent change in average areal concentration versus the timing between pre and post-chemotherapy patients is shown in Figure 5-4. Positive values indicate a higher number of cells post-chemotherapy. It appears that there is a greater change in the number of stem cells per area when the time between both pre and post chemotherapy is small. There was a decrease in HSCs post-chemotherapy in patients 4, 6, 9, and 11. An increase in HSCs post-chemotherapy was seen for Patients 2, 3, 5, 7, 8, 10 and 12. However, no consistent trend has been found to suggest a reason for such changes in HSC population. Similar heterogeneity post-chemotherapy has been previously found, and marrow only seems to return to normal after 18 months of clinical remission (Martinez-Jaramillo *et al.*, 2004; Yao *et al.*, 2000).

Effect on Cellularity

Cellularity is used to determine the amount of fat in the marrow, where 100% cellularity indicates purely active marrow and 0% cellularity indicates entirely fatty marrow. Bone marrow cellularity has been noted to increase as a result of damage to the hematopoietic microenvironment (Jensen *et al.*, 1990; Orazi *et al.*, 1992). Thus, patients with lymphoma seem to have a higher fat content (lower cellularity) than that found in normal marrow at diagnosis, which increases with treatment. However, studies have shown that this decrease in fat content and subsequent increase in hematopoietic tissue subsides once the patient is in remission, and a higher cellularity indicates a normal hematopoietic microenvironment (Moulopoulos and Dimopoulos, 1997).

In the present study, cellularity was found to be lower than the normal value of 48% (Cristy, 1981) for 6 of 12 patients pre-chemotherapy. Fat fraction ranged from 30.6% for patient 7 to 80.4% for patient 8. As expected, cellularity increased or stayed the same post-chemotherapy for 10 of 12 patients, as shown in Figure 5-5. Interestingly, the two patients who did not have an increase in hematopoietic tissue post-chemotherapy were patients 3 and 8 whom both had experimental (non CHOP) treatments.

Dose Implications

Radioimmunotherapy guarantees some amount of marrow toxicity since there is no specific marker to target only diseased cells. If the radiopharmaceutical is uniformly distributed throughout the marrow, absorbed dose would accurately be measured by averaging the dose over marrow cavities, as all radiosensitive cells would receive the same radiation dose. This is what is implicitly assumed in current dosimetry methods to predict marrow toxicity. However, radiopharmaceuticals that localize on bone surfaces (non-uniform distributions) would result in higher marrow toxicity, as this is the preferential location of the radiosensitive cell population. In this case, absorbed dose should not simply be averaged over the marrow cavities, but should instead to weighted by the amount of cells at individual locations throughout bone marrow, as proposed by Watchman et al (2007).

Lymphoma patients have shown to have less radiosensitive cells in the red bone marrow overall when compared to non-NHL marrow, with no changes in HSC population due to chemotherapy. This signifies that (1) marrow toxicity may be inherently higher in NHL patients simply due to hematopoietic alterations, and (2) chemotherapy does not seem to affect the hematopoietic environment negatively and does not seem to result in marrow toxicity as a function of HSC death. For radioimmunotherapy, the timing or nature of previous chemotherapy regimens appears to be less important to numbers of HSC although the numbers of more

differentiated progenitors were not evaluated in our study. However, care should be taken in general when predicting absorbed dose in lymphoma patients, as current methods do not assume preferential location or a lower concentration of the radiosensitive cell population.

Conclusion

This paper serves to determine the mean concentration and spatial gradient in NHL patients to provide a better prediction of marrow toxicity. The effect of chemotherapy on the bone marrow was also explored due to its common use with radioimmunotherapy. Twelve patients with diffuse, non-Hodgkin's lymphoma undergoing chemotherapy were studied both before and after treatment. It was found that the mean concentration of HSCs was lower in NHL patients when compared to marrow from patients without NHL, and did follow a spatial gradient whereby cell concentration decreased with depth into marrow cavities. Chemotherapy was found to have no negative effect on the HSC population. Thus, current procedures used to predict marrow toxicity should be updated to include a spatial gradient and inherently lower HSC concentration. It is hoped that this will help better estimate marrow toxicity in diseased marrow

Table 5-1. Pertinent data for all 12 patients, in both pre and post-chemotherapy biopsies.

Specimen No.		1	2	3	4	5	6	7	8	9	10	11	12	Totals
Age		48	75	55	45	24	65	25	14	30	70	47	15	
Gender		Female	Female	Female	Female	Female	Male	Female	Male	Female	Female	Male	Male	
Disease		Large B-cell non-Hodgkin's Lymphoma	Large B-cell non-Hodgkin's Lymphoma	Follicular B-cell non-Hodgkin's Lymphoma	Mantle B-cell non-Hodgkin's Lymphoma	Large B-cell non-Hodgkin's Lymphoma	Large B-cell non-Hodgkin's Lymphoma	Large B-cell non-Hodgkin's Lymphoma	Large B-cell non-Hodgkin's Lymphoma	Large B-cell non-Hodgkin's Lymphoma	Large B-cell non-Hodgkin's Lymphoma	Large B-cell non-Hodgkin's Lymphoma	Large B-cell non-Hodgkin's Lymphoma	
Treatment		CHOP-R x 8 RICE	CHOP-R x 6	Cytoxan Vincristine Prednisone Fludarabine/ Interferon	Leukeran/ Prednisone CHOP-R x 6	CHOP x 4 XRT CHOP-R x 5 ICE x 1	CHOP x 3 XRT RICE x 3	CHOP x 4 XRT VP-16/ Rituxan x 3	XRT Trial Rituximab Rasburicase	CHOP-R x 6 XRT RICE x 2	CHOP-R x 3	CHOP-R x 6 RICE x 2	Cyclophos-phamide Rituximab x 5	
Time Between Biopsies		14 months	4 months	5 months	44 months	52 months	23 months	10 months	11 months	10 months	2 months	9 months	5 months	
Cellularity (%)	*Pre-chemotherapy*	54.3%	46.9%	47.5%	86.4%	79.2%	59.1%	30.6%	80.4%	50.2%	52.9%	38.7%	46.8%	n/a
	Post-chemotherapy	86.1%	61.5%	22.8%	84.1%	77.5%	67.0%	50.4%	39.1%	53.1%	65.0%	55.8%	51.7%	n/a
Specimen Fractional Weight	*Pre-chemotherapy*	0.10	0.05	0.13	0.07	0.10	0.06	0.08	0.05	0.10	0.13	0.05	0.07	1.00
	Post-chemotherapy	0.10	0.12	0.11	0.09	0.10	0.05	0.06	0.04	0.08	0.08	0.11	0.07	1.00
Total Marrow Area (mm^2)	*Pre-chemotherapy*	18.13	8.63	23.10	12.18	18.04	10.85	13.99	9.14	17.50	22.55	9.65	13.10	176.84
	Post-chemotherapy	21.97	27.07	24.92	20.86	21.54	10.47	12.41	8.07	18.67	16.87	23.63	15.26	221.73
Active Marrow Area (mm^2)	*Pre-chemotherapy*	9.83	4.05	10.97	10.52	14.28	6.41	4.28	7.35	8.78	11.92	3.74	6.13	98.26
	Post-chemotherapy	18.92	16.64	5.68	17.55	16.70	7.01	6.25	3.16	9.92	10.96	13.17	7.89	133.86
Total Cell Count	*Pre-chemotherapy*	83	4	105	38	35	38	12	54	164	68	155	142	898
	Post-chemotherapy	*157*	*114*	*133*	*26*	*52*	*16*	*37*	*66*	*141*	*124*	*192*	*210*	1268

Table 5-2. Mean cellular concentration and error for both normocellular and diseased marrow.

		non-NHL	NHL	
			Pre-Chemo	Post-Chemo
Cellular Concentration (Total Marrow)	Mean	9.03	5.08	5.72
	Error	1.47	1.13	0.93
	# Samples	12	12	12
Cellular Concentration (Active Marrow)	Mean		10.18	11.37
	Error		2.81	2.28
	# Samples		12	12

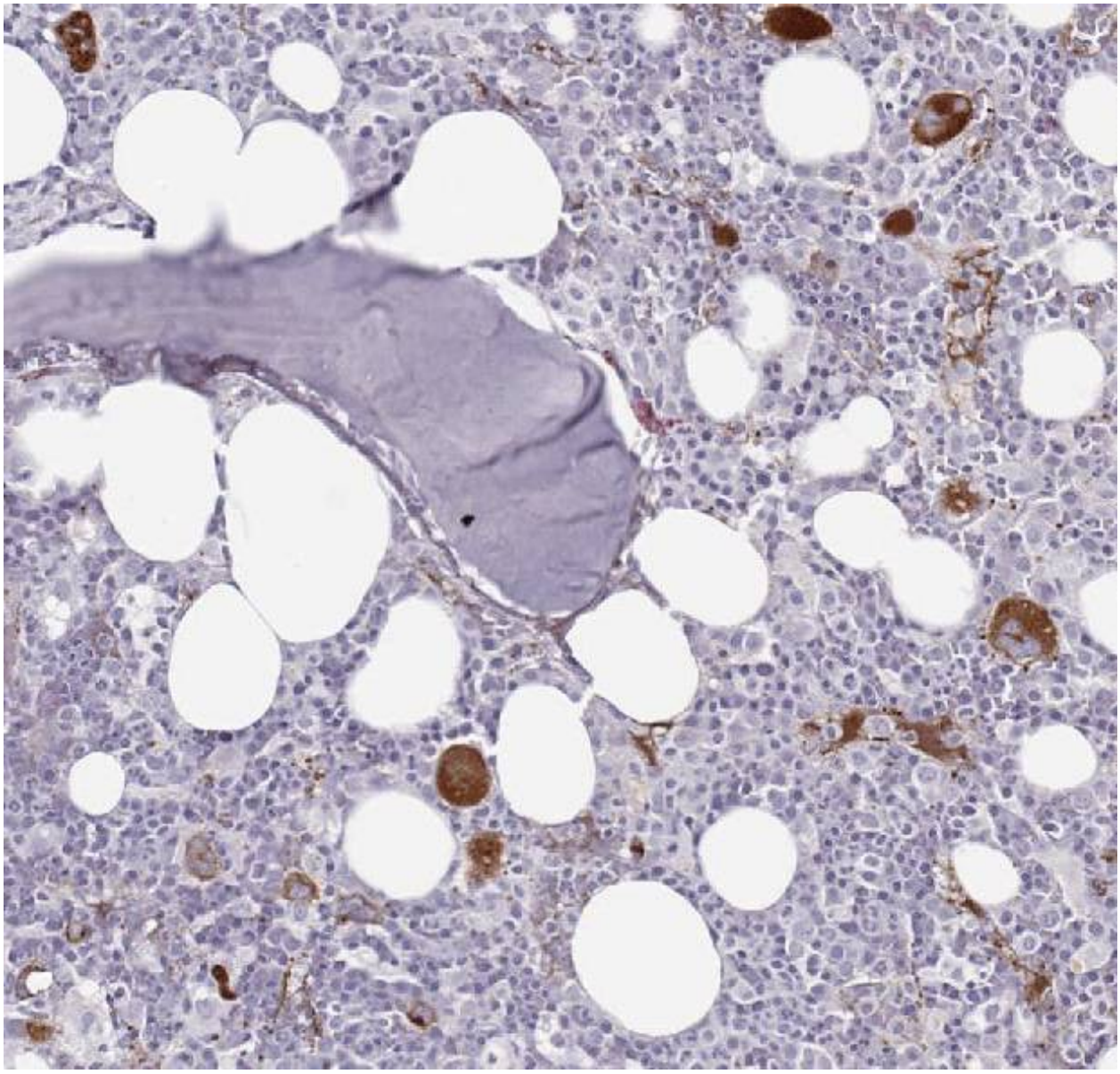

Figure 5-1. Co-stained biopsy showing CD34+/CD31- (red) hematopoietic stem and progenitor cells and CD34+/CD31+ (brown) endothelial tissue.

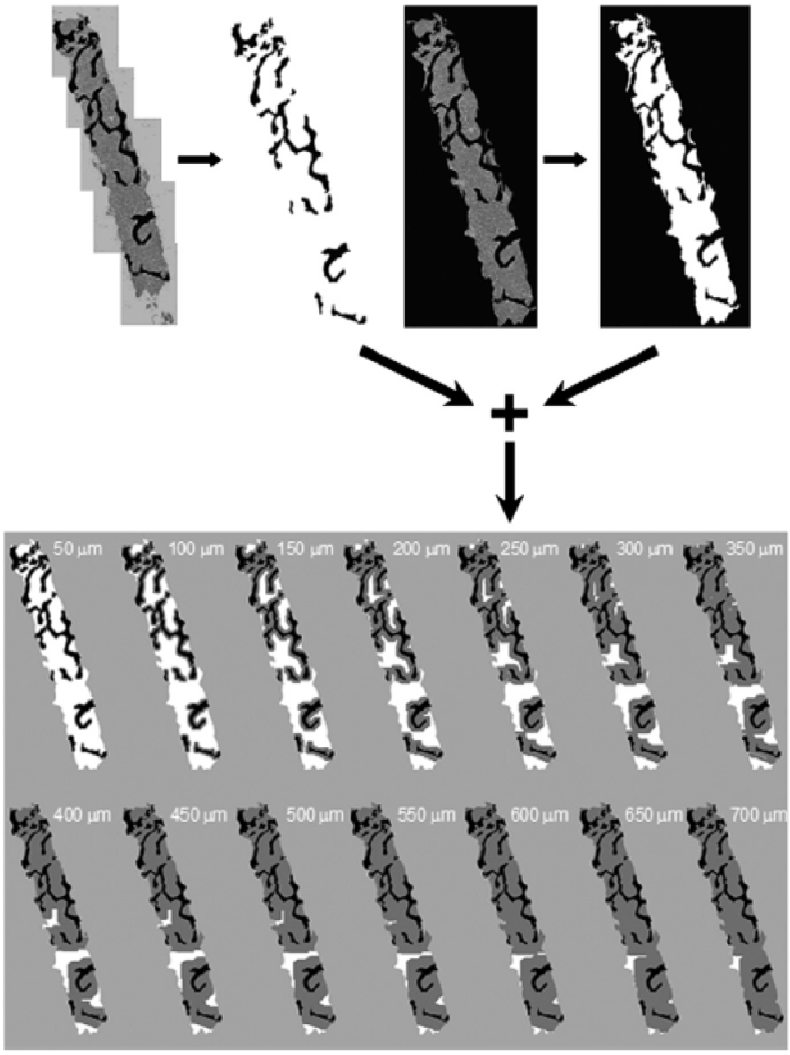

Figure 5-2. Binary digital images of total marrow (white) and trabeculae (black) are combined and trabeculae are expanded to determine area of marrow in 50 µm bins (Watchman *et al.*, 2007).

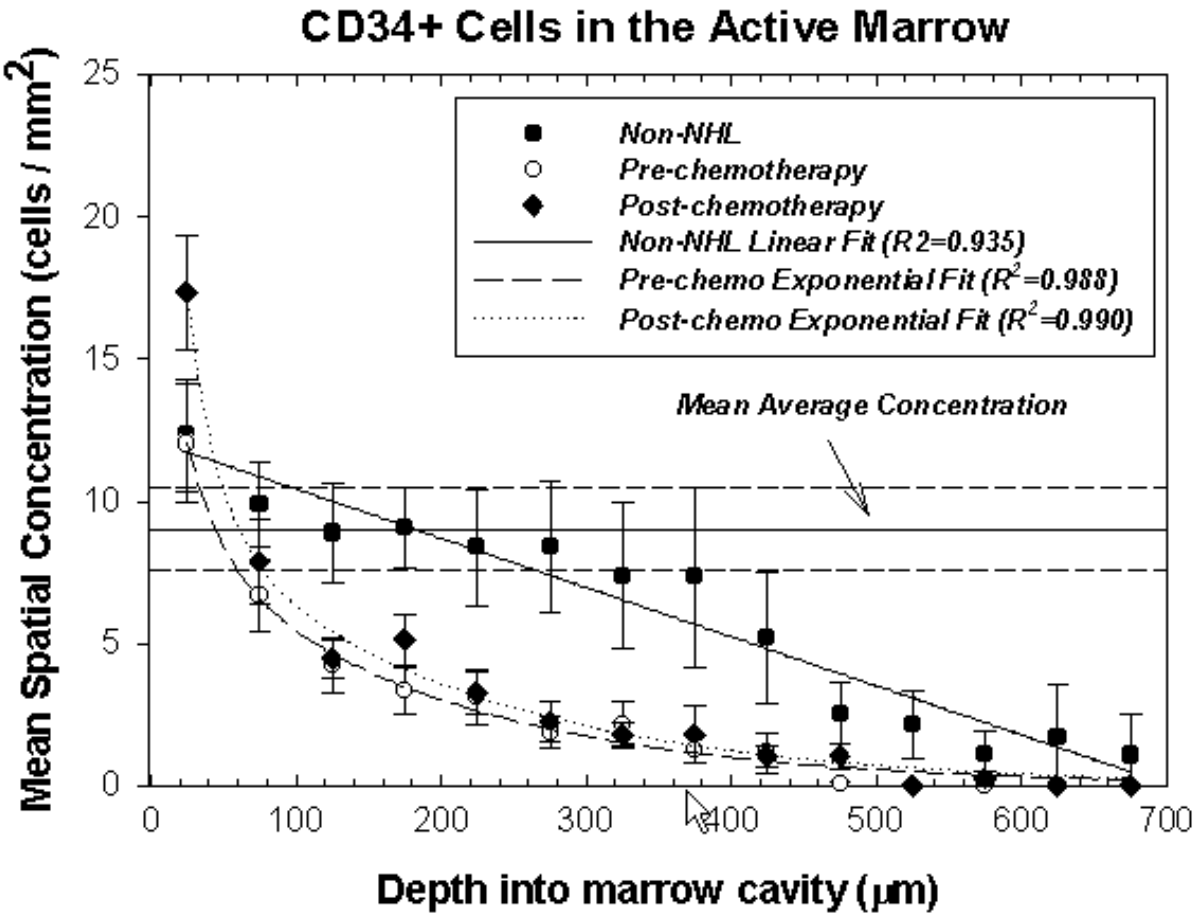

Figure 5-3. CD34+ cell concentration as a function of depth into marrow cavities.

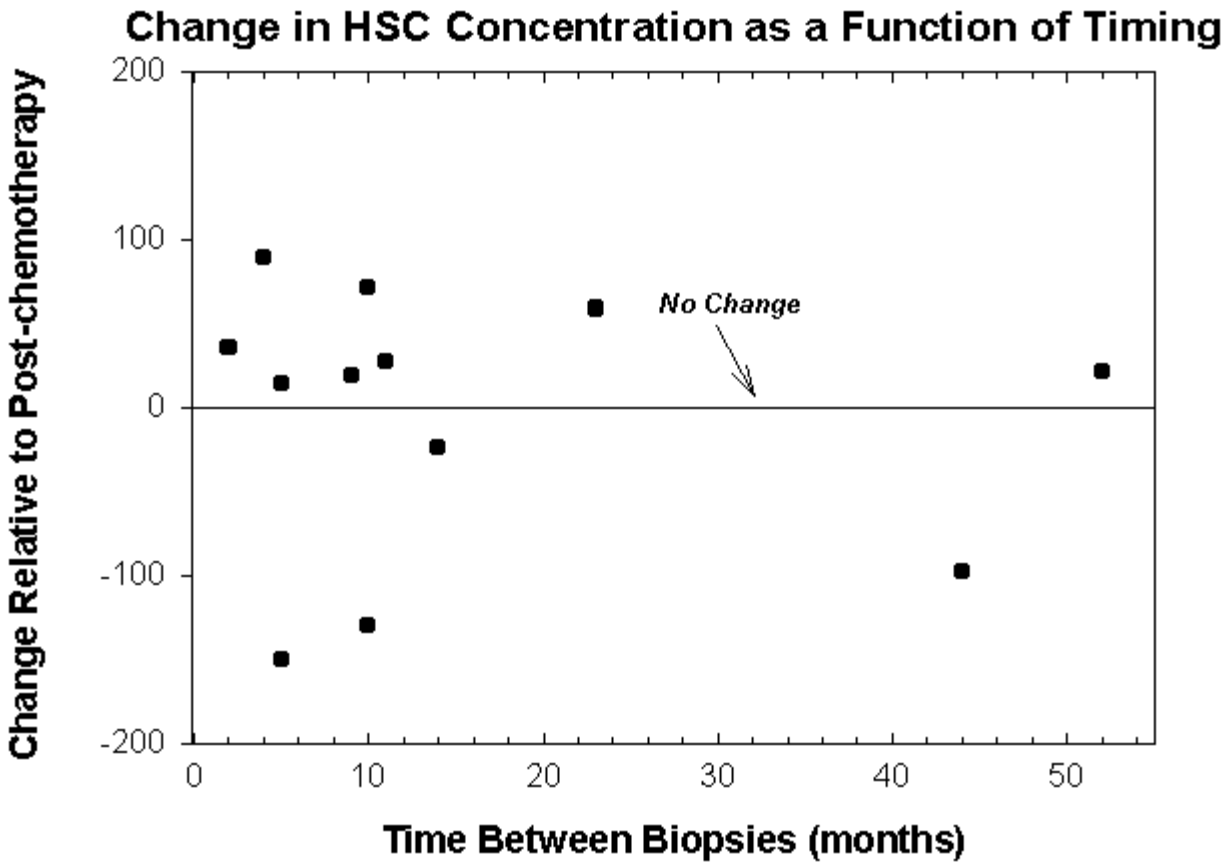

Figure 5-4. Change in HSC concentration as a function of time between biopsies.

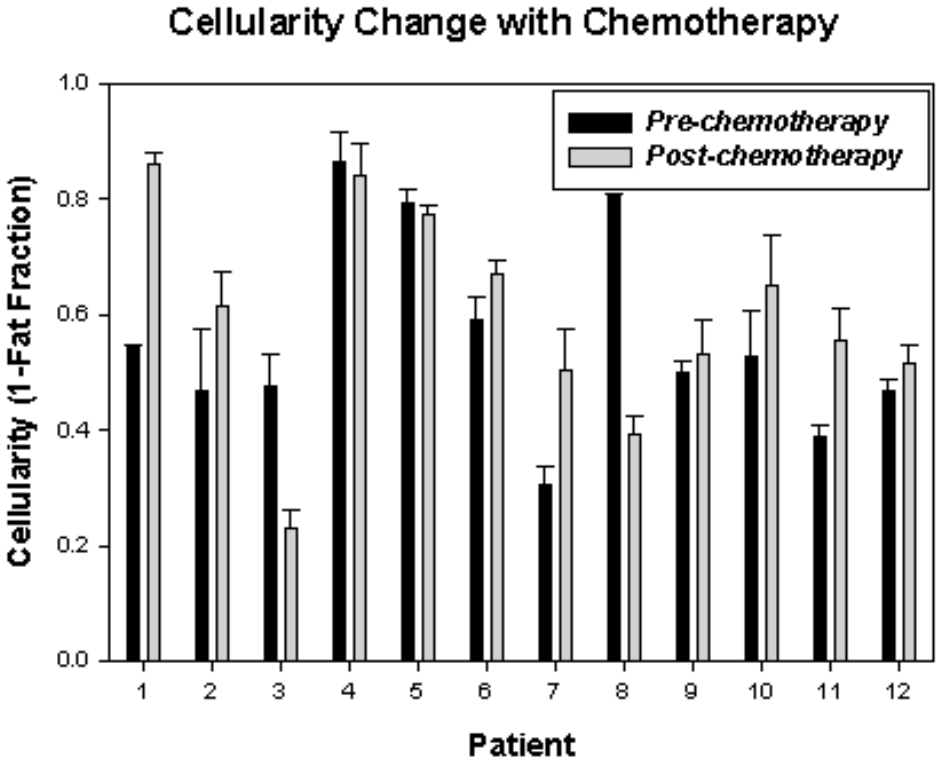

Figure 5-5. Cellularity changes before and after chemotherapy.

CHAPTER 6
CONCLUSIONS AND FUTURE WORK

Conclusions

To predict the risk of bone cancer, an accurate assessment of skeletal tissues is necessary. This requires both a patient specific model of the active marrow, as well as proper modeling of the location and concentration of radiosensitive cells. The individual patients skeletal structure must be known on a macrostructural scale (correct skeletal size) and a microstructural size (trabecular structure). Furthermore, the osteoprogenitor cell and hematopoietic stem cell populations must be accurately known for realistic absorbed dose estimates. In radioimmunotherapy, little work has been done to determine these factors. Also, there are no models to date that assess the differences in gender for patient specific assessments of radiation absorbed dose.

Current ICRP models used to predict radiation dose and toxicity rely on a Reference Man model that is outdated and unsalable. Skeletal factors such as marrow masses and cellularities come from several independent sources dating back to 1926 (Custer, 1974; Trotter and Hixon, 1974; Mechanik, 1926). Moreover, absorbed fractions are based on 2D optical scanning methods of only seven bone sites (Whitwell, 1973). Perhaps the most striking problem is the inability of scaling to tailor absorbed fractions and S values to specific patients. Recent work has also shown that ICRP tissue definitions for the endosteum may be incorrect, and may require increasing the size of the radiosensitive region from 10 μm to 50 μm (Bolch *et al.*, 2007). Furthermore, studies have identified a spatial gradient in the hematopoietic stem cell leading to inaccuracies in current dose estimates which rely on methodologies that average absorbed dose over marrow cavities (Watchman *et al.*, 2007). These methods also assume normal bone marrow

in terms of the concentration and location of stem cells, which is unrealistic of patients undergoing radioimmunotherapy.

Chapter 3 provides a complete skeletal mass database for a reference female model to be used to provide a patient specific scalable model for accurate dose assessment in radiation protection and medical applications. No model for a female subject has previously been given, and this paper serves to provide a companion skeletal reference model to the adult male. The mass database comes from actual macrostructural patient data (ex-vivo CT) as well as accurate trabecular structure (microCT). Specific absorbed fractions are provided using Paired Image Radiation Transport, where the macrostructure and microstructure of the actual, same patient is combined (Shah *et al.*, 2005b). Hopefully, this model will be used to better assess dose estimates of the female population.

Biopsies are widely used to assess blood disease, and their usefulness for predicting marrow health was explored in Chapter 4. In that study, it was determined whether hematopoietic cellular distributions found in biopsy specimens would yield the same result that would have been found had a larger field of view been used. Also, possible directional dependence (anisotropy) in the hematopoietic stem cell concentration was discussed. The mean concentration of HSCs was found to be the same in both simulated biopsies and autopsies, signifying the accuracy in using small fields to measure cellular concentration as a surrogate for larger field of views. Furthermore, no anisotropy was found, signifying that a biopsy should provide an accurate assessment of marrow health.

Chapter 5 served to determine the mean concentration and spatial gradient in lymphoma patients to provide a better prediction of marrow toxicity. The effect of chemotherapy on the bone marrow was also explored due to its common use with radioimmunotherapy. It was found

that the mean concentration of HSCs was lower in lymphoma patients when compared to normocellular marrow, and did follow a spatial gradient whereby cell concentration decreased with depth into marrow cavities. Chemotherapy was found to have no negative effect on the HSC population. Thus, current procedures used to predict marrow toxicity should be updated to include a spatial gradient and inherently lower HSC concentration. It is hoped that this would help better estimate marrow toxicity in diseased marrow.

Future Work

This dissertation enhances work already performed in the ALRADS group at the University of Florida, and allows room for further applications. Specifically, improvements in the skeletal database can be made by adding more reference individuals of varying skeletal health through use of PIRT for 3D radiation transport. Also, reference S values can be determined for the reference female model for several radionuclides of interest in current therapeutic regimes. Then, clinical applications through scalability are achievable. Lastly, cellular measurements can be improved for faster and more realistic determinations of concentrations and gradients.

Improvements in Skeletal Database

The current skeletal database of UF reference individuals now consists of a male and female cancer patient, but needs to be expanded to include more individuals of varying skeletal health. The trabecular microstructure is known to change with age, thus to accurately predict absorbed dose for an individual, age related changes should available in our database (Atkinson, 1965). Perhaps more prevalent is the known changes in trabeculae with osteoporosis, signifying the need for individuals with varying skeletal health (Berne, 1993). Studies have also shown changes in bone mineral density with menstruation status, with a markedly larger population of women with osteoporosis post-menopause (Yao *et al.*, 2001). Thus, it is proposed that future

reference individuals for women are assembled based on menopausal status instead of age. Building a library of trabecular microstructures and skeletal macrostructures, one will be able to "mix and match" images for more patient specific scaling. Work is currently underway in the ALRADS group for younger reference subjects including pediatric patients. Furthermore, new methods of modeling such as 'hybrid' phantoms that combine both the realistic anatomy of voxel phantoms and flexibility of stylized phantoms are realized.

Reference S Values for UFRF

Current methods of assessing absorbed dose require knowledge of the cumulated activity and radionuclide S value through the MIRD schema. The S value is the dose received by they target organ per disintegration in the source, and depends on the absorbed fraction, mass of the target tissue, and the mean energy emitted for the radionuclide used in therapy. These values should be assembled for the reference female model for several radionuclides used in current therapeutic regimes. Possible radionuclides to be used should include P-33, Sm-153, Sr-89, P-32, Y-90, and I-131. After averaging over all skeletal sites, S values should be compared to those currently in use.

Improvements in Cellular Measurements

To alleviate the time to count CD34+ cells, fluorescent staining should be used to eliminate use of visually defining positive cells in the microscope. Using this method, several stains can be applied at once to decrease the chance of falsely selecting a co-stained (brown) cell as a stem cell (red). With sufficient code writing, this will also allow for automation in measurements from cells to the nearest bone trabeculae. Most notably, work should be performed to develop 3D models of bone marrow to reduce errors induced by edge effects. The use of fiducially markers, novel imaging techniques, and software development should be explored to co-register the z plane in biopsies. Moreover, more patients should be enrolled for both normal and diseased

patients to increase reliability and allow for age and gender assessments of the hematopoietic stem cell lines. Variation in spatial gradient with bone site is recognized, but further investigations would more conclusively evaluate any bone site dependence (Bourke *et al.*, in press). Lastly, the osteoprogenitor cell population should be studied to better define the region of the endosteum for better predictions of cancer risk.

Scalability and Clinical Applications

The absorbed fractions, masses, and S values from this work lends itself well to better estimates of absorbed dose in clinical applications, but only if the models are conveniently scalable. Studies have been made to predict and scale spongiosa volumes and masses and using statistical methods (Brindle *et al.*, 2006b; Brindle *et al.*, 2006c; Pichardo *et al.*, 2007). However, these methods are not feasible on a large scale and software development is necessary. Using image based software, a quick pelvic CT scan of a radionuclide therapy patient could estimate patient specific S values almost immediately. Furthermore, image based measurements of marrow cellularity will allow for active marrow to be known in that radioimmunotherapy patient for a better prediction of marrow toxicity.

APPENDIX A
TABLES OF SPECIFIC ABSORBED FRACTION

This appendix tabulates values of Specific Absorbed Fraction (SAF) for UFRF for any combination of source (TAM, TBS, TBV, TAM_{50}, TIM) and target (TAM, TAM_{50}) regions in the entire skeleton containing active marrow for a range of cellularities (10% to 100%). Absorbed Fraction (AF) values were normalized to the mass of the target (and cellularity) to report SAF. For the TAM irradiating the TAM, marrow cellularity is varied. For all sources irradiating the TAM or $TAM_{50,}$ ICRP reference cellularity is used.

Table A-1. UFRF absorbed fraction for all sources irradiating the active marrow in the cranium.

Cranium ϕ (TAM← TAM) Cellularity												Cranium ϕ (TAM← r_s) Source Tissue r_s			
Energy (MeV)	100%	90%	80%	70%	60%	50%	40%	30%	20%	10%	38% (ICRP 70)	TIM	TBS	TBV	CBS_{HC} or CBV
0.010	2.01E-02	2.23E-02	2.50E-02	2.85E-02	3.32E-02	3.97E-02	4.96E-02	6.58E-02	9.84E-02	1.96E-01	5.20E-02	5.45E-04	1.08E-02	3.15E-05	7.74E-07
0.015	2.00E-02	2.21E-02	2.47E-02	2.81E-02	3.26E-02	3.89E-02	4.84E-02	6.42E-02	9.57E-02	1.90E-01	5.09E-02	1.10E-03	1.08E-02	6.06E-05	1.70E-06
0.020	1.99E-02	2.19E-02	2.44E-02	2.77E-02	3.20E-02	3.80E-02	4.71E-02	6.22E-02	9.24E-02	1.83E-01	4.95E-02	1.82E-03	1.07E-02	1.02E-04	2.77E-06
0.030	1.96E-02	2.14E-02	2.36E-02	2.65E-02	3.03E-02	3.57E-02	4.37E-02	5.71E-02	8.39E-02	1.64E-01	4.58E-02	3.59E-03	1.06E-02	2.06E-04	5.93E-06
0.040	1.92E-02	2.07E-02	2.26E-02	2.51E-02	2.84E-02	3.29E-02	3.98E-02	5.12E-02	7.40E-02	1.43E-01	4.16E-02	5.63E-03	1.04E-02	3.31E-04	1.02E-05
0.050	1.88E-02	2.00E-02	2.16E-02	2.36E-02	2.62E-02	3.00E-02	3.56E-02	4.49E-02	6.36E-02	1.20E-01	3.71E-02	7.77E-03	1.02E-02	4.78E-04	1.53E-05
0.060	1.83E-02	1.93E-02	2.05E-02	2.21E-02	2.41E-02	2.71E-02	3.14E-02	3.87E-02	5.33E-02	9.70E-02	3.26E-02	9.81E-03	1.00E-02	6.33E-04	1.99E-05
0.080	1.73E-02	1.79E-02	1.86E-02	1.94E-02	2.06E-02	2.22E-02	2.46E-02	2.86E-02	3.66E-02	6.05E-02	2.52E-02	1.28E-02	9.55E-03	9.63E-04	3.26E-05
0.10	1.64E-02	1.67E-02	1.71E-02	1.77E-02	1.84E-02	1.93E-02	2.08E-02	2.32E-02	2.79E-02	4.22E-02	2.12E-02	1.37E-02	9.10E-03	1.28E-03	4.66E-05
0.15	1.39E-02	1.41E-02	1.43E-02	1.45E-02	1.48E-02	1.53E-02	1.60E-02	1.70E-02	1.92E-02	2.57E-02	1.61E-02	1.28E-02	8.34E-03	2.10E-03	8.45E-05
0.20	1.16E-02	1.17E-02	1.19E-02	1.20E-02	1.22E-02	1.25E-02	1.29E-02	1.36E-02	1.49E-02	1.88E-02	1.30E-02	1.09E-02	7.58E-03	2.87E-03	1.29E-04
0.30	8.50E-03	8.58E-03	8.63E-03	8.69E-03	8.80E-03	8.96E-03	9.18E-03	9.50E-03	1.02E-02	1.24E-02	9.22E-03	8.11E-03	6.38E-03	3.93E-03	2.06E-04
0.40	7.17E-03	7.21E-03	7.25E-03	7.30E-03	7.37E-03	7.48E-03	7.62E-03	7.86E-03	8.33E-03	9.76E-03	7.66E-03	6.91E-03	5.83E-03	4.31E-03	2.80E-04
0.50	6.35E-03	6.38E-03	6.42E-03	6.45E-03	6.50E-03	6.60E-03	6.69E-03	7.06E-03	7.43E-03	8.50E-03	6.82E-03	6.06E-03	5.33E-03	4.44E-03	3.56E-04
0.60	6.16E-03	6.18E-03	6.21E-03	6.26E-03	6.30E-03	6.35E-03	6.43E-03	6.57E-03	6.86E-03	7.73E-03	6.46E-03	6.02E-03	5.34E-03	4.49E-03	4.31E-04
0.80	5.69E-03	5.72E-03	5.73E-03	5.73E-03	5.78E-03	5.79E-03	5.86E-03	5.96E-03	6.16E-03	6.75E-03	5.87E-03	5.60E-03	5.11E-03	4.48E-03	5.52E-04
1.0	5.37E-03	5.38E-03	5.40E-03	5.43E-03	5.48E-03	5.49E-03	5.54E-03	5.62E-03	5.78E-03	6.10E-03	5.55E-03	5.30E-03	4.99E-03	4.45E-03	6.61E-04
1.5	4.89E-03	4.90E-03	4.91E-03	4.92E-03	4.93E-03	4.95E-03	4.99E-03	5.07E-03	5.17E-03	5.46E-03	5.00E-03	4.85E-03	4.60E-03	4.30E-03	7.94E-04
2.0	4.59E-03	4.59E-03	4.61E-03	4.62E-03	4.64E-03	4.66E-03	4.68E-03	4.72E-03	4.79E-03	5.02E-03	4.69E-03	4.58E-03	4.39E-03	4.15E-03	8.10E-04
3.0	4.20E-03	4.20E-03	4.21E-03	4.23E-03	4.22E-03	4.22E-03	4.24E-03	4.29E-03	4.34E-03	4.48E-03	4.25E-03	4.21E-03	4.08E-03	3.93E-03	7.23E-04
4.0	3.95E-03	3.96E-03	3.97E-03	3.99E-03	3.99E-03	3.98E-03	4.00E-03	4.03E-03	4.08E-03	4.15E-03	4.00E-03	3.95E-03	3.87E-03	3.76E-03	6.13E-04
5.0	3.78E-03	3.79E-03	3.79E-03	3.80E-03	3.80E-03	3.80E-03	3.82E-03	3.84E-03	3.87E-03	3.96E-03	3.82E-03	3.77E-03	3.71E-03	3.63E-03	5.28E-04
6.0	3.63E-03	3.64E-03	3.65E-03	3.66E-03	3.66E-03	3.67E-03	3.68E-03	3.69E-03	3.71E-03	3.79E-03	3.68E-03	3.64E-03	3.59E-03	3.52E-03	4.59E-04
8.0	3.43E-03	3.43E-03	3.43E-03	3.44E-03	3.44E-03	3.44E-03	3.45E-03	3.47E-03	3.49E-03	3.54E-03	3.45E-03	3.42E-03	3.39E-03	3.34E-03	3.73E-04
10.0	3.26E-03	3.27E-03	3.27E-03	3.27E-03	3.28E-03	3.28E-03	3.28E-03	3.29E-03	3.31E-03	3.36E-03	3.28E-03	3.26E-03	3.23E-03	3.19E-03	3.13E-04

Table A-2. UFRF absorbed fraction for all sources irradiating the shallow active marrow in the cranium.

Cranium ϕ (TAM_{50}← TAM) Cellularity												Cranium ϕ (TAM_{50}← r_s) Source Tissue r_s			
Energy (MeV)	100%	90%	80%	70%	60%	50%	40%	30%	20%	10%	38% (ICRP 70)	TIM	TBS	TBV	CBS_{HC} or CBV
0.010	3.07E-02	3.29E-02	3.58E-02	3.94E-02	4.42E-02	5.10E-02	6.11E-02	7.81E-02	1.10E-01	2.04E-01	6.38E-02	3.88E-04	2.86E-02	8.38E-05	7.44E-07
0.015	2.04E-02	2.26E-02	2.54E-02	2.89E-02	3.35E-02	4.02E-02	5.00E-02	6.63E-02	9.92E-02	1.98E-01	5.25E-02	8.03E-04	2.85E-02	1.66E-04	1.73E-06
0.020	2.01E-02	2.23E-02	2.49E-02	2.83E-02	3.28E-02	3.91E-02	4.85E-02	6.43E-02	9.59E-02	1.91E-01	5.10E-02	1.32E-03	2.82E-02	2.70E-04	2.93E-06
0.030	1.94E-02	2.13E-02	2.36E-02	2.66E-02	3.07E-02	3.64E-02	4.48E-02	5.89E-02	8.72E-02	1.72E-01	4.71E-02	2.61E-03	2.74E-02	5.40E-04	5.72E-06
0.040	1.85E-02	2.01E-02	2.21E-02	2.47E-02	2.82E-02	3.30E-02	4.03E-02	5.14E-02	7.67E-02	1.50E-01	4.22E-02	4.17E-03	2.65E-02	8.58E-04	9.94E-06
0.050	1.75E-02	1.88E-02	2.05E-02	2.26E-02	2.55E-02	2.95E-02	3.54E-02	4.54E-02	6.53E-02	1.25E-01	3.70E-02	5.86E-03	2.55E-02	1.23E-03	1.45E-05
0.060	1.64E-02	1.75E-02	1.88E-02	2.05E-02	2.27E-02	2.58E-02	3.05E-02	3.83E-02	5.39E-02	1.01E-01	3.17E-02	7.46E-03	2.43E-02	1.60E-03	2.03E-05
0.080	1.48E-02	1.61E-02	1.69E-02	1.83E-02	1.97E-02	2.23E-02	2.66E-02	3.63E-02	5.14E-02	2.30E-02	9.78E-03	2.00E-02	2.30E-03	3.16E-05	
0.10	1.31E-02	1.39E-02	1.39E-02	1.45E-02	1.53E-02	1.63E-02	1.79E-02	2.05E-02	2.57E-02	4.14E-02	1.83E-02	1.04E-02	1.74E-02	2.75E-03	4.34E-05
0.15	1.09E-02	1.11E-02	1.13E-02	1.16E-02	1.19E-02	1.24E-02	1.31E-02	1.42E-02	1.66E-02	2.36E-02	1.32E-02	9.81E-03	1.23E-02	3.48E-03	7.74E-05
0.20	9.38E-03	9.46E-03	9.60E-03	9.77E-03	9.99E-03	1.03E-02	1.07E-02	1.14E-02	1.28E-02	1.71E-02	1.18E-02	8.67E-03	9.72E-03	3.96E-03	1.23E-04
0.30	7.41E-03	7.49E-03	7.54E-03	7.60E-03	7.72E-03	7.86E-03	8.11E-03	8.50E-03	9.27E-03	1.16E-02	8.17E-03	7.00E-03	7.46E-03	4.59E-03	2.01E-04
0.40	6.59E-03	6.63E-03	6.68E-03	6.73E-03	6.81E-03	6.93E-03	7.08E-03	7.32E-03	7.83E-03	9.37E-03	7.11E-03	6.24E-03	6.60E-03	4.81E-03	2.78E-04
0.50	6.19E-03	6.22E-03	6.25E-03	6.28E-03	6.35E-03	6.45E-03	6.56E-03	6.74E-03	7.14E-03	8.34E-03	6.59E-03	5.88E-03	6.17E-03	4.84E-03	3.54E-04
0.60	5.93E-03	5.97E-03	6.01E-03	6.05E-03	6.09E-03	6.13E-03	6.24E-03	6.41E-03	6.71E-03	7.62E-03	6.27E-03	5.66E-03	5.94E-03	4.83E-03	4.32E-04
0.80	5.61E-03	5.64E-03	5.65E-03	5.67E-03	5.70E-03	5.75E-03	5.82E-03	5.94E-03	6.15E-03	6.78E-03	5.94E-03	5.38E-03	5.51E-03	4.79E-03	5.52E-04
1.0	5.39E-03	5.40E-03	5.41E-03	5.44E-03	5.43E-03	5.49E-03	5.55E-03	5.65E-03	5.80E-03	6.26E-03	5.57E-03	5.16E-03	5.27E-03	4.70E-03	6.72E-04
1.5	5.01E-03	5.02E-03	5.03E-03	5.05E-03	5.06E-03	5.08E-03	5.12E-03	5.20E-03	5.31E-03	5.64E-03	5.14E-03	4.84E-03	4.87E-03	4.52E-03	8.04E-04
2.0	4.75E-03	4.76E-03	4.78E-03	4.80E-03	4.81E-03	4.83E-03	4.85E-03	4.89E-03	4.97E-03	5.23E-03	4.86E-03	4.60E-03	4.65E-03	4.37E-03	8.24E-04
3.0	4.40E-03	4.40E-03	4.42E-03	4.44E-03	4.44E-03	4.43E-03	4.46E-03	4.50E-03	4.56E-03	4.75E-03	4.46E-03	4.27E-03	4.30E-03	4.12E-03	7.38E-04
4.0	4.17E-03	4.18E-03	4.19E-03	4.20E-03	4.21E-03	4.21E-03	4.22E-03	4.24E-03	4.28E-03	4.40E-03	4.22E-03	4.04E-03	4.07E-03	3.94E-03	6.27E-04
5.0	4.00E-03	4.01E-03	4.01E-03	4.01E-03	4.02E-03	4.03E-03	4.05E-03	4.08E-03	4.11E-03	4.21E-03	4.05E-03	3.87E-03	3.90E-03	3.81E-03	5.42E-04
6.0	3.87E-03	3.87E-03	3.88E-03	3.89E-03	3.89E-03	3.90E-03	3.91E-03	3.93E-03	3.96E-03	4.04E-03	3.91E-03	3.75E-03	3.78E-03	3.70E-03	4.70E-04
8.0	3.65E-03	3.66E-03	3.66E-03	3.67E-03	3.67E-03	3.68E-03	3.69E-03	3.70E-03	3.73E-03	3.81E-03	3.69E-03	3.54E-03	3.56E-03	3.51E-03	3.79E-04
10.0	3.49E-03	3.49E-03	3.50E-03	3.50E-03	3.50E-03	3.51E-03	3.51E-03	3.52E-03	3.54E-03	3.61E-03	3.51E-03	3.36E-03	3.39E-03	3.35E-03	3.20E-04

Table A-3. UFRF absorbed fraction for all sources irradiating the active marrow in the clavicles.

Clavicles ϕ (TAM← TAM) Cellularity												Clavicles ϕ (TAM← r_S) Source Tissue r_S			
Energy (MeV)	100%	90%	80%	70%	60%	50%	40%	30%	20%	10%	33% (ICRP 70)	TM	TBS	TBV	CBS_{wc} or CBV
0.010	3.90E-02	4.32E-02	4.84E-02	5.52E-02	6.42E-02	7.38E-02	9.57E-02	1.27E-01	1.90E-01	3.79E-01	1.16E-01	1.22E-03	2.09E-02	1.86E-04	6.55E-06
0.015	3.90E-02	4.30E-02	4.81E-02	5.46E-02	6.33E-02	7.36E-02	9.38E-02	1.24E-01	1.85E-01	3.68E-01	1.13E-01	2.48E-03	2.09E-02	3.94E-04	1.21E-05
0.020	3.89E-02	4.28E-02	4.77E-02	5.39E-02	6.22E-02	7.39E-02	9.14E-02	1.20E-01	1.79E-01	3.53E-01	1.10E-01	4.07E-03	2.09E-02	6.41E-04	2.10E-05
0.030	3.88E-02	4.23E-02	4.66E-02	5.21E-02	5.95E-02	6.98E-02	8.54E-02	1.11E-01	1.63E-01	3.18E-01	1.02E-01	8.07E-03	2.10E-02	1.28E-03	4.10E-05
0.040	3.87E-02	4.17E-02	4.53E-02	5.01E-02	5.63E-02	6.51E-02	7.83E-02	1.00E-01	1.44E-01	2.70E-01	9.23E-02	1.27E-02	2.10E-02	2.10E-03	6.57E-05
0.050	3.86E-02	4.10E-02	4.40E-02	4.79E-02	5.30E-02	6.01E-02	7.09E-02	8.87E-02	1.25E-01	2.32E-01	8.22E-02	1.76E-02	2.12E-02	3.00E-03	1.01E-04
0.060	3.85E-02	4.04E-02	4.27E-02	4.57E-02	4.97E-02	5.53E-02	6.36E-02	7.75E-02	1.05E-01	1.89E-01	7.24E-02	2.24E-02	2.12E-02	4.02E-03	1.39E-04
0.080	3.82E-02	3.93E-02	4.06E-02	4.23E-02	4.44E-02	4.75E-02	5.20E-02	5.98E-02	7.47E-02	1.20E-01	5.68E-02	2.88E-02	2.16E-02	6.11E-03	2.23E-04
0.10	3.79E-02	3.86E-02	3.94E-02	4.05E-02	4.18E-02	4.36E-02	4.64E-02	5.10E-02	5.99E-02	8.67E-02	4.93E-02	3.32E-02	2.20E-02	8.32E-03	3.19E-04
0.15	3.72E-02	3.75E-02	3.79E-02	3.85E-02	3.91E-02	4.01E-02	4.13E-02	4.34E-02	4.76E-02	6.00E-02	4.27E-02	3.54E-02	2.43E-02	1.38E-02	5.67E-04
0.20	3.64E-02	3.66E-02	3.69E-02	3.73E-02	3.77E-02	3.84E-02	3.92E-02	4.06E-02	4.32E-02	5.08E-02	4.01E-02	3.56E-02	2.65E-02	1.86E-02	8.65E-04
0.30	3.50E-02	3.53E-02	3.54E-02	3.57E-02	3.59E-02	3.63E-02	3.68E-02	3.76E-02	3.90E-02	4.31E-02	3.73E-02	3.48E-02	2.92E-02	2.47E-02	1.45E-03
0.40	3.39E-02	3.41E-02	3.42E-02	3.44E-02	3.46E-02	3.50E-02	3.53E-02	3.58E-02	3.68E-02	3.97E-02	3.56E-02	3.40E-02	3.02E-02	2.72E-02	2.11E-03
0.50	3.29E-02	3.31E-02	3.32E-02	3.33E-02	3.35E-02	3.37E-02	3.40E-02	3.45E-02	3.52E-02	3.73E-02	3.43E-02	3.31E-02	3.03E-02	2.82E-02	2.75E-03
0.60	3.20E-02	3.21E-02	3.22E-02	3.23E-02	3.25E-02	3.27E-02	3.29E-02	3.33E-02	3.39E-02	3.56E-02	3.31E-02	3.22E-02	3.01E-02	2.88E-02	3.34E-03
0.80	3.02E-02	3.03E-02	3.04E-02	3.05E-02	3.06E-02	3.08E-02	3.10E-02	3.12E-02	3.17E-02	3.29E-02	3.11E-02	3.04E-02	2.92E-02	2.82E-02	4.40E-03
1.0	2.86E-02	2.86E-02	2.87E-02	2.88E-02	2.89E-02	2.91E-02	2.92E-02	2.95E-02	2.97E-02	3.05E-02	2.94E-02	2.88E-02	2.79E-02	2.73E-02	5.30E-03
1.5	2.48E-02	2.48E-02	2.48E-02	2.49E-02	2.50E-02	2.51E-02	2.52E-02	2.53E-02	2.55E-02	2.60E-02	2.52E-02	2.50E-02	2.50E-02	2.48E-02	6.57E-03
2.0	2.14E-02	2.15E-02	2.16E-02	2.16E-02	2.17E-02	2.17E-02	2.17E-02	2.18E-02	2.19E-02	2.25E-02	2.18E-02	2.15E-02	2.20E-02	2.18E-02	6.94E-03
3.0	1.66E-02	1.66E-02	1.65E-02	1.65E-02	1.65E-02	1.66E-02	1.66E-02	1.67E-02	1.68E-02	1.70E-02	1.67E-02	1.64E-02	1.69E-02	1.68E-02	6.08E-03
4.0	1.30E-02	1.29E-02	1.29E-02	1.29E-02	1.30E-02	1.30E-02	1.30E-02	1.30E-02	1.31E-02	1.32E-02	1.30E-02	1.29E-02	1.31E-02	1.32E-02	5.05E-03
5.0	1.04E-02	1.04E-02	1.04E-02	1.05E-02	1.05E-02	1.04E-02	1.05E-02	1.05E-02	1.06E-02	1.07E-02	1.05E-02	1.04E-02	1.06E-02	1.06E-02	4.16E-03
6.0	8.62E-03	8.66E-03	8.64E-03	8.61E-03	8.65E-03	8.72E-03	8.71E-03	8.70E-03	8.73E-03	8.83E-03	8.71E-03	8.54E-03	8.82E-03	8.73E-03	3.50E-03
8.0	6.45E-03	6.42E-03	6.43E-03	6.45E-03	6.45E-03	6.45E-03	6.46E-03	6.48E-03	6.50E-03	6.57E-03	6.47E-03	6.39E-03	6.52E-03	6.49E-03	2.68E-03
10.0	5.13E-03	5.11E-03	5.11E-03	5.12E-03	5.12E-03	5.11E-03	5.14E-03	5.16E-03	5.21E-03	5.26E-03	5.17E-03	5.13E-03	5.20E-03	5.20E-03	2.16E-03

Table A-4. UFRF absorbed fraction for all sources irradiating the shallow active marrow in the clavicles.

Clavicles ϕ (TAM_{SV}← TAM) Cellularity												Clavicles ϕ (TAM_{SV}← r_S) Source Tissue r_S			
Energy (MeV)	100%	90%	80%	70%	60%	50%	40%	30%	20%	10%	33% (ICRP 70)	TM	TBS	TBV	CBS_{wc} or CBV
0.010	3.88E-02	4.29E-02	4.82E-02	5.51E-02	6.42E-02	7.69E-02	9.59E-02	1.27E-01	1.91E-01	3.83E-01	1.16E-01	8.14E-04	4.92E-01	4.38E-03	5.60E-06
0.015	3.84E-02	4.27E-02	4.77E-02	5.41E-02	6.23E-02	7.52E-02	9.38E-02	1.25E-01	1.87E-01	3.76E-01	1.13E-01	1.66E-03	4.89E-01	9.23E-03	7.33E-06
0.020	3.82E-02	4.25E-02	4.70E-02	5.33E-02	6.13E-02	7.38E-02	9.14E-02	1.21E-01	1.80E-01	3.59E-01	1.10E-01	2.61E-03	4.85E-01	1.50E-02	1.88E-05
0.030	3.67E-02	4.08E-02	4.48E-02	5.06E-02	5.83E-02	5.90E-02	8.48E-02	1.11E-01	1.65E-01	3.26E-01	1.02E-01	5.10E-03	4.75E-01	2.96E-02	3.76E-05
0.040	3.56E-02	3.81E-02	4.23E-02	4.72E-02	5.37E-02	6.27E-02	7.85E-02	9.85E-02	1.46E-01	2.84E-01	9.15E-02	8.31E-03	4.61E-01	4.74E-02	6.96E-05
0.050	3.38E-02	3.69E-02	3.97E-02	4.38E-02	4.91E-02	5.66E-02	6.77E-02	8.62E-02	1.24E-01	2.36E-01	7.94E-02	1.17E-02	4.46E-01	6.64E-02	7.22E-05
0.060	3.26E-02	3.49E-02	3.71E-02	4.02E-02	4.43E-02	5.02E-02	5.89E-02	7.34E-02	1.03E-01	1.90E-01	6.81E-02	1.54E-02	4.28E-01	8.64E-02	1.14E-04
0.080	3.00E-02	3.11E-02	3.24E-02	3.42E-02	3.65E-02	3.99E-02	4.49E-02	5.32E-02	6.98E-02	1.20E-01	5.82E-02	2.09E-02	3.65E-01	1.18E-01	1.91E-04
0.10	2.87E-02	2.96E-02	3.04E-02	3.14E-02	3.27E-02	3.44E-02	3.74E-02	4.23E-02	5.21E-02	8.14E-02	4.95E-02	2.32E-02	2.98E-01	1.34E-01	2.64E-04
0.15	2.81E-02	2.89E-02	2.98E-02	2.95E-02	3.02E-02	3.12E-02	3.24E-02	3.45E-02	3.89E-02	5.22E-02	3.38E-02	2.61E-02	2.01E-01	1.37E-01	4.54E-04
0.20	2.89E-02	2.91E-02	2.93E-02	2.97E-02	3.02E-02	3.10E-02	3.21E-02	3.39E-02	3.65E-02	4.42E-02	3.32E-02	2.77E-02	1.51E-01	1.21E-01	7.01E-04
0.30	3.04E-02	3.00E-02	3.07E-02	3.00E-02	3.11E-02	3.15E-02	3.21E-02	3.31E-02	3.40E-02	3.83E-02	3.27E-02	2.89E-02	1.02E-01	9.27E-02	1.20E-03
0.40	3.08E-02	3.09E-02	3.11E-02	3.14E-02	3.13E-02	3.19E-02	3.22E-02	3.27E-02	3.37E-02	3.67E-02	3.25E-02	3.09E-02	8.13E-02	7.63E-02	1.84E-03
0.50	3.03E-02	3.03E-02	3.09E-02	3.10E-02	3.11E-02	3.11E-02	3.14E-02	3.18E-02	3.27E-02	3.53E-02	3.17E-02	3.10E-02	6.99E-02	6.70E-02	2.47E-03
0.60	3.02E-02	3.04E-02	3.04E-02	3.05E-02	3.09E-02	3.16E-02	3.15E-02	3.13E-02	3.19E-02	3.39E-02	3.14E-02	3.01E-02	6.28E-02	6.09E-02	2.89E-03
0.80	2.90E-02	2.96E-02	2.95E-02	2.94E-02	2.94E-02	2.94E-02	2.96E-02	3.00E-02	3.06E-02	3.26E-02	2.98E-02	2.94E-02	5.33E-02	5.23E-02	3.83E-03
1.0	2.81E-02	2.79E-02	2.80E-02	2.81E-02	2.84E-02	2.88E-02	2.90E-02	2.92E-02	2.95E-02	3.05E-02	2.91E-02	2.80E-02	4.89E-02	4.69E-02	4.75E-03
1.5	2.45E-02	2.48E-02	2.48E-02	2.48E-02	2.49E-02	2.51E-02	2.51E-02	2.52E-02	2.55E-02	2.64E-02	2.52E-02	2.50E-02	3.78E-02	3.73E-02	6.04E-03
2.0	2.18E-02	2.17E-02	2.18E-02	2.21E-02	2.22E-02	2.19E-02	2.20E-02	2.22E-02	2.24E-02	2.33E-02	2.21E-02	2.19E-02	3.18E-02	3.18E-02	6.43E-03
3.0	1.69E-02	1.69E-02	1.69E-02	1.69E-02	1.68E-02	1.68E-02	1.69E-02	1.72E-02	1.73E-02	1.77E-02	1.71E-02	1.69E-02	2.34E-02	2.34E-02	5.78E-03
4.0	1.33E-02	1.31E-02	1.32E-02	1.33E-02	1.34E-02	1.34E-02	1.34E-02	1.34E-02	1.34E-02	1.36E-02	1.34E-02	1.32E-02	1.79E-02	1.80E-02	4.86E-03
5.0	1.07E-02	1.07E-02	1.07E-02	1.07E-02	1.07E-02	1.07E-02	1.07E-02	1.08E-02	1.08E-02	1.11E-02	1.08E-02	1.07E-02	1.44E-02	1.44E-02	3.90E-03
6.0	8.80E-03	8.82E-03	8.79E-03	8.76E-03	8.83E-03	8.87E-03	8.87E-03	8.88E-03	8.94E-03	9.13E-03	8.88E-03	8.69E-03	1.20E-02	1.19E-02	3.52E-03
8.0	6.56E-03	6.59E-03	6.56E-03	6.56E-03	6.55E-03	6.56E-03	6.58E-03	6.61E-03	6.66E-03	6.80E-03	6.60E-03	6.55E-03	8.92E-03	8.88E-03	2.63E-03
10.0	5.20E-03	5.23E-03	5.23E-03	5.22E-03	5.23E-03	5.24E-03	5.26E-03	5.29E-03	5.32E-03	5.43E-03	5.28E-03	5.21E-03	7.10E-03	7.14E-03	2.09E-03

Table A-5. UFRF absorbed fraction for all sources irradiating the active marrow in the mandible.

Mandible ϕ (TAM← TAM) Cellularity												Mandible ϕ (TAM← r_{Si}) Source Tissue r_i			
Energy (MeV)	100%	90%	80%	70%	60%	50%	40%	30%	20%	10%	35% (ICRP 70)	TM	TBS	TBV	CES_{wc} or 2BV
0.010	7.08E-02	7.84E-02	8.79E-02	1.00E-01	1.17E-01	1.39E-01	1.74E-01	2.31E-01	3.45E-01	6.89E-01	1.83E-01	2.19E-03	379E-02	3.04E-04	1.34E-06
0.015	7.07E-02	7.81E-02	8.73E-02	9.92E-02	1.15E-01	1.37E-01	1.70E-01	2.26E-01	3.36E-01	6.68E-01	1.79E-01	4.44E-03	379E-02	6.30E-04	2.28E-06
0.020	7.06E-02	7.77E-02	8.65E-02	9.78E-02	1.13E-01	1.34E-01	1.66E-01	2.19E-01	3.25E-01	6.42E-01	1.74E-01	7.32E-03	380E-02	1.01E-03	2.07E-06
0.030	7.04E-02	7.07E-02	8.49E-02	9.46E-02	1.08E-01	1.27E-01	1.58E-01	2.02E-01	2.98E-01	5.78E-01	1.62E-01	1.44E-02	379E-02	2.04E-03	8.42E-06
0.040	7.01E-02	7.55E-02	8.22E-02	9.08E-02	1.02E-01	1.18E-01	1.42E-01	1.82E-01	2.62E-01	5.02E-01	1.48E-01	2.27E-02	378E-02	3.32E-03	1.03E-05
0.050	6.98E-02	7.42E-02	7.97E-02	8.67E-02	9.63E-02	1.09E-01	1.29E-01	1.61E-01	2.26E-01	4.22E-01	1.34E-01	3.14E-02	377E-02	4.78E-03	1.46E-05
0.060	6.94E-02	7.29E-02	7.72E-02	8.27E-02	9.05E-02	1.00E-01	1.15E-01	1.41E-01	1.91E-01	3.43E-01	1.19E-01	4.00E-02	377E-02	6.37E-03	1.99E-05
0.080	6.88E-02	7.07E-02	7.31E-02	7.61E-02	8.01E-02	8.57E-02	9.39E-02	1.08E-01	1.35E-01	2.18E-01	9.61E-02	5.31E-02	376E-02	9.67E-03	3.11E-05
0.10	6.81E-02	6.93E-02	7.08E-02	7.27E-02	7.51E-02	7.85E-02	8.35E-02	9.19E-02	1.08E-01	1.57E-01	8.48E-02	6.68E-02	380E-02	1.32E-02	4.60E-05
0.15	6.62E-02	6.69E-02	6.78E-02	6.88E-02	6.98E-02	7.15E-02	7.39E-02	7.79E-02	8.54E-02	1.08E-01	7.45E-02	6.20E-02	409E-02	2.23E-02	7.28E-05
0.20	6.44E-02	6.49E-02	6.56E-02	6.61E-02	6.69E-02	6.79E-02	6.94E-02	7.19E-02	7.65E-02	9.04E-02	6.98E-02	6.18E-02	444E-02	3.08E-02	1.04E-04
0.30	6.20E-02	6.21E-02	6.27E-02	6.31E-02	6.38E-02	6.42E-02	6.51E-02	6.66E-02	6.92E-02	7.70E-02	6.53E-02	6.08E-02	498E-02	4.20E-02	1.86E-04
0.40	6.07E-02	6.10E-02	6.13E-02	6.16E-02	6.20E-02	6.24E-02	6.31E-02	6.42E-02	6.59E-02	7.10E-02	6.33E-02	5.99E-02	524E-02	4.73E-02	2.35E-04
0.60	6.00E-02	6.03E-02	6.04E-02	6.07E-02	6.13E-02	6.14E-02	6.10E-02	6.20E-02	6.41E-02	6.80E-02	6.21E-02	6.03E-02	538E-02	5.01E-02	2.70E-04
0.80	5.95E-02	5.97E-02	5.99E-02	6.01E-02	6.04E-02	6.08E-02	6.12E-02	6.19E-02	6.29E-02	6.61E-02	6.13E-02	5.90E-02	547E-02	5.18E-02	3.21E-04
1.0	5.87E-02	5.88E-02	5.91E-02	5.93E-02	5.96E-02	5.99E-02	6.02E-02	6.08E-02	6.15E-02	6.39E-02	6.03E-02	5.85E-02	555E-02	5.37E-02	4.54E-04
1.5	5.82E-02	5.84E-02	5.86E-02	5.88E-02	5.90E-02	5.92E-02	5.95E-02	6.00E-02	6.06E-02	6.25E-02	5.96E-02	5.80E-02	558E-02	5.44E-02	5.39E-04
2.0	5.72E-02	5.73E-02	5.75E-02	5.77E-02	5.79E-02	5.81E-02	5.84E-02	5.88E-02	5.91E-02	6.03E-02	5.84E-02	5.71E-02	556E-02	5.47E-02	7.22E-04
3.0	5.63E-02	5.63E-02	5.66E-02	5.69E-02	5.73E-02	5.73E-02	5.74E-02	5.77E-02	5.81E-02	5.90E-02	5.75E-02	5.63E-02	552E-02	5.45E-02	8.53E-04
4.0	5.47E-02	5.48E-02	5.50E-02	5.52E-02	5.53E-02	5.55E-02	5.57E-02	5.60E-02	5.62E-02	5.70E-02	5.57E-02	5.47E-02	540E-02	5.36E-02	8.69E-04
5.0	5.21E-02	5.19E-02	5.27E-02	5.37E-02	5.32E-02	5.25E-02	5.26E-02	5.28E-02	5.30E-02	5.34E-02	5.27E-02	5.19E-02	515E-02	5.24E-02	7.12E-04
6.0	5.09E-02	5.09E-02	5.13E-02	5.22E-02	5.17E-02	5.11E-02	5.12E-02	5.14E-02	5.16E-02	5.21E-02	5.12E-02	5.05E-02	502E-02	5.18E-02	6.38E-04
8.0	4.84E-02	4.79E-02	4.93E-02	5.08E-02	5.08E-02	4.96E-02	4.93E-02	4.88E-02	4.89E-02	4.93E-02	4.93E-02	4.79E-02	477E-02	5.11E-02	5.08E-04
10.0	4.62E-02	4.53E-02	4.67E-02	4.82E-02	4.81E-02	4.80E-02	4.74E-02	4.63E-02	4.64E-02	4.66E-02	4.72E-02	4.54E-02	454E-02	5.03E-02	4.18E-04

Table A-6. UFRF absorbed fraction for all sources irradiating the shallow active marrow in the mandible.

Mandible ϕ (TAM_{50}← TAM) Cellularity												Mandible ϕ (TAM_{50}← r_{Si}) Source Tissue r_i			
Energy (MeV)	100%	90%	80%	70%	60%	50%	40%	30%	20%	10%	35% (ICRP 70)	TM	TBS	TBV	CES_{wc} or 2BV
0.010	6.93E-02	6.99E-02	7.86E-02	9.00E-02	1.08E-01	1.29E-01	1.55E-01	2.06E-01	3.08E-01	6.19E-01	1.63E-01	1.22E-03	353E-01	2.84E-03	6.07E-06
0.015	6.22E-02	6.93E-02	7.74E-02	8.78E-02	1.02E-01	1.22E-01	1.52E-01	2.02E-01	3.01E-01	5.97E-01	1.60E-01	2.58E-03	351E-01	5.86E-03	1.33E-05
0.020	6.13E-02	6.73E-02	7.60E-02	8.64E-02	1.00E-01	1.20E-01	1.48E-01	1.96E-01	2.91E-01	5.77E-01	1.55E-01	4.26E-03	349E-01	9.33E-03	1.06E-05
0.030	5.99E-02	6.51E-02	7.34E-02	8.17E-02	9.43E-02	1.11E-01	1.37E-01	1.81E-01	2.67E-01	5.24E-01	1.41E-01	8.39E-03	341E-01	1.86E-02	3.23E-05
0.040	5.77E-02	6.23E-02	6.85E-02	7.63E-02	8.69E-02	1.02E-01	1.24E-01	1.62E-01	2.35E-01	4.54E-01	1.30E-01	1.35E-02	331E-01	2.99E-02	6.43E-05
0.050	5.50E-02	5.87E-02	6.42E-02	7.13E-02	7.97E-02	9.15E-02	1.10E-01	1.40E-01	2.01E-01	3.83E-01	1.15E-01	1.92E-02	320E-01	4.22E-02	8.42E-05
0.060	5.27E-02	5.56E-02	5.96E-02	6.46E-02	7.11E-02	8.10E-02	9.51E-02	1.19E-01	1.66E-01	3.08E-01	9.89E-02	2.47E-02	307E-01	5.49E-02	1.10E-04
0.080	4.82E-02	5.00E-02	5.22E-02	5.51E-02	5.88E-02	6.40E-02	7.18E-02	8.47E-02	1.11E-01	1.89E-01	7.38E-02	3.30E-02	264E-01	7.63E-02	1.81E-04
0.10	4.58E-02	4.69E-02	4.79E-02	4.96E-02	5.19E-02	5.51E-02	6.02E-02	6.86E-02	8.42E-02	1.31E-01	6.15E-02	3.66E-02	217E-01	8.91E-02	2.58E-04
0.15	4.36E-02	4.41E-02	4.48E-02	4.57E-02	4.69E-02	4.82E-02	5.06E-02	5.46E-02	6.15E-02	8.22E-02	5.13E-02	3.98E-02	151E-01	9.75E-02	4.23E-04
0.20	4.48E-02	4.47E-02	4.51E-02	4.57E-02	4.69E-02	4.77E-02	4.90E-02	5.11E-02	5.53E-02	6.77E-02	4.93E-02	4.24E-02	120E-01	9.33E-02	5.66E-04
0.30	4.70E-02	4.72E-02	4.75E-02	4.80E-02	4.82E-02	4.86E-02	4.96E-02	5.14E-02	5.35E-02	5.99E-02	4.99E-02	4.58E-02	917E-02	8.00E-02	1.04E-03
0.40	4.67E-02	4.69E-02	4.89E-02	4.92E-02	4.95E-02	4.99E-02	5.04E-02	5.14E-02	5.29E-02	5.73E-02	5.06E-02	4.77E-02	794E-02	7.19E-02	1.35E-03
0.50	4.93E-02	4.94E-02	4.97E-02	5.00E-02	5.03E-02	5.08E-02	5.13E-02	5.20E-02	5.31E-02	5.65E-02	5.14E-02	4.90E-02	720E-02	6.69E-02	1.51E-03
0.60	4.99E-02	4.99E-02	5.01E-02	5.04E-02	5.07E-02	5.11E-02	5.15E-02	5.23E-02	5.31E-02	5.55E-02	5.17E-02	4.94E-02	676E-02	6.33E-02	1.90E-03
0.80	5.04E-02	5.03E-02	5.07E-02	5.09E-02	5.11E-02	5.16E-02	5.18E-02	5.21E-02	5.28E-02	5.49E-02	5.18E-02	5.01E-02	624E-02	5.92E-02	2.64E-03
1.0	5.04E-02	5.03E-02	5.08E-02	5.10E-02	5.12E-02	5.14E-02	5.17E-02	5.22E-02	5.26E-02	5.40E-02	5.18E-02	5.03E-02	597E-02	5.71E-02	3.12E-03
1.5	5.01E-02	5.03E-02	5.05E-02	5.08E-02	5.09E-02	5.11E-02	5.13E-02	5.17E-02	5.20E-02	5.28E-02	5.14E-02	5.00E-02	563E-02	5.47E-02	4.24E-03
2.0	4.96E-02	4.93E-02	4.99E-02	5.00E-02	5.02E-02	5.05E-02	5.07E-02	5.10E-02	5.13E-02	5.22E-02	5.07E-02	4.97E-02	543E-02	5.31E-02	4.90E-03
3.0	4.85E-02	4.89E-02	4.87E-02	4.89E-02	4.91E-02	4.93E-02	4.95E-02	4.98E-02	4.99E-02	5.05E-02	4.95E-02	4.85E-02	516E-02	5.08E-02	5.03E-03
4.0	4.77E-02	4.75E-02	4.78E-02	4.79E-02	4.79E-02	4.81E-02	4.83E-02	4.86E-02	4.86E-02	4.89E-02	4.83E-02	4.73E-02	497E-02	5.01E-02	4.69E-03
5.0	4.67E-02	4.63E-02	4.64E-02	4.66E-02	4.67E-02	4.69E-02	4.70E-02	4.72E-02	4.73E-02	4.77E-02	4.70E-02	4.62E-02	482E-02	4.85E-02	4.12E-03
6.0	4.58E-02	4.53E-02	4.52E-02	4.53E-02	4.55E-02	4.57E-02	4.58E-02	4.60E-02	4.61E-02	4.64E-02	4.59E-02	4.51E-02	467E-02	4.77E-02	3.69E-03
8.0	4.38E-02	4.29E-02	4.30E-02	4.32E-02	4.38E-02	4.42E-02	4.40E-02	4.37E-02	4.38E-02	4.40E-02	4.40E-02	4.29E-02	441E-02	4.69E-02	2.94E-03
10.0	4.18E-02	4.08E-02	4.08E-02	4.09E-02	4.17E-02	4.29E-02	4.24E-02	4.15E-02	4.15E-02	4.17E-02	4.22E-02	4.07E-02	417E-02	4.63E-02	2.43E-03

Table A-7. UFRF absorbed fraction for all sources irradiating the active marrow in the scapulae.

Scapulae ϕ (TAM← TAM) Cellularity												Scapulae ϕ (TAM← r_S) Source Tissue r_s			
Energy (MeV)	100%	90%	80%	70%	60%	50%	40%	30%	20%	10%	38% (ICRP 70)	TM	TBS	TBV	CBS_{HC} or CBV
0.010	2.21E-02	2.44E-02	2.74E-02	3.12E-02	3.63E-02	4.36E-02	5.42E-02	7.20E-02	1.08E-01	2.15E-01	5.70E-02	6.61E-04	1.18E-02	6.89E-05	3.55E-06
0.015	2.20E-02	2.43E-02	2.72E-02	3.09E-02	3.58E-02	4.27E-02	5.31E-02	7.03E-02	1.05E-01	2.08E-01	5.58E-02	1.37E-03	1.18E-02	1.40E-04	6.76E-06
0.020	2.20E-02	2.43E-02	2.69E-02	3.05E-02	3.52E-02	4.18E-02	5.17E-02	6.82E-02	1.01E-01	2.00E-01	5.43E-02	2.24E-03	1.18E-02	2.25E-04	1.05E-05
0.030	2.19E-02	2.38E-02	2.62E-02	2.94E-02	3.36E-02	3.94E-02	4.82E-02	6.28E-02	9.21E-02	1.80E-01	5.05E-02	4.43E-03	1.17E-02	4.90E-04	2.29E-05
0.040	2.17E-02	2.34E-02	2.56E-02	2.81E-02	3.17E-02	3.67E-02	4.41E-02	5.69E-02	8.34E-02	1.60E-01	4.81E-02	6.97E-03	1.17E-02	7.48E-04	3.53E-05
0.050	2.15E-02	2.29E-02	2.49E-02	2.69E-02	2.97E-02	3.37E-02	3.98E-02	5.00E-02	7.32E-02	1.31E-01	4.14E-02	9.62E-03	1.16E-02	1.06E-03	6.09E-05
0.060	2.13E-02	2.24E-02	2.37E-02	2.54E-02	2.77E-02	3.08E-02	3.56E-02	4.35E-02	5.82E-02	1.06E-01	3.60E-02	1.22E-02	1.15E-02	1.42E-03	7.83E-05
0.080	2.09E-02	2.15E-02	2.23E-02	2.32E-02	2.45E-02	2.62E-02	2.86E-02	3.31E-02	4.16E-02	6.73E-02	2.94E-02	1.62E-02	1.14E-02	2.18E-03	1.24E-04
0.10	2.05E-02	2.09E-02	2.13E-02	2.19E-02	2.27E-02	2.37E-02	2.53E-02	2.79E-02	3.30E-02	4.83E-02	2.57E-02	1.78E-02	1.13E-02	2.94E-03	1.81E-04
0.15	1.93E-02	1.96E-02	1.98E-02	2.00E-02	2.04E-02	2.10E-02	2.17E-02	2.29E-02	2.53E-02	3.23E-02	2.19E-02	1.83E-02	1.16E-02	4.94E-03	3.41E-04
0.20	1.82E-02	1.83E-02	1.85E-02	1.87E-02	1.89E-02	1.92E-02	1.97E-02	2.04E-02	2.19E-02	2.64E-02	1.98E-02	1.78E-02	1.20E-02	6.85E-03	4.94E-04
0.30	1.63E-02	1.64E-02	1.65E-02	1.66E-02	1.67E-02	1.69E-02	1.72E-02	1.76E-02	1.84E-02	2.07E-02	1.72E-02	1.61E-02	1.25E-02	9.51E-03	8.15E-04
0.40	1.51E-02	1.51E-02	1.52E-02	1.53E-02	1.54E-02	1.55E-02	1.57E-02	1.60E-02	1.65E-02	1.81E-02	1.58E-02	1.49E-02	1.28E-02	1.07E-02	1.13E-03
0.50	1.42E-02	1.43E-02	1.44E-02	1.44E-02	1.45E-02	1.46E-02	1.47E-02	1.50E-02	1.54E-02	1.65E-02	1.48E-02	1.42E-02	1.24E-02	1.10E-02	1.43E-03
0.60	1.36E-02	1.37E-02	1.37E-02	1.38E-02	1.38E-02	1.39E-02	1.40E-02	1.42E-02	1.46E-02	1.64E-02	1.40E-02	1.36E-02	1.22E-02	1.10E-02	1.72E-03
0.80	1.25E-02	1.25E-02	1.25E-02	1.26E-02	1.26E-02	1.27E-02	1.28E-02	1.29E-02	1.31E-02	1.38E-02	1.28E-02	1.25E-02	1.15E-02	1.08E-02	2.14E-03
1.0	1.15E-02	1.16E-02	1.16E-02	1.16E-02	1.17E-02	1.17E-02	1.18E-02	1.19E-02	1.21E-02	1.26E-02	1.18E-02	1.15E-02	1.08E-02	1.02E-02	2.38E-03
1.5	9.62E-03	9.57E-03	9.60E-03	9.65E-03	9.68E-03	9.72E-03	9.77E-03	9.85E-03	9.97E-03	1.03E-02	9.79E-03	9.62E-03	9.13E-03	8.79E-03	2.65E-03
2.0	8.08E-03	8.08E-03	8.11E-03	8.17E-03	8.14E-03	8.11E-03	8.14E-03	8.20E-03	8.30E-03	8.60E-03	8.15E-03	8.02E-03	7.73E-03	7.48E-03	2.58E-03
3.0	5.97E-03	6.08E-03	6.01E-03	5.92E-03	5.95E-03	5.99E-03	6.04E-03	6.12E-03	6.25E-03	6.26E-03	6.05E-03	5.98E-03	5.79E-03	5.65E-03	2.19E-03
4.0	4.64E-03	4.63E-03	4.64E-03	4.65E-03	4.65E-03	4.66E-03	4.66E-03	4.66E-03	4.70E-03	4.83E-03	4.66E-03	4.58E-03	4.44E-03	4.35E-03	1.78E-03
5.0	3.74E-03	3.76E-03	3.75E-03	3.74E-03	3.76E-03	3.79E-03	3.79E-03	3.79E-03	3.83E-03	3.93E-03	3.79E-03	3.71E-03	3.63E-03	3.56E-03	1.47E-03
6.0	3.14E-03	3.15E-03	3.16E-03	3.17E-03	3.16E-03	3.16E-03	3.17E-03	3.20E-03	3.22E-03	3.28E-03	3.18E-03	3.14E-03	3.04E-03	2.96E-03	1.26E-03
8.0	2.39E-03	2.38E-03	2.38E-03	2.38E-03	2.38E-03	2.38E-03	2.39E-03	2.41E-03	2.42E-03	2.47E-03	2.39E-03	2.36E-03	2.30E-03	2.25E-03	9.78E-04
10.0	1.90E-03	1.91E-03	1.91E-03	1.91E-03	1.91E-03	1.91E-03	1.92E-03	1.93E-03	1.94E-03	2.00E-03	1.92E-03	1.90E-03	1.86E-03	1.79E-03	7.87E-04

Table A-8. UFRF absorbed fraction for all sources irradiating the shallow active marrow in the scapulae.

Scapulae ϕ (TAM_{SV}← TAM) Cellularity												Scapulae ϕ (TAM_{SV}← r_S) Source Tissue r_s			
Energy (MeV)	100%	90%	80%	70%	60%	50%	40%	30%	20%	10%	38% (ICRP 70)	TM	TBS	TBV	CBS_{HC} or CBV
0.010	2.03E-02	2.25E-02	2.53E-02	2.88E-02	3.35E-02	4.02E-02	5.01E-02	6.68E-02	9.98E-02	1.99E-01	5.38E-02	3.92E-04	7.91E-02	4.62E-04	3.21E-06
0.015	2.02E-02	2.23E-02	2.50E-02	2.85E-02	3.31E-02	3.96E-02	4.93E-02	6.04E-02	9.70E-02	1.94E-01	5.28E-02	8.04E-04	7.89E-02	5.37E-04	5.38E-06
0.020	1.99E-02	2.20E-02	2.45E-02	2.78E-02	3.22E-02	3.84E-02	4.77E-02	6.53E-02	9.42E-02	1.87E-01	5.02E-02	1.33E-03	7.80E-02	1.50E-03	6.72E-06
0.030	1.92E-02	2.11E-02	2.34E-02	2.64E-02	3.03E-02	3.58E-02	4.41E-02	5.19E-02	8.65E-02	1.68E-01	4.63E-02	2.65E-03	7.62E-02	3.00E-03	1.98E-05
0.040	1.85E-02	2.01E-02	2.21E-02	2.48E-02	2.83E-02	3.29E-02	3.98E-02	5.17E-02	7.85E-02	1.47E-01	4.35E-02	3.96E-03	7.48E-02	4.83E-03	3.11E-05
0.050	1.76E-02	1.89E-02	2.05E-02	2.26E-02	2.54E-02	2.93E-02	3.53E-02	4.52E-02	6.46E-02	1.23E-01	3.88E-02	6.00E-03	7.15E-02	6.76E-03	5.21E-05
0.060	1.67E-02	1.77E-02	1.90E-02	2.06E-02	2.28E-02	2.59E-02	3.05E-02	3.82E-02	5.33E-02	9.87E-02	3.37E-02	7.69E-03	6.84E-02	8.84E-03	6.80E-05
0.080	1.50E-02	1.59E-02	1.64E-02	1.73E-02	1.85E-02	2.02E-02	2.27E-02	2.69E-02	3.53E-02	6.03E-02	2.34E-02	1.02E-02	5.86E-02	1.23E-02	9.70E-05
0.10	1.40E-02	1.44E-02	1.48E-02	1.53E-02	1.61E-02	1.72E-02	1.87E-02	2.13E-02	2.63E-02	4.15E-02	1.91E-02	1.12E-02	4.81E-02	1.45E-02	1.46E-04
0.15	1.28E-02	1.29E-02	1.31E-02	1.34E-02	1.38E-02	1.43E-02	1.50E-02	1.61E-02	1.83E-02	2.51E-02	1.51E-02	1.16E-02	3.30E-02	1.63E-02	2.61E-04
0.20	1.23E-02	1.24E-02	1.26E-02	1.28E-02	1.30E-02	1.33E-02	1.37E-02	1.44E-02	1.57E-02	1.98E-02	1.38E-02	1.17E-02	2.57E-02	1.63E-02	3.90E-04
0.30	1.20E-02	1.20E-02	1.21E-02	1.22E-02	1.23E-02	1.25E-02	1.27E-02	1.31E-02	1.39E-02	1.61E-02	1.29E-02	1.10E-02	1.93E-02	1.51E-02	6.51E-04
0.40	1.16E-02	1.17E-02	1.18E-02	1.18E-02	1.19E-02	1.20E-02	1.22E-02	1.25E-02	1.29E-02	1.42E-02	1.22E-02	1.15E-02	1.66E-02	1.41E-02	9.31E-04
0.50	1.13E-02	1.13E-02	1.14E-02	1.15E-02	1.15E-02	1.16E-02	1.17E-02	1.19E-02	1.23E-02	1.33E-02	1.18E-02	1.12E-02	1.51E-02	1.33E-02	1.21E-03
0.60	1.10E-02	1.11E-02	1.11E-02	1.11E-02	1.11E-02	1.12E-02	1.13E-02	1.15E-02	1.18E-02	1.27E-02	1.13E-02	1.09E-02	1.41E-02	1.28E-02	1.43E-03
0.80	1.04E-02	1.05E-02	1.03E-02	1.04E-02	1.04E-02	1.04E-02	1.05E-02	1.07E-02	1.09E-02	1.15E-02	1.06E-02	1.03E-02	1.26E-02	1.17E-02	1.82E-03
1.0	9.73E-03	9.73E-03	9.75E-03	9.77E-03	9.79E-03	9.80E-03	9.89E-03	1.00E-02	1.02E-02	1.06E-02	9.92E-03	9.68E-03	1.15E-02	1.08E-02	2.06E-03
1.5	8.26E-03	8.27E-03	8.28E-03	8.29E-03	8.32E-03	8.36E-03	8.40E-03	8.46E-03	8.58E-03	8.96E-03	8.41E-03	8.24E-03	9.37E-03	8.98E-03	2.34E-03
2.0	6.98E-03	7.01E-03	7.03E-03	7.04E-03	7.06E-03	7.08E-03	7.08E-03	7.18E-03	7.28E-03	7.51E-03	7.09E-03	6.94E-03	7.83E-03	7.59E-03	2.37E-03
3.0	5.27E-03	5.29E-03	5.25E-03	5.20E-03	5.23E-03	5.28E-03	5.32E-03	5.40E-03	5.46E-03	5.65E-03	5.34E-03	5.24E-03	5.85E-03	5.68E-03	1.98E-03
4.0	4.11E-03	4.09E-03	4.10E-03	4.11E-03	4.11E-03	4.10E-03	4.11E-03	4.13E-03	4.17E-03	4.28E-03	4.12E-03	4.06E-03	4.50E-03	4.37E-03	1.80E-03
5.0	3.32E-03	3.31E-03	3.33E-03	3.33E-03	3.31E-03	3.37E-03	3.37E-03	3.37E-03	3.40E-03	3.51E-03	3.37E-03	3.31E-03	3.67E-03	3.56E-03	1.32E-03
6.0	2.79E-03	2.79E-03	2.79E-03	2.81E-03	2.81E-03	2.80E-03	2.82E-03	2.85E-03	2.87E-03	2.94E-03	2.82E-03	2.79E-03	3.07E-03	2.97E-03	1.14E-03
8.0	2.13E-03	2.13E-03	2.12E-03	2.11E-03	2.11E-03	2.12E-03	2.12E-03	2.14E-03	2.15E-03	2.20E-03	2.13E-03	2.09E-03	2.32E-03	2.26E-03	8.90E-04
10.0	1.69E-03	1.70E-03	1.70E-03	1.70E-03	1.70E-03	1.70E-03	1.71E-03	1.13E-03	1.75E-03	1.79E-03	1.72E-03	1.69E-03	1.87E-03	1.80E-03	7.22E-04

Table A-9. UFRF absorbed fraction for all sources irradiating the active marrow in the sternum.

Sternum ϕ (TAM← TAM) Cellularity												Sternum ϕ (TAM← r_S) Source Tissue r_S			
Energy (MeV)	100%	90%	80%	70%	60%	50%	40%	30%	20%	10%	70% (ICRP 70)	TM	TBS	TBV	CBS_{HC} or CBV
0.010	3.21E-02	3.56E-02	3.99E-02	4.55E-02	5.29E-02	6.32E-02	7.88E-02	1.05E-01	1.57E-01	3.12E-01	4.55E-02	1.01E-03	1.73E-02	2.36E-04	7.48E-06
0.015	3.21E-02	3.54E-02	3.96E-02	4.50E-02	5.22E-02	6.22E-02	7.72E-02	1.02E-01	1.52E-01	3.03E-01	4.50E-02	2.05E-03	1.73E-02	4.84E-04	1.33E-05
0.020	3.21E-02	3.53E-02	3.93E-02	4.44E-02	5.13E-02	6.09E-02	7.53E-02	9.93E-02	1.47E-01	2.91E-01	4.44E-02	3.39E-03	1.73E-02	8.01E-04	2.30E-05
0.030	3.20E-02	3.49E-02	3.84E-02	4.30E-02	4.91E-02	5.76E-02	7.03E-02	9.16E-02	1.34E-01	2.62E-01	4.30E-02	6.70E-03	1.75E-02	1.58E-03	4.73E-05
0.040	3.20E-02	3.44E-02	3.74E-02	4.13E-02	4.69E-02	5.37E-02	6.46E-02	8.26E-02	1.19E-01	2.27E-01	4.13E-02	1.03E-02	1.77E-02	2.60E-03	8.16E-05
0.050	3.19E-02	3.39E-02	3.64E-02	3.95E-02	4.38E-02	4.97E-02	5.85E-02	7.32E-02	1.03E-01	1.91E-01	3.95E-02	1.46E-02	1.79E-02	3.72E-03	1.15E-04
0.060	3.19E-02	3.34E-02	3.53E-02	3.78E-02	4.11E-02	4.57E-02	5.26E-02	6.40E-02	8.69E-02	1.55E-01	3.78E-02	1.86E-02	1.80E-02	4.95E-03	1.55E-04
0.080	3.17E-02	3.29E-02	3.37E-02	3.51E-02	3.69E-02	3.94E-02	4.31E-02	4.94E-02	6.17E-02	9.89E-02	3.51E-02	2.47E-02	1.86E-02	7.54E-03	2.56E-04
0.10	3.16E-02	3.21E-02	3.26E-02	3.37E-02	3.48E-02	3.53E-02	3.85E-02	4.23E-02	4.97E-02	7.18E-02	3.37E-02	2.75E-02	1.94E-02	1.02E-02	3.72E-04
0.15	3.12E-02	3.15E-02	3.16E-02	3.22E-02	3.28E-02	3.30E-02	3.40E-02	3.64E-02	3.98E-02	5.00E-02	3.22E-02	2.94E-02	2.21E-02	1.61E-02	6.73E-04
0.20	3.08E-02	3.10E-02	3.12E-02	3.15E-02	3.19E-02	3.24E-02	3.31E-02	3.42E-02	3.64E-02	4.26E-02	3.15E-02	2.98E-02	2.44E-02	2.06E-02	1.06E-03
0.30	3.00E-02	3.01E-02	3.03E-02	3.05E-02	3.07E-02	3.11E-02	3.15E-02	3.21E-02	3.33E-02	3.69E-02	3.05E-02	2.98E-02	2.66E-02	2.48E-02	1.77E-03
0.40	2.93E-02	2.94E-02	2.96E-02	2.97E-02	2.99E-02	3.01E-02	3.04E-02	3.09E-02	3.17E-02	3.40E-02	2.97E-02	2.91E-02	2.71E-02	2.60E-02	2.53E-03
0.50	2.85E-02	2.87E-02	2.88E-02	2.89E-02	2.90E-02	2.93E-02	2.96E-02	2.98E-02	3.04E-02	3.21E-02	2.89E-02	2.84E-02	2.70E-02	2.62E-02	3.26E-03
0.60	2.78E-02	2.79E-02	2.80E-02	2.81E-02	2.83E-02	2.86E-02	2.88E-02	2.90E-02	2.95E-02	3.11E-02	2.81E-02	2.76E-02	2.67E-02	2.61E-02	4.07E-03
0.80	2.64E-02	2.65E-02	2.66E-02	2.66E-02	2.68E-02	2.69E-02	2.70E-02	2.72E-02	2.76E-02	2.87E-02	2.66E-02	2.65E-02	2.57E-02	2.53E-02	5.23E-03
1.0	2.52E-02	2.53E-02	2.53E-02	2.54E-02	2.55E-02	2.57E-02	2.58E-02	2.59E-02	2.62E-02	2.69E-02	2.54E-02	2.53E-02	2.45E-02	2.43E-02	6.10E-03
1.5	2.19E-02	2.20E-02	2.21E-02	2.22E-02	2.23E-02	2.24E-02	2.24E-02	2.25E-02	2.27E-02	2.32E-02	2.22E-02	2.21E-02	2.16E-02	2.15E-02	7.39E-03
2.0	1.92E-02	1.92E-02	1.92E-02	1.93E-02	1.92E-02	1.92E-02	1.93E-02	1.96E-02	1.97E-02	2.00E-02	1.93E-02	1.92E-02	1.88E-02	1.88E-02	7.69E-03
3.0	1.47E-02	1.47E-02	1.48E-02	1.48E-02	1.47E-02	1.47E-02	1.47E-02	1.48E-02	1.50E-02	1.54E-02	1.48E-02	1.47E-02	1.44E-02	1.45E-02	6.91E-03
4.0	1.15E-02	1.17E-02	1.17E-02	1.17E-02	1.17E-02	1.17E-02	1.18E-02	1.19E-02	1.20E-02	1.22E-02	1.17E-02	1.17E-02	1.16E-02	1.15E-02	5.90E-03
5.0	9.68E-03	9.58E-03	9.64E-03	9.71E-03	9.67E-03	9.52E-03	9.71E-03	9.67E-03	9.92E-03	1.01E-02	9.71E-03	9.63E-03	9.39E-03	9.44E-03	5.02E-03
6.0	8.24E-03	8.08E-03	8.11E-03	8.14E-03	8.18E-03	8.23E-03	8.23E-03	8.24E-03	8.36E-03	8.32E-03	8.14E-03	8.07E-03	8.04E-03	8.00E-03	4.33E-03
8.0	6.23E-03	6.23E-03	6.22E-03	6.20E-03	6.24E-03	6.29E-03	6.26E-03	6.21E-03	6.34E-03	6.34E-03	6.20E-03	6.16E-03	6.02E-03	6.08E-03	3.41E-03
10.0	4.96E-03	4.93E-03	4.98E-03	5.00E-03	4.99E-03	4.97E-03	4.99E-03	5.02E-03	5.03E-03	5.07E-03	5.00E-03	4.93E-03	4.86E-03	4.89E-03	2.72E-03

Table A-10. UFRF absorbed fraction for all sources irradiating the shallow active marrow in the sternum.

Sternum ϕ (TAM_{SV}← TAM) Cellularity												Sternum ϕ (TAM_{SV}← r_S) Source Tissue r_S			
Energy (MeV)	100%	90%	80%	70%	60%	50%	40%	30%	20%	10%	70% (ICRP 70)	TM	TBS	TBV	CBS_{HC} or CBV
0.010	2.71E-02	3.03E-02	3.39E-02	3.86E-02	4.45E-02	5.28E-02	6.60E-02	8.81E-02	1.32E-01	2.65E-01	3.86E-02	5.55E-04	8.00E-01	1.10E-02	2.23E-06
0.015	2.68E-02	2.99E-02	3.33E-02	3.79E-02	4.42E-02	5.26E-02	6.58E-02	8.78E-02	1.30E-01	2.60E-01	3.79E-02	1.13E-03	7.94E-01	2.23E-02	1.34E-05
0.020	2.65E-02	2.91E-02	3.24E-02	3.66E-02	4.25E-02	5.09E-02	6.36E-02	8.48E-02	1.26E-01	2.49E-01	3.66E-02	1.85E-03	7.88E-01	3.67E-02	2.33E-05
0.030	2.59E-02	2.82E-02	3.14E-02	3.55E-02	4.08E-02	4.83E-02	5.93E-02	7.75E-02	1.14E-01	2.25E-01	3.55E-02	3.63E-03	7.72E-01	7.19E-02	4.80E-05
0.040	2.51E-02	2.70E-02	2.98E-02	3.34E-02	3.79E-02	4.40E-02	5.36E-02	6.86E-02	1.01E-01	1.97E-01	3.34E-02	5.46E-03	7.51E-01	1.15E-01	6.34E-05
0.050	2.41E-02	2.58E-02	2.80E-02	3.08E-02	3.45E-02	3.97E-02	4.76E-02	6.07E-02	8.65E-02	1.64E-01	3.08E-02	8.48E-03	7.26E-01	1.60E-01	1.16E-04
0.060	2.30E-02	2.44E-02	2.62E-02	2.84E-02	3.12E-02	3.51E-02	4.14E-02	5.18E-02	7.17E-02	1.31E-01	2.84E-02	1.14E-02	6.95E-01	2.05E-01	1.37E-04
0.080	2.16E-02	2.27E-02	2.36E-02	2.47E-02	2.61E-02	2.80E-02	3.15E-02	3.14E-02	4.81E-02	8.02E-02	2.47E-02	1.51E-02	5.92E-01	2.78E-01	2.11E-04
0.10	2.12E-02	2.14E-02	2.21E-02	2.31E-02	2.39E-02	2.51E-02	2.72E-02	3.06E-02	3.70E-02	5.61E-02	2.31E-02	1.72E-02	4.83E-01	3.06E-01	2.73E-04
0.15	2.12E-02	2.14E-02	2.18E-02	2.24E-02	2.29E-02	2.34E-02	2.46E-02	2.68E-02	2.94E-02	3.77E-02	2.24E-02	1.99E-02	3.21E-01	2.78E-01	5.23E-04
0.20	2.25E-02	2.29E-02	2.28E-02	2.27E-02	2.33E-02	2.33E-02	2.39E-02	2.49E-02	2.71E-02	3.34E-02	2.27E-02	2.15E-02	2.32E-01	2.18E-01	8.33E-04
0.30	2.34E-02	2.30E-02	2.30E-02	2.37E-02	2.39E-02	2.40E-02	2.44E-02	2.49E-02	2.61E-02	2.85E-02	2.37E-02	2.20E-02	1.41E-01	1.33E-01	1.31E-03
0.40	2.34E-02	2.31E-02	2.35E-02	2.41E-02	2.43E-02	2.39E-02	2.42E-02	2.48E-02	2.58E-02	2.79E-02	2.41E-02	2.30E-02	1.05E-01	1.00E-01	1.96E-03
0.50	2.31E-02	2.30E-02	2.31E-02	2.33E-02	2.36E-02	2.37E-02	2.39E-02	2.41E-02	2.46E-02	2.62E-02	2.33E-02	2.27E-02	8.58E-02	8.28E-02	2.78E-03
0.60	2.22E-02	2.24E-02	2.31E-02	2.34E-02	2.38E-02	2.38E-02	2.39E-02	2.40E-02	2.44E-02	2.58E-02	2.34E-02	2.24E-02	7.28E-02	7.14E-02	3.29E-03
0.80	2.17E-02	2.21E-02	2.21E-02	2.22E-02	2.23E-02	2.25E-02	2.27E-02	2.31E-02	2.32E-02	2.34E-02	2.22E-02	2.19E-02	5.88E-02	5.61E-02	4.26E-03
1.0	2.08E-02	2.07E-02	2.09E-02	2.12E-02	2.09E-02	2.04E-02	2.09E-02	2.17E-02	2.18E-02	2.23E-02	2.12E-02	2.08E-02	4.86E-02	4.77E-02	5.20E-03
1.5	1.82E-02	1.80E-02	1.86E-02	1.90E-02	1.92E-02	1.94E-02	1.91E-02	1.87E-02	1.88E-02	1.89E-02	1.90E-02	1.90E-02	3.58E-02	3.50E-02	8.16E-03
2.0	1.60E-02	1.57E-02	1.60E-02	1.65E-02	1.66E-02	1.64E-02	1.64E-02	1.64E-02	1.64E-02	1.62E-02	1.65E-02	1.57E-02	2.87E-02	2.83E-02	8.58E-03
3.0	1.24E-02	1.23E-02	1.23E-02	1.25E-02	1.25E-02	1.25E-02	1.26E-02	1.26E-02	1.26E-02	1.27E-02	1.25E-02	1.25E-02	2.06E-02	2.02E-02	5.79E-03
4.0	9.74E-03	9.77E-03	9.82E-03	9.88E-03	9.88E-03	9.84E-03	9.90E-03	1.00E-02	1.01E-02	1.03E-02	9.88E-03	9.76E-03	1.62E-02	1.54E-02	4.96E-03
5.0	8.11E-03	8.03E-03	8.10E-03	8.17E-03	8.13E-03	8.04E-03	8.18E-03	8.21E-03	8.39E-03	8.29E-03	8.17E-03	8.06E-03	1.30E-02	1.29E-02	4.25E-03
6.0	6.83E-03	6.73E-03	6.78E-03	6.78E-03	6.87E-03	6.99E-03	6.99E-03	6.99E-03	7.00E-03	7.05E-03	6.78E-03	6.73E-03	1.09E-02	1.08E-02	3.75E-03
8.0	5.20E-03	5.23E-03	5.26E-03	5.23E-03	5.25E-03	5.27E-03	5.22E-03	5.15E-03	5.17E-03	5.23E-03	5.23E-03	5.18E-03	8.21E-03	8.15E-03	2.90E-03
10.0	4.17E-03	4.16E-03	4.19E-03	4.22E-03	4.13E-03	4.13E-03	4.16E-03	4.20E-03	4.19E-03	4.19E-03	4.22E-03	4.13E-03	6.69E-03	6.56E-03	2.32E-03

Table A-11. UFRF absorbed fraction for all sources irradiating the active marrow in the ribs.

Ribs $\phi(TAM \leftarrow TAM)$ Cellularity												Ribs $\phi(TAM \leftarrow r_S)$ Source Tissue r_S			
Energy (MeV)	100%	90%	80%	70%	60%	50%	40%	30%	20%	10%	70% (ICRP 70)	TM	TBS	TBV	CBS_{HC} or CBV
0.010	8.34E-03	9.24E-03	1.04E-02	1.18E-02	1.37E-02	1.34E-02	2.05E-02	2.72E-02	4.07E-02	8.11E-02	1.18E-02	2.57E-04	4.46E-03	4.08E-05	1.36E-06
0.015	8.33E-03	9.20E-03	1.03E-02	1.17E-02	1.35E-02	1.32E-02	2.01E-02	2.66E-02	3.96E-02	7.87E-02	1.17E-02	5.25E-04	4.47E-03	8.26E-05	2.76E-06
0.020	8.32E-03	9.15E-03	1.02E-02	1.15E-02	1.33E-02	1.58E-02	1.96E-02	2.58E-02	3.82E-02	7.56E-02	1.15E-02	8.63E-04	4.47E-03	1.37E-04	4.58E-06
0.030	8.29E-03	9.02E-03	9.94E-03	1.11E-02	1.27E-02	1.49E-02	1.82E-02	2.37E-02	3.48E-02	6.78E-02	1.11E-02	1.71E-03	4.48E-03	2.74E-04	9.23E-06
0.040	8.23E-03	8.87E-03	9.69E-03	1.07E-02	1.20E-02	1.39E-02	1.67E-02	2.14E-02	3.05E-02	5.85E-02	1.07E-02	2.68E-03	4.48E-03	4.14E-04	1.02E-05
0.050	8.20E-03	8.71E-03	9.35E-03	1.02E-02	1.13E-02	1.28E-02	1.51E-02	1.89E-02	2.65E-02	4.94E-02	1.02E-02	3.71E-03	4.48E-03	5.40E-04	2.30E-05
0.060	8.15E-03	8.55E-03	9.05E-03	9.69E-03	1.05E-02	1.17E-02	1.36E-02	1.65E-02	2.24E-02	4.02E-02	9.69E-03	4.70E-03	4.50E-03	6.53E-04	3.08E-05
0.080	8.04E-03	8.29E-03	8.54E-03	8.80E-03	9.37E-03	1.00E-02	1.10E-02	1.29E-02	1.58E-02	2.54E-02	8.80E-03	6.21E-03	4.53E-03	1.20E-03	4.80E-05
0.10	7.92E-03	8.06E-03	8.23E-03	8.46E-03	8.75E-03	9.15E-03	9.73E-03	1.07E-02	1.26E-02	1.84E-02	8.46E-03	6.85E-03	4.58E-03	1.77E-03	7.10E-05
0.15	7.60E-03	7.68E-03	7.77E-03	7.88E-03	8.02E-03	8.22E-03	8.49E-03	8.95E-03	9.83E-03	1.25E-02	7.88E-03	7.14E-03	4.98E-03	2.88E-03	1.30E-04
0.20	7.30E-03	7.36E-03	7.41E-03	7.49E-03	7.58E-03	7.72E-03	7.89E-03	8.17E-03	8.72E-03	1.04E-02	7.49E-03	7.04E-03	5.33E-03	3.76E-03	1.95E-04
0.30	6.79E-03	6.82E-03	6.86E-03	6.91E-03	6.98E-03	7.04E-03	7.14E-03	7.31E-03	7.60E-03	8.49E-03	6.91E-03	6.88E-03	5.63E-03	4.67E-03	3.33E-04
0.40	6.35E-03	6.39E-03	6.42E-03	6.45E-03	6.49E-03	6.55E-03	6.61E-03	6.72E-03	6.93E-03	7.53E-03	6.45E-03	6.28E-03	5.59E-03	4.95E-03	4.73E-04
0.50	5.98E-03	6.00E-03	6.03E-03	6.06E-03	6.09E-03	6.14E-03	6.19E-03	6.26E-03	6.41E-03	6.86E-03	6.06E-03	5.84E-03	5.44E-03	4.94E-03	6.06E-04
0.60	6.68E-03	6.68E-03	6.80E-03	6.71E-03	6.74E-03	6.79E-03	6.82E-03	6.80E-03	6.91E-03	6.88E-03	6.71E-03	5.61E-03	5.22E-03	4.81E-03	7.21E-04
0.80	5.08E-03	5.08E-03	5.10E-03	5.11E-03	5.14E-03	5.17E-03	5.20E-03	5.25E-03	5.34E-03	5.59E-03	5.11E-03	5.05E-03	4.78E-03	4.52E-03	9.35E-04
1.0	4.60E-03	4.61E-03	4.62E-03	4.63E-03	4.65E-03	4.68E-03	4.70E-03	4.73E-03	4.80E-03	5.01E-03	4.63E-03	4.59E-03	4.39E-03	4.15E-03	1.05E-03
1.5	3.74E-03	3.74E-03	3.76E-03	3.78E-03	3.78E-03	3.79E-03	3.81E-03	3.83E-03	3.88E-03	4.02E-03	3.78E-03	3.72E-03	3.59E-03	3.44E-03	1.08E-03
2.0	3.17E-03	3.18E-03	3.18E-03	3.18E-03	3.20E-03	3.21E-03	3.22E-03	3.23E-03	3.26E-03	3.36E-03	3.18E-03	3.16E-03	3.05E-03	2.95E-03	9.73E-04
3.0	2.48E-03	2.48E-03	2.48E-03	2.47E-03	2.48E-03	2.50E-03	2.50E-03	2.52E-03	2.54E-03	2.59E-03	2.47E-03	2.46E-03	2.39E-03	2.34E-03	7.33E-04
4.0	2.09E-03	2.08E-03	2.08E-03	2.08E-03	2.09E-03	2.10E-03	2.11E-03	2.12E-03	2.14E-03	2.19E-03	2.08E-03	2.07E-03	2.03E-03	1.99E-03	5.64E-04
5.0	1.84E-03	1.84E-03	1.84E-03	1.84E-03	1.85E-03	1.87E-03	1.87E-03	1.87E-03	1.88E-03	1.92E-03	1.84E-03	1.84E-03	1.79E-03	1.77E-03	4.55E-04
6.0	1.66E-03	1.66E-03	1.67E-03	1.67E-03	1.67E-03	1.68E-03	1.68E-03	1.69E-03	1.71E-03	1.74E-03	1.67E-03	1.66E-03	1.63E-03	1.61E-03	3.75E-04
8.0	1.42E-03	1.42E-03	1.42E-03	1.43E-03	1.43E-03	1.44E-03	1.44E-03	1.44E-03	1.45E-03	1.48E-03	1.43E-03	1.43E-03	1.41E-03	1.40E-03	2.84E-04
10.0	1.26E-03	1.26E-03	1.26E-03	1.26E-03	1.27E-03	1.27E-03	1.28E-03	1.28E-03	1.29E-03	1.31E-03	1.26E-03	1.26E-03	1.25E-03	1.24E-03	2.30E-04

Table A-12. UFRF absorbed fraction for all sources irradiating the shallow active marrow in the ribs.

Ribs $\phi(TAM_{SV} \leftarrow TAM)$ Cellularity												Ribs $\phi(TAM_{SV} \leftarrow r_S)$ Source Tissue r_S			
Energy (MeV)	100%	90%	80%	70%	60%	50%	40%	30%	20%	10%	70% (ICRP 70)	TM	TBS	TBV	CBS_{HC} or CBV
0.010	6.93E-03	7.63E-03	8.62E-03	9.83E-03	1.14E-02	1.37E-02	1.71E-02	2.27E-02	3.39E-02	6.76E-02	9.83E-03	1.40E-04	4.84E-02	4.43E-04	9.19E-07
0.015	6.86E-03	7.53E-03	8.50E-03	9.68E-03	1.12E-02	1.34E-02	1.67E-02	2.22E-02	3.31E-02	6.59E-02	9.65E-03	2.82E-04	4.81E-02	8.53E-04	2.48E-06
0.020	6.79E-03	7.43E-03	8.35E-03	9.48E-03	1.10E-02	1.31E-02	1.62E-02	2.15E-02	3.19E-02	6.33E-02	9.48E-03	4.67E-04	4.77E-02	1.47E-03	3.68E-06
0.030	6.61E-03	7.21E-03	7.98E-03	8.98E-03	1.03E-02	1.22E-02	1.50E-02	1.98E-02	2.92E-02	5.74E-02	8.98E-03	9.27E-04	4.68E-02	2.91E-03	7.91E-06
0.040	6.34E-03	6.89E-03	7.55E-03	8.40E-03	9.55E-03	1.12E-02	1.36E-02	1.77E-02	2.58E-02	5.00E-02	8.40E-03	1.50E-03	4.56E-02	4.64E-03	1.13E-05
0.050	6.07E-03	6.53E-03	7.06E-03	7.75E-03	8.73E-03	1.00E-02	1.21E-02	1.54E-02	2.20E-02	4.17E-02	7.75E-03	2.12E-03	4.41E-02	6.56E-03	1.73E-05
0.060	5.77E-03	6.11E-03	6.56E-03	7.12E-03	7.85E-03	8.86E-03	1.04E-02	1.30E-02	1.82E-02	3.36E-02	7.12E-03	2.74E-03	4.25E-02	8.52E-03	2.48E-05
0.080	5.30E-03	5.47E-03	5.72E-03	6.03E-03	6.45E-03	7.03E-03	7.90E-03	9.35E-03	1.21E-02	2.04E-02	6.03E-03	3.62E-03	3.65E-02	1.18E-02	3.62E-05
0.10	5.00E-03	5.11E-03	5.26E-03	5.45E-03	5.72E-03	6.05E-03	6.57E-03	7.44E-03	9.13E-03	1.42E-02	5.45E-03	4.01E-03	2.98E-02	1.36E-02	5.11E-05
0.15	4.77E-03	4.82E-03	4.89E-03	4.98E-03	5.12E-03	5.27E-03	5.52E-03	5.92E-03	6.69E-03	8.99E-03	4.98E-03	4.33E-03	2.07E-02	1.40E-02	9.62E-05
0.20	4.75E-03	4.79E-03	4.83E-03	4.91E-03	4.98E-03	5.07E-03	5.21E-03	5.48E-03	5.94E-03	7.38E-03	4.91E-03	4.54E-03	1.59E-02	1.25E-02	1.47E-04
0.30	4.73E-03	4.77E-03	4.78E-03	4.82E-03	4.86E-03	4.90E-03	5.00E-03	5.10E-03	5.41E-03	6.15E-03	4.82E-03	4.61E-03	1.11E-02	9.80E-03	2.43E-04
0.40	4.57E-03	4.59E-03	4.62E-03	4.64E-03	4.67E-03	4.70E-03	4.77E-03	4.89E-03	5.05E-03	5.54E-03	4.64E-03	4.47E-03	8.93E-03	8.21E-03	3.59E-04
0.50	4.37E-03	4.40E-03	4.40E-03	4.41E-03	4.41E-03	4.47E-03	4.51E-03	4.58E-03	4.71E-03	5.09E-03	4.41E-03	4.31E-03	7.82E-03	7.17E-03	4.76E-04
0.60	4.17E-03	4.19E-03	4.15E-03	4.18E-03	4.13E-03	4.22E-03	4.26E-03	4.32E-03	4.42E-03	4.72E-03	4.18E-03	4.11E-03	6.72E-03	6.39E-03	5.70E-04
0.80	3.76E-03	3.79E-03	3.78E-03	3.77E-03	3.79E-03	3.79E-03	3.82E-03	3.88E-03	3.95E-03	4.17E-03	3.77E-03	3.72E-03	5.57E-03	5.35E-03	7.26E-04
1.0	3.39E-03	3.40E-03	3.40E-03	3.41E-03	3.42E-03	3.44E-03	3.47E-03	3.50E-03	3.56E-03	3.74E-03	3.41E-03	3.39E-03	4.85E-03	4.65E-03	8.15E-04
1.5	2.74E-03	2.75E-03	2.75E-03	2.76E-03	2.76E-03	2.80E-03	2.80E-03	2.81E-03	2.85E-03	2.98E-03	2.76E-03	2.72E-03	3.67E-03	3.58E-03	8.34E-04
2.0	2.33E-03	2.33E-03	2.33E-03	2.33E-03	2.34E-03	2.35E-03	2.37E-03	2.39E-03	2.42E-03	2.49E-03	2.33E-03	2.34E-03	3.01E-03	2.98E-03	7.49E-04
3.0	1.83E-03	1.83E-03	1.83E-03	1.84E-03	1.85E-03	1.86E-03	1.86E-03	1.86E-03	1.88E-03	1.94E-03	1.84E-03	1.80E-03	2.29E-03	2.28E-03	5.50E-04
4.0	1.55E-03	1.55E-03	1.55E-03	1.56E-03	1.58E-03	1.56E-03	1.57E-03	1.59E-03	1.60E-03	1.64E-03	1.56E-03	1.54E-03	1.89E-03	1.88E-03	4.23E-04
5.0	1.38E-03	1.38E-03	1.38E-03	1.38E-03	1.39E-03	1.39E-03	1.40E-03	1.40E-03	1.41E-03	1.45E-03	1.38E-03	1.37E-03	1.66E-03	1.66E-03	3.41E-04
6.0	1.25E-03	1.26E-03	1.26E-03	1.26E-03	1.27E-03	1.27E-03	1.27E-03	1.28E-03	1.29E-03	1.32E-03	1.26E-03	1.26E-03	1.49E-03	1.49E-03	2.81E-04
8.0	1.09E-03	1.09E-03	1.08E-03	1.09E-03	1.09E-03	1.10E-03	1.10E-03	1.10E-03	1.11E-03	1.14E-03	1.09E-03	1.09E-03	1.26E-03	1.27E-03	2.13E-04
10.0	9.70E-04	9.67E-04	9.68E-04	9.71E-04	9.73E-04	9.78E-04	9.78E-04	9.17E-04	9.85E-04	1.01E-03	9.71E-04	9.67E-04	1.12E-03	1.11E-03	1.74E-04

Table A-13. UFRF absorbed fraction for all sources irradiating the active marrow in the cervical vertebrae.

Cervical Vertebrae ϕ (TAM← TAM) Cellularity												Cervical Vertebrae ϕ (TAM← r_S) Source Tissue r_S			
Energy (MeV)	100%	90%	80%	70%	60%	50%	40%	30%	20%	10%	70% (ICRP 70)	TM	TBS	TBV	CBS_{HC} or CBV
0.010	3.91E-02	4.33E-02	4.86E-02	5.53E-02	6.44E-02	7.70E-02	9.60E-02	1.28E-01	1.91E-01	3.80E-01	5.53E-02	1.17E-03	2.08E-02	1.27E-04	5.45E-06
0.015	3.90E-02	4.31E-02	4.82E-02	5.47E-02	6.35E-02	7.57E-02	9.40E-02	1.25E-01	1.86E-01	3.69E-01	5.47E-02	2.40E-03	2.09E-02	2.62E-04	1.08E-05
0.020	3.89E-02	4.28E-02	4.77E-02	5.39E-02	6.23E-02	7.40E-02	9.15E-02	1.21E-01	1.79E-01	3.55E-01	5.39E-02	3.93E-03	2.08E-02	4.32E-04	1.93E-05
0.030	3.87E-02	4.25E-02	4.84E-02	5.29E-02	5.94E-02	6.98E-02	8.63E-02	1.11E-01	1.63E-01	3.19E-01	5.29E-02	7.77E-03	2.06E-02	8.63E-04	3.84E-05
0.040	3.84E-02	4.13E-02	4.50E-02	4.97E-02	5.60E-02	6.48E-02	7.80E-02	1.00E-01	1.44E-01	2.76E-01	4.97E-02	1.23E-02	2.06E-02	1.40E-03	6.14E-05
0.050	3.80E-02	4.04E-02	4.34E-02	4.73E-02	5.24E-02	5.96E-02	7.04E-02	8.84E-02	1.24E-01	2.32E-01	4.73E-02	1.69E-02	2.05E-02	2.01E-03	8.91E-05
0.060	3.76E-02	3.96E-02	4.19E-02	4.48E-02	4.88E-02	5.44E-02	6.29E-02	7.69E-02	1.05E-01	1.88E-01	4.48E-02	2.14E-02	2.03E-02	2.68E-03	1.22E-04
0.080	3.68E-02	3.79E-02	3.92E-02	4.08E-02	4.30E-02	4.51E-02	5.07E-02	5.83E-02	7.35E-02	1.19E-01	4.08E-02	2.82E-02	2.00E-02	4.06E-03	1.93E-04
0.10	3.59E-02	3.66E-02	3.74E-02	3.85E-02	3.98E-02	4.17E-02	4.44E-02	4.90E-02	5.81E-02	8.52E-02	3.85E-02	3.09E-02	1.99E-02	5.51E-03	2.90E-04
0.15	3.36E-02	3.39E-02	3.43E-02	3.48E-02	3.55E-02	3.54E-02	3.77E-02	3.99E-02	4.40E-02	5.63E-02	3.48E-02	3.14E-02	2.04E-02	9.27E-03	5.18E-04
0.20	3.12E-02	3.15E-02	3.18E-02	3.21E-02	3.25E-02	3.31E-02	3.39E-02	3.53E-02	3.78E-02	4.53E-02	3.21E-02	2.89E-02	2.11E-02	1.28E-02	7.84E-04
0.30	2.76E-02	2.77E-02	2.79E-02	2.81E-02	2.84E-02	2.87E-02	2.92E-02	2.99E-02	3.12E-02	3.53E-02	2.81E-02	2.69E-02	2.21E-02	1.78E-02	1.29E-03
0.40	2.54E-02	2.54E-02	2.56E-02	2.57E-02	2.59E-02	2.62E-02	2.64E-02	2.69E-02	2.79E-02	3.07E-02	2.57E-02	2.50E-02	2.19E-02	1.92E-02	1.76E-03
0.60	2.30E-02	2.30E-02	2.30E-02	2.32E-02	2.33E-02	2.34E-02	2.37E-02	2.41E-02	2.48E-02	2.70E-02	2.32E-02	2.36E-02	2.13E-02	1.91E-02	2.10E-03
0.80	2.26E-02	2.26E-02	2.26E-02	2.30E-02	2.30E-02	2.31E-02	2.33E-02	2.36E-02	2.41E-02	2.59E-02	2.30E-02	2.24E-02	2.07E-02	1.92E-02	2.62E-03
1.0	2.05E-02	2.06E-02	2.07E-02	2.08E-02	2.08E-02	2.09E-02	2.10E-02	2.12E-02	2.16E-02	2.28E-02	2.08E-02	2.05E-02	1.92E-02	1.81E-02	3.16E-03
1.5	1.54E-02	1.53E-02	1.53E-02	1.54E-02	1.54E-02	1.55E-02	1.56E-02	1.57E-02	1.59E-02	1.64E-02	1.54E-02	1.52E-02	1.47E-02	1.43E-02	3.97E-03
2.0	1.27E-02	1.28E-02	1.28E-02	1.28E-02	1.28E-02	1.28E-02	1.28E-02	1.29E-02	1.31E-02	1.34E-02	1.28E-02	1.26E-02	1.23E-02	1.21E-02	3.63E-03
3.0	8.98E-03	9.04E-03	8.99E-03	8.93E-03	9.04E-03	9.20E-03	9.17E-03	9.11E-03	9.21E-03	9.50E-03	8.93E-03	9.10E-03	8.74E-03	8.63E-03	3.01E-03
4.0	6.81E-03	6.82E-03	6.83E-03	6.86E-03	6.84E-03	6.82E-03	6.79E-03	6.75E-03	6.85E-03	7.14E-03	6.86E-03	6.75E-03	6.62E-03	6.44E-03	2.38E-03
5.0	5.34E-03	5.35E-03	5.37E-03	5.40E-03	5.41E-03	5.41E-03	5.42E-03	5.42E-03	5.49E-03	5.70E-03	5.40E-03	5.35E-03	5.23E-03	5.13E-03	1.91E-03
6.0	4.44E-03	4.43E-03	4.44E-03	4.46E-03	4.48E-03	4.50E-03	4.50E-03	4.49E-03	4.54E-03	4.70E-03	4.46E-03	4.40E-03	4.31E-03	4.24E-03	1.64E-03
8.0	3.33E-03	3.33E-03	3.31E-03	3.31E-03	3.33E-03	3.33E-03	3.33E-03	3.36E-03	3.40E-03	3.53E-03	3.31E-03	3.27E-03	3.23E-03	3.18E-03	1.26E-03
10.0	2.66E-03	2.64E-03	2.63E-03	2.63E-03	2.65E-03	2.67E-03	2.67E-03	2.69E-03	2.71E-03	2.80E-03	2.63E-03	2.62E-03	2.56E-03	2.54E-03	9.63E-04

Table A-14. UFRF absorbed fraction for all sources irradiating the shallow active marrow in the cervical vertebrae.

Cervical Vertebrae ϕ (TAM_{SV}← TAM) Cellularity												Cervical Vertebrae ϕ (TAM_{SV}← r_S) Source Tissue r_S			
Energy (MeV)	100%	90%	80%	70%	60%	50%	40%	30%	20%	10%	70% (ICRP 70)	TM	TBS	TBV	CBS_{HC} or CBV
0.010	3.51E-02	3.98E-02	4.57E-02	5.39E-02	6.57E-02	8.35E-02	8.67E-02	1.15E-01	1.73E-01	3.44E-01	4.99E-02	6.84E-04	1.23E-01	7.46E-04	4.27E-06
0.015	3.47E-02	3.93E-02	4.31E-02	4.90E-02	5.73E-02	6.82E-02	8.49E-02	1.13E-01	1.68E-01	3.34E-01	4.90E-02	1.40E-03	1.22E-01	1.54E-03	9.48E-06
0.020	3.43E-02	3.73E-02	4.23E-02	4.81E-02	5.57E-02	6.63E-02	8.24E-02	1.09E-01	1.62E-01	3.22E-01	4.81E-02	2.25E-03	1.21E-01	2.52E-03	1.62E-05
0.030	3.32E-02	3.61E-02	4.03E-02	4.56E-02	5.23E-02	6.19E-02	7.63E-02	1.00E-01	1.49E-01	2.93E-01	4.55E-02	4.55E-03	1.19E-01	4.99E-03	3.07E-05
0.040	3.18E-02	3.46E-02	3.80E-02	4.24E-02	4.83E-02	5.65E-02	6.89E-02	8.55E-02	1.31E-01	2.54E-01	4.24E-02	7.36E-03	1.15E-01	8.00E-03	5.51E-05
0.050	3.03E-02	3.25E-02	3.54E-02	3.91E-02	4.38E-02	5.06E-02	6.06E-02	7.74E-02	1.11E-01	2.12E-01	3.91E-02	1.03E-02	1.10E-01	1.13E-02	7.82E-05
0.060	2.89E-02	3.05E-02	3.28E-02	3.57E-02	3.94E-02	4.47E-02	5.25E-02	6.66E-02	9.18E-02	1.70E-01	3.57E-02	1.32E-02	1.05E-01	1.46E-02	1.08E-04
0.080	2.60E-02	2.71E-02	2.84E-02	3.00E-02	3.22E-02	3.48E-02	3.92E-02	4.66E-02	6.12E-02	1.05E-01	3.00E-02	1.76E-02	9.03E-02	2.05E-02	1.58E-04
0.10	2.43E-02	2.49E-02	2.57E-02	2.66E-02	2.79E-02	2.97E-02	3.23E-02	3.66E-02	4.53E-02	7.13E-02	2.66E-02	1.93E-02	7.36E-02	2.40E-02	2.39E-04
0.15	2.23E-02	2.28E-02	2.30E-02	2.35E-02	2.40E-02	2.48E-02	2.61E-02	2.83E-02	3.21E-02	4.36E-02	2.35E-02	2.02E-02	5.05E-02	2.69E-02	4.22E-04
0.20	2.10E-02	2.13E-02	2.21E-02	2.23E-02	2.27E-02	2.31E-02	2.40E-02	2.50E-02	2.69E-02	3.31E-02	2.23E-02	2.04E-02	3.90E-02	2.68E-02	6.55E-04
0.30	2.12E-02	2.13E-02	2.14E-02	2.16E-02	2.13E-02	2.21E-02	2.25E-02	2.32E-02	2.45E-02	2.85E-02	2.16E-02	2.08E-02	3.08E-02	2.48E-02	1.09E-03
0.40	2.06E-02	2.09E-02	2.09E-02	2.10E-02	2.11E-02	2.13E-02	2.16E-02	2.22E-02	2.30E-02	2.54E-02	2.10E-02	2.01E-02	2.69E-02	2.31E-02	1.49E-03
0.50	1.98E-02	2.01E-02	2.01E-02	2.01E-02	2.01E-02	2.02E-02	2.05E-02	2.12E-02	2.18E-02	2.36E-02	2.01E-02	1.98E-02	2.48E-02	2.22E-02	1.88E-03
0.60	1.91E-02	1.93E-02	1.92E-02	1.93E-02	1.94E-02	1.96E-02	1.97E-02	2.00E-02	2.05E-02	2.22E-02	1.93E-02	1.90E-02	2.31E-02	2.10E-02	2.31E-03
0.80	1.76E-02	1.79E-02	1.78E-02	1.80E-02	1.79E-02	1.79E-02	1.81E-02	1.84E-02	1.87E-02	1.97E-02	1.80E-02	1.76E-02	2.05E-02	1.91E-02	2.80E-03
1.0	1.62E-02	1.63E-02	1.63E-02	1.64E-02	1.65E-02	1.65E-02	1.66E-02	1.68E-02	1.71E-02	1.80E-02	1.64E-02	1.62E-02	1.86E-02	1.75E-02	3.23E-03
1.5	1.35E-02	1.34E-02	1.34E-02	1.35E-02	1.35E-02	1.36E-02	1.37E-02	1.38E-02	1.40E-02	1.43E-02	1.35E-02	1.34E-02	1.48E-02	1.43E-02	3.58E-03
2.0	1.13E-02	1.13E-02	1.13E-02	1.13E-02	1.13E-02	1.13E-02	1.13E-02	1.14E-02	1.16E-02	1.20E-02	1.13E-02	1.11E-02	1.22E-02	1.19E-02	3.31E-03
3.0	7.97E-03	8.03E-03	8.02E-03	7.97E-03	8.08E-03	8.23E-03	8.20E-03	8.15E-03	8.20E-03	8.36E-03	7.97E-03	8.02E-03	8.70E-03	8.49E-03	2.68E-03
4.0	6.06E-03	6.06E-03	6.08E-03	6.11E-03	6.08E-03	6.04E-03	6.02E-03	6.00E-03	6.07E-03	6.32E-03	6.11E-03	6.08E-03	6.67E-03	6.36E-03	2.16E-03
5.0	4.73E-03	4.73E-03	4.75E-03	4.80E-03	4.81E-03	4.82E-03	4.82E-03	4.83E-03	4.90E-03	5.11E-03	4.80E-03	4.75E-03	5.21E-03	5.07E-03	1.74E-03
6.0	3.93E-03	3.94E-03	3.95E-03	3.96E-03	3.98E-03	4.00E-03	3.99E-03	3.98E-03	4.04E-03	4.19E-03	3.96E-03	3.93E-03	4.30E-03	4.20E-03	1.48E-03
8.0	2.97E-03	2.94E-03	2.95E-03	2.95E-03	2.94E-03	2.93E-03	2.95E-03	2.98E-03	3.01E-03	3.10E-03	2.95E-03	2.92E-03	3.22E-03	3.12E-03	1.14E-03
10.0	2.38E-03	2.34E-03	2.34E-03	2.35E-03	2.38E-03	2.37E-03	2.38E-03	2.39E-03	2.42E-03	2.49E-03	2.35E-03	2.34E-03	2.55E-03	2.51E-03	8.61E-04

Table A-15. UFRF absorbed fraction for all sources irradiating the active marrow in the thoracic vertebrae.

Thoracic Vertebrae ϕ (TAM← TAM) Cellularity												Thoracic Vertebrae ϕ (TAM← r_S) Source Tissue r_S			
Energy (MeV)	100%	90%	80%	70%	60%	50%	40%	30%	20%	10%	70% (ICRP 70)	TM	TBS	TBV	CBS_{HC} or CBV
0.010	6.28E-03	6.95E-03	7.80E-03	8.89E-03	1.03E-02	1.24E-02	1.54E-02	2.05E-02	3.06E-02	6.11E-02	8.89E-03	1.93E-04	3.36E-03	2.85E-05	1.09E-06
0.015	6.27E-03	6.93E-03	7.74E-03	8.79E-03	1.02E-02	1.22E-02	1.51E-02	2.00E-02	2.98E-02	5.92E-02	8.79E-03	3.94E-04	3.37E-03	5.78E-05	2.61E-06
0.020	6.26E-03	6.89E-03	7.67E-03	8.67E-03	1.00E-02	1.19E-02	1.47E-02	1.94E-02	2.88E-02	5.70E-02	8.67E-03	6.48E-04	3.37E-03	9.52E-05	4.44E-06
0.030	6.24E-03	6.86E-03	7.59E-03	8.58E-03	9.87E-03	1.17E-02	1.37E-02	1.79E-02	2.62E-02	5.12E-02	8.58E-03	1.28E-03	3.36E-03	1.90E-04	8.69E-06
0.040	6.21E-03	6.69E-03	7.28E-03	8.04E-03	9.05E-03	1.06E-02	1.26E-02	1.61E-02	2.32E-02	4.45E-02	8.04E-03	2.02E-03	3.36E-03	3.10E-04	1.42E-05
0.050	6.18E-03	6.57E-03	7.05E-03	7.67E-03	8.49E-03	9.85E-03	1.14E-02	1.43E-02	2.00E-02	3.73E-02	7.67E-03	2.79E-03	3.36E-03	4.43E-04	2.07E-05
0.060	6.15E-03	6.49E-03	6.87E-03	7.31E-03	7.95E-03	8.95E-03	1.03E-02	1.24E-02	1.68E-02	3.07E-02	7.31E-03	3.56E-03	3.35E-03	5.93E-04	2.81E-05
0.080	6.07E-03	6.24E-03	6.45E-03	6.72E-03	7.07E-03	7.56E-03	8.30E-03	9.52E-03	1.20E-02	1.92E-02	6.72E-03	4.70E-03	3.36E-03	9.02E-04	4.59E-05
0.10	5.99E-03	6.10E-03	6.23E-03	6.40E-03	6.61E-03	6.91E-03	7.35E-03	8.09E-03	9.54E-03	1.39E-02	6.40E-03	5.19E-03	3.38E-03	1.23E-03	6.65E-05
0.15	5.77E-03	5.83E-03	5.90E-03	5.98E-03	6.09E-03	6.23E-03	6.44E-03	6.79E-03	7.46E-03	9.45E-03	5.98E-03	5.44E-03	3.65E-03	2.07E-03	1.21E-04
0.20	5.57E-03	5.61E-03	5.65E-03	5.70E-03	5.77E-03	5.86E-03	6.00E-03	6.22E-03	6.64E-03	7.88E-03	5.70E-03	5.37E-03	3.86E-03	2.85E-03	1.83E-04
0.30	5.24E-03	5.27E-03	5.30E-03	5.34E-03	5.37E-03	5.42E-03	5.50E-03	5.63E-03	5.85E-03	6.53E-03	5.34E-03	5.15E-03	4.39E-03	3.83E-03	3.06E-04
0.40	5.03E-03	5.05E-03	5.07E-03	5.10E-03	5.13E-03	5.17E-03	5.23E-03	5.31E-03	5.46E-03	5.92E-03	5.10E-03	4.97E-03	4.51E-03	4.18E-03	4.26E-04
0.60	4.88E-03	4.89E-03	4.90E-03	4.92E-03	4.95E-03	4.98E-03	5.03E-03	5.10E-03	5.21E-03	5.56E-03	4.92E-03	4.83E-03	4.60E-03	4.38E-03	6.46E-04
0.80	4.71E-03	4.74E-03	4.75E-03	4.77E-03	4.79E-03	4.83E-03	4.88E-03	4.91E-03	5.01E-03	5.29E-03	4.77E-03	4.70E-03	4.44E-03	4.24E-03	8.42E-04
0.80	4.46E-03	4.47E-03	4.48E-03	4.50E-03	4.51E-03	4.54E-03	4.57E-03	4.62E-03	4.68E-03	4.86E-03	4.50E-03	4.46E-03	4.27E-03	4.15E-03	8.11E-04
1.0	4.23E-03	4.24E-03	4.25E-03	4.27E-03	4.27E-03	4.29E-03	4.31E-03	4.35E-03	4.40E-03	4.58E-03	4.27E-03	4.22E-03	4.09E-03	3.99E-03	9.16E-04
1.5	3.70E-03	3.71E-03	3.72E-03	3.74E-03	3.75E-03	3.76E-03	3.78E-03	3.80E-03	3.83E-03	3.92E-03	3.74E-03	3.72E-03	3.63E-03	3.57E-03	1.02E-03
2.0	3.29E-03	3.30E-03	3.30E-03	3.30E-03	3.30E-03	3.31E-03	3.32E-03	3.34E-03	3.35E-03	3.41E-03	3.30E-03	3.27E-03	3.24E-03	3.20E-03	9.91E-04
3.0	2.62E-03	2.60E-03	2.62E-03	2.65E-03	2.64E-03	2.34E-03	2.65E-03	2.68E-03	2.68E-03	2.71E-03	2.65E-03	2.62E-03	2.59E-03	2.56E-03	8.33E-04
4.0	2.12E-03	2.13E-03	2.13E-03	2.13E-03	2.13E-03	2.13E-03	2.14E-03	2.15E-03	2.16E-03	2.19E-03	2.13E-03	2.12E-03	2.10E-03	2.10E-03	7.05E-04
5.0	1.76E-03	1.78E-03	1.77E-03	1.75E-03	1.78E-03	1.77E-03	1.77E-03	1.78E-03	1.79E-03	1.82E-03	1.75E-03	1.76E-03	1.76E-03	1.73E-03	5.98E-04
6.0	1.49E-03	1.49E-03	1.49E-03	1.49E-03	1.49E-03	1.49E-03	1.49E-03	1.49E-03	1.49E-03	1.52E-03	1.49E-03	1.48E-03	1.48E-03	1.46E-03	5.13E-04
8.0	1.13E-03	1.13E-03	1.13E-03	1.13E-03	1.13E-03	1.13E-03	1.13E-03	1.13E-03	1.13E-03	1.15E-03	1.13E-03	1.11E-03	1.10E-03	1.09E-03	3.99E-04
10.0	8.92E-04	8.96E-04	8.94E-04	8.92E-04	8.92E-04	8.91E-04	8.96E-04	9.00E-04	9.02E-04	9.09E-04	8.92E-04	8.90E-04	8.83E-04	8.74E-04	3.22E-04

Table A-16. UFRF absorbed fraction for all sources irradiating the shallow active marrow in the thoracic vertebrae.

Thoracic Vertebrae ϕ (TAM_{SV}← TAM) Cellularity												Thoracic Vertebrae ϕ (TAM_{SV}← r_S) Source Tissue r_S			
Energy (MeV)	100%	90%	80%	70%	60%	50%	40%	30%	20%	10%	70% (ICRP 70)	TM	TBS	TBV	CBS_{HC} or CBV
0.010	6.62E-03	6.24E-03	7.01E-03	8.07E-03	9.53E-03	1.17E-02	1.49E-02	1.99E-02	2.78E-02	5.55E-02	8.07E-03	1.13E-04	3.35E-02	2.84E-04	7.57E-07
0.015	5.57E-03	6.17E-03	6.92E-03	7.88E-03	9.14E-03	1.09E-02	1.36E-02	1.81E-02	2.71E-02	5.39E-02	7.88E-03	2.27E-04	3.33E-02	5.71E-04	2.36E-06
0.020	5.52E-03	6.09E-03	6.80E-03	7.72E-03	8.95E-03	1.07E-02	1.32E-02	1.75E-02	2.61E-02	5.20E-02	7.72E-03	3.77E-04	3.31E-02	9.40E-04	3.64E-06
0.030	5.34E-03	5.95E-03	6.59E-03	7.34E-03	8.43E-03	9.94E-03	1.23E-02	1.61E-02	2.39E-02	4.69E-02	7.34E-03	7.48E-04	3.23E-02	1.86E-03	7.19E-06
0.040	5.13E-03	5.57E-03	6.12E-03	6.82E-03	7.73E-03	9.12E-03	1.11E-02	1.44E-02	2.11E-02	4.10E-02	6.82E-03	1.20E-03	3.14E-02	2.98E-03	1.26E-05
0.050	4.90E-03	5.23E-03	5.73E-03	6.30E-03	7.13E-03	8.21E-03	9.83E-03	1.25E-02	1.79E-02	3.43E-02	6.30E-03	1.72E-03	3.04E-02	4.17E-03	1.74E-05
0.060	4.68E-03	4.93E-03	5.33E-03	5.78E-03	6.37E-03	7.20E-03	8.46E-03	1.06E-02	1.48E-02	2.76E-02	5.78E-03	2.19E-03	2.91E-02	5.46E-03	2.4 E-05
0.080	4.30E-03	4.44E-03	4.64E-03	4.90E-03	5.21E-03	5.71E-03	6.42E-03	7.60E-03	9.94E-03	1.70E-02	4.90E-03	2.94E-03	2.50E-02	7.58E-03	3.76E-05
0.10	4.04E-03	4.17E-03	4.28E-03	4.42E-03	4.64E-03	4.95E-03	5.38E-03	6.09E-03	7.51E-03	1.18E-02	4.42E-03	3.25E-03	2.04E-02	8.76E-03	5.23E-05
0.15	3.90E-03	3.91E-03	3.98E-03	4.06E-03	4.17E-03	4.32E-03	4.51E-03	4.83E-03	5.46E-03	7.34E-03	4.06E-03	3.54E-03	1.40E-02	9.38E-03	9.63E-05
0.20	3.84E-03	3.80E-03	4.00E-03	4.09E-03	4.13E-03	4.23E-03	4.35E-03	4.55E-03	4.92E-03	6.03E-03	4.05E-03	3.73E-03	1.00E-02	9.70E-03	1.56E-04
0.30	4.11E-03	4.15E-03	4.16E-03	4.20E-03	4.21E-03	4.30E-03	4.36E-03	4.46E-03	4.68E-03	5.35E-03	4.20E-03	4.02E-03	7.88E-03	6.92E-03	2.58E-04
0.40	4.15E-03	4.19E-03	4.20E-03	4.22E-03	4.25E-03	4.30E-03	4.38E-03	4.48E-03	4.69E-03	5.01E-03	4.22E-03	4.12E-03	6.58E-03	5.97E-03	3.68E-04
0.50	4.13E-03	4.18E-03	4.15E-03	4.18E-03	4.23E-03	4.22E-03	4.29E-03	4.32E-03	4.43E-03	4.75E-03	4.18E-03	4.08E-03	5.90E-03	5.47E-03	4.7 E-04
0.60	4.01E-03	4.03E-03	4.08E-03	4.09E-03	4.11E-03	4.14E-03	4.17E-03	4.23E-03	4.32E-03	4.59E-03	4.09E-03	4.02E-03	5.47E-03	5.12E-03	5.61E-04
0.80	3.87E-03	3.90E-03	3.91E-03	3.92E-03	3.99E-03	3.94E-03	3.97E-03	4.03E-03	4.09E-03	4.27E-03	3.92E-03	3.85E-03	4.92E-03	4.66E-03	7.11E-04
1.0	3.70E-03	3.80E-03	3.71E-03	3.72E-03	3.73E-03	3.74E-03	3.76E-03	3.80E-03	3.85E-03	4.00E-03	3.72E-03	3.68E-03	4.52E-03	4.34E-03	8.18E-04
1.5	3.27E-03	3.24E-03	3.29E-03	3.30E-03	3.31E-03	3.32E-03	3.33E-03	3.35E-03	3.39E-03	3.50E-03	3.30E-03	3.28E-03	3.80E-03	3.71E-03	9.18E-04
2.0	2.93E-03	2.90E-03	2.92E-03	2.93E-03	2.93E-03	2.93E-03	2.94E-03	2.95E-03	2.97E-03	3.02E-03	2.93E-03	2.90E-03	3.30E-03	3.23E-03	8.83E-04
3.0	2.34E-03	2.30E-03	2.34E-03	2.37E-03	2.33E-03	2.35E-03	2.36E-03	2.39E-03	2.40E-03	2.42E-03	2.37E-03	2.35E-03	2.60E-03	2.56E-03	7.56E-04
4.0	1.91E-03	1.89E-03	1.90E-03	1.90E-03	1.90E-03	1.91E-03	1.91E-03	1.92E-03	1.93E-03	1.97E-03	1.90E-03	1.90E-03	2.10E-03	2.08E-03	6.31E-04
5.0	1.57E-03	1.56E-03	1.58E-03	1.57E-03	1.58E-03	1.58E-03	1.59E-03	1.59E-03	1.60E-03	1.64E-03	1.57E-03	1.57E-03	1.74E-03	1.71E-03	5.38E-04
6.0	1.33E-03	1.33E-03	1.33E-03	1.33E-03	1.33E-03	1.34E-03	1.34E-03	1.33E-03	1.33E-03	1.35E-03	1.33E-03	1.32E-03	1.47E-03	1.44E-03	4.83E-04
8.0	1.00E-03	9.97E-04	9.98E-04	1.00E-03	1.00E-03	9.99E-04	1.00E-03	1.01E-03	1.01E-03	1.03E-03	1.00E-03	9.92E-04	1.09E-03	1.07E-03	3.61E-04
10.0	7.95E-04	8.01E-04	8.01E-04	8.01E-04	8.00E-04	7.98E-04	8.01E-04	8.05E-04	8.09E-04	8.20E-04	8.01E-04	7.97E-04	8.77E-04	8.59E-04	2.89E-04

Table A-17. UFRF absorbed fraction for all sources irradiating the active marrow in the lumbar vertebrae.

Lumbar Vertebrae ϕ (TAM← TAM) Cellularity												Lumbar Vertebrae ϕ (TAM← r_S) Source Tissue r_S			
Energy (MeV)	100%	90%	80%	70%	60%	50%	40%	30%	20%	10%	70% (ICRP 70)	TM	TBS	TBV	CBS_{HC} or CBV
0.010	7.05E-03	7.81E-03	8.76E-03	9.98E-03	1.16E-02	1.39E-02	1.73E-02	2.30E-02	3.44E-02	6.86E-02	9.98E-03	2.16E-04	3.78E-03	3.02E-05	1.21E-06
0.015	7.05E-03	7.78E-03	8.70E-03	9.88E-03	1.15E-02	1.37E-02	1.70E-02	2.25E-02	3.35E-02	6.66E-02	9.88E-03	4.42E-04	3.78E-03	6.16E-05	2.32E-06
0.020	7.04E-03	7.74E-03	8.62E-03	9.75E-03	1.13E-02	1.34E-02	1.65E-02	2.18E-02	3.23E-02	6.40E-02	9.75E-03	7.29E-04	3.78E-03	1.01E-04	4.04E-06
0.030	7.02E-03	7.04E-03	8.42E-03	9.42E-03	1.08E-02	1.28E-02	1.04E-02	2.01E-02	2.95E-02	5.75E-02	9.42E-03	1.40E-03	3.78E-03	2.06E-04	8.63E-06
0.040	6.99E-03	7.53E-03	8.18E-03	9.04E-03	1.02E-02	1.18E-02	1.42E-02	1.81E-02	2.61E-02	5.00E-02	9.04E-03	2.27E-03	3.77E-03	3.33E-04	1.45E-05
0.050	6.96E-03	7.39E-03	7.93E-03	8.63E-03	9.66E-03	1.09E-02	1.28E-02	1.61E-02	2.25E-02	4.19E-02	8.63E-03	3.15E-03	3.76E-03	4.78E-04	2.10E-05
0.060	6.93E-03	7.29E-03	7.79E-03	8.43E-03	9.36E-03	1.07E-02	1.25E-02	1.56E-02	2.16E-02	3.97E-02	8.43E-03	4.00E-03	3.77E-03	6.28E-04	2.78E-05
0.080	6.85E-03	7.04E-03	7.28E-03	7.59E-03	7.98E-03	8.53E-03	9.36E-03	1.07E-02	1.35E-02	2.16E-02	7.59E-03	5.31E-03	3.77E-03	9.74E-04	4.46E-05
0.10	6.78E-03	6.90E-03	7.05E-03	7.23E-03	7.48E-03	7.82E-03	8.31E-03	9.13E-03	1.08E-02	1.57E-02	7.23E-03	5.87E-03	3.83E-03	1.33E-03	6.65E-05
0.15	6.57E-03	6.64E-03	6.71E-03	6.80E-03	6.93E-03	7.10E-03	7.32E-03	7.70E-03	8.45E-03	1.07E-02	6.80E-03	6.18E-03	4.12E-03	2.25E-03	1.24E-04
0.20	6.36E-03	6.40E-03	6.45E-03	6.52E-03	6.60E-03	6.71E-03	6.87E-03	7.12E-03	7.58E-03	8.97E-03	6.52E-03	6.14E-03	4.46E-03	3.12E-03	1.89E-04
0.30	6.04E-03	6.07E-03	6.10E-03	6.14E-03	6.19E-03	6.26E-03	6.35E-03	6.49E-03	6.74E-03	7.51E-03	6.14E-03	5.93E-03	5.00E-03	4.29E-03	3.08E-04
0.40	5.83E-03	5.85E-03	5.88E-03	5.91E-03	5.94E-03	5.99E-03	6.05E-03	6.15E-03	6.32E-03	6.83E-03	5.91E-03	5.78E-03	5.19E-03	4.78E-03	4.26E-04
0.60	5.68E-03	5.69E-03	5.71E-03	5.73E-03	5.76E-03	5.80E-03	5.86E-03	5.92E-03	6.05E-03	6.43E-03	5.73E-03	5.63E-03	5.22E-03	4.91E-03	4.42E-04
0.80	5.52E-03	5.55E-03	5.57E-03	5.60E-03	5.63E-03	5.68E-03	5.70E-03	5.76E-03	5.87E-03	6.18E-03	5.60E-03	5.51E-03	5.19E-03	4.95E-03	4.41E-04
0.90	5.30E-03	5.30E-03	5.32E-03	5.35E-03	5.38E-03	5.38E-03	5.41E-03	5.47E-03	5.55E-03	5.78E-03	5.35E-03	5.28E-03	5.06E-03	4.90E-03	4.34E-04
1.0	5.08E-03	5.09E-03	5.10E-03	5.11E-03	5.13E-03	5.17E-03	5.20E-03	5.25E-03	5.30E-03	5.44E-03	5.11E-03	5.05E-03	4.90E-03	4.78E-03	4.23E-04
1.5	4.57E-03	4.58E-03	4.59E-03	4.60E-03	4.61E-03	4.63E-03	4.66E-03	4.70E-03	4.75E-03	4.87E-03	4.60E-03	4.57E-03	4.47E-03	4.40E-03	3.92E-04
2.0	4.13E-03	4.14E-03	4.16E-03	4.19E-03	4.21E-03	4.24E-03	4.24E-03	4.24E-03	4.27E-03	4.34E-03	4.19E-03	4.15E-03	4.07E-03	4.02E-03	3.72E-04
3.0	3.47E-03	3.47E-03	3.46E-03	3.44E-03	3.46E-03	3.49E-03	3.51E-03	3.54E-03	3.56E-03	3.61E-03	3.44E-03	3.44E-03	3.42E-03	3.38E-03	3.00E-04
4.0	2.92E-03	2.92E-03	2.93E-03	2.94E-03	2.94E-03	2.94E-03	2.95E-03	2.96E-03	2.97E-03	2.99E-03	2.94E-03	2.92E-03	2.89E-03	2.85E-03	2.60E-04
5.0	2.49E-03	2.49E-03	2.49E-03	2.50E-03	2.50E-03	2.50E-03	2.51E-03	2.51E-03	2.52E-03	2.55E-03	2.50E-03	2.47E-03	2.46E-03	2.46E-03	2.60E-04
6.0	2.14E-03	2.14E-03	2.14E-03	2.15E-03	2.14E-03	2.13E-03	2.14E-03	2.14E-03	2.15E-03	2.18E-03	2.15E-03	2.12E-03	2.11E-03	2.09E-03	6.85E-04
8.0	1.63E-03	1.63E-03	1.63E-03	1.64E-03	1.64E-03	1.64E-03	1.63E-03	1.63E-03	1.63E-03	1.66E-03	1.64E-03	1.63E-03	1.61E-03	1.60E-03	5.47E-04
10.0	1.31E-03	1.30E-03	1.30E-03	1.30E-03	1.30E-03	1.31E-03	1.31E-03	1.30E-03	1.31E-03	1.32E-03	1.30E-03	1.30E-03	1.28E-03	1.28E-03	4.38E-04

Table A-18. UFRF absorbed fraction for all sources irradiating the shallow active marrow in the lumbar vertebrae.

Lumbar Vertebrae ϕ (TAM_{50}← TAM) Cellularity												Lumbar Vertebrae ϕ (TAM_{50}← r_S) Source Tissue r_S			
Energy (MeV)	100%	90%	80%	70%	60%	50%	40%	30%	20%	10%	70% (ICRP 70)	TM	TBS	TBV	CBS_{HC} or CBV
0.010	6.34E-03	7.08E-03	7.96E-03	9.10E-03	1.08E-02	1.28E-02	1.56E-02	2.07E-02	3.10E-02	6.20E-02	9.10E-03	1.24E-04	4.27E-02	3.41E-04	9.84E-07
0.015	6.25E-03	6.91E-03	7.74E-03	8.81E-03	1.02E-02	1.22E-02	1.53E-02	2.03E-02	3.03E-02	6.04E-02	8.81E-03	2.61E-04	4.25E-02	6.93E-04	1.52E-06
0.020	6.18E-03	6.82E-03	7.63E-03	8.67E-03	1.01E-02	1.20E-02	1.49E-02	1.96E-02	2.93E-02	5.83E-02	8.67E-03	4.23E-04	4.21E-02	1.14E-03	3.98E-06
0.030	6.02E-03	6.67E-03	7.39E-03	8.19E-03	9.41E-03	1.11E-02	1.37E-02	1.81E-02	2.67E-02	5.29E-02	8.19E-03	8.47E-04	4.12E-02	2.29E-03	7.37E-06
0.040	5.77E-03	6.27E-03	6.88E-03	7.67E-03	8.74E-03	1.02E-02	1.24E-02	1.61E-02	2.35E-02	4.58E-02	7.67E-03	1.35E-03	4.00E-02	3.63E-03	1.26E-05
0.050	5.52E-03	5.93E-03	6.43E-03	7.09E-03	7.97E-03	9.20E-03	1.10E-02	1.41E-02	2.02E-02	3.85E-02	7.09E-03	1.91E-03	3.86E-02	5.11E-03	1.83E-05
0.060	5.24E-03	5.61E-03	5.99E-03	6.49E-03	7.17E-03	8.13E-03	9.57E-03	1.20E-02	1.67E-02	3.06E-02	6.49E-03	2.48E-03	3.71E-02	6.68E-03	2.60E-05
0.080	4.85E-03	5.00E-03	5.23E-03	5.52E-03	5.91E-03	6.47E-03	7.25E-03	8.56E-03	1.12E-02	1.91E-02	5.52E-03	3.30E-03	3.17E-02	9.26E-03	3.51E-05
0.10	4.56E-03	4.69E-03	4.81E-03	5.01E-03	5.24E-03	5.56E-03	6.05E-03	6.86E-03	8.40E-03	1.30E-02	5.01E-03	3.68E-03	2.58E-02	1.07E-02	5.47E-05
0.15	4.41E-03	4.49E-03	4.51E-03	4.59E-03	4.72E-03	4.89E-03	5.13E-03	5.52E-03	6.19E-03	8.20E-03	4.59E-03	4.02E-03	1.75E-02	1.14E-02	1.00E-04
0.20	4.47E-03	4.53E-03	4.50E-03	4.62E-03	4.73E-03	4.81E-03	4.93E-03	5.14E-03	5.50E-03	6.63E-03	4.62E-03	4.23E-03	1.33E-02	1.09E-02	1.51E-04
0.30	4.71E-03	4.79E-03	4.79E-03	4.82E-03	4.85E-03	4.89E-03	4.97E-03	5.11E-03	5.35E-03	6.09E-03	4.82E-03	4.63E-03	9.63E-03	8.47E-03	2.54E-04
0.40	4.82E-03	4.86E-03	4.84E-03	4.89E-03	4.91E-03	4.95E-03	5.01E-03	5.10E-03	5.26E-03	5.73E-03	4.89E-03	4.73E-03	7.98E-03	7.14E-03	3.56E-04
0.50	4.80E-03	4.81E-03	4.82E-03	4.84E-03	4.88E-03	4.93E-03	4.98E-03	5.07E-03	5.14E-03	5.49E-03	4.84E-03	4.78E-03	7.11E-03	6.55E-03	4.58E-04
0.60	4.75E-03	4.79E-03	4.77E-03	4.79E-03	4.84E-03	4.91E-03	4.94E-03	5.00E-03	5.09E-03	5.38E-03	4.79E-03	4.76E-03	6.63E-03	6.13E-03	5.70E-04
0.80	4.63E-03	4.63E-03	4.63E-03	4.66E-03	4.68E-03	4.67E-03	4.69E-03	4.73E-03	4.80E-03	5.00E-03	4.66E-03	4.57E-03	5.94E-03	5.59E-03	7.36E-04
1.0	4.47E-03	4.49E-03	4.48E-03	4.47E-03	4.52E-03	4.55E-03	4.56E-03	4.58E-03	4.63E-03	4.76E-03	4.47E-03	4.40E-03	5.51E-03	5.25E-03	8.71E-04
1.5	4.08E-03	4.07E-03	4.08E-03	4.10E-03	4.13E-03	4.11E-03	4.13E-03	4.17E-03	4.20E-03	4.29E-03	4.10E-03	4.08E-03	4.73E-03	4.59E-03	9.90E-04
2.0	3.67E-03	3.69E-03	3.69E-03	3.69E-03	3.73E-03	3.78E-03	3.78E-03	3.77E-03	3.79E-03	3.84E-03	3.69E-03	3.68E-03	4.18E-03	4.07E-03	1.07E-03
3.0	3.10E-03	3.11E-03	3.09E-03	3.07E-03	3.13E-03	3.12E-03	3.13E-03	3.15E-03	3.17E-03	3.21E-03	3.07E-03	3.06E-03	3.41E-03	3.36E-03	8.94E-04
4.0	2.60E-03	2.61E-03	2.63E-03	2.63E-03	2.63E-03	2.63E-03	2.64E-03	2.64E-03	2.66E-03	2.67E-03	2.63E-03	2.62E-03	2.90E-03	2.70E-03	8.02E-04
5.0	2.24E-03	2.23E-03	2.23E-03	2.24E-03	2.24E-03	2.23E-03	2.24E-03	2.26E-03	2.27E-03	2.29E-03	2.24E-03	2.21E-03	2.42E-03	2.41E-03	6.88E-04
6.0	1.92E-03	1.93E-03	1.92E-03	1.92E-03	1.92E-03	1.91E-03	1.92E-03	1.93E-03	1.93E-03	1.94E-03	1.92E-03	1.90E-03	2.08E-03	2.04E-03	6.16E-04
8.0	1.46E-03	1.46E-03	1.46E-03	1.46E-03	1.46E-03	1.46E-03	1.46E-03	1.45E-03	1.46E-03	1.48E-03	1.46E-03	1.45E-03	1.59E-03	1.55E-03	4.90E-04
10.0	1.18E-03	1.19E-03	1.16E-03	1.17E-03	1.17E-03	1.18E-03	1.17E-03	1.17E-03	1.18E-03	1.19E-03	1.17E-03	1.17E-03	1.27E-03	1.25E-03	3.96E-04

Table A-19. UFRF absorbed fraction for all sources irradiating the active marrow in the sacrum.

	Sacrum ϕ (TAM ← TAM) Cellularity											Sacrum ϕ (TAM ← r_S) Source Tissue r_S			
Energy (MeV)	100%	90%	80%	70%	60%	50%	40%	30%	20%	10%	70% (ICRP 70)	TAM	TBS	TBV	CBS_{vc} or CBV
0.010	1.21E-02	1.34E-02	1.50E-02	1.71E-02	1.99E-02	2.38E-02	2.97E-02	3.94E-02	5.89E-02	1.17E-01	1.71E-02	3.78E-04	6.51E-03	6.54E-05	1.88E-06
0.015	1.21E-02	1.33E-02	1.49E-02	1.69E-02	1.96E-02	2.34E-02	2.91E-02	3.85E-02	5.74E-02	1.14E-01	1.69E-02	7.74E-04	6.51E-03	1.31E-04	3.85E-06
0.020	1.21E-02	1.33E-02	1.48E-02	1.67E-02	1.93E-02	2.29E-02	2.83E-02	3.73E-02	5.54E-02	1.10E-01	1.67E-02	1.26E-03	6.53E-03	2.18E-04	6.51E-06
0.030	1.20E-02	1.31E-02	1.45E-02	1.62E-02	1.85E-02	2.17E-02	2.66E-02	3.45E-02	5.05E-02	9.85E-02	1.62E-02	2.51E-03	6.55E-03	4.39E-04	1.39E-05
0.040	1.20E-02	1.29E-02	1.41E-02	1.55E-02	1.75E-02	2.02E-02	2.43E-02	3.11E-02	4.47E-02	8.59E-02	1.55E-02	3.90E-03	6.56E-03	7.10E-04	2.23E-05
0.050	1.20E-02	1.27E-02	1.37E-02	1.49E-02	1.64E-02	1.87E-02	2.20E-02	2.75E-02	3.86E-02	7.18E-02	1.49E-02	5.48E-03	6.58E-03	1.02E-03	3.26E-05
0.060	1.20E-02	1.26E-02	1.33E-02	1.42E-02	1.54E-02	1.72E-02	1.98E-02	2.41E-02	3.27E-02	5.86E-02	1.42E-02	6.95E-03	6.60E-03	1.36E-03	4.59E-05
0.080	1.19E-02	1.23E-02	1.28E-02	1.32E-02	1.38E-02	1.48E-02	1.62E-02	1.85E-02	2.32E-02	3.72E-02	1.32E-02	9.24E-03	6.68E-03	2.06E-03	7.42E-05
0.10	1.18E-02	1.20E-02	1.23E-02	1.26E-02	1.30E-02	1.36E-02	1.45E-02	1.59E-02	1.87E-02	2.70E-02	1.26E-02	1.03E-02	6.83E-03	2.80E-03	1.07E-04
0.15	1.16E-02	1.18E-02	1.19E-02	1.21E-02	1.23E-02	1.26E-02	1.30E-02	1.36E-02	1.49E-02	1.87E-02	1.21E-02	1.10E-02	7.57E-03	4.59E-03	2.09E-04
0.20	1.15E-02	1.15E-02	1.16E-02	1.17E-02	1.19E-02	1.21E-02	1.23E-02	1.28E-02	1.35E-02	1.59E-02	1.17E-02	1.11E-02	8.24E-03	6.11E-03	3.30E-04
0.30	1.11E-02	1.12E-02	1.13E-02	1.13E-02	1.14E-02	1.15E-02	1.17E-02	1.19E-02	1.24E-02	1.37E-02	1.13E-02	1.10E-02	9.15E-03	7.90E-03	5.67E-04
0.40	1.09E-02	1.09E-02	1.10E-02	1.10E-02	1.11E-02	1.12E-02	1.13E-02	1.15E-02	1.18E-02	1.26E-02	1.10E-02	1.08E-02	9.38E-03	8.54E-03	8.31E-04
0.50	1.06E-02	1.07E-02	1.07E-02	1.08E-02	1.09E-02	1.09E-02	1.10E-02	1.12E-02	1.14E-02	1.20E-02	1.08E-02	1.06E-02	9.44E-03	8.79E-03	1.04E-03
0.60	1.04E-02	1.06E-02	1.06E-02	1.06E-02	1.06E-02	1.07E-02	1.07E-02	1.08E-02	1.10E-02	1.16E-02	1.06E-02	1.04E-02	9.46E-03	9.02E-03	1.30E-03
0.80	1.00E-02	1.01E-02	1.01E-02	1.01E-02	1.02E-02	1.02E-02	1.03E-02	1.04E-02	1.05E-02	1.09E-02	1.01E-02	1.00E-02	9.37E-03	9.01E-03	1.67E-03
1.0	9.66E-03	9.73E-03	9.75E-03	9.79E-03	9.83E-03	9.89E-03	9.91E-03	9.95E-03	1.01E-02	1.04E-02	9.79E-03	9.67E-03	9.14E-03	8.91E-03	1.95E-03
1.5	8.89E-03	8.90E-03	8.93E-03	8.96E-03	9.00E-03	9.07E-03	9.07E-03	9.06E-03	9.16E-03	9.46E-03	8.96E-03	8.95E-03	8.55E-03	8.39E-03	2.36E-03
2.0	8.16E-03	8.18E-03	8.17E-03	8.14E-03	8.20E-03	8.28E-03	8.31E-03	8.36E-03	8.39E-03	8.49E-03	8.14E-03	8.17E-03	7.92E-03	7.86E-03	2.57E-03
3.0	6.93E-03	6.95E-03	6.95E-03	6.94E-03	6.98E-03	7.09E-03	7.02E-03	7.00E-03	7.03E-03	7.12E-03	6.94E-03	6.89E-03	6.81E-03	6.78E-03	2.50E-03
4.0	5.95E-03	5.88E-03	5.91E-03	5.95E-03	5.94E-03	5.93E-03	5.94E-03	5.96E-03	5.97E-03	6.02E-03	5.95E-03	5.87E-03	5.81E-03	5.81E-03	2.33E-03
5.0	5.07E-03	5.09E-03	5.10E-03	5.12E-03	5.11E-03	5.10E-03	5.11E-03	5.13E-03	5.17E-03	5.29E-03	5.12E-03	5.10E-03	5.01E-03	4.92E-03	2.03E-03
6.0	4.43E-03	4.43E-03	4.44E-03	4.45E-03	4.45E-03	4.46E-03	4.46E-03	4.48E-03	4.49E-03	4.54E-03	4.45E-03	4.40E-03	4.37E-03	4.38E-03	1.90E-03
8.0	3.49E-03	3.49E-03	3.48E-03	3.48E-03	3.50E-03	3.52E-03	3.51E-03	3.47E-03	3.49E-03	3.55E-03	3.48E-03	3.50E-03	3.46E-03	3.42E-03	1.55E-03
10.0	2.82E-03	2.86E-03	2.88E-03	2.87E-03	2.85E-03	2.83E-03	2.85E-03	2.89E-03	2.90E-03	2.92E-03	2.87E-03	2.86E-03	2.82E-03	2.80E-03	1.28E-03

Table A-20. UFRF absorbed fraction for all sources irradiating the shallow active marrow in the sacrum.

	Sacrum ϕ (TAM_{50} ← TAM) Cellularity											Sacrum ϕ (TAM_{50} ← r_S) Source Tissue r_S			
Energy (MeV)	100%	90%	80%	70%	60%	50%	40%	30%	20%	10%	70% (ICRP 70)	TAM	TBS	TBV	CBS_{vc} or CBV
0.010	1.08E-02	1.21E-02	1.36E-02	1.56E-02	1.80E-02	2.15E-02	2.68E-02	3.56E-02	5.38E-02	1.08E-01	1.56E-02	2.18E-04	1.63E-01	1.64E-03	6.72E-07
0.015	1.08E-02	1.20E-02	1.34E-02	1.51E-02	1.75E-02	2.11E-02	2.62E-02	3.49E-02	5.24E-02	1.05E-01	1.51E-02	4.01E-04	1.62E-01	3.28E-03	2.30E-06
0.020	1.06E-02	1.16E-02	1.30E-02	1.48E-02	1.73E-02	2.01E-02	2.52E-02	3.37E-02	5.07E-02	1.02E-01	1.48E-02	7.27E-04	1.61E-01	5.43E-03	6.34E-06
0.030	1.02E-02	1.11E-02	1.24E-02	1.41E-02	1.63E-02	1.93E-02	2.38E-02	3.11E-02	4.63E-02	9.17E-02	1.41E-02	1.43E-03	1.57E-01	1.07E-02	1.07E-05
0.040	9.78E-03	1.08E-02	1.18E-02	1.32E-02	1.50E-02	1.75E-02	2.13E-02	2.77E-02	4.10E-02	8.08E-02	1.32E-02	2.35E-03	1.52E-01	1.72E-02	2.30E-05
0.050	9.49E-03	1.03E-02	1.11E-02	1.23E-02	1.38E-02	1.59E-02	1.89E-02	2.39E-02	3.47E-02	6.69E-02	1.23E-02	3.33E-03	1.47E-01	2.40E-02	2.96E-05
0.060	9.08E-03	9.57E-03	1.03E-02	1.12E-02	1.24E-02	1.40E-02	1.65E-02	2.08E-02	2.91E-02	5.39E-02	1.12E-02	4.34E-03	1.41E-01	3.11E-02	3.99E-05
0.080	8.40E-03	8.70E-03	9.12E-03	9.65E-03	1.03E-02	1.12E-02	1.26E-02	1.49E-02	1.96E-02	3.33E-02	9.65E-03	5.84E-03	1.20E-01	4.25E-02	7.36E-05
0.10	8.01E-03	8.33E-03	8.60E-03	8.88E-03	9.29E-03	9.86E-03	1.06E-02	1.19E-02	1.46E-02	2.27E-02	8.88E-03	6.50E-03	9.79E-02	4.81E-02	9.32E-05
0.15	7.97E-03	8.09E-03	8.18E-03	8.37E-03	8.53E-03	8.75E-03	9.09E-03	9.67E-03	1.10E-02	1.48E-02	8.37E-03	7.32E-03	6.69E-02	4.82E-02	1.96E-04
0.20	8.20E-03	8.29E-03	8.38E-03	8.55E-03	8.62E-03	8.73E-03	8.93E-03	9.26E-03	1.00E-02	1.24E-02	8.55E-03	7.75E-03	5.08E-02	4.26E-02	3.00E-04
0.30	8.71E-03	8.70E-03	8.84E-03	8.93E-03	8.99E-03	9.00E-03	9.10E-03	9.17E-03	9.73E-03	1.14E-02	8.93E-03	8.43E-03	3.48E-02	3.23E-02	5.04E-04
0.40	8.71E-03	8.74E-03	8.86E-03	9.02E-03	8.99E-03	8.94E-03	8.99E-03	9.08E-03	9.46E-03	1.06E-02	9.02E-03	8.64E-03	2.82E-02	2.73E-02	7.15E-04
0.50	8.63E-03	8.73E-03	8.86E-03	9.02E-03	9.01E-03	8.99E-03	9.09E-03	9.25E-03	9.54E-03	1.04E-02	9.02E-03	8.72E-03	2.49E-02	2.44E-02	8.96E-04
0.60	8.60E-03	8.81E-03	8.74E-03	8.66E-03	8.77E-03	8.81E-03	8.93E-03	9.15E-03	9.38E-03	1.01E-02	8.66E-03	8.56E-03	2.21E-02	2.22E-02	1.21E-03
0.80	8.39E-03	8.49E-03	8.50E-03	8.57E-03	8.59E-03	8.62E-03	8.69E-03	8.80E-03	8.93E-03	9.29E-03	8.57E-03	8.65E-03	1.85E-02	1.85E-02	1.50E-03
1.0	8.22E-03	8.32E-03	8.34E-03	8.37E-03	8.41E-03	8.54E-03	8.57E-03	8.61E-03	8.77E-03	9.26E-03	8.37E-03	8.36E-03	1.60E-02	1.62E-02	1.81E-03
1.5	7.81E-03	7.87E-03	7.85E-03	7.83E-03	7.86E-03	7.87E-03	7.87E-03	7.87E-03	8.02E-03	8.48E-03	7.83E-03	7.79E-03	1.25E-02	1.24E-02	2.13E-03
2.0	7.10E-03	7.29E-03	7.28E-03	7.28E-03	7.38E-03	7.40E-03	7.44E-03	7.50E-03	7.52E-03	7.56E-03	7.28E-03	7.24E-03	1.05E-02	1.04E-02	2.31E-03
3.0	6.17E-03	6.19E-03	6.12E-03	6.03E-03	6.13E-03	6.28E-03	6.20E-03	6.08E-03	6.19E-03	6.51E-03	6.03E-03	6.22E-03	8.31E-03	8.32E-03	2.31E-03
4.0	5.23E-03	5.30E-03	5.30E-03	5.31E-03	5.33E-03	5.36E-03	5.33E-03	5.29E-03	5.32E-03	5.41E-03	5.31E-03	5.20E-03	6.85E-03	6.82E-03	2.09E-03
5.0	4.63E-03	4.69E-03	4.68E-03	4.60E-03	4.63E-03	4.68E-03	4.66E-03	4.60E-03	4.60E-03	4.84E-03	4.60E-03	4.63E-03	5.91E-03	5.79E-03	1.86E-03
6.0	3.96E-03	3.93E-03	3.96E-03	4.00E-03	4.00E-03	4.00E-03	3.97E-03	3.91E-03	3.98E-03	4.16E-03	4.00E-03	3.92E-03	5.05E-03	5.10E-03	1.72E-03
8.0	3.11E-03	3.12E-03	3.12E-03	3.10E-03	3.13E-03	3.16E-03	3.14E-03	3.11E-03	3.14E-03	3.25E-03	3.10E-03	3.17E-03	3.97E-03	3.96E-03	1.41E-03
10.0	2.51E-03	2.53E-03	2.58E-03	2.58E-03	2.55E-03	2.52E-03	2.53E-03	2.56E-03	2.59E-03	2.69E-03	2.58E-03	2.56E-03	3.21E-03	3.22E-03	1.17E-03

Table A-21. UFRF absorbed fraction for all sources irradiating the active marrow in the ossa coxae.

Ossa Coxae ϕ (TAM← TAM) Cellularity												Ossa Coxae ϕ (TAM← r_{si}) Source Tissue r_i			
Energy (MeV)	100%	90%	80%	70%	60%	50%	40%	30%	20%	10%	85% (ICRP 70)	TM	TBS	TBV	CES_{WC} or 2BV
0.010	2.69E-03	2.93E-03	3.34E-03	3.81E-03	4.43E-03	5.30E-03	6.60E-03	8.78E-03	1.31E-02	2.62E-02	5.52E-03	8.21E-05	1.44E-03	1.12E-05	3.36E-07
0.015	2.69E-03	2.97E-03	3.32E-03	3.77E-03	4.37E-03	5.21E-03	6.47E-03	8.67E-03	1.28E-02	2.54E-02	5.42E-03	1.69E-04	1.44E-03	2.33E-05	6.80E-07
0.020	2.68E-03	2.95E-03	3.29E-03	3.72E-03	4.29E-03	5.10E-03	6.30E-03	8.31E-03	1.23E-02	2.44E-02	5.30E-03	2.77E-04	1.44E-03	3.81E-05	1.19E-06
0.030	2.67E-03	2.91E-03	3.21E-03	3.63E-03	4.19E-03	4.82E-03	6.09E-03	7.67E-03	1.12E-02	2.15E-02	4.95E-03	5.48E-04	1.44E-03	7.64E-05	2.57E-06
0.040	2.66E-03	2.87E-03	3.12E-03	3.44E-03	3.88E-03	4.49E-03	5.40E-03	6.52E-03	9.95E-03	1.90E-02	4.44E-03	8.61E-04	1.44E-03	1.25E-04	4.23E-06
0.050	2.65E-03	2.82E-03	3.02E-03	3.29E-03	3.64E-03	4.14E-03	4.88E-03	6.12E-03	8.59E-03	1.60E-02	4.20E-03	1.20E-03	1.44E-03	1.79E-04	6.01E-06
0.060	2.64E-03	2.79E-03	2.93E-03	3.13E-03	3.41E-03	3.79E-03	4.37E-03	5.23E-03	7.29E-03	1.30E-02	3.89E-03	1.52E-03	1.44E-03	2.27E-04	8.47E-06
0.080	2.61E-03	2.63E-03	2.77E-03	2.88E-03	3.03E-03	3.25E-03	3.56E-03	4.08E-03	5.12E-03	8.24E-03	3.30E-03	2.02E-03	1.44E-03	3.62E-04	1.40E-05
0.10	2.57E-03	2.62E-03	2.60E-03	2.75E-03	2.84E-03	2.97E-03	3.16E-03	3.47E-03	4.10E-03	5.96E-03	3.90E-03	2.23E-03	1.46E-03	4.90E-04	2.01E-05
0.15	2.49E-03	2.51E-03	2.54E-03	2.58E-03	2.62E-03	2.68E-03	2.77E-03	2.92E-03	3.20E-03	4.06E-03	2.70E-03	2.33E-03	1.58E-03	6.12E-04	3.84E-05
0.20	2.40E-03	2.42E-03	2.44E-03	2.47E-03	2.49E-03	2.53E-03	2.59E-03	2.68E-03	2.86E-03	3.40E-03	2.34E-03	2.29E-03	1.69E-03	1.10E-03	5.73E-05
0.30	2.27E-03	2.29E-03	2.30E-03	2.31E-03	2.33E-03	2.36E-03	2.39E-03	2.44E-03	2.53E-03	2.83E-03	2.36E-03	2.18E-03	1.81E-03	1.44E-03	9.70E-05
0.40	2.18E-03	2.19E-03	2.20E-03	2.21E-03	2.22E-03	2.25E-03	2.27E-03	2.30E-03	2.37E-03	2.58E-03	2.25E-03	2.08E-03	1.82E-03	1.55E-03	1.42E-04
0.60	2.11E-03	2.13E-03	2.13E-03	2.14E-03	2.15E-03	2.17E-03	2.19E-03	2.22E-03	2.27E-03	2.42E-03	2.17E-03	1.99E-03	1.79E-03	1.59E-03	1.79E-04
0.80	2.06E-03	2.06E-03	2.07E-03	2.08E-03	2.09E-03	2.11E-03	2.12E-03	2.14E-03	2.18E-03	2.30E-03	2.11E-03	1.91E-03	1.75E-03	1.58E-03	2.11E-04
1.0	1.97E-03	1.97E-03	1.98E-03	1.99E-03	1.99E-03	2.01E-03	2.02E-03	2.04E-03	2.06E-03	2.15E-03	2.01E-03	1.80E-03	1.68E-03	1.57E-03	2.82E-04
1.5	1.89E-03	1.91E-03	1.90E-03	1.91E-03	1.92E-03	1.93E-03	1.94E-03	1.94E-03	1.97E-03	2.04E-03	1.93E-03	1.71E-03	1.61E-03	1.54E-03	3.38E-04
2.0	1.72E-03	1.73E-03	1.73E-03	1.74E-03	1.74E-03	1.75E-03	1.76E-03	1.77E-03	1.79E-03	1.83E-03	1.75E-03	1.53E-03	1.48E-03	1.46E-03	4.46E-04
3.0	1.59E-03	1.59E-03	1.59E-03	1.60E-03	1.60E-03	1.61E-03	1.61E-03	1.61E-03	1.62E-03	1.66E-03	1.61E-03	1.39E-03	1.37E-03	1.36E-03	5.14E-04
4.0	1.34E-03	1.34E-03	1.34E-03	1.35E-03	1.35E-03	1.35E-03	1.36E-03	1.37E-03	1.38E-03	1.40E-03	1.35E-03	1.16E-03	1.16E-03	1.17E-03	5.50E-04
5.0	1.14E-03	1.13E-03	1.13E-03	1.13E-03	1.13E-03	1.13E-03	1.13E-03	1.13E-03	1.13E-03	1.13E-03	1.13E-03	9.86E-04	1.00E-03	1.01E-03	5.43E-04
6.0	9.90E-04	9.90E-04	9.94E-04	9.98E-04	1.00E-03	1.01E-03	1.00E-03	1.00E-03	1.01E-03	1.02E-03	1.01E-03	8.64E-04	8.74E-04	8.85E-04	5.04E-04
8.0	8.68E-04	8.68E-04	8.70E-04	8.78E-04	8.73E-04	8.72E-04	8.74E-04	8.78E-04	8.81E-04	8.89E-04	8.73E-04	7.53E-04	7.63E-04	7.73E-04	4.70E-04
10.0	5.67E-04	5.73E-04	5.71E-04	5.69E-04	5.72E-04	5.77E-04	5.75E-04	5.12E-04	5.75E-04	5.84E-04	5.77E-04	5.02E-04	5.03E-04	5.11E-04	3.44E-04

Table A-22. UFRF absorbed fraction for all sources irradiating the shallow active marrow in the ossa coxae.

Ossa Coxae ϕ (TAM_{SV}← TAM) Cellularity												Ossa Coxae ϕ (TAM_{SV}← r_{Si}) Source Tissue r_i			
Energy (MeV)	100%	90%	80%	70%	60%	50%	40%	30%	20%	10%	85% (ICRP 70)	TM	TBS	TBV	CES_{WC} or 2BV
0.010	2.41E-03	2.61E-03	3.00E-03	3.42E-03	3.98E-03	3.76E-02	5.94E-03	7.92E-03	1.19E-02	2.37E-02	4.96E-03	4.58E-05	1.43E-02	1.12E-04	2.76E-07
0.015	2.38E-03	2.64E-03	2.95E-03	3.36E-03	3.90E-03	4.65E-03	5.81E-03	7.73E-03	1.16E-02	2.30E-02	4.84E-03	9.59E-05	1.43E-02	2.31E-04	6.18E-07
0.020	2.35E-03	2.59E-03	2.89E-03	3.28E-03	3.80E-03	4.54E-03	5.64E-03	7.47E-03	1.11E-02	2.21E-02	4.72E-03	1.58E-04	1.41E-02	3.77E-04	1.01E-06
0.030	2.27E-03	2.49E-03	2.77E-03	3.13E-03	3.63E-03	4.34E-03	5.39E-03	6.97E-03	1.03E-02	2.00E-02	4.49E-03	3.12E-04	1.39E-02	7.46E-04	1.92E-06
0.040	2.19E-03	2.38E-03	2.61E-03	2.92E-03	3.33E-03	3.90E-03	4.74E-03	6.16E-03	8.94E-03	1.73E-02	4.94E-03	5.00E-04	1.34E-02	1.20E-03	4.09E-06
0.050	2.10E-03	2.29E-03	2.45E-03	2.69E-03	3.02E-03	3.48E-03	4.17E-03	5.24E-03	7.66E-03	1.46E-02	3.98E-03	7.13E-04	1.30E-02	1.68E-03	5.82E-06
0.060	2.00E-03	2.11E-03	2.27E-03	2.47E-03	2.73E-03	3.10E-03	3.64E-03	4.53E-03	6.35E-03	1.18E-02	3.19E-03	9.10E-04	1.24E-02	2.16E-03	7.48E-06
0.080	1.82E-03	1.90E-03	1.90E-03	2.10E-03	2.21E-03	2.43E-03	2.73E-03	3.23E-03	4.23E-03	7.20E-03	2.48E-03	1.23E-03	1.05E-02	3.00E-03	1.16E-05
0.10	1.74E-03	1.79E-03	1.83E-03	1.90E-03	1.99E-03	2.10E-03	2.29E-03	2.60E-03	3.20E-03	5.01E-03	2.73E-03	1.37E-03	8.64E-03	3.42E-03	1.69E-05
0.15	1.68E-03	1.70E-03	1.72E-03	1.75E-03	1.80E-03	1.87E-03	1.95E-03	2.08E-03	2.36E-03	3.19E-03	1.88E-03	1.50E-03	5.93E-03	3.60E-03	2.98E-05
0.20	1.67E-03	1.71E-03	1.73E-03	1.75E-03	1.77E-03	1.80E-03	1.85E-03	1.82E-03	2.08E-03	2.01E-03	1.81E-03	1.56E-03	4.57E-03	3.32E-03	4.55E-05
0.30	1.74E-03	1.74E-03	1.76E-03	1.78E-03	1.80E-03	1.82E-03	1.85E-03	1.89E-03	1.97E-03	2.24E-03	1.83E-03	1.66E-03	3.28E-03	2.76E-03	8.11E-05
0.40	1.74E-03	1.75E-03	1.77E-03	1.78E-03	1.79E-03	1.79E-03	1.82E-03	1.86E-03	1.93E-03	2.15E-03	1.80E-03	1.64E-03	2.76E-03	2.47E-03	1.19E-04
0.50	1.71E-03	1.73E-03	1.74E-03	1.76E-03	1.77E-03	1.77E-03	1.79E-03	1.83E-03	1.87E-03	1.99E-03	1.76E-03	1.59E-03	2.50E-03	2.31E-03	1.52E-04
0.60	1.69E-03	1.72E-03	1.72E-03	1.73E-03	1.73E-03	1.74E-03	1.76E-03	1.78E-03	1.82E-03	1.92E-03	1.74E-03	1.56E-03	2.30E-03	2.19E-03	1.81E-04
0.80	1.65E-03	1.65E-03	1.66E-03	1.66E-03	1.68E-03	1.69E-03	1.69E-03	1.69E-03	1.73E-03	1.84E-03	1.69E-03	1.49E-03	2.08E-03	2.01E-03	2.47E-04
1.0	1.61E-03	1.62E-03	1.62E-03	1.62E-03	1.63E-03	1.64E-03	1.64E-03	1.65E-03	1.67E-03	1.73E-03	1.64E-03	1.44E-03	1.90E-03	1.90E-03	2.98E-04
1.5	1.49E-03	1.50E-03	1.50E-03	1.52E-03	1.52E-03	1.52E-03	1.53E-03	1.53E-03	1.55E-03	1.60E-03	1.52E-03	1.31E-03	1.84E-03	1.88E-03	3.91E-04
2.0	1.38E-03	1.38E-03	1.38E-03	1.40E-03	1.40E-03	1.40E-03	1.41E-03	1.41E-03	1.42E-03	1.47E-03	1.40E-03	1.21E-03	1.47E-03	1.49E-03	4.59E-04
3.0	1.18E-03	1.17E-03	1.18E-03	1.18E-03	1.18E-03	1.19E-03	1.19E-03	1.21E-03	1.21E-03	1.23E-03	1.19E-03	1.02E-03	1.21E-03	1.24E-03	4.94E-04
4.0	1.01E-03	1.03E-03	1.03E-03	1.03E-03	1.03E-03	1.03E-03	1.03E-03	1.03E-03	1.03E-03	1.06E-03	1.03E-03	8.78E-04	1.03E-03	1.06E-03	4.92E-04
5.0	8.83E-04	8.70E-04	8.81E-04	8.84E-04	8.87E-04	8.90E-04	8.92E-04	8.94E-04	8.95E-04	8.99E-04	8.90E-04	7.61E-04	8.86E-04	9.11E-04	4.56E-04
6.0	7.72E-04	7.68E-04	7.74E-04	7.81E-04	7.79E-04	7.75E-04	7.77E-04	7.80E-04	7.83E-04	7.90E-04	7.78E-04	6.71E-04	7.71E-04	7.93E-04	4.22E-04
8.0	6.15E-04	6.20E-04	6.18E-04	6.16E-04	6.17E-04	6.19E-04	6.19E-04	6.20E-04	6.21E-04	6.24E-04	6.19E-04	5.39E-04	6.10E-04	6.28E-04	3.63E-04
10.0	5.05E-04	5.10E-04	5.10E-04	5.10E-04	5.13E-04	5.18E-04	5.16E-04	5.13E-04	5.16E-04	5.24E-04	5.17E-04	4.45E-04	5.04E-04	5.17E-04	3.11E-04

Table A-23. UFRF absorbed fraction for all sources irradiating the active marrow in the proximal humeri.

Proximal Humeri ϕ (TAM← TAM) Cellularity												Proximal Humeri ϕ (TAM← r_S) Source Tissue r_S			
Energy (MeV)	100%	90%	80%	70%	60%	50%	40%	30%	20%	10%	25% (ICRP 70)	TM	TBS	TBV	CBS_{WC} or CBV
0.010	1.10E-02	1.23E-02	1.37E-02	1.56E-02	1.81E-02	2.17E-02	2.70E-02	3.59E-02	5.38E-02	1.07E-01	4.31E-02	3.38E-04	5.92E-03	5.37E-05	1.41E-06
0.015	1.10E-02	1.23E-02	1.36E-02	1.54E-02	1.79E-02	2.14E-02	2.66E-02	3.51E-02	5.23E-02	1.04E-01	4.20E-02	7.07E-04	5.90E-03	1.06E-04	3.44E-06
0.020	1.10E-02	1.21E-02	1.35E-02	1.52E-02	1.76E-02	2.09E-02	2.58E-02	3.41E-02	5.05E-02	9.99E-02	4.06E-02	1.16E-03	5.91E-03	1.74E-04	5.33E-06
0.030	1.10E-02	1.20E-02	1.32E-02	1.47E-02	1.68E-02	1.98E-02	2.41E-02	3.10E-02	4.61E-02	8.99E-02	3.73E-02	2.29E-03	5.93E-03	3.32E-04	9.79E-06
0.040	1.10E-02	1.18E-02	1.28E-02	1.42E-02	1.60E-02	1.84E-02	2.22E-02	2.84E-02	4.08E-02	7.81E-02	3.33E-02	3.61E-03	5.94E-03	5.63E-04	1.73E-05
0.050	1.09E-02	1.16E-02	1.25E-02	1.35E-02	1.50E-02	1.70E-02	2.01E-02	2.51E-02	3.53E-02	6.57E-02	2.92E-02	4.99E-03	5.94E-03	8.31E-04	2.79E-05
0.060	1.09E-02	1.14E-02	1.21E-02	1.30E-02	1.41E-02	1.57E-02	1.80E-02	2.20E-02	2.98E-02	5.30E-02	2.51E-02	6.38E-03	5.94E-03	1.08E-03	3.32E-05
0.080	1.09E-02	1.13E-02	1.15E-02	1.20E-02	1.26E-02	1.35E-02	1.48E-02	1.69E-02	2.12E-02	3.40E-02	1.86E-02	8.51E-03	6.01E-03	1.69E-03	5.73E-05
0.10	1.08E-02	1.10E-02	1.12E-02	1.15E-02	1.19E-02	1.24E-02	1.32E-02	1.45E-02	1.70E-02	2.46E-02	1.55E-02	9.46E-03	6.11E-03	2.29E-03	8.42E-05
0.15	1.06E-02	1.07E-02	1.08E-02	1.10E-02	1.12E-02	1.15E-02	1.18E-02	1.24E-02	1.36E-02	1.71E-02	1.29E-02	1.02E-02	6.69E-03	3.85E-03	1.43E-04
0.20	1.05E-02	1.05E-02	1.06E-02	1.07E-02	1.09E-02	1.11E-02	1.13E-02	1.17E-02	1.24E-02	1.47E-02	1.20E-02	1.03E-02	7.37E-03	5.28E-03	2.26E-04
0.30	1.02E-02	1.03E-02	1.03E-02	1.04E-02	1.05E-02	1.06E-02	1.07E-02	1.10E-02	1.13E-02	1.25E-02	1.11E-02	1.02E-02	8.32E-03	7.71E-03	3.74E-04
0.40	1.01E-02	1.01E-02	1.02E-02	1.02E-02	1.03E-02	1.03E-02	1.04E-02	1.06E-02	1.09E-02	1.16E-02	1.07E-02	1.01E-02	8.73E-03	7.87E-03	5.52E-04
0.60	1.00E-02	1.00E-02	1.00E-02	1.01E-02	1.01E-02	1.02E-02	1.03E-02	1.04E-02	1.06E-02	1.12E-02	1.06E-02	1.00E-02	8.88E-03	8.20E-03	7.08E-04
0.80	9.83E-03	9.88E-03	9.89E-03	9.93E-03	9.98E-03	1.00E-02	1.01E-02	1.02E-02	1.04E-02	1.09E-02	1.03E-02	9.92E-03	8.89E-03	8.39E-03	8.47E-04
0.80	9.60E-03	9.63E-03	9.65E-03	9.69E-03	9.74E-03	9.81E-03	9.84E-03	9.90E-03	1.00E-02	1.04E-02	9.95E-03	9.72E-03	8.90E-03	8.49E-03	1.20E-03
1.0	9.39E-03	9.43E-03	9.45E-03	9.48E-03	9.52E-03	9.57E-03	9.60E-03	9.64E-03	9.74E-03	1.01E-02	9.68E-03	9.51E-03	8.81E-03	8.48E-03	1.48E-03
1.5	8.84E-03	8.91E-03	8.93E-03	8.97E-03	8.99E-03	9.02E-03	9.06E-03	9.12E-03	9.19E-03	9.40E-03	9.15E-03	8.98E-03	8.48E-03	8.23E-03	2.02E-03
2.0	8.31E-03	8.33E-03	8.35E-03	8.38E-03	8.42E-03	8.47E-03	8.49E-03	8.53E-03	8.59E-03	8.76E-03	8.55E-03	8.46E-03	8.03E-03	7.89E-03	2.31E-03
3.0	7.39E-03	7.38E-03	7.39E-03	7.41E-03	7.44E-03	7.48E-03	7.49E-03	7.50E-03	7.53E-03	7.65E-03	7.51E-03	7.48E-03	7.26E-03	7.17E-03	2.61E-03
4.0	6.54E-03	6.54E-03	6.52E-03	6.49E-03	6.50E-03	6.51E-03	6.55E-03	6.62E-03	6.63E-03	6.66E-03	6.62E-03	6.57E-03	6.40E-03	6.41E-03	2.56E-03
5.0	5.69E-03	5.68E-03	5.72E-03	5.78E-03	5.77E-03	5.77E-03	5.78E-03	5.79E-03	5.80E-03	5.82E-03	5.79E-03	5.77E-03	5.62E-03	5.62E-03	2.31E-03
6.0	5.10E-03	5.10E-03	5.09E-03	5.07E-03	5.09E-03	5.12E-03	5.11E-03	5.09E-03	5.10E-03	5.14E-03	5.09E-03	5.10E-03	5.03E-03	5.05E-03	2.15E-03
8.0	3.98E-03	4.00E-03	4.00E-03	4.00E-03	3.99E-03	3.98E-03	3.99E-03	4.00E-03	4.02E-03	4.07E-03	4.01E-03	3.96E-03	3.96E-03	3.97E-03	1.77E-03
10.0	3.23E-03	3.21E-03	3.21E-03	3.21E-03	3.22E-03	3.24E-03	3.22E-03	3.20E-03	3.21E-03	3.25E-03	3.21E-03	3.18E-03	3.20E-03	3.16E-03	1.48E-03

Table A-24. UFRF absorbed fraction for all sources irradiating the shallow active marrow in the proximal humeri.

Proximal Humeri ϕ (TAM_{SV}← TAM) Cellularity												Proximal Humer ϕ (TAM_{SV}← r_S) Source Tissue r_S			
Energy (MeV)	100%	90%	80%	70%	60%	50%	40%	30%	20%	10%	25% (ICRP 70)	TM	TBS	TBV	CBS_{WC} or CBV
0.010	9.54E-03	1.09E-02	1.19E-02	1.35E-02	1.56E-02	1.90E-02	2.37E-02	3.15E-02	4.72E-02	9.44E-02	3.77E-02	2.01E-04	1.21E-01	1.10E-03	4.10E-06
0.015	9.40E-03	1.04E-02	1.17E-02	1.34E-02	1.55E-02	1.86E-02	2.30E-02	3.05E-02	4.58E-02	9.14E-02	3.66E-02	3.92E-04	1.20E-01	2.17E-03	5.30E-06
0.020	9.37E-03	1.04E-02	1.16E-02	1.32E-02	1.52E-02	1.81E-02	2.24E-02	2.97E-02	4.43E-02	8.81E-02	3.56E-02	6.37E-04	1.19E-01	3.54E-03	4.04E-06
0.030	9.09E-03	9.91E-03	1.10E-02	1.24E-02	1.43E-02	1.70E-02	2.09E-02	2.74E-02	4.03E-02	7.91E-02	3.25E-02	1.27E-03	1.17E-01	7.06E-03	1.10E-05
0.040	8.78E-03	9.54E-03	1.05E-02	1.17E-02	1.32E-02	1.53E-02	1.88E-02	2.45E-02	3.56E-02	6.90E-02	2.89E-02	2.10E-03	1.14E-01	1.11E-02	2.03E-05
0.050	8.36E-03	9.01E-03	9.75E-03	1.07E-02	1.22E-02	1.39E-02	1.67E-02	2.14E-02	3.06E-02	5.83E-02	2.51E-02	2.89E-03	1.10E-01	1.60E-02	3.01E-05
0.060	8.03E-03	8.32E-03	8.95E-03	9.76E-03	1.08E-02	1.23E-02	1.45E-02	1.81E-02	2.54E-02	4.74E-02	2.10E-02	3.72E-03	1.05E-01	2.04E-02	3.81E-05
0.080	7.33E-03	7.59E-03	7.94E-03	8.43E-03	8.99E-03	9.77E-03	1.10E-02	1.29E-02	1.70E-02	2.93E-02	1.46E-02	5.15E-03	9.04E-02	2.87E-02	5.31E-05
0.10	6.99E-03	7.15E-03	7.38E-03	7.67E-03	8.05E-03	8.60E-03	9.30E-03	1.05E-02	1.29E-02	2.02E-02	1.14E-02	5.62E-03	7.34E-02	3.29E-02	7.82E-05
0.15	6.85E-03	6.89E-03	7.00E-03	7.13E-03	7.27E-03	7.47E-03	7.79E-03	8.34E-03	9.37E-03	1.25E-02	8.75E-03	6.29E-03	5.01E-02	3.44E-02	1.20E-04
0.20	6.94E-03	7.11E-03	7.22E-03	7.33E-03	7.44E-03	7.55E-03	7.71E-03	7.98E-03	8.74E-03	1.11E-02	8.27E-03	6.01E-03	3.83E-02	3.12E-02	1.61E-04
0.30	7.59E-03	7.59E-03	7.60E-03	7.74E-03	7.81E-03	7.90E-03	8.01E-03	8.18E-03	8.60E-03	9.85E-03	8.35E-03	7.41E-03	2.70E-02	2.42E-02	3.56E-04
0.40	7.69E-03	7.69E-03	7.73E-03	7.84E-03	7.95E-03	8.10E-03	8.14E-03	8.20E-03	8.40E-03	8.99E-03	8.26E-03	7.70E-03	2.18E-02	2.01E-02	5.24E-04
0.50	7.83E-03	7.78E-03	7.78E-03	7.73E-03	7.85E-03	8.01E-03	8.13E-03	8.34E-03	8.42E-03	8.67E-03	8.37E-03	7.88E-03	1.92E-02	1.81E-02	6.72E-04
0.60	7.79E-03	7.85E-03	7.94E-03	7.94E-03	7.98E-03	8.02E-03	8.07E-03	8.15E-03	8.29E-03	8.72E-03	8.20E-03	8.01E-03	1.74E-02	1.69E-02	8.12E-04
0.80	7.80E-03	7.71E-03	7.73E-03	7.75E-03	7.80E-03	7.88E-03	7.91E-03	7.97E-03	8.12E-03	8.57E-03	8.03E-03	7.94E-03	1.53E-02	1.51E-02	1.16E-03
1.0	7.63E-03	7.60E-03	7.70E-03	7.71E-03	7.75E-03	7.82E-03	7.83E-03	7.86E-03	8.02E-03	8.49E-03	7.92E-03	7.72E-03	1.39E-02	1.40E-02	1.43E-03
1.5	7.27E-03	7.39E-03	7.37E-03	7.38E-03	7.39E-03	7.41E-03	7.48E-03	7.60E-03	7.83E-03	8.27E-03	7.71E-03	7.85E-03	1.19E-02	1.19E-02	1.85E-03
2.0	7.03E-03	6.90E-03	6.94E-03	6.98E-03	7.03E-03	7.09E-03	7.14E-03	7.22E-03	7.24E-03	7.30E-03	7.22E-03	7.00E-03	1.04E-02	1.04E-02	2.02E-03
3.0	6.24E-03	6.26E-03	6.28E-03	6.32E-03	6.33E-03	6.33E-03	6.34E-03	6.34E-03	6.36E-03	6.41E-03	6.35E-03	6.28E-03	8.52E-03	8.47E-03	2.16E-03
4.0	5.62E-03	5.63E-03	5.64E-03	5.66E-03	5.67E-03	5.67E-03	5.67E-03	5.72E-03	5.73E-03	5.70E-03	5.70E-03	5.66E-03	7.16E-03	7.33E-03	2.16E-03
5.0	4.90E-03	4.92E-03	4.95E-03	4.99E-03	5.00E-03	5.01E-03	5.00E-03	4.99E-03	5.01E-03	5.07E-03	5.00E-03	5.01E-03	6.18E-03	6.24E-03	1.92E-03
6.0	4.38E-03	4.41E-03	4.39E-03	4.37E-03	4.39E-03	4.41E-03	4.41E-03	4.42E-03	4.43E-03	4.47E-03	4.42E-03	4.41E-03	5.47E-03	5.56E-03	1.81E-03
8.0	3.46E-03	3.47E-03	3.47E-03	3.48E-03	3.48E-03	3.48E-03	3.47E-03	3.44E-03	3.47E-03	3.57E-03	3.48E-03	3.46E-03	4.31E-03	4.36E-03	1.50E-03
10.0	2.80E-03	2.78E-03	2.78E-03	2.79E-03	2.79E-03	2.79E-03	2.79E-03	2.79E-03	2.80E-03	2.85E-03	2.80E-03	2.79E-03	3.49E-03	3.46E-03	1.25E-03

Table A-25. UFRF absorbed fraction for all sources irradiating the active marrow in the proximal femora.

Proximal Femora ϕ (TAM← TAM) Cellularity												Proximal Femora ϕ (TAM← r_s) Source Tissue r_s			
Energy (MeV)	100%	90%	80%	70%	60%	50%	40%	30%	20%	10%	25% (ICRP 70)	TM	TBS	TBV	CBS_{HC} or CBV
0.010	5.87E-03	6.50E-03	7.29E-03	8.31E-03	9.66E-03	1.16E-02	1.44E-02	1.92E-02	2.86E-02	5.71E-02	2.30E-02	1.87E-04	3.14E-03	1.96E-05	7.56E-07
0.015	5.86E-03	6.47E-03	7.24E-03	8.22E-03	9.63E-03	1.14E-02	1.41E-02	1.87E-02	2.79E-02	5.54E-02	2.24E-02	3.80E-04	3.14E-03	4.04E-05	1.81E-06
0.020	5.85E-03	6.44E-03	7.17E-03	8.11E-03	9.36E-03	1.11E-02	1.38E-02	1.81E-02	2.69E-02	5.33E-02	2.17E-02	6.24E-04	3.14E-03	6.57E-05	2.93E-06
0.030	5.82E-03	6.34E-03	6.99E-03	7.83E-03	8.94E-03	1.06E-02	1.28E-02	1.67E-02	2.45E-02	4.79E-02	1.98E-02	1.23E-03	3.13E-03	1.32E-04	5.72E-06
0.040	5.79E-03	6.23E-03	6.79E-03	7.50E-03	8.45E-03	9.78E-03	1.18E-02	1.51E-02	2.17E-02	4.16E-02	1.77E-02	1.93E-03	3.11E-03	2.14E-04	9.95E-06
0.050	5.75E-03	6.12E-03	6.57E-03	7.14E-03	7.92E-03	9.00E-03	1.06E-02	1.33E-02	1.87E-02	3.50E-02	1.55E-02	2.68E-03	3.09E-03	3.07E-04	1.43E-05
0.060	5.71E-03	6.00E-03	6.35E-03	6.80E-03	7.40E-03	8.25E-03	9.51E-03	1.16E-02	1.58E-02	2.84E-02	1.33E-02	3.41E-03	3.07E-03	4.08E-04	1.94E-05
0.080	5.63E-03	5.79E-03	5.98E-03	6.23E-03	6.57E-03	7.03E-03	7.72E-03	8.87E-03	1.11E-02	1.80E-02	9.70E-03	4.53E-03	3.05E-03	6.25E-04	3.18E-05
0.10	5.54E-03	5.64E-03	5.76E-03	5.92E-03	6.12E-03	6.40E-03	6.82E-03	7.51E-03	8.87E-03	1.30E-02	8.05E-03	5.01E-03	3.04E-03	8.51E-04	4.51E-05
0.15	5.29E-03	5.34E-03	5.40E-03	5.48E-03	5.59E-03	5.72E-03	5.92E-03	6.24E-03	6.86E-03	8.73E-03	6.40E-03	5.20E-03	3.19E-03	1.46E-03	8.18E-05
0.20	5.03E-03	5.08E-03	5.12E-03	5.17E-03	5.24E-03	5.33E-03	5.45E-03	5.65E-03	6.03E-03	7.19E-03	5.80E-03	5.08E-03	3.38E-03	2.06E-03	1.22E-04
0.30	4.65E-03	4.67E-03	4.70E-03	4.74E-03	4.77E-03	4.83E-03	4.90E-03	5.01E-03	5.22E-03	5.85E-03	5.10E-03	4.77E-03	3.71E-03	2.83E-03	2.00E-04
0.40	4.43E-03	4.45E-03	4.47E-03	4.50E-03	4.52E-03	4.56E-03	4.61E-03	4.70E-03	4.84E-03	5.27E-03	4.75E-03	4.58E-03	3.85E-03	3.33E-03	2.80E-04
0.60	4.32E-03	4.33E-03	4.34E-03	4.36E-03	4.38E-03	4.41E-03	4.47E-03	4.53E-03	4.63E-03	4.94E-03	4.67E-03	4.48E-03	3.88E-03	3.49E-03	3.66E-04
0.80	4.24E-03	4.25E-03	4.27E-03	4.28E-03	4.31E-03	4.34E-03	4.37E-03	4.41E-03	4.50E-03	4.75E-03	4.45E-03	4.41E-03	3.88E-03	3.55E-03	4.26E-04
1.0	4.00E-03	4.01E-03	4.03E-03	4.04E-03	4.05E-03	4.08E-03	4.09E-03	4.13E-03	4.17E-03	4.32E-03	4.15E-03	4.17E-03	3.80E-03	3.60E-03	6.59E-04
1.5	3.77E-03	3.78E-03	3.79E-03	3.80E-03	3.81E-03	3.82E-03	3.84E-03	3.87E-03	3.90E-03	3.99E-03	3.88E-03	3.93E-03	3.84E-03	3.82E-03	8.37E-04
2.0	3.56E-03	3.56E-03	3.57E-03	3.58E-03	3.59E-03	3.61E-03	3.61E-03	3.63E-03	3.66E-03	3.73E-03	3.64E-03	3.73E-03	3.48E-03	3.39E-03	9.37E-04
3.0	3.18E-03	3.18E-03	3.19E-03	3.20E-03	3.21E-03	3.23E-03	3.23E-03	3.23E-03	3.24E-03	3.28E-03	3.23E-03	3.32E-03	3.14E-03	3.08E-03	1.04E-03
4.0	2.85E-03	2.84E-03	2.85E-03	2.86E-03	2.87E-03	2.88E-03	2.88E-03	2.88E-03	2.90E-03	2.94E-03	2.88E-03	2.97E-03	2.82E-03	2.79E-03	1.06E-03
5.0	2.55E-03	2.56E-03	2.56E-03	2.55E-03	2.56E-03	2.56E-03	2.57E-03	2.58E-03	2.59E-03	2.61E-03	2.58E-03	2.65E-03	2.53E-03	2.52E-03	1.04E-03
6.0	2.28E-03	2.29E-03	2.29E-03	2.29E-03	2.29E-03	2.30E-03	2.30E-03	2.30E-03	2.31E-03	2.33E-03	2.31E-03	2.38E-03	2.26E-03	2.24E-03	1.01E-03
8.0	1.84E-03	1.85E-03	1.85E-03	1.84E-03	1.85E-03	1.85E-03	1.85E-03	1.85E-03	1.85E-03	1.88E-03	1.85E-03	1.91E-03	1.83E-03	1.82E-03	9.03E-04
10.0	1.51E-03	1.51E-03	1.51E-03	1.52E-03	1.51E-03	1.51E-03	1.51E-03	1.51E-03	1.52E-03	1.54E-03	1.52E-03	1.56E-03	1.50E-03	1.49E-03	7.86E-04

Table A-26. UFRF absorbed fraction for all sources irradiating the shallow active marrow in the proximal femora.

Proximal Femora ϕ (TAM_{SH}← TAM) Cellularity												Proximal Femora ϕ (TAM_{SH}← r_s) Source Tissue r_s			
Energy (MeV)	100%	90%	80%	70%	60%	50%	40%	30%	20%	10%	25% (ICRP 70)	TM	TBS	TBV	CBS_{HC} or CBV
0.010	5.48E-03	6.08E-03	6.83E-03	7.80E-03	9.08E-03	1.09E-02	1.36E-02	1.80E-02	2.70E-02	5.39E-02	2.16E-02	1.11E-04	2.30E-02	1.44E-04	6.24E-07
0.015	5.43E-03	6.03E-03	6.74E-03	7.67E-03	8.92E-03	1.07E-02	1.33E-02	1.76E-02	2.63E-02	5.23E-02	2.11E-02	2.25E-04	2.28E-02	2.96E-04	1.84E-06
0.020	5.35E-03	5.93E-03	6.60E-03	7.50E-03	8.72E-03	1.04E-02	1.29E-02	1.70E-02	2.54E-02	5.04E-02	2.03E-02	3.77E-04	2.27E-02	4.77E-04	3.41E-06
0.030	5.19E-03	5.75E-03	6.31E-03	7.11E-03	8.13E-03	9.67E-03	1.19E-02	1.57E-02	2.31E-02	4.56E-02	1.86E-02	7.49E-04	2.21E-02	9.47E-04	6.05E-06
0.040	4.98E-03	5.41E-03	5.94E-03	6.63E-03	7.54E-03	8.82E-03	1.08E-02	1.40E-02	2.04E-02	3.97E-02	1.65E-02	1.20E-03	2.15E-02	1.52E-03	1.06E-05
0.050	4.73E-03	5.09E-03	5.53E-03	6.09E-03	6.85E-03	7.91E-03	9.50E-03	1.22E-02	1.74E-02	3.31E-02	1.42E-02	1.69E-03	2.07E-02	2.14E-03	1.43E-05
0.060	4.49E-03	4.77E-03	5.12E-03	5.57E-03	6.13E-03	6.98E-03	8.21E-03	1.03E-02	1.44E-02	2.67E-02	1.19E-02	2.10E-03	1.98E-02	2.77E-03	1.83E-05
0.080	4.08E-03	4.23E-03	4.41E-03	4.65E-03	4.98E-03	5.45E-03	6.13E-03	7.18E-03	9.56E-03	1.64E-02	8.19E-03	2.90E-03	1.70E-02	3.90E-03	3.01E-05
0.10	3.81E-03	3.91E-03	4.03E-03	4.18E-03	4.39E-03	4.69E-03	5.09E-03	5.76E-03	7.13E-03	1.12E-02	6.31E-03	3.21E-03	1.38E-02	4.58E-03	4.18E-05
0.15	3.54E-03	3.60E-03	3.65E-03	3.72E-03	3.82E-03	3.95E-03	4.14E-03	4.45E-03	5.06E-03	6.88E-03	4.99E-03	3.41E-03	9.54E-03	5.10E-03	7.58E-05
0.20	3.40E-03	3.54E-03	3.60E-03	3.69E-03	3.68E-03	3.77E-03	3.89E-03	4.08E-03	4.45E-03	5.55E-03	4.23E-03	3.54E-03	7.49E-03	5.08E-03	1.08E-04
0.30	3.57E-03	3.59E-03	3.62E-03	3.65E-03	3.68E-03	3.73E-03	3.80E-03	3.91E-03	4.12E-03	4.74E-03	3.99E-03	3.68E-03	5.69E-03	4.58E-03	1.88E-04
0.40	3.61E-03	3.62E-03	3.63E-03	3.65E-03	3.68E-03	3.73E-03	3.78E-03	3.85E-03	3.98E-03	4.37E-03	3.91E-03	3.75E-03	5.02E-03	4.31E-03	2.67E-04
0.50	3.57E-03	3.58E-03	3.58E-03	3.64E-03	3.68E-03	3.70E-03	3.74E-03	3.80E-03	3.89E-03	4.17E-03	3.84E-03	3.77E-03	4.88E-03	4.18E-03	3.46E-04
0.60	3.59E-03	3.53E-03	3.60E-03	3.64E-03	3.64E-03	3.65E-03	3.68E-03	3.73E-03	3.80E-03	4.02E-03	3.76E-03	3.76E-03	4.46E-03	4.07E-03	4.11E-04
0.80	3.52E-03	3.55E-03	3.56E-03	3.57E-03	3.58E-03	3.59E-03	3.62E-03	3.66E-03	3.70E-03	3.84E-03	3.68E-03	3.72E-03	4.19E-03	3.93E-03	5.43E-04
1.0	3.49E-03	3.49E-03	3.49E-03	3.50E-03	3.52E-03	3.54E-03	3.56E-03	3.58E-03	3.63E-03	3.77E-03	3.60E-03	3.67E-03	3.99E-03	3.80E-03	6.31E-04
1.5	3.32E-03	3.33E-03	3.34E-03	3.34E-03	3.35E-03	3.38E-03	3.39E-03	3.41E-03	3.44E-03	3.53E-03	3.42E-03	3.51E-03	3.69E-03	3.57E-03	7.58E-04
2.0	3.18E-03	3.17E-03	3.18E-03	3.19E-03	3.20E-03	3.22E-03	3.23E-03	3.24E-03	3.26E-03	3.31E-03	3.25E-03	3.37E-03	3.45E-03	3.37E-03	8.82E-04
3.0	2.87E-03	2.86E-03	2.87E-03	2.88E-03	2.90E-03	2.93E-03	2.92E-03	2.92E-03	2.93E-03	2.99E-03	2.92E-03	3.03E-03	3.07E-03	3.00E-03	9.78E-04
4.0	2.60E-03	2.60E-03	2.60E-03	2.60E-03	2.61E-03	2.62E-03	2.61E-03	2.61E-03	2.63E-03	2.66E-03	2.61E-03	2.72E-03	2.73E-03	2.69E-03	9.06E-04
5.0	2.33E-03	2.34E-03	2.33E-03	2.33E-03	2.33E-03	2.33E-03	2.34E-03	2.35E-03	2.36E-03	2.39E-03	2.36E-03	2.44E-03	2.44E-03	2.43E-03	9.81E-04
6.0	2.08E-03	2.09E-03	2.10E-03	2.10E-03	2.12E-03	2.11E-03	2.11E-03	2.11E-03	2.11E-03	2.13E-03	2.11E-03	2.20E-03	2.18E-03	2.17E-03	9.47E-04
8.0	1.69E-03	1.69E-03	1.69E-03	1.69E-03	1.69E-03	1.70E-03	1.70E-03	1.69E-03	1.70E-03	1.72E-03	1.70E-03	1.77E-03	1.76E-03	1.75E-03	8.46E-04
10.0	1.39E-03	1.38E-03	1.38E-03	1.39E-03	1.39E-03	1.38E-03	1.39E-03	1.39E-03	1.39E-03	1.40E-03	1.39E-03	1.45E-03	1.45E-03	1.43E-03	7.34E-04

APPENDIX B
GRAPHS OF SPECIFIC ABORBED FRACTION

This appendix graphs Specific Absorbed Fraction (SAF) data for UFRF for any combination of source (TAM, TBS, TBV, TAM_{50}, TIM) and target (TAM, TAM_{50}) regions in the entire skeleton containing active marrow for a range of cellularities (10% to 100%). Absorbed Fraction (AF) values were normalized to the mass of the target (and cellularity) to report SAF. For the TAM irradiating the TAM, marrow cellularity is varied. For all sources irradiating the TAM or $TAM_{50,}$ ICRP reference cellularity is used.

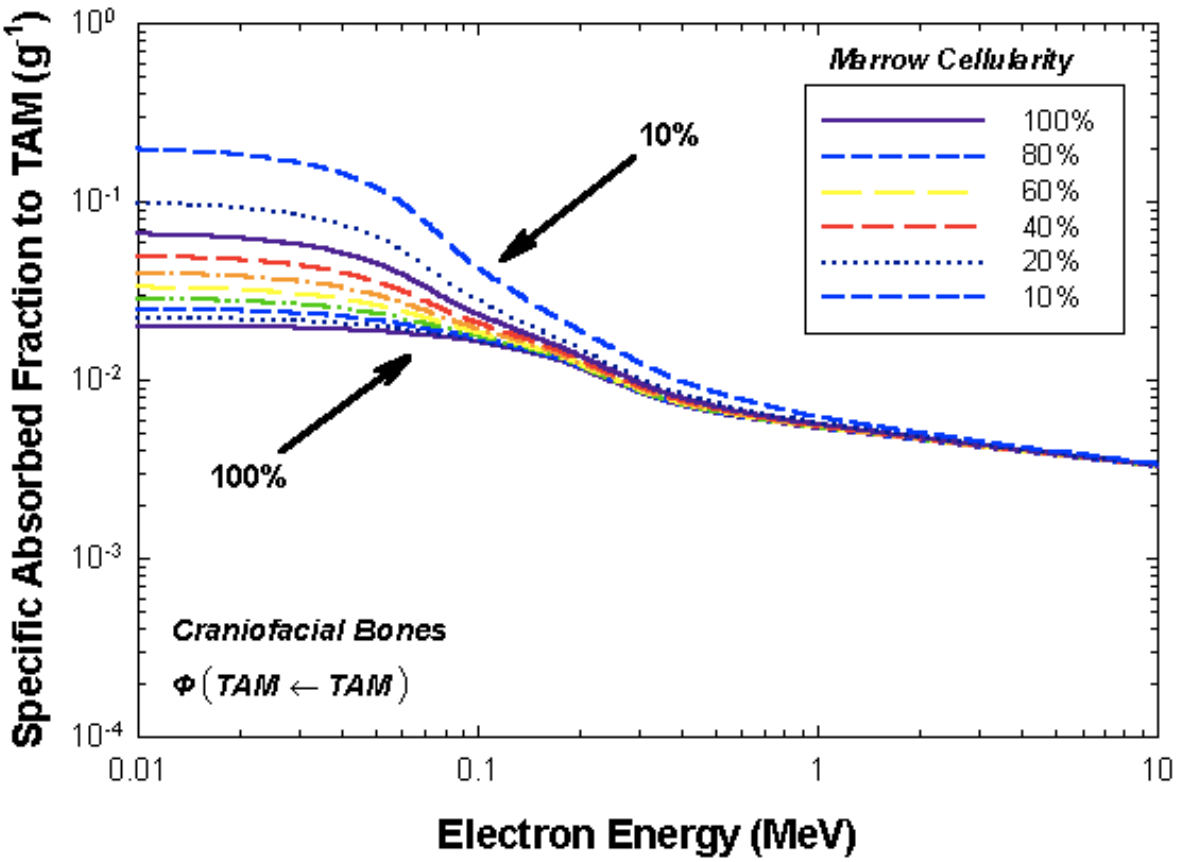

Figure B-1. Specific absorbed fraction for the TAM irradiating the TAM for the cranium.

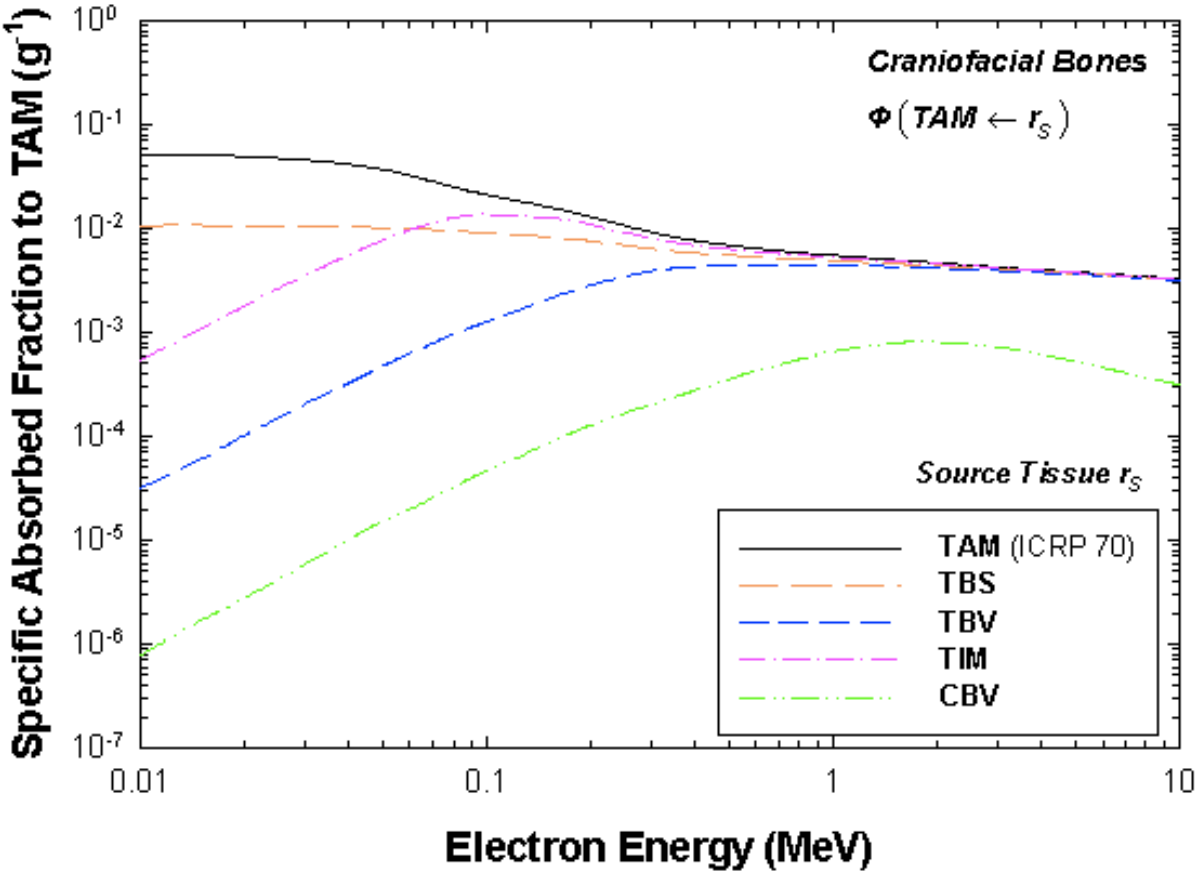

Figure B-2. Specific absorbed fraction for all sources irradiating the TAM for the cranium.

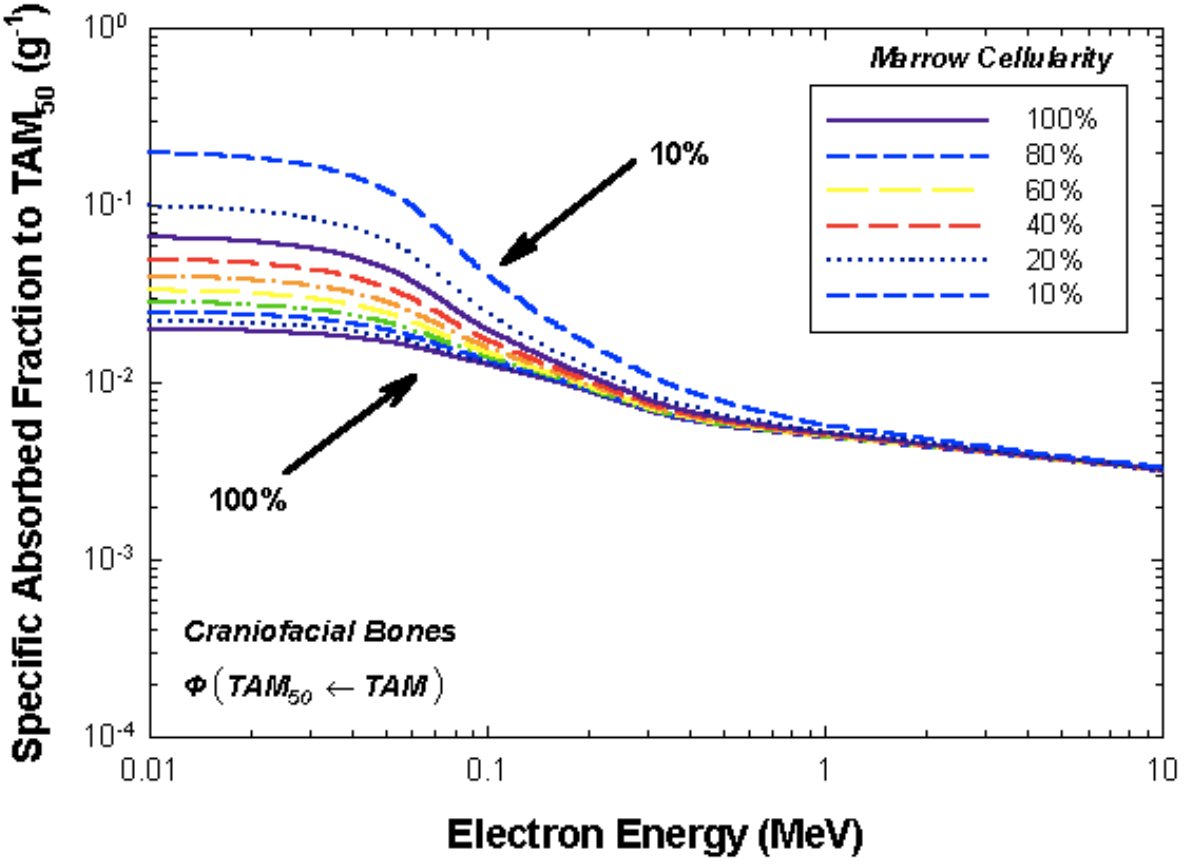

Figure B-3. Specific absorbed fraction for the TAM irradiating the TAM_{50} for the cranium.

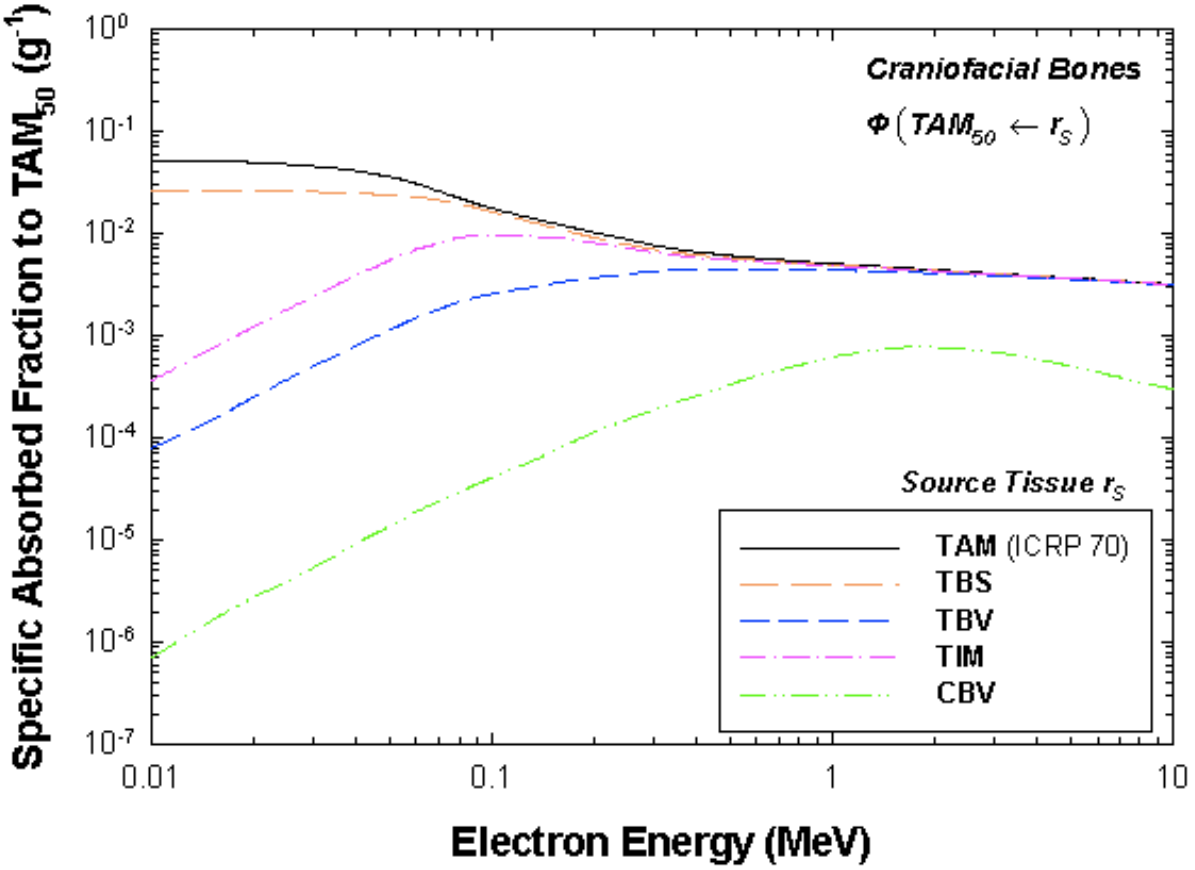

Figure B-4. Specific absorbed fraction for all sources irradiating the TAM_{50} for the cranium.

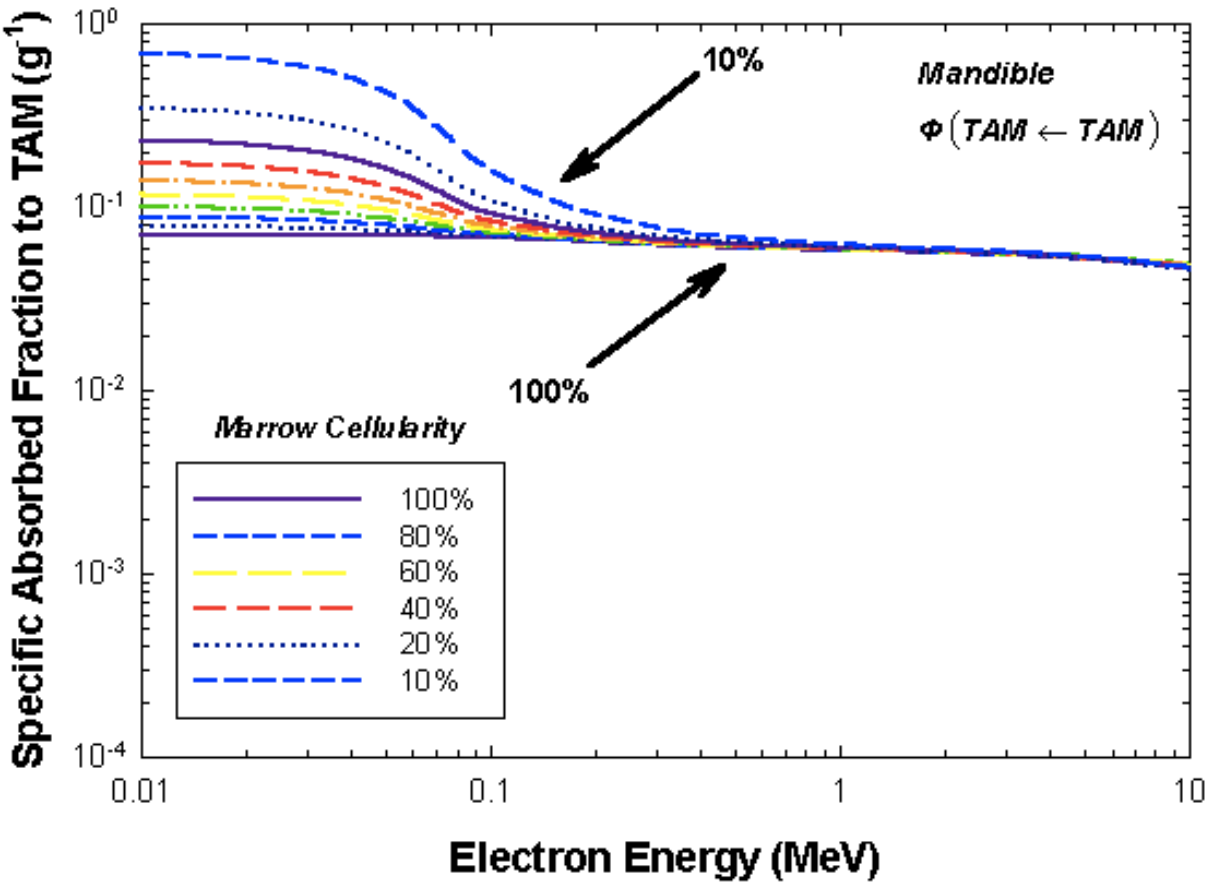

Figure B-5. Specific absorbed fraction for the TAM irradiating the TAM for the mandible.

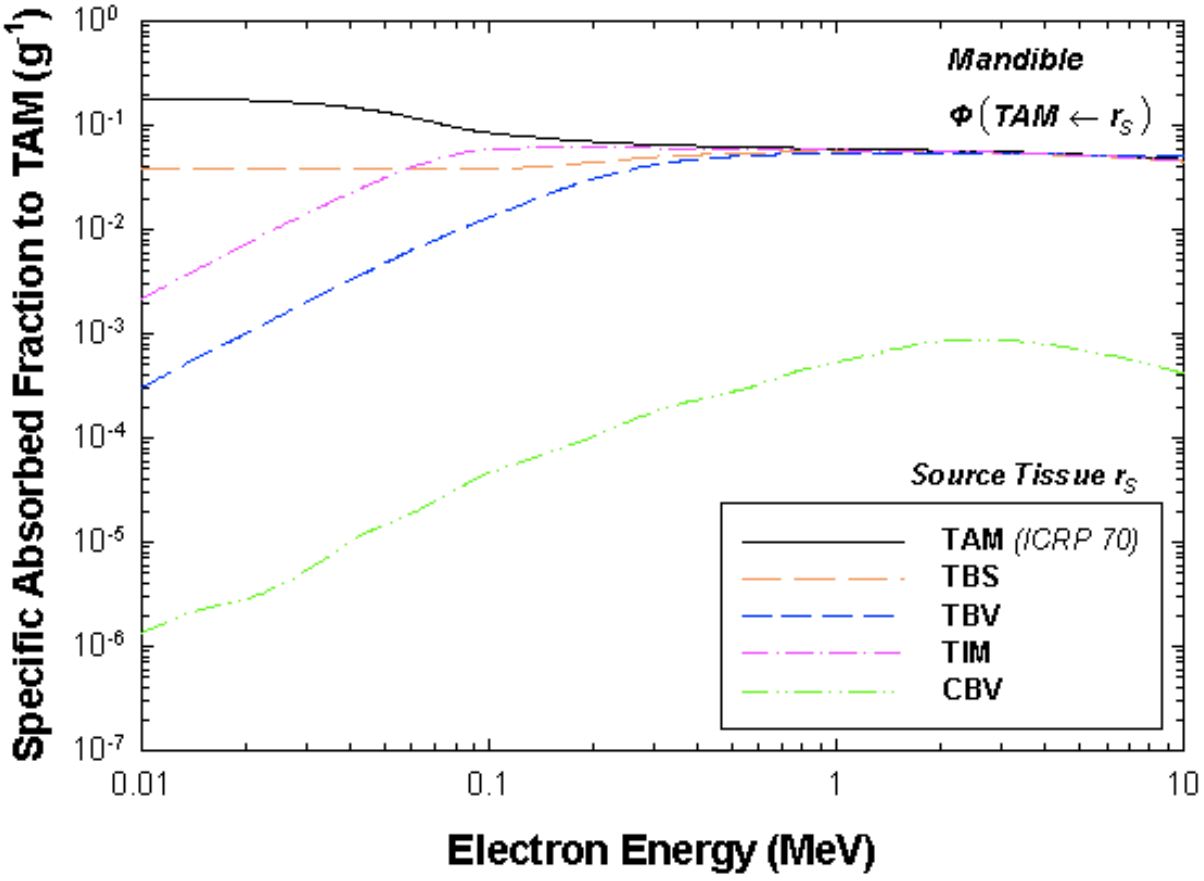

Figure B-6. Specific absorbed fraction for all sources irradiating the TAM for the mandible.

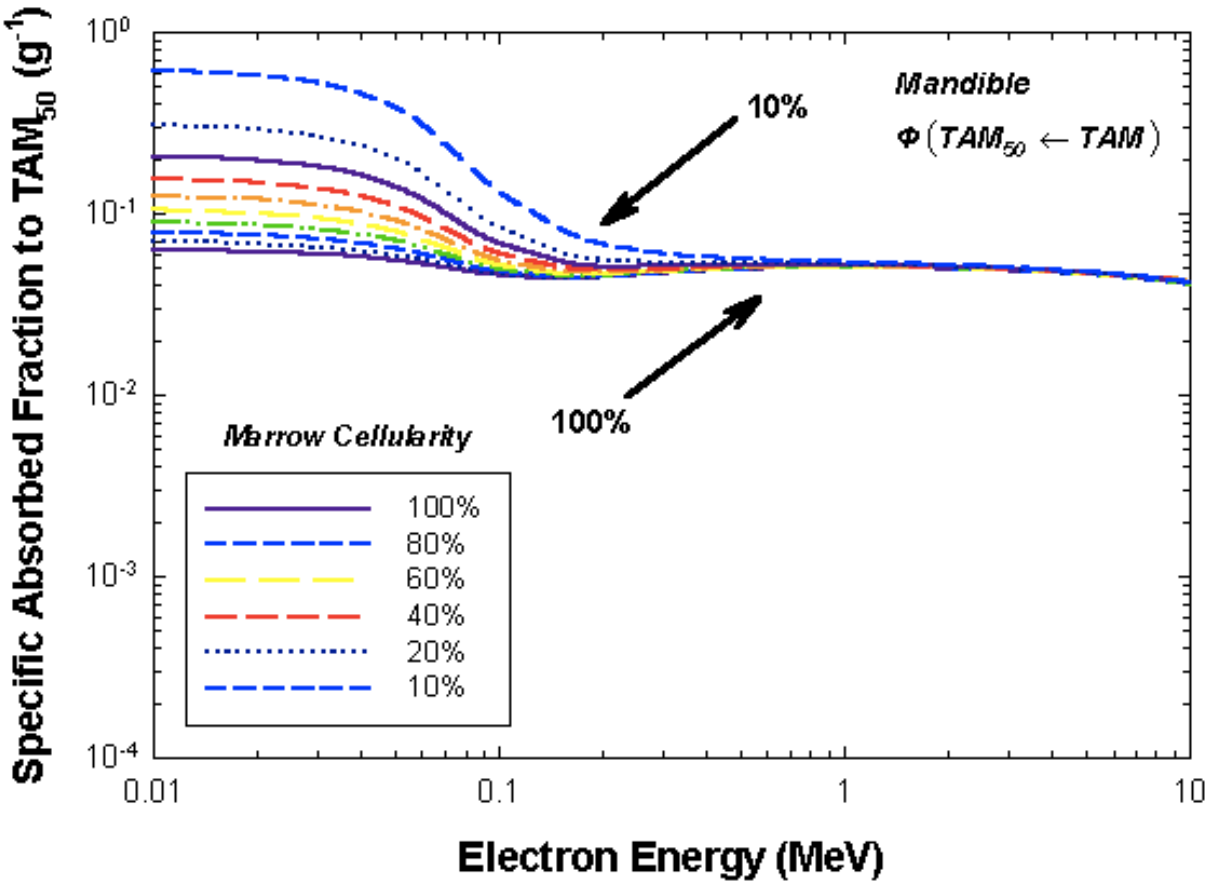

Figure B-7. Specific absorbed fraction for the TAM irradiating the TAM_{50} for the mandible.

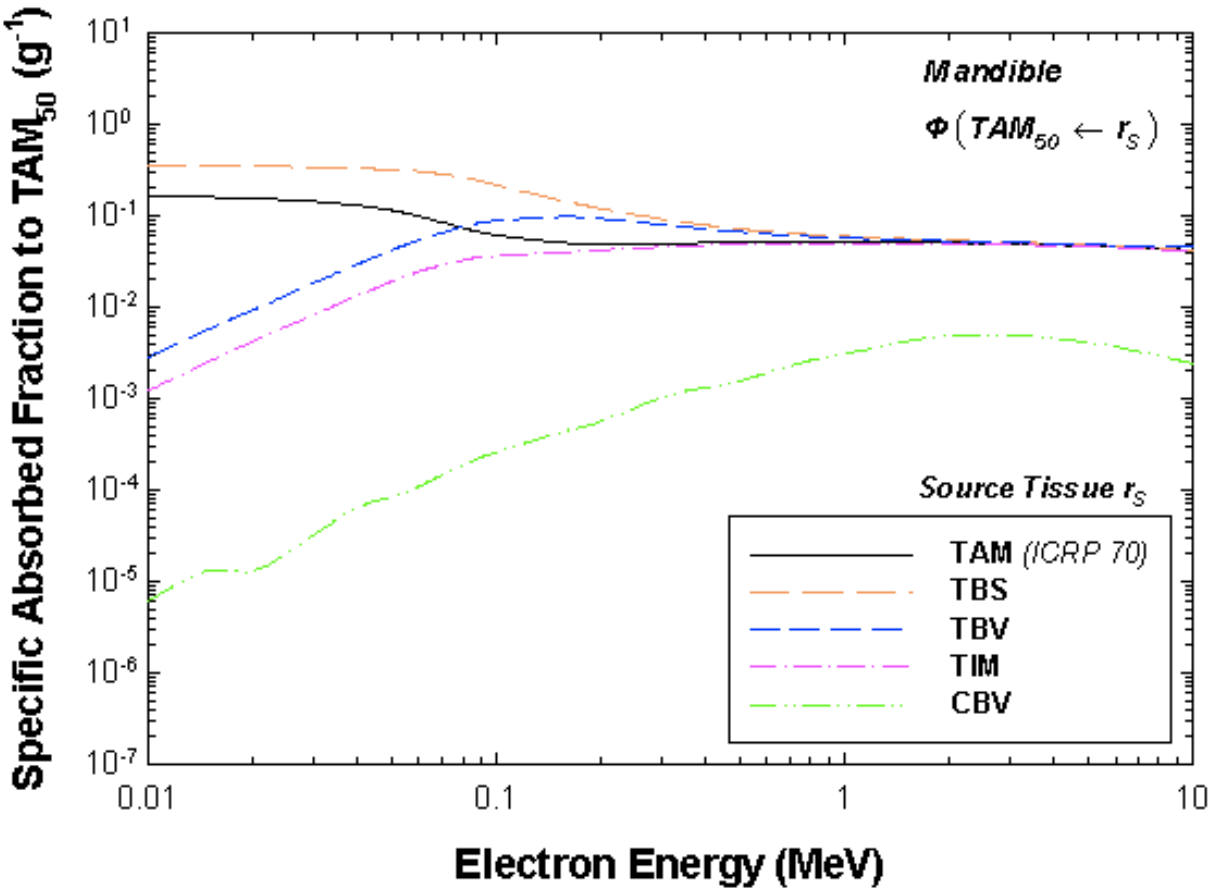

Figure B-8. Specific absorbed fraction for all sources irradiating the TAM_{50} for the mandible.

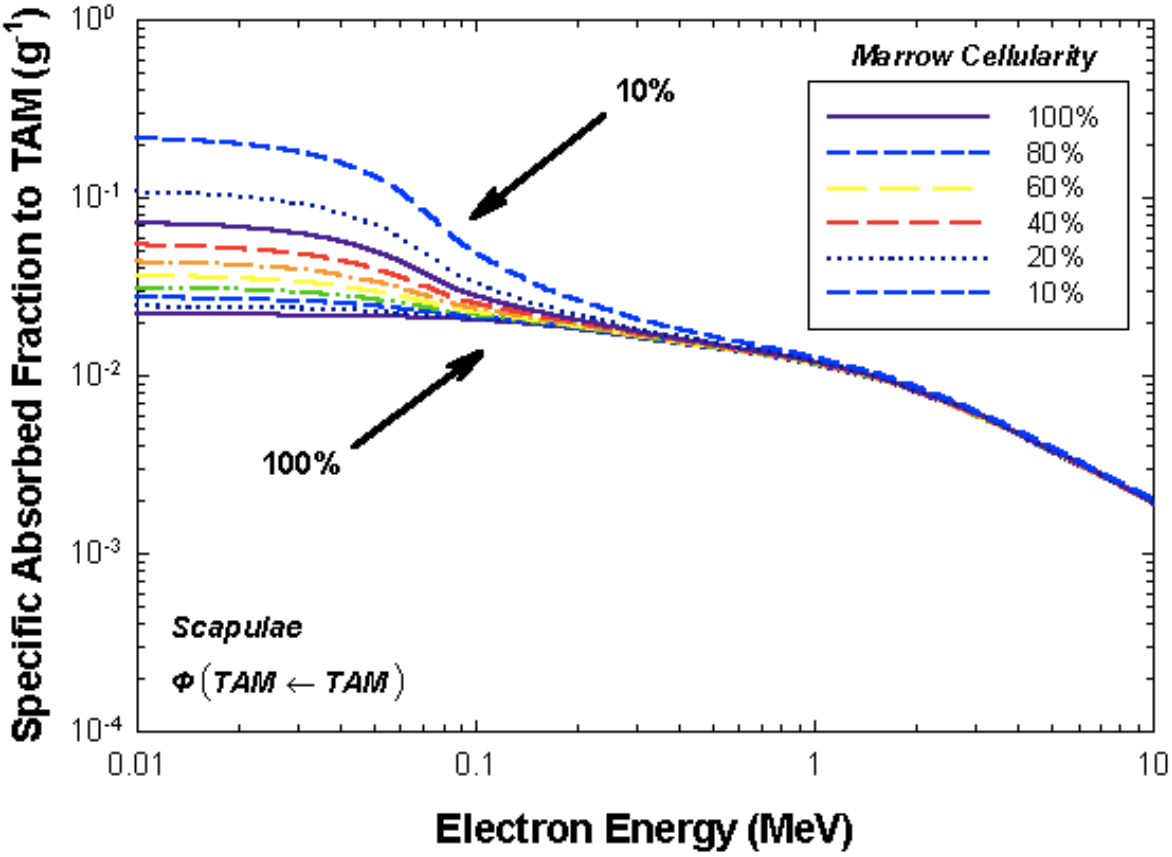

Figure B-9. Specific absorbed fraction for the TAM irradiating the TAM for the scapulae.

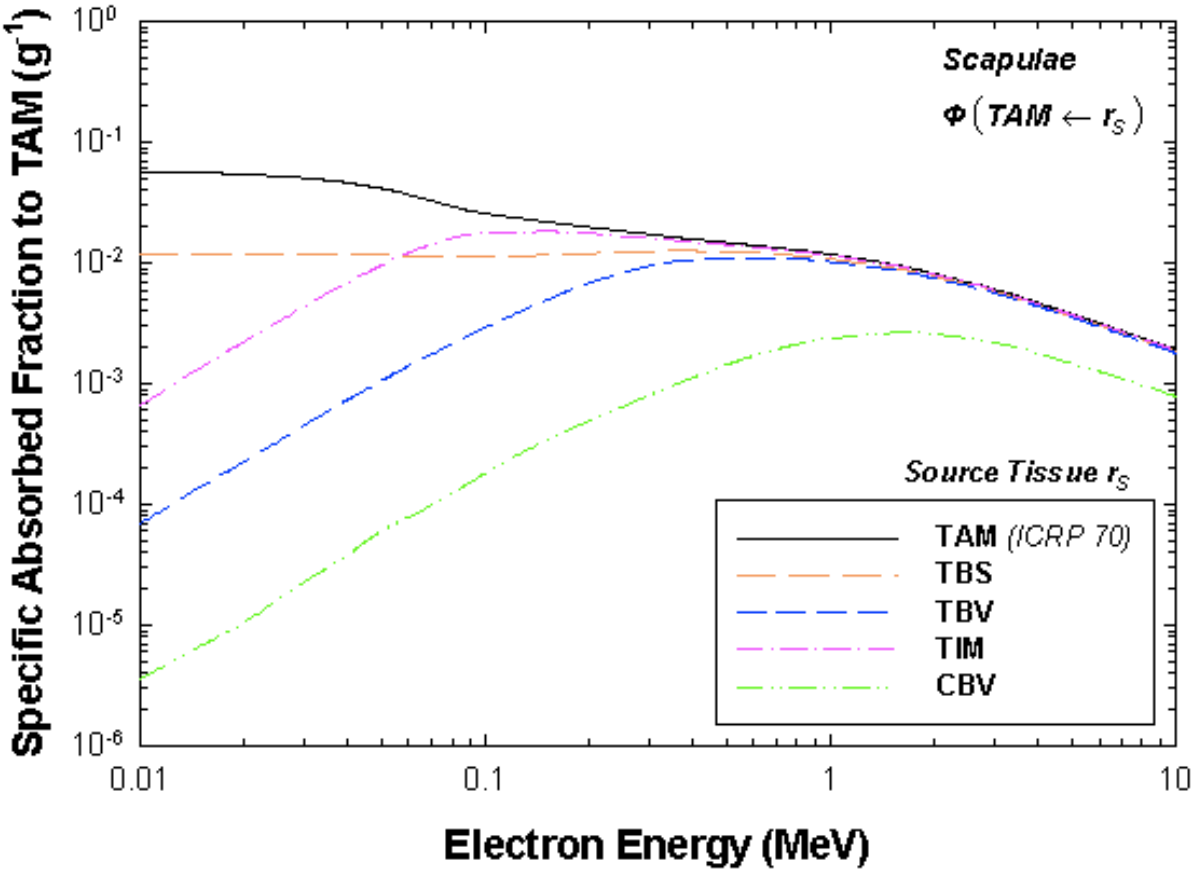

Figure B-10. Specific absorbed fraction for all sources irradiating the TAM for the scapulae.

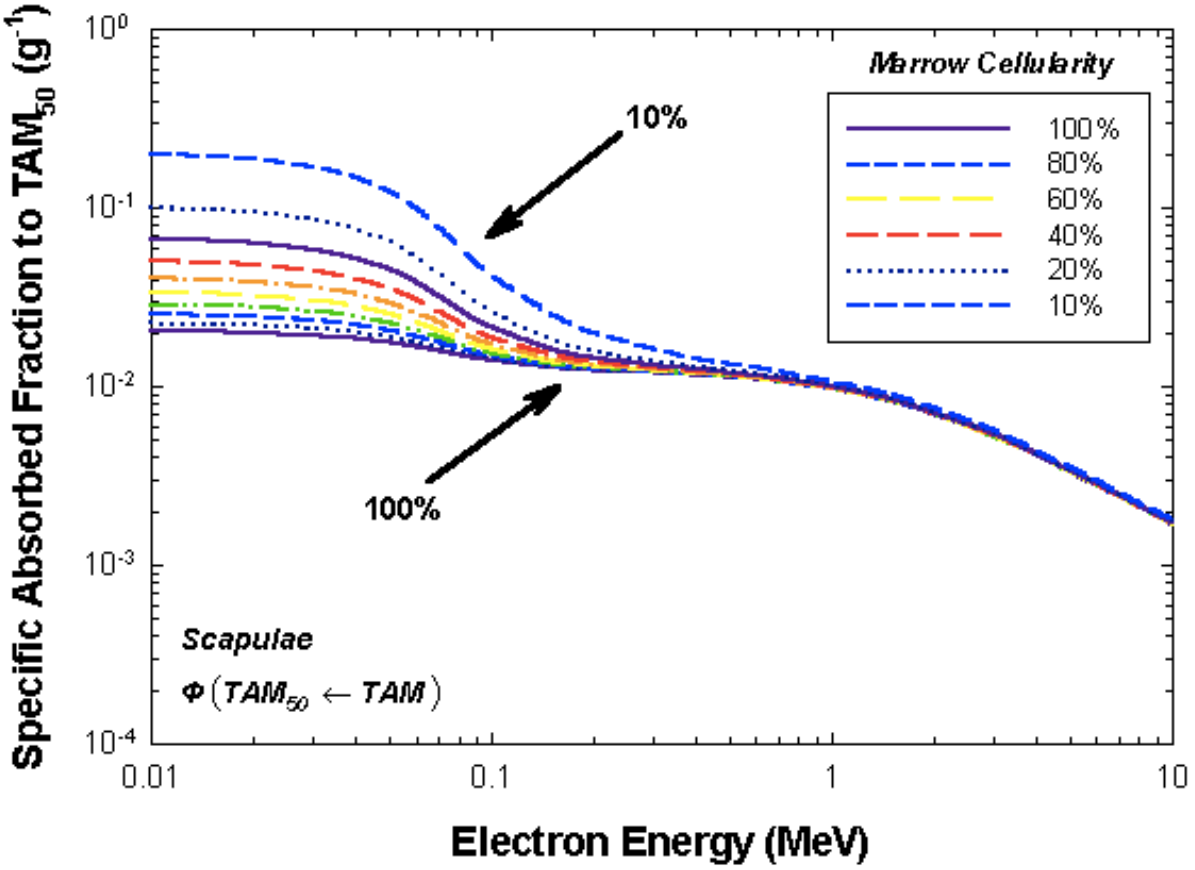

Figure B-11. Specific absorbed fraction for the TAM irradiating the TAM_{50} for the scapulae.

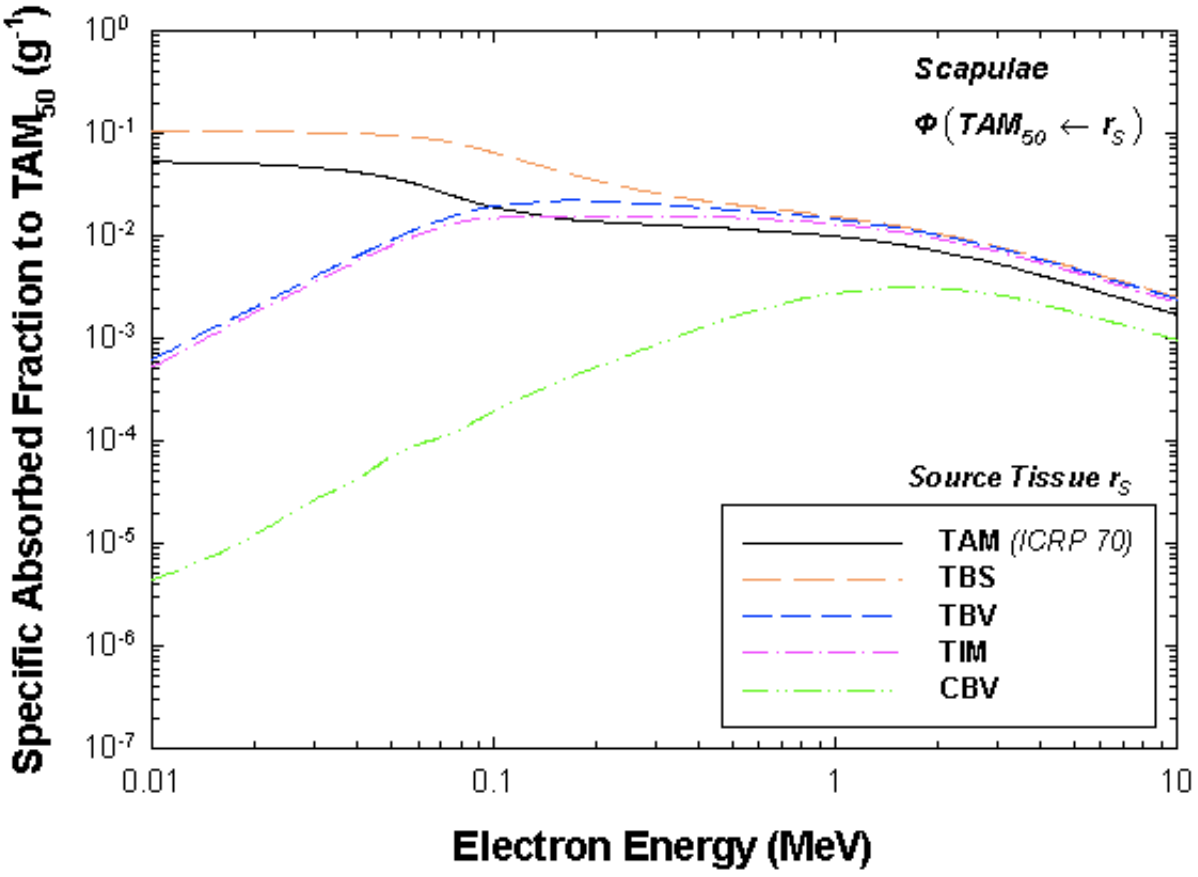

Figure B-12. Specific absorbed fraction for all sources irradiating the TAM_{50} for the scapulae.

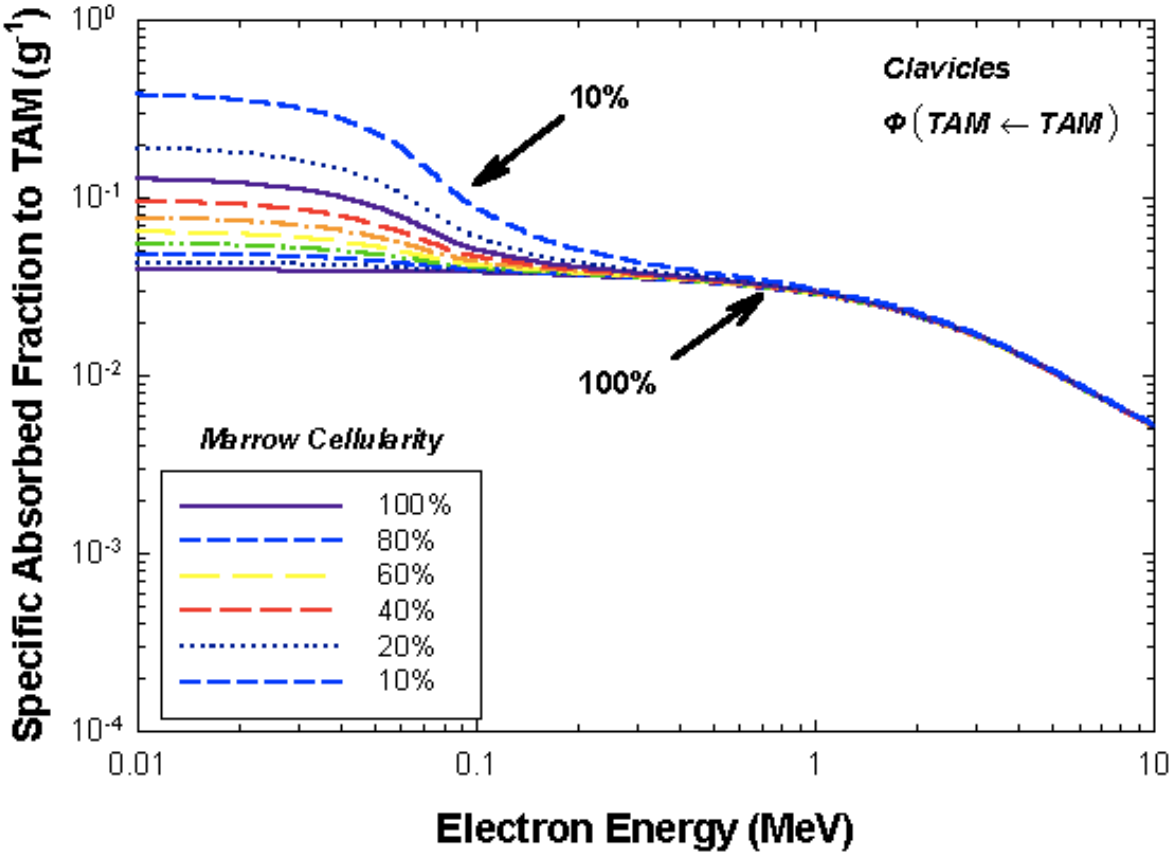

Figure B-13. Specific absorbed fraction for the TAM irradiating the TAM for the clavicles.

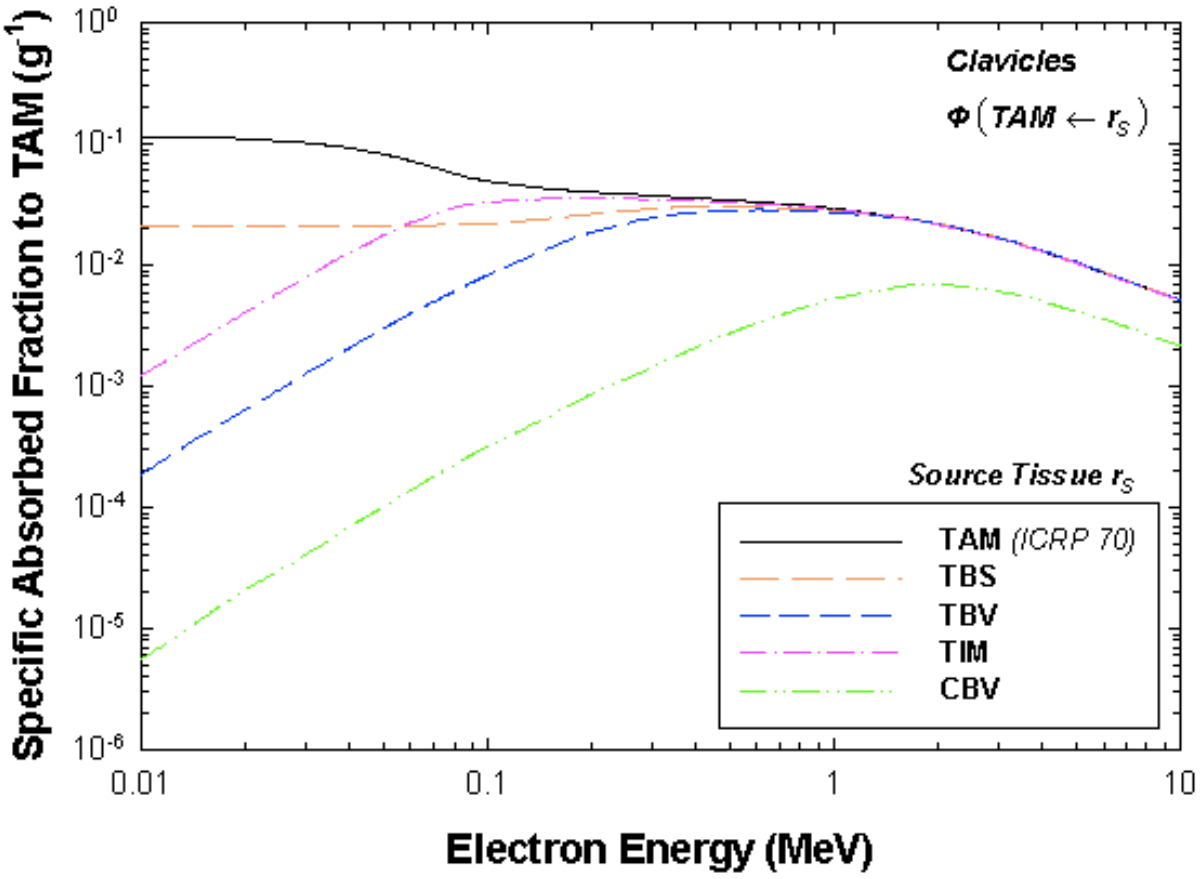

Figure B-14. Specific absorbed fraction for all sources irradiating the TAM for the clavicles.

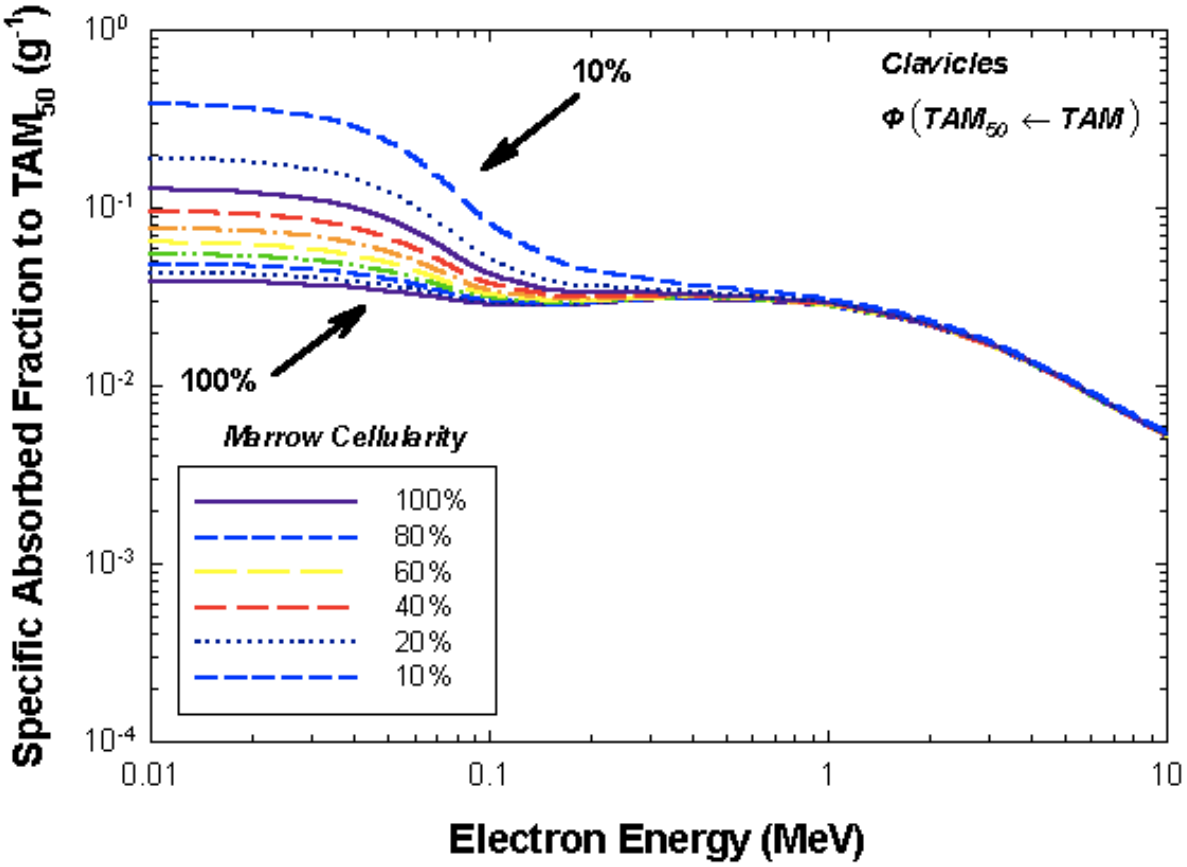

Figure B-15. Specific absorbed fraction for the TAM irradiating the TAM_{50} for the clavicles.

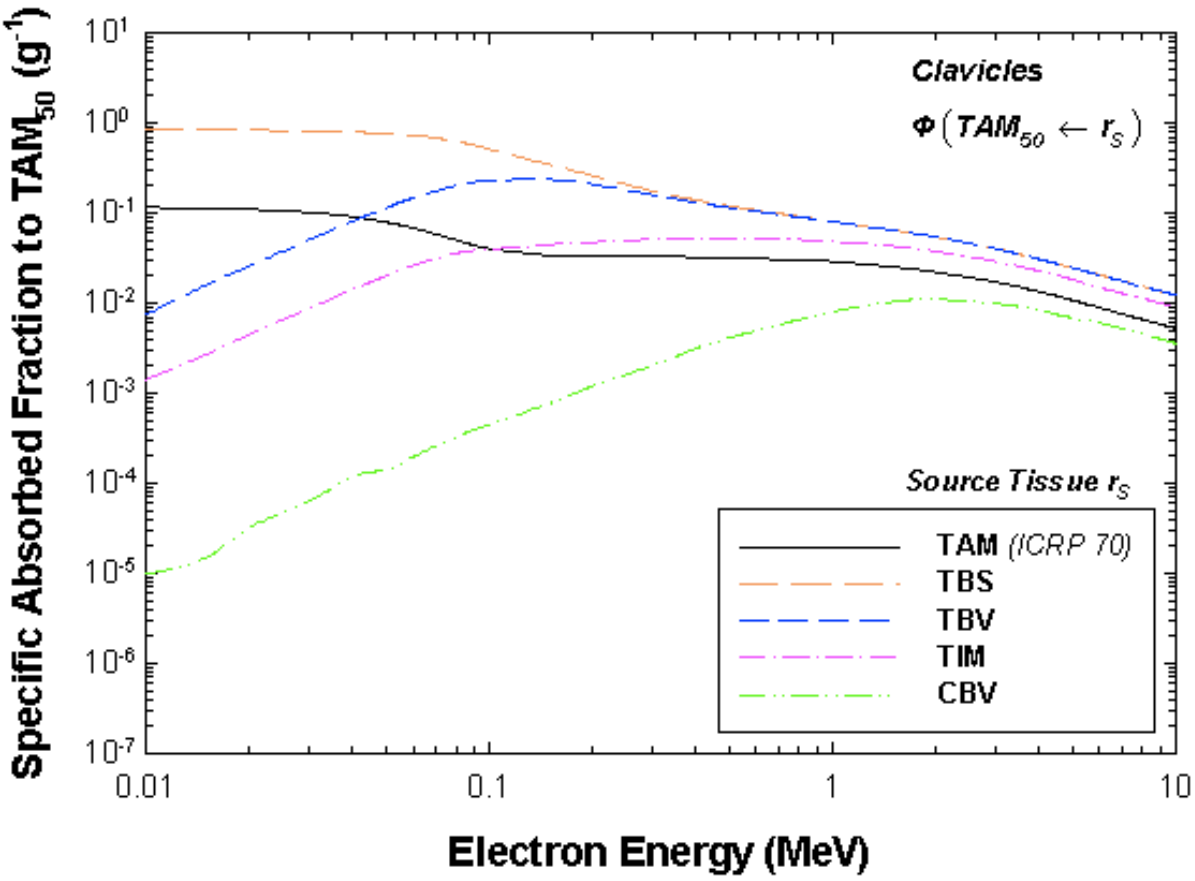

Figure B-16. Specific absorbed fraction for all sources irradiating the TAM_{50} for the clavicles.

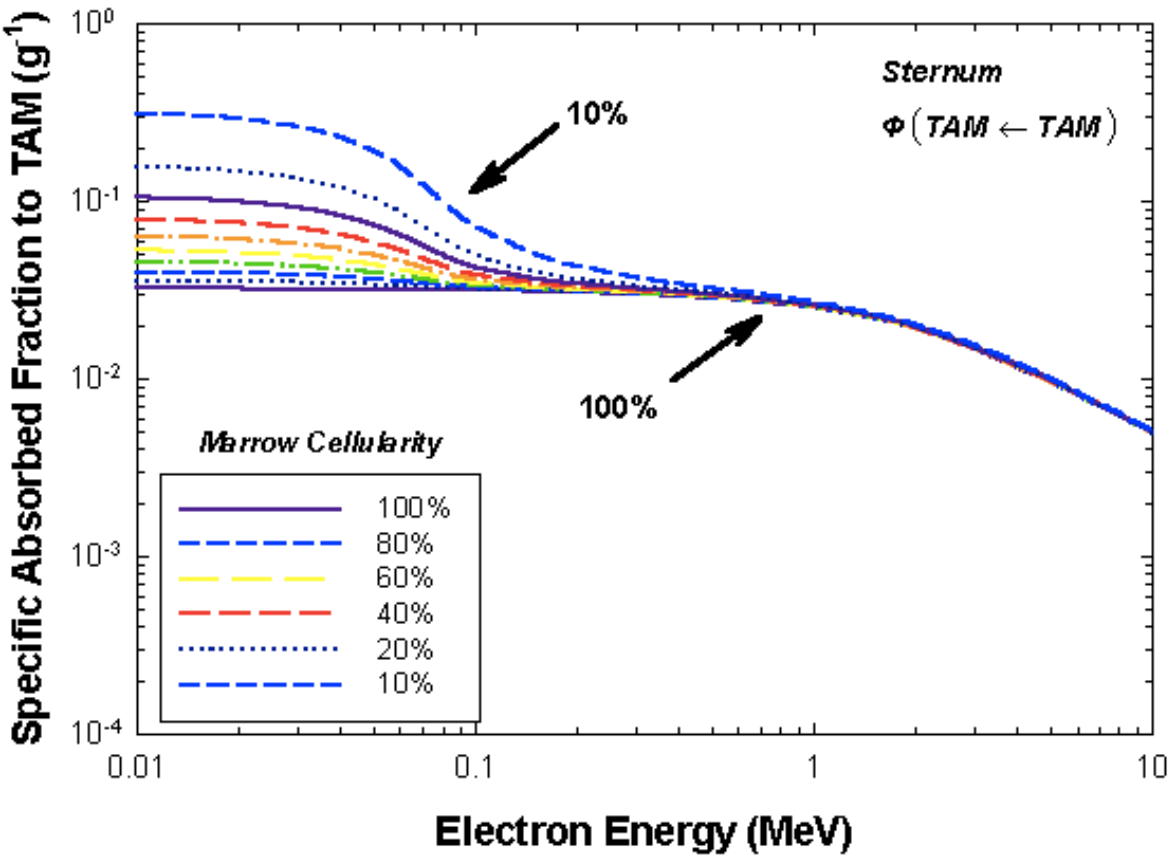

Figure B-17. Specific absorbed fraction for the TAM irradiating the TAM for the sternum.

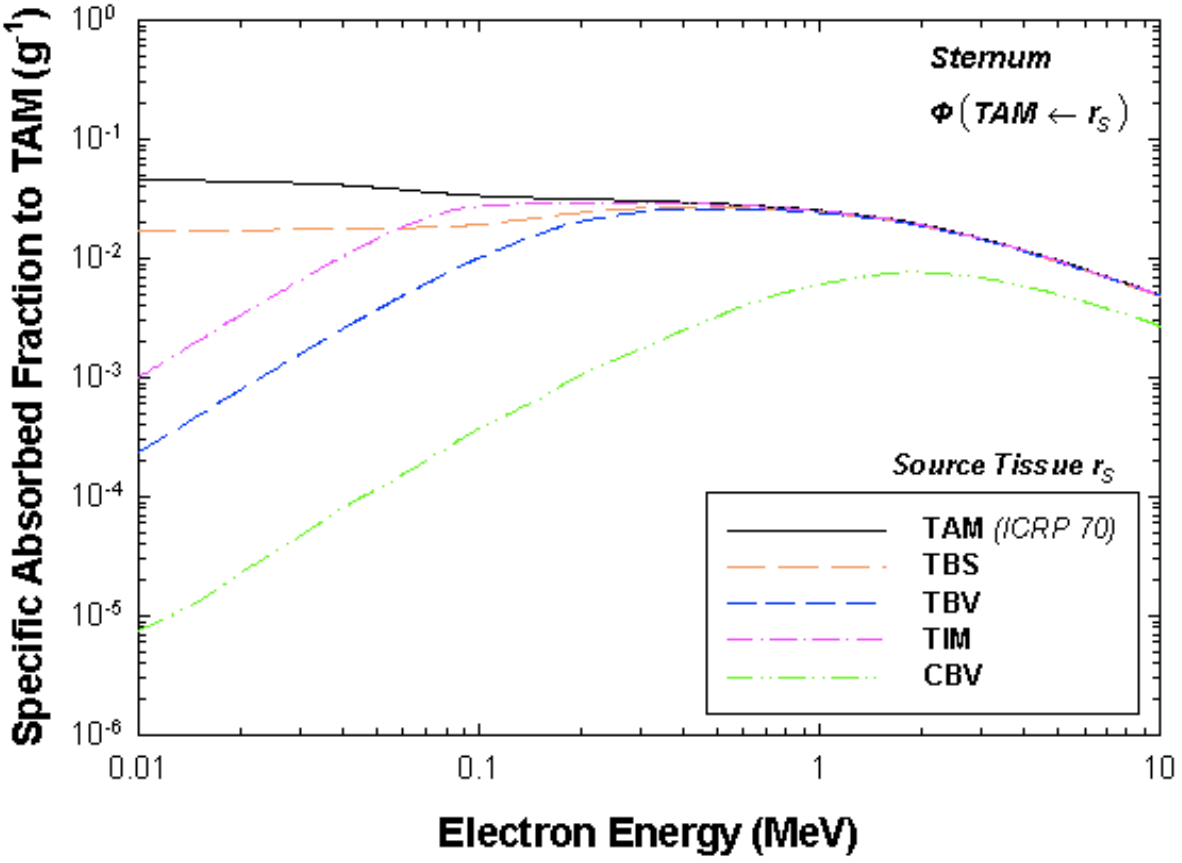

Figure B-18. Specific absorbed fraction for all sources irradiating the TAM for the sternum.

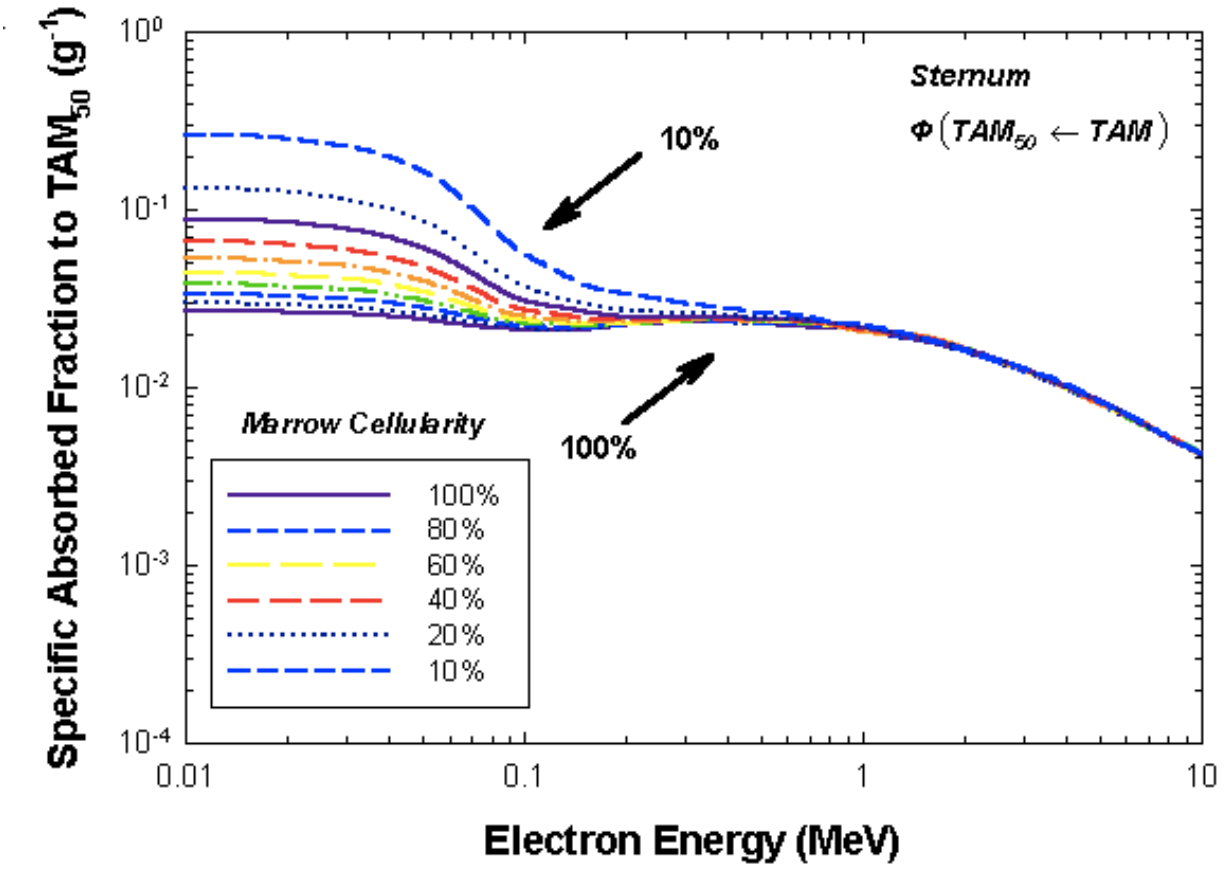

Figure B-19. Specific absorbed fraction for the TAM irradiating the TAM_{50} for the sternum.

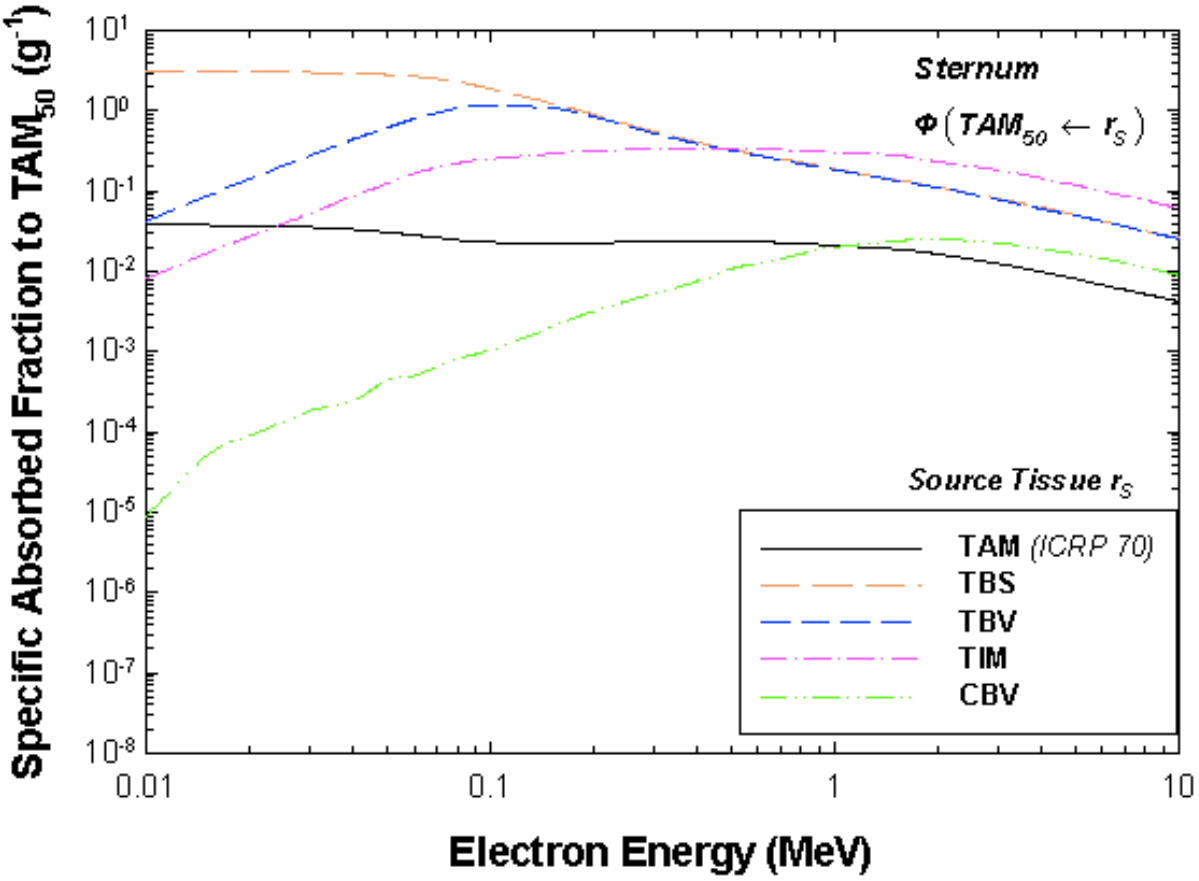

Figure B-20. Specific absorbed fraction for all sources irradiating the TAM_{50} for the sternum.

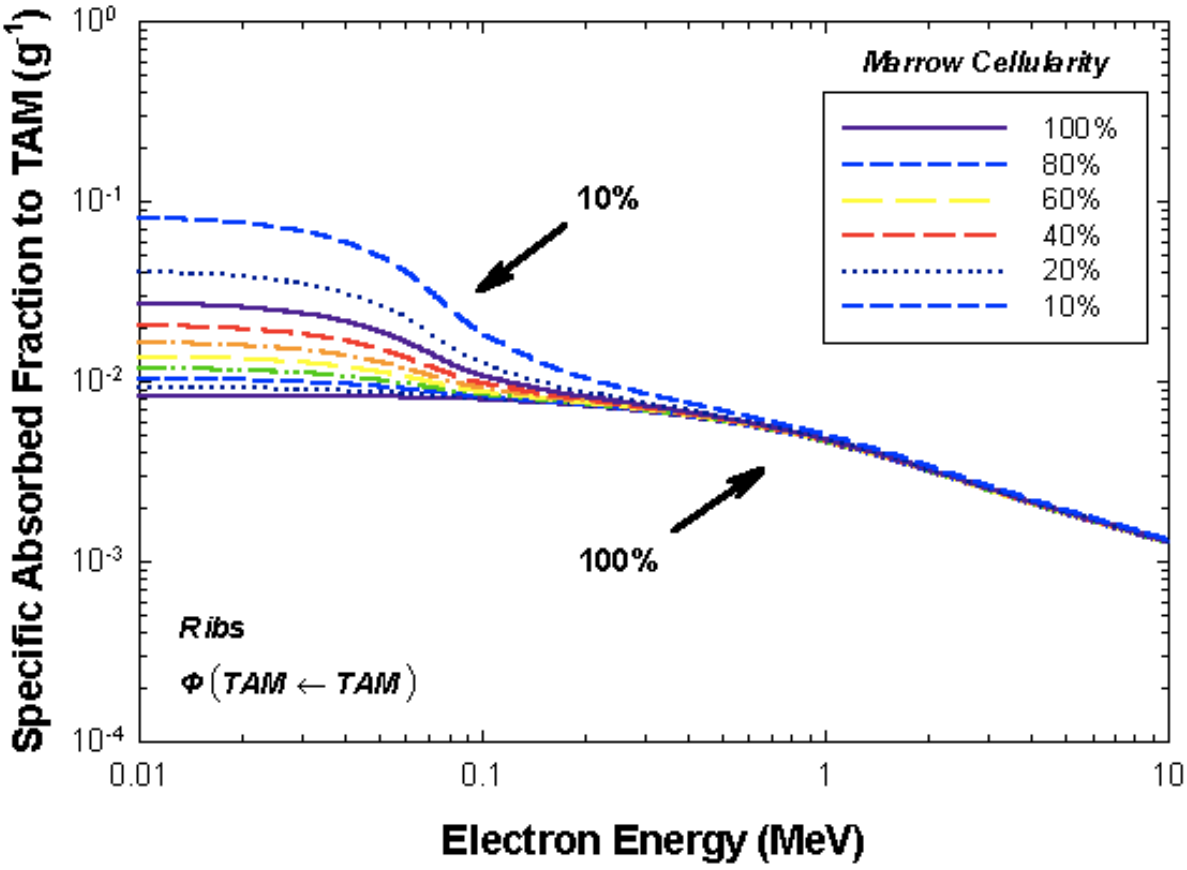

Figure B-21. Specific absorbed fraction for the TAM irradiating the TAM for the ribs.

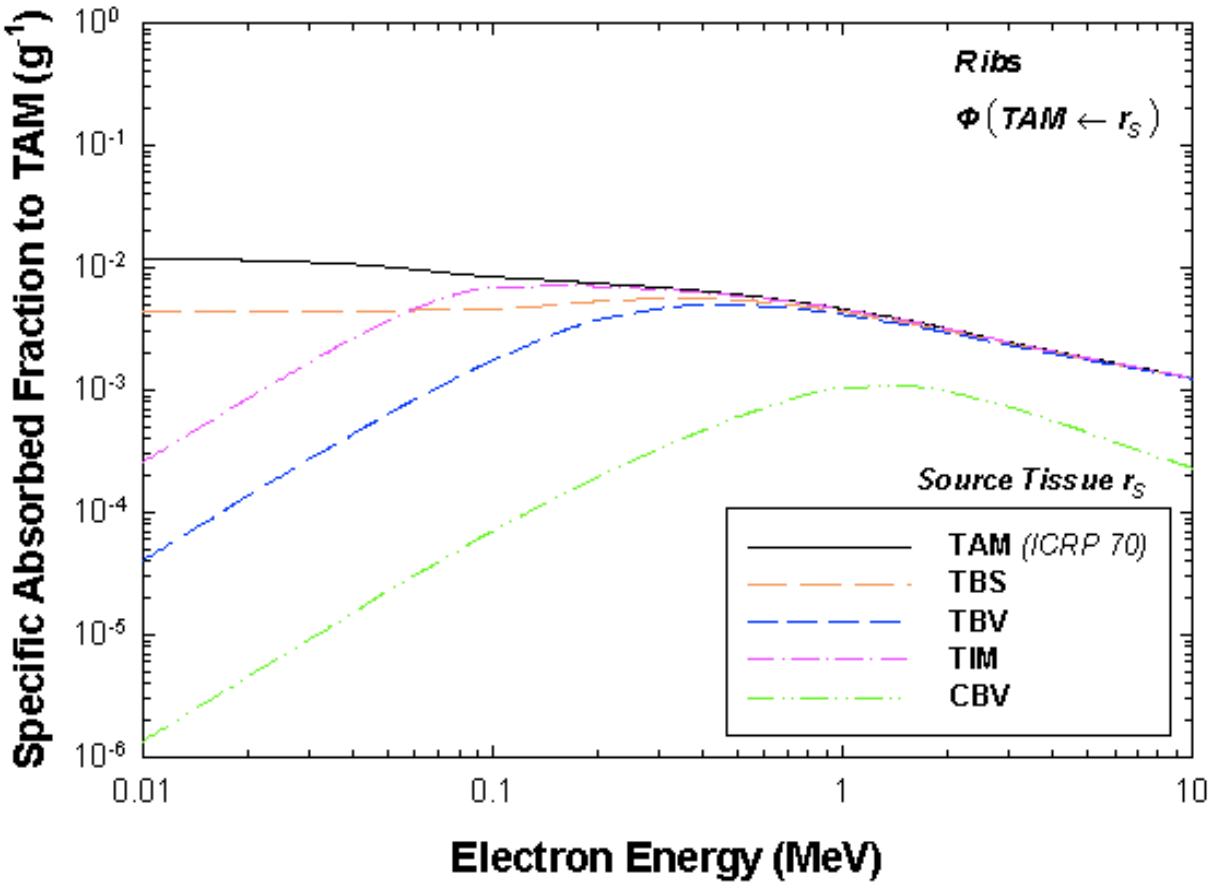

Figure B-22. Specific absorbed fraction for all sources irradiating the TAM for the ribs.

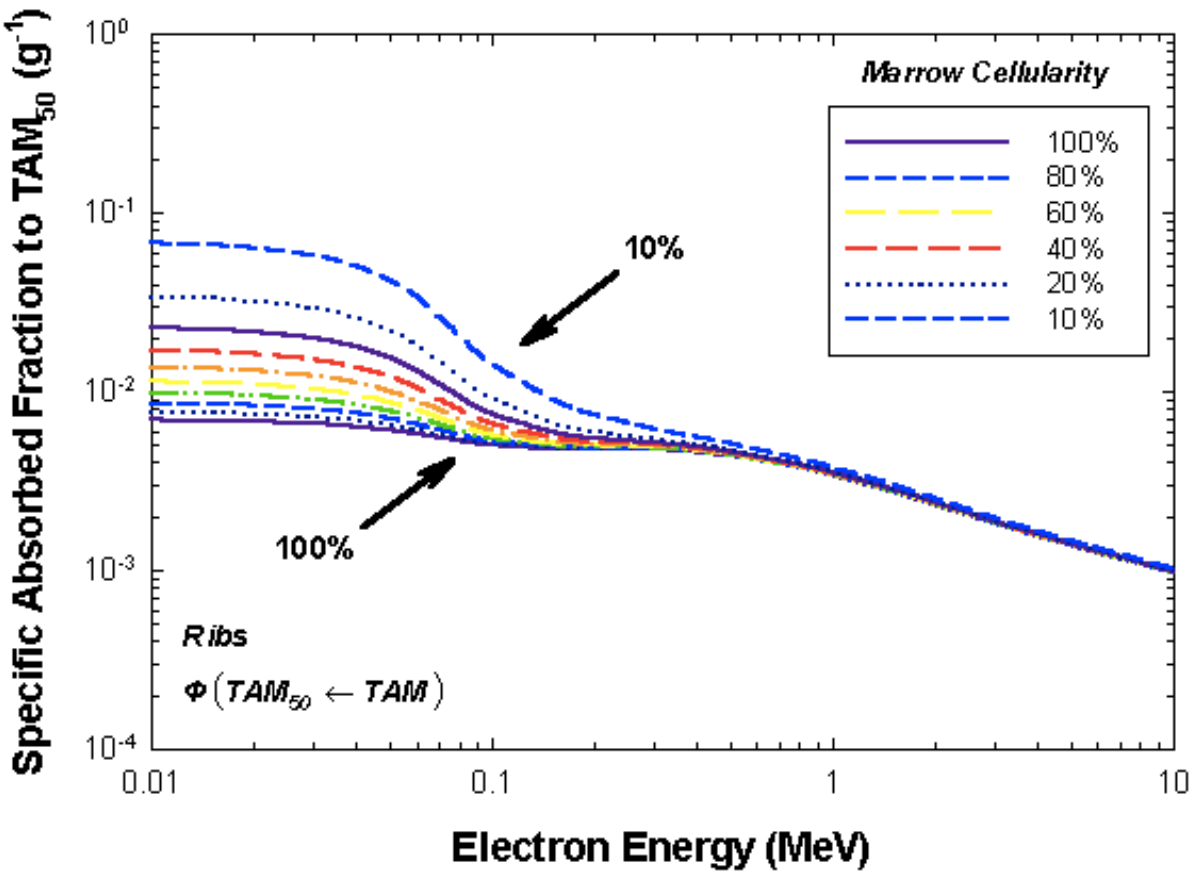

Figure B-23. Specific absorbed fraction for the TAM irradiating the TAM_{50} for the ribs.

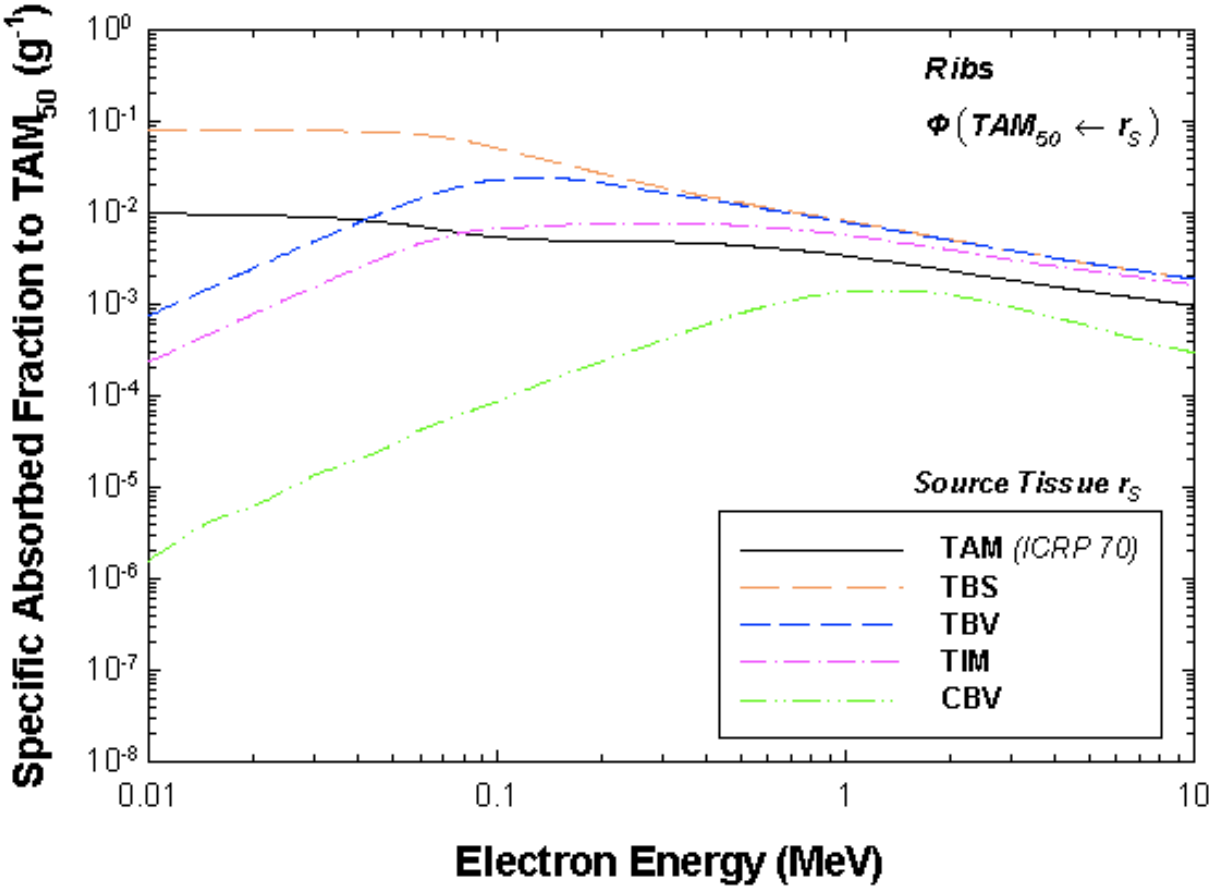

Figure B-24. Specific absorbed fraction for all sources irradiating the TAM_{50} for the ribs.

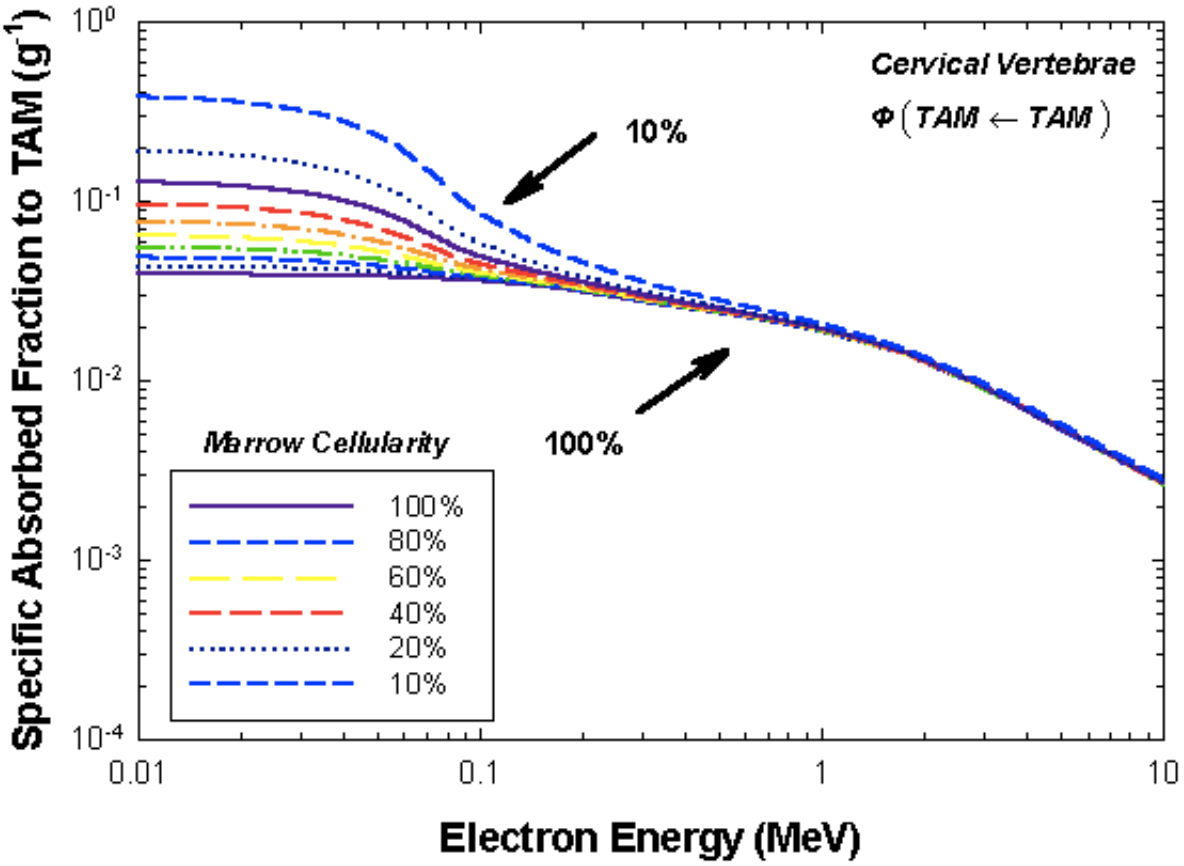

Figure B-25. Specific absorbed fraction for the TAM irradiating the TAM for the cervical vertebrae.

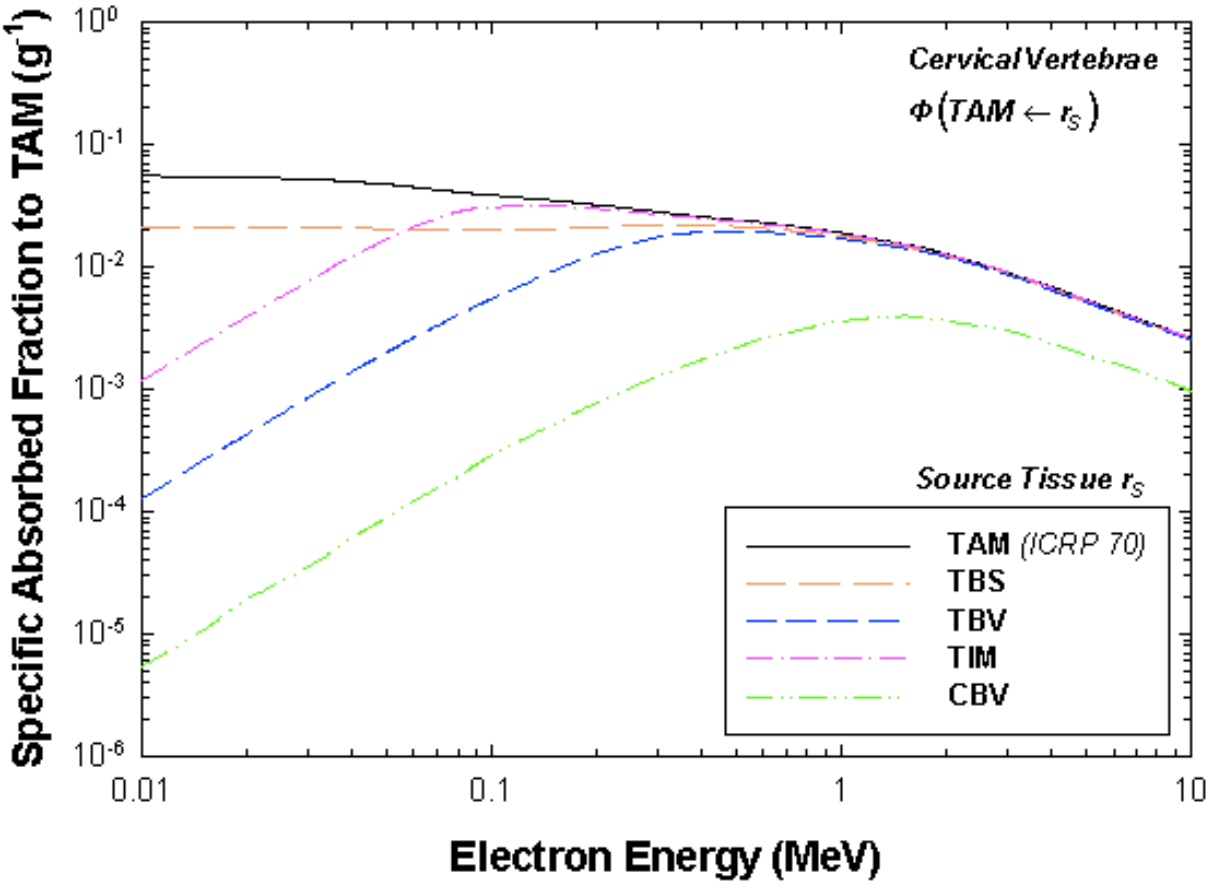

Figure B-26. Specific absorbed fraction for all sources irradiating the TAM for the cervical vertebrae.

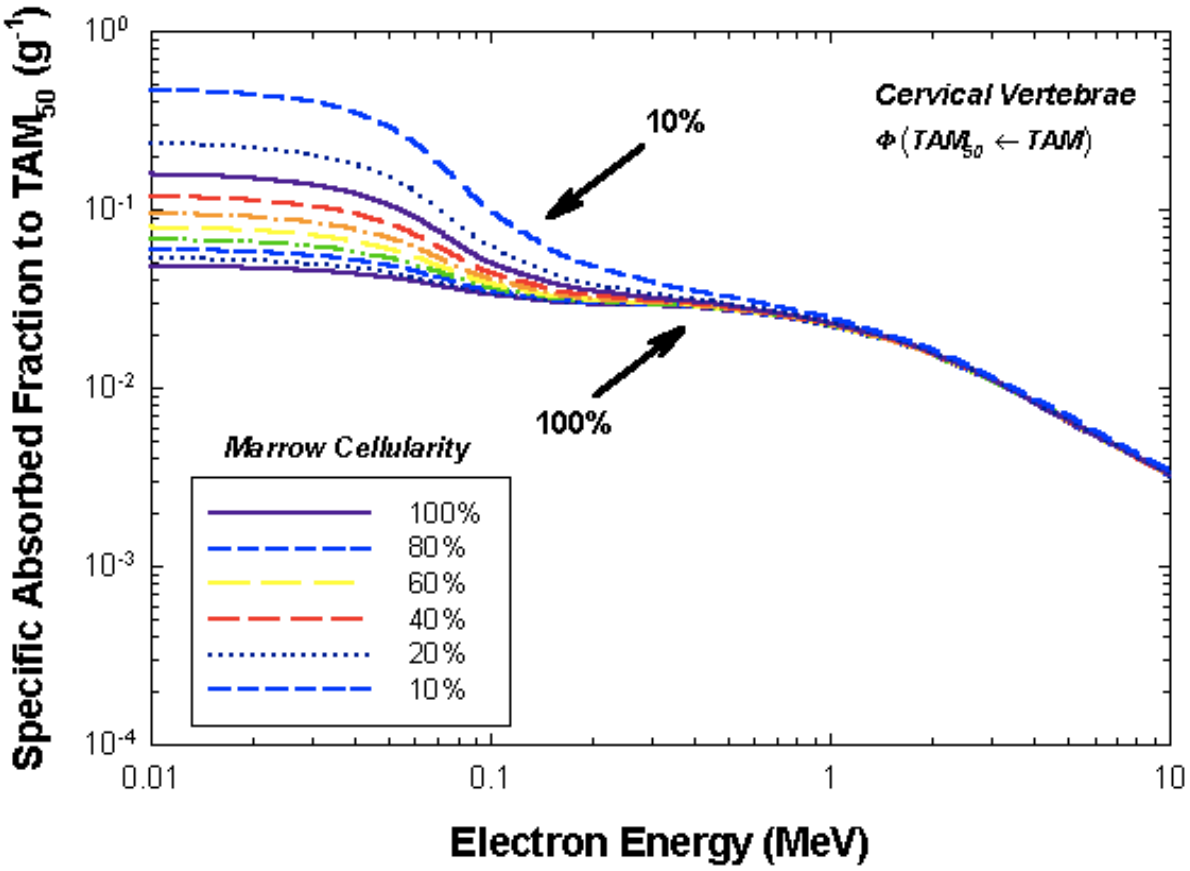

Figure B-27. Specific absorbed fraction for the TAM irradiating the TAM_{50} for the cervical vertebrae.

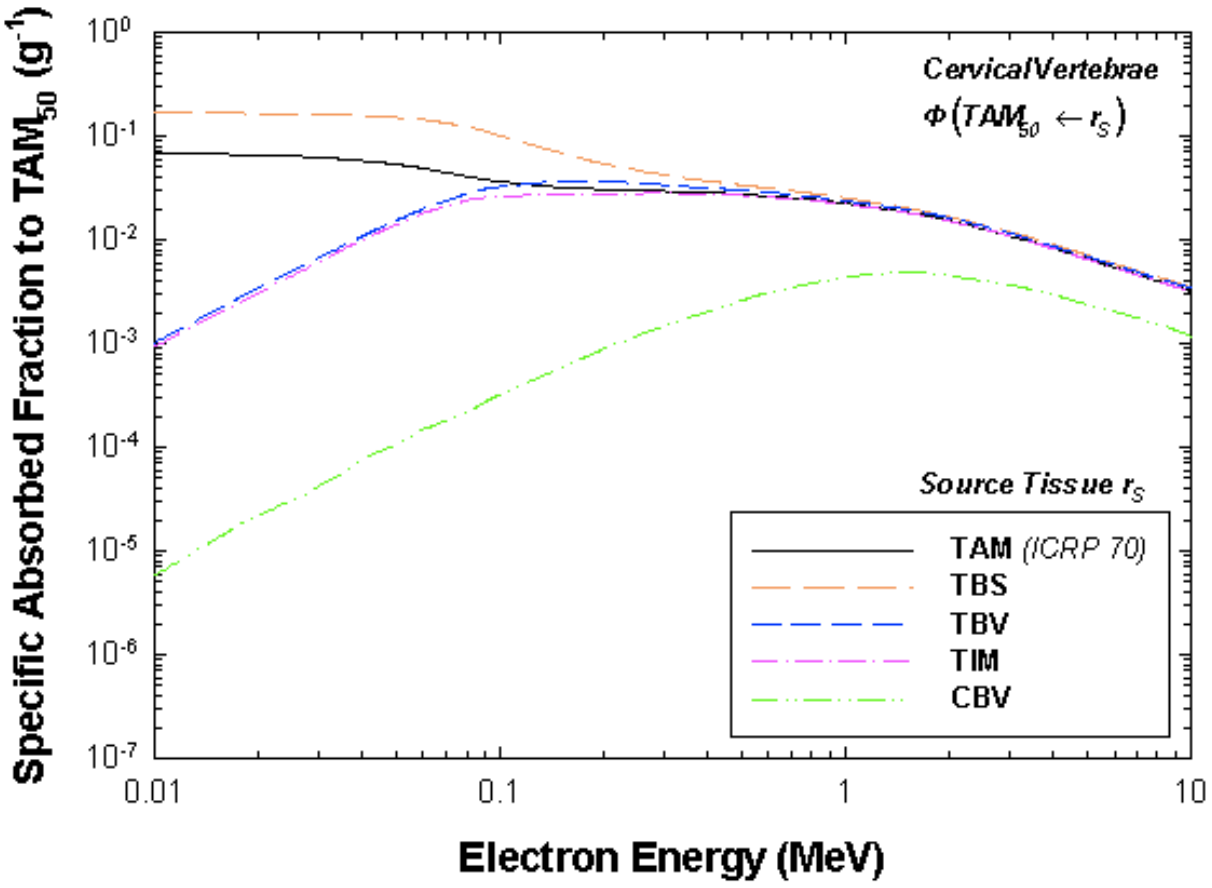

Figure B-28. Specific absorbed fraction for all sources irradiating the TAM_{50} for the cervical vertebrae.

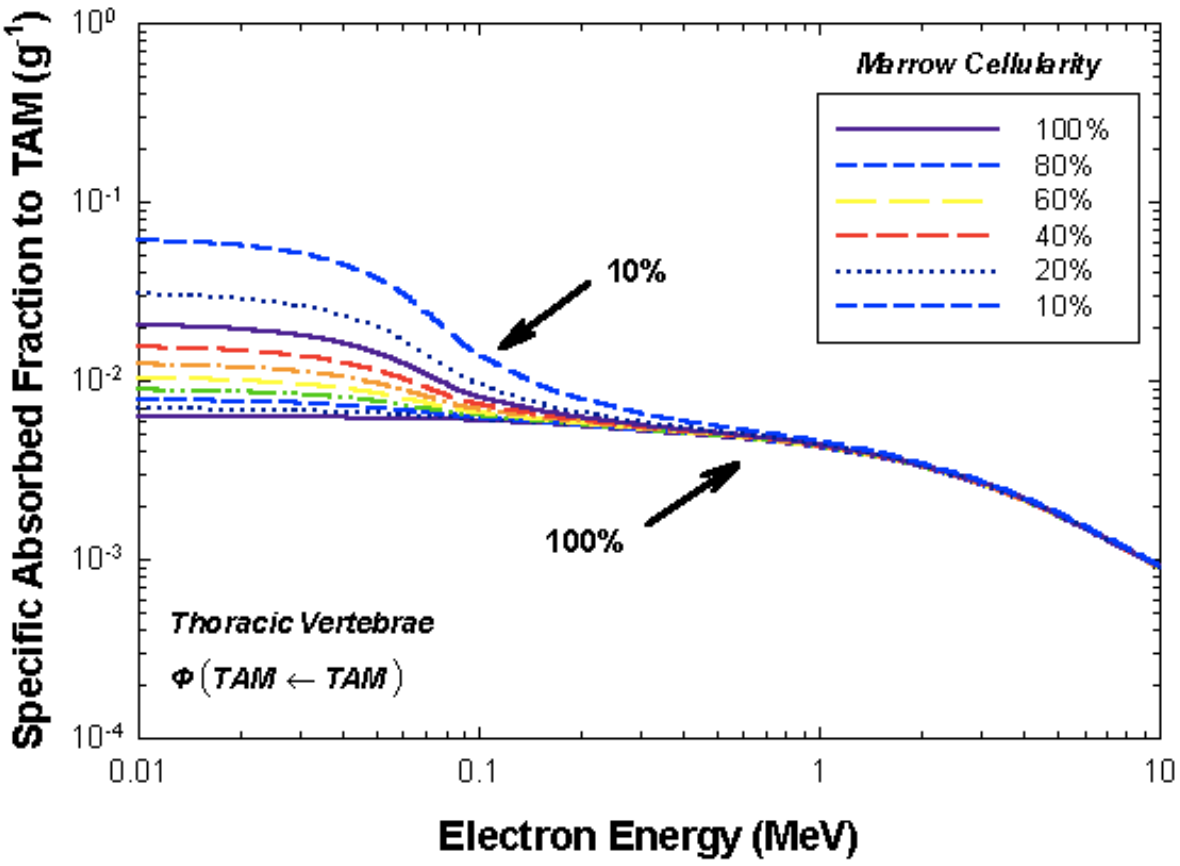

Figure B-29. Specific absorbed fraction for the TAM irradiating the TAM for the thoracic vertebrae.

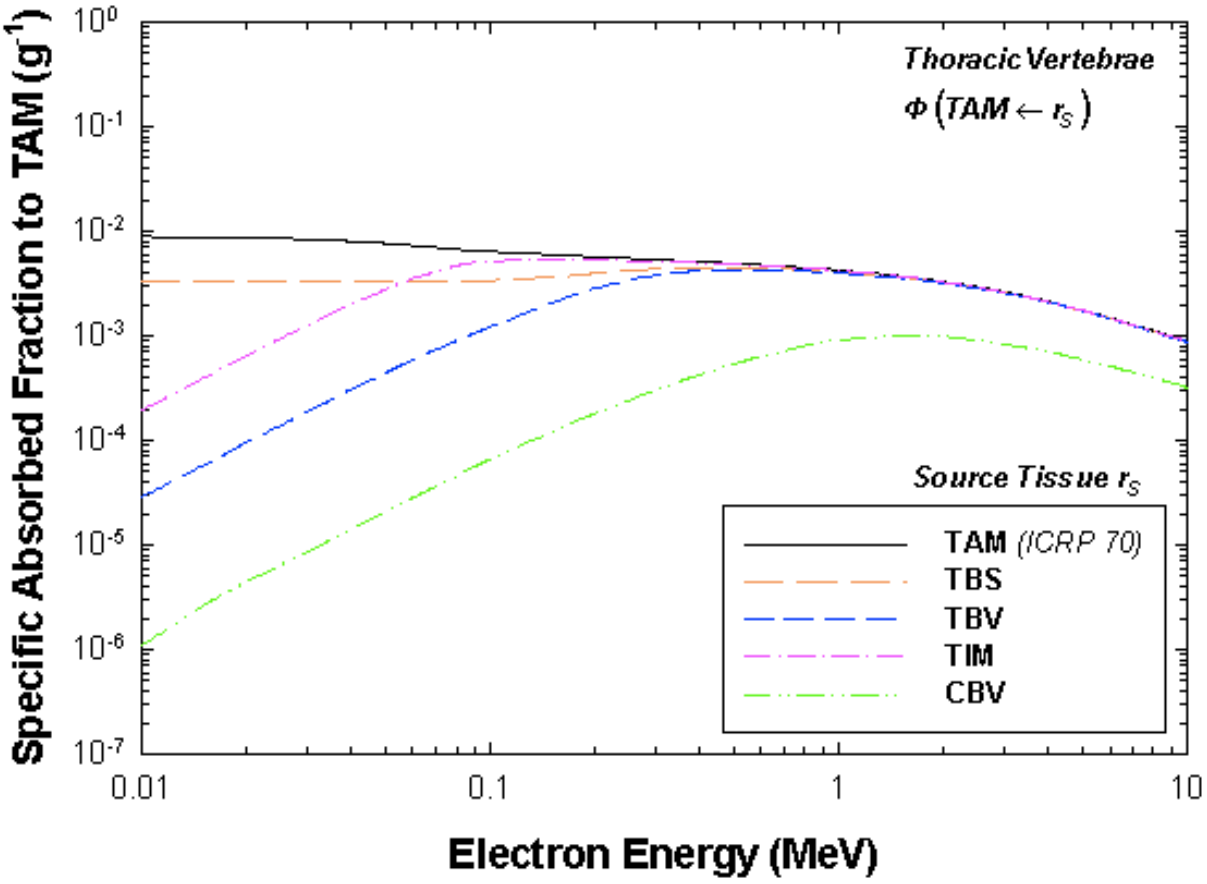

Figure B-30. Specific absorbed fraction for all sources irradiating the TAM for the thoracic vertebrae.

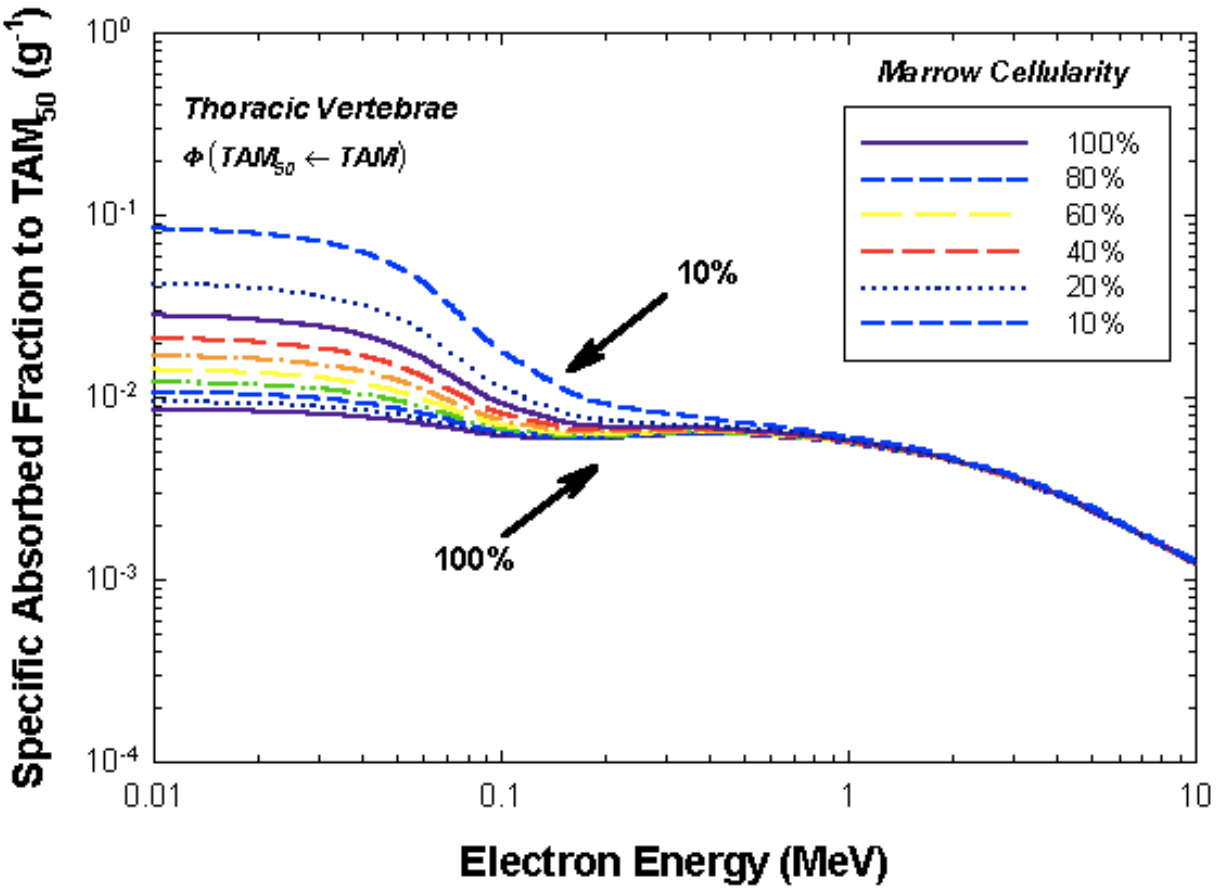

Figure B-31. Specific absorbed fraction for the TAM irradiating the TAM_{50} for the thoracic vertebrae.

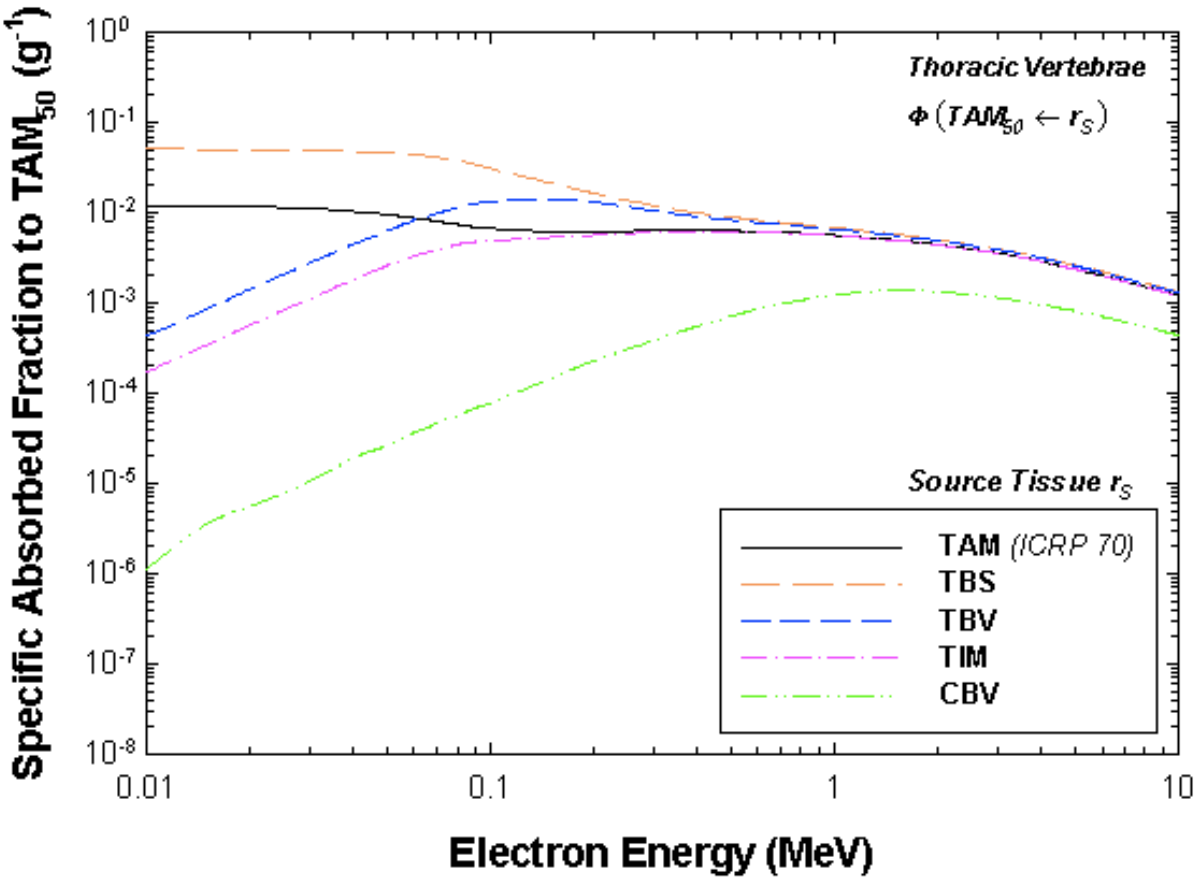

Figure B-32. Specific absorbed fraction for all sources irradiating the TAM_{50} for the thoracic vertebrae.

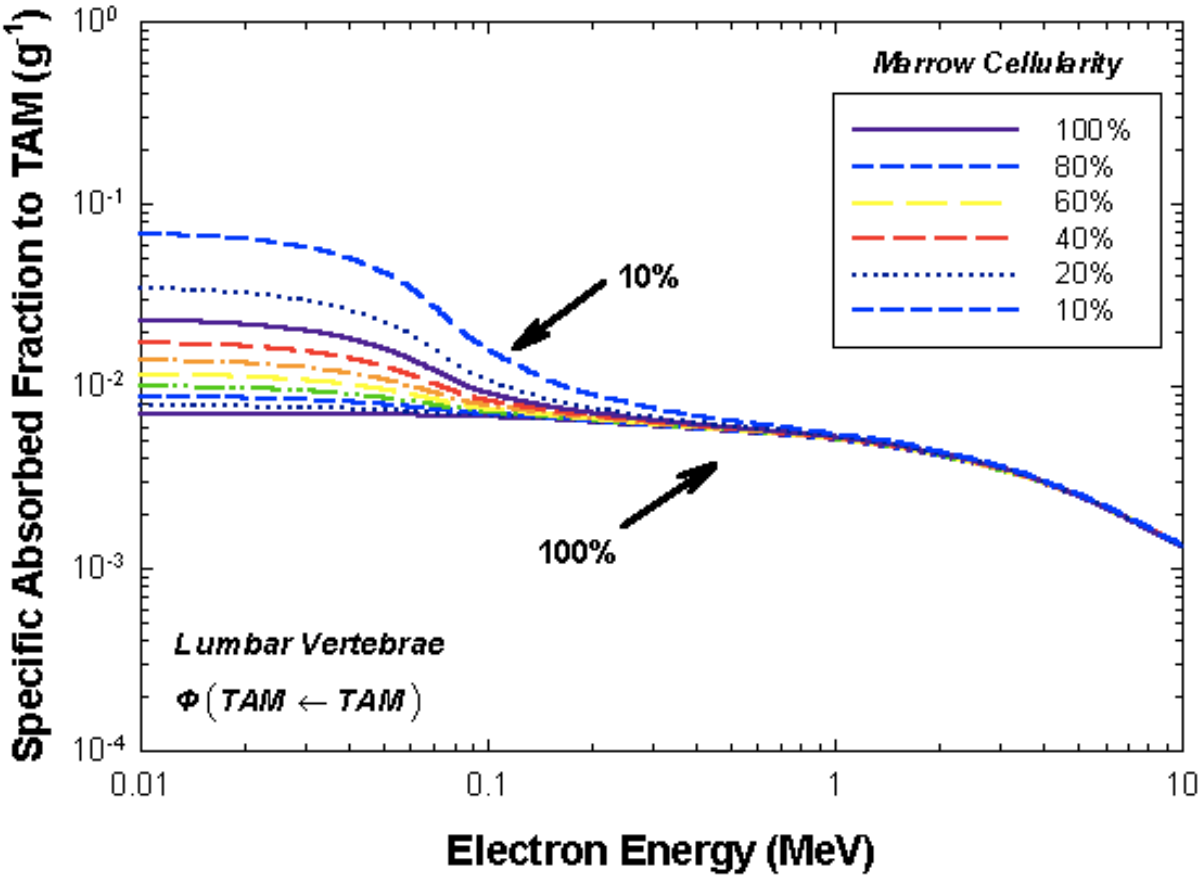

Figure B-33. Specific absorbed fraction for the TAM irradiating the TAM for the lumbar vertebrae.

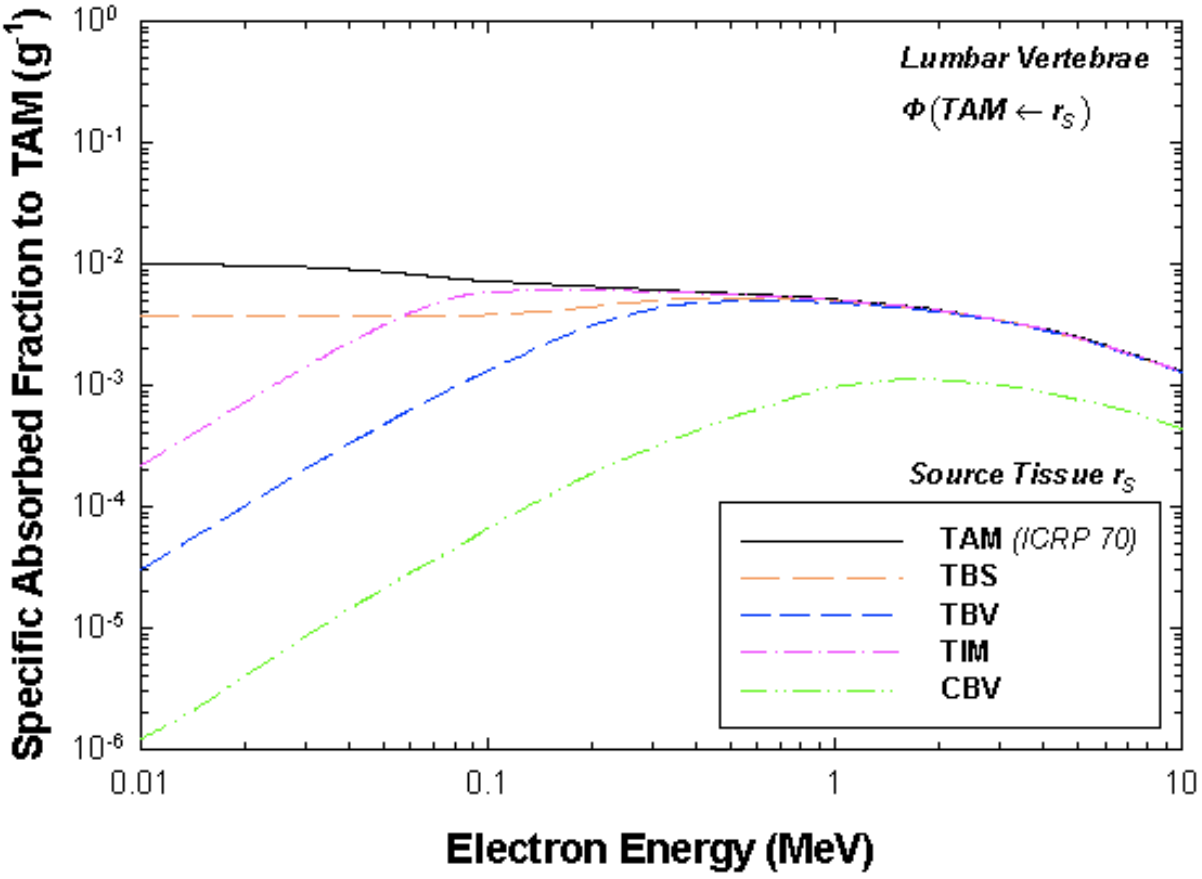

Figure B-34. Specific absorbed fraction for all sources irradiating the TAM for the lumbar vertebrae.

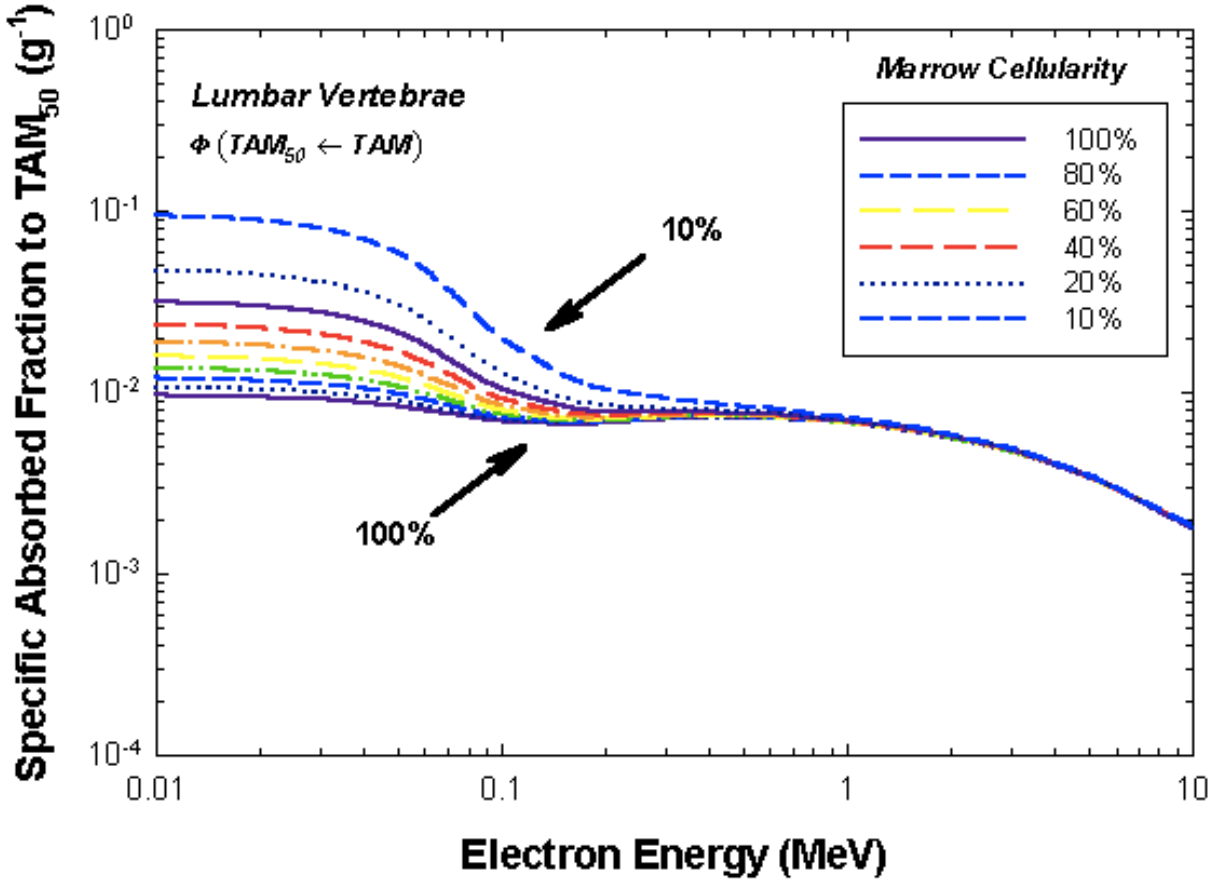

Figure B-35. Specific absorbed fraction for the TAM irradiating the TAM_{50} for the lumbar vertebrae.

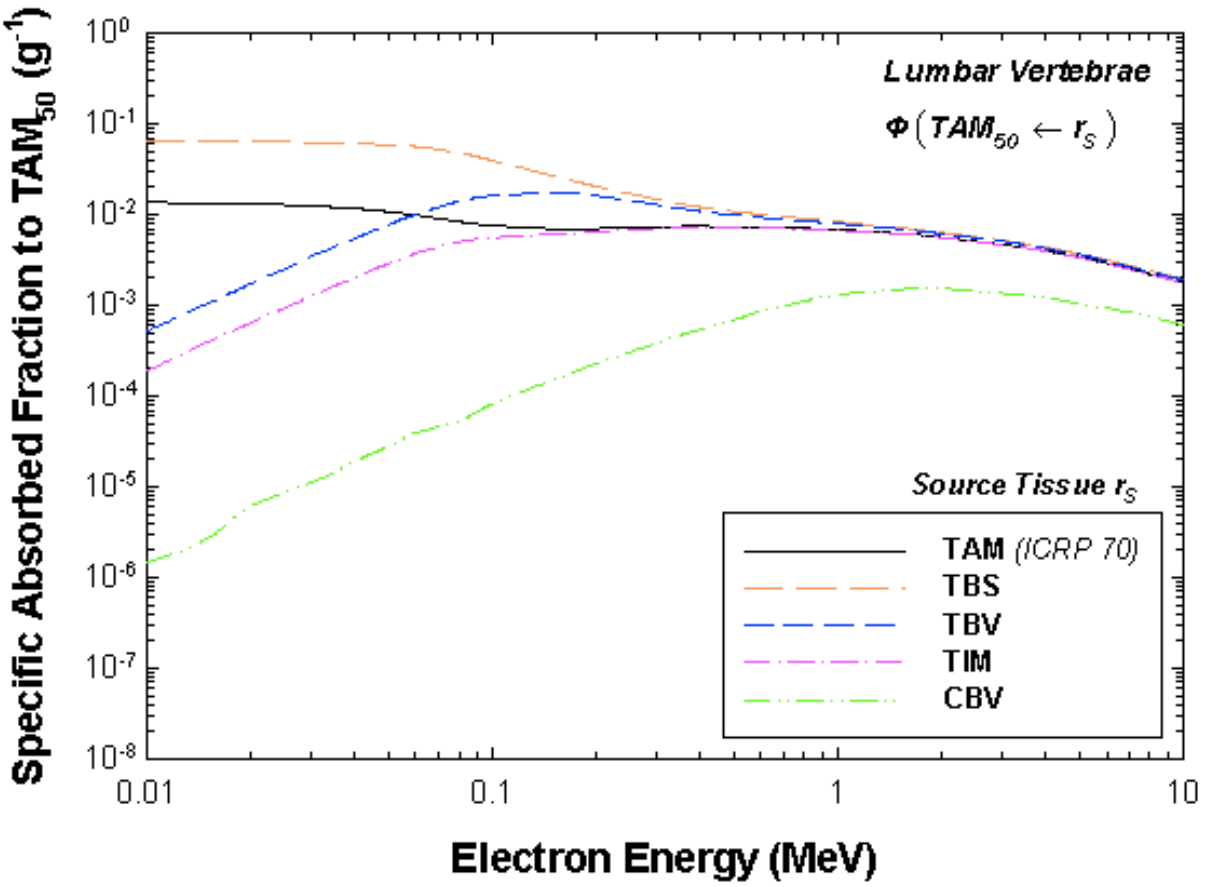

Figure B-36. Specific absorbed fraction for all sources irradiating the TAM_{50} for the lumbar vertebrae.

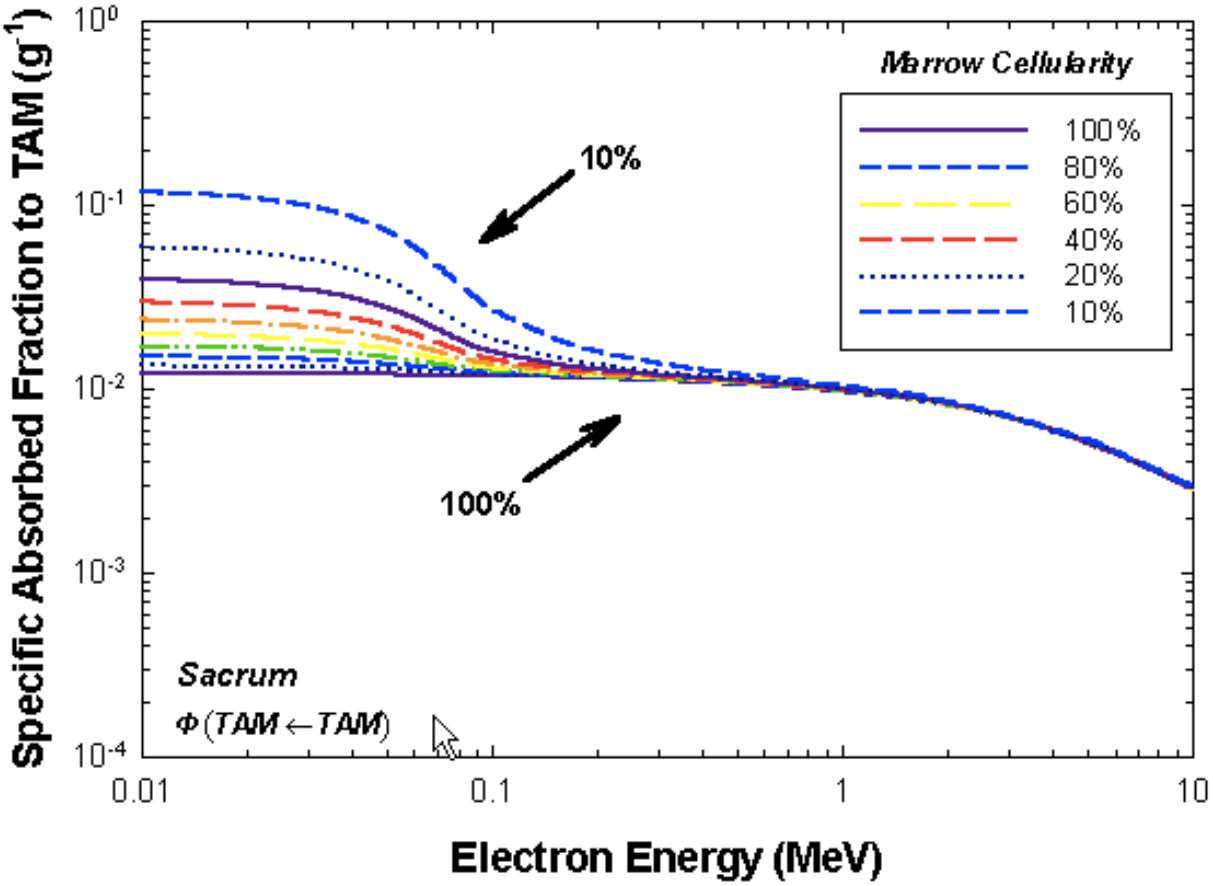

Figure B-37. Specific absorbed fraction for the TAM irradiating the TAM for the sacrum.

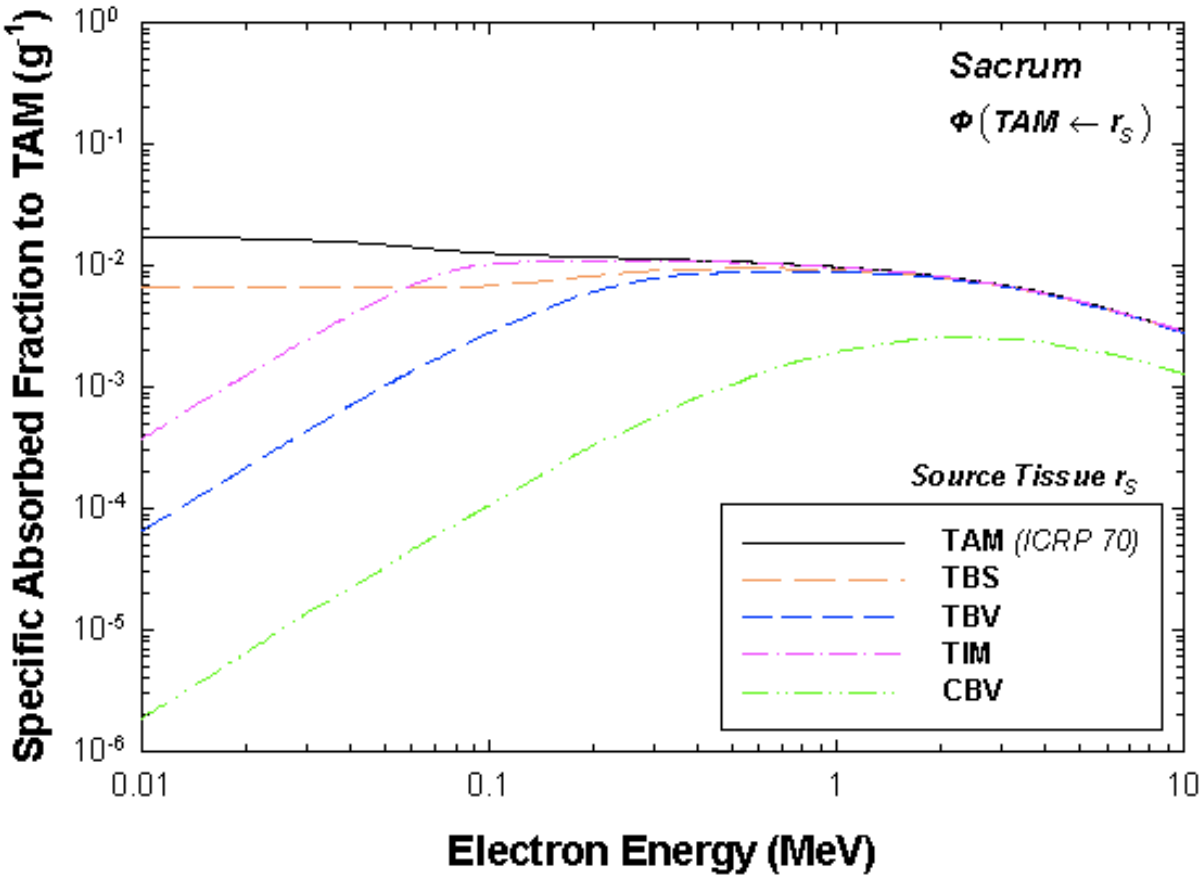

Figure B-38. Specific absorbed fraction for all sources irradiating the TAM for the sacrum.

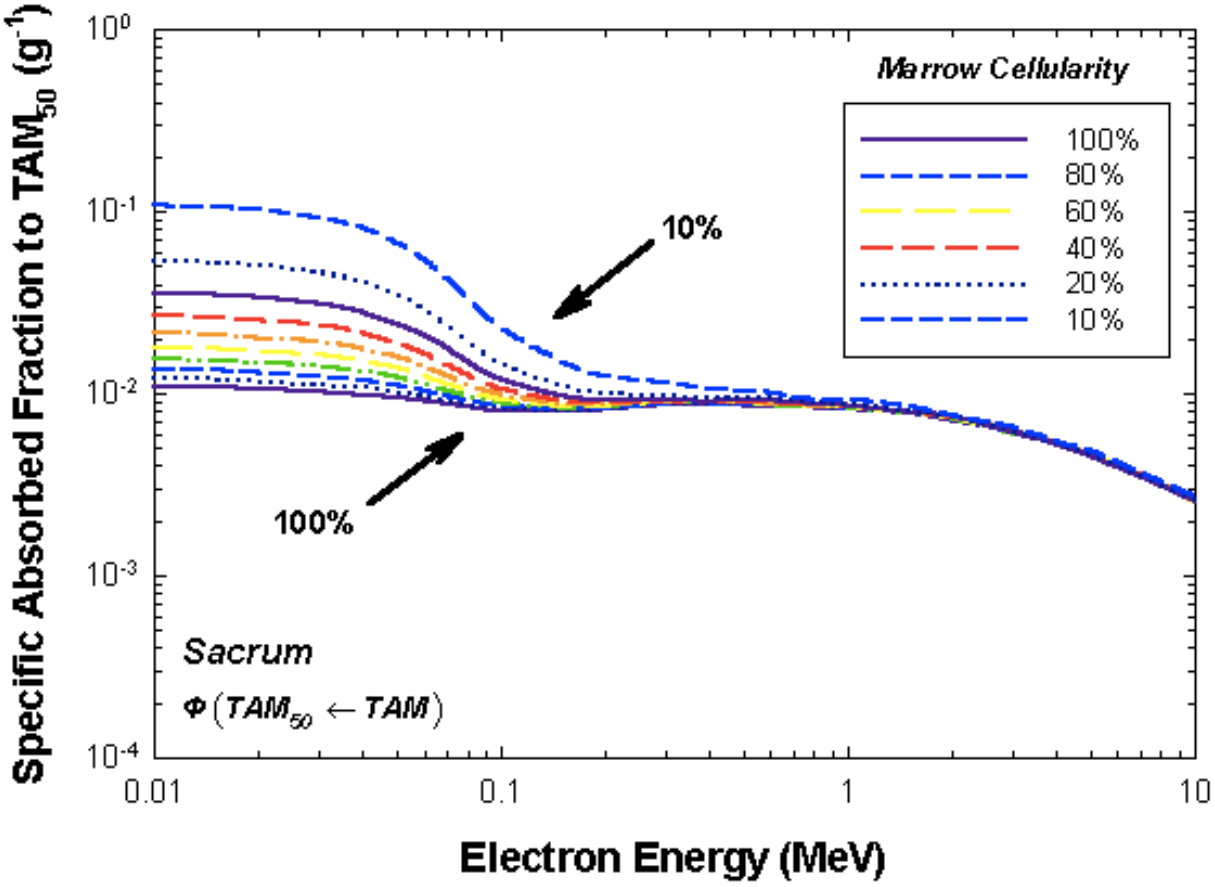

Figure B-39. Specific absorbed fraction for the TAM irradiating the TAM_{50} for the sacrum.

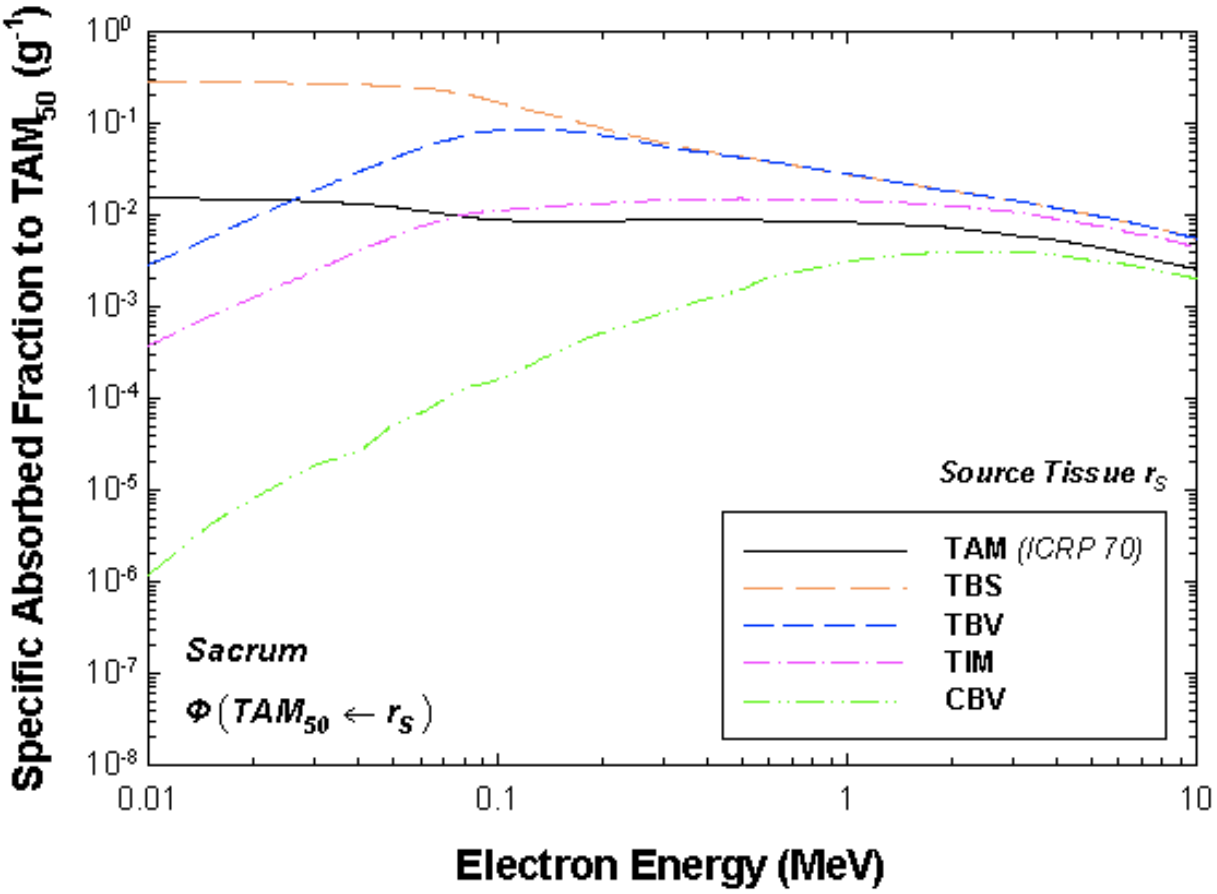

Figure B-40. Specific absorbed fraction for all sources irradiating the TAM_{50} for the sacrum.

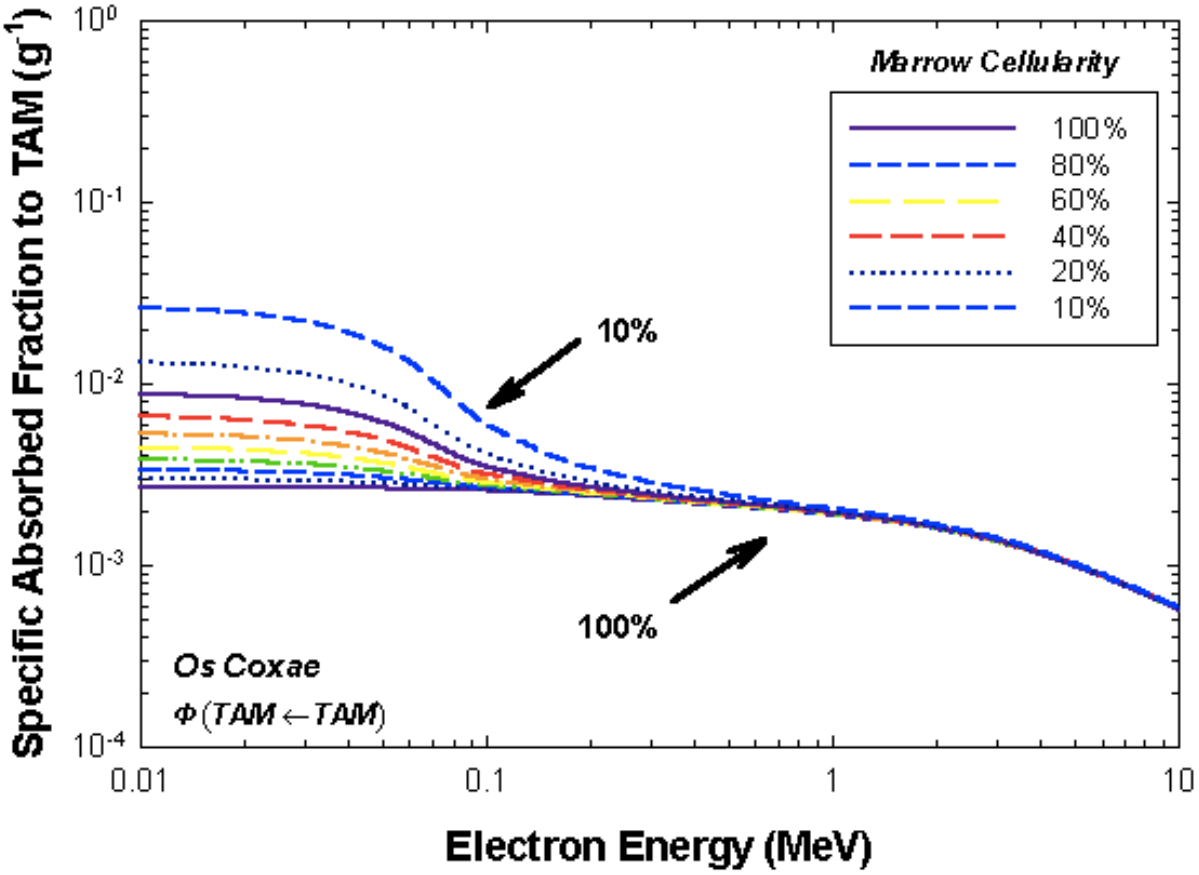

Figure B-41. Specific absorbed fraction for the TAM irradiating the TAM for the os coxae.

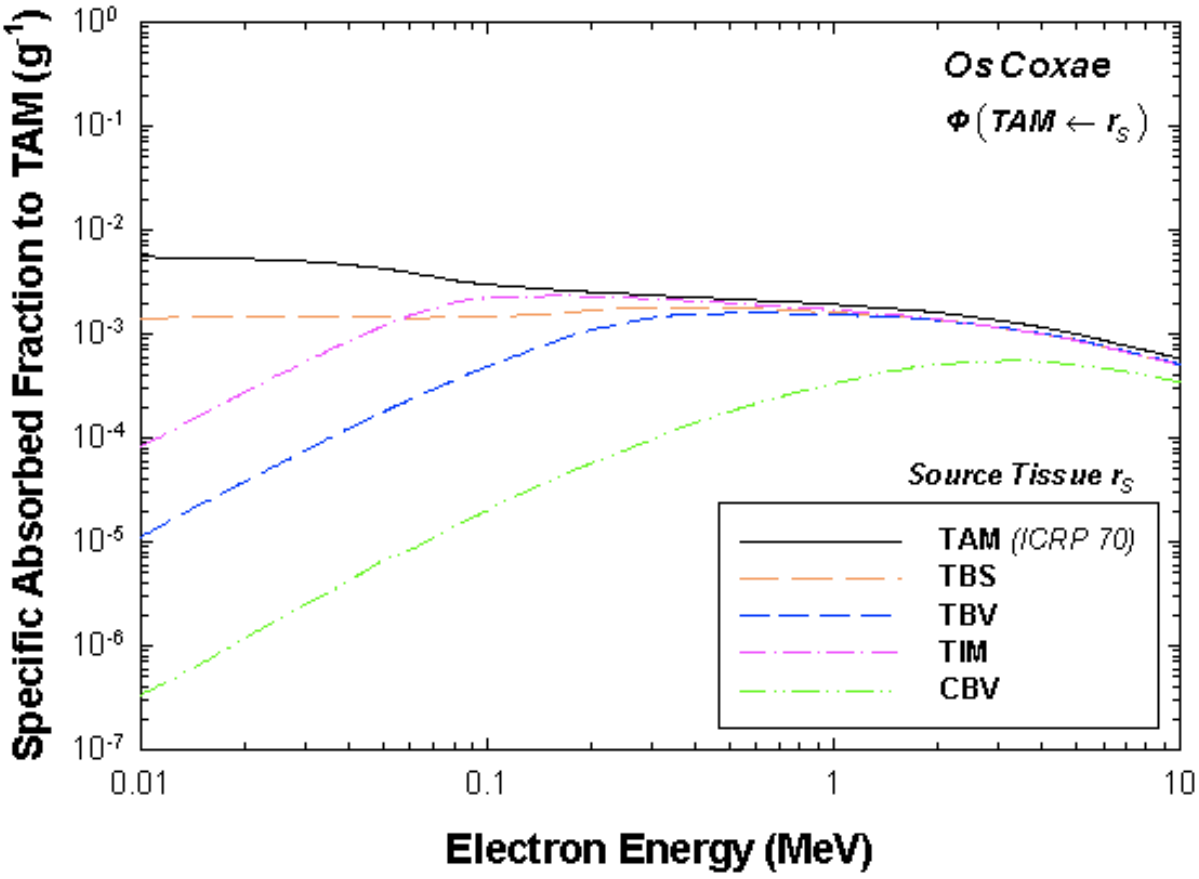

Figure B-42. Specific absorbed fraction for all sources irradiating the TAM for the os coxae.

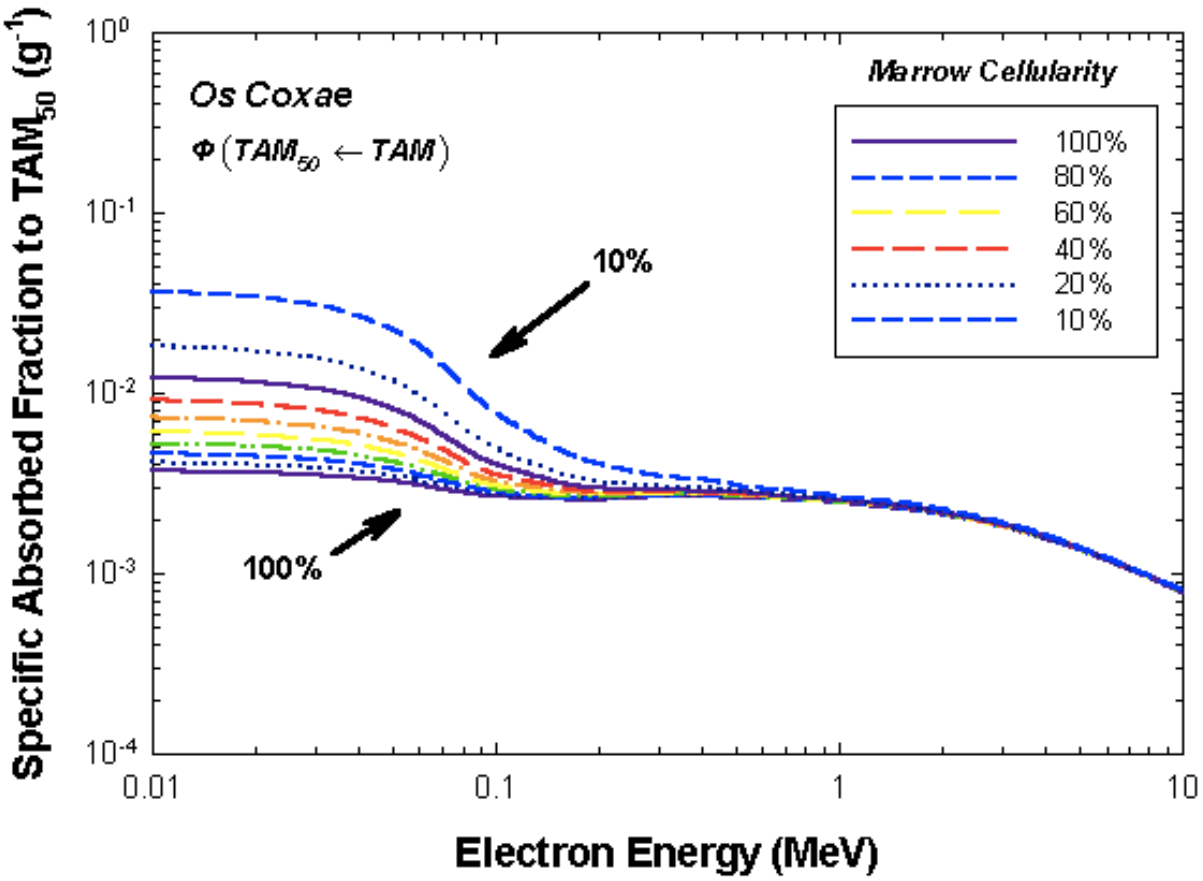

Figure B-43. Specific absorbed fraction for the TAM irradiating the TAM_{50} for the os coxae.

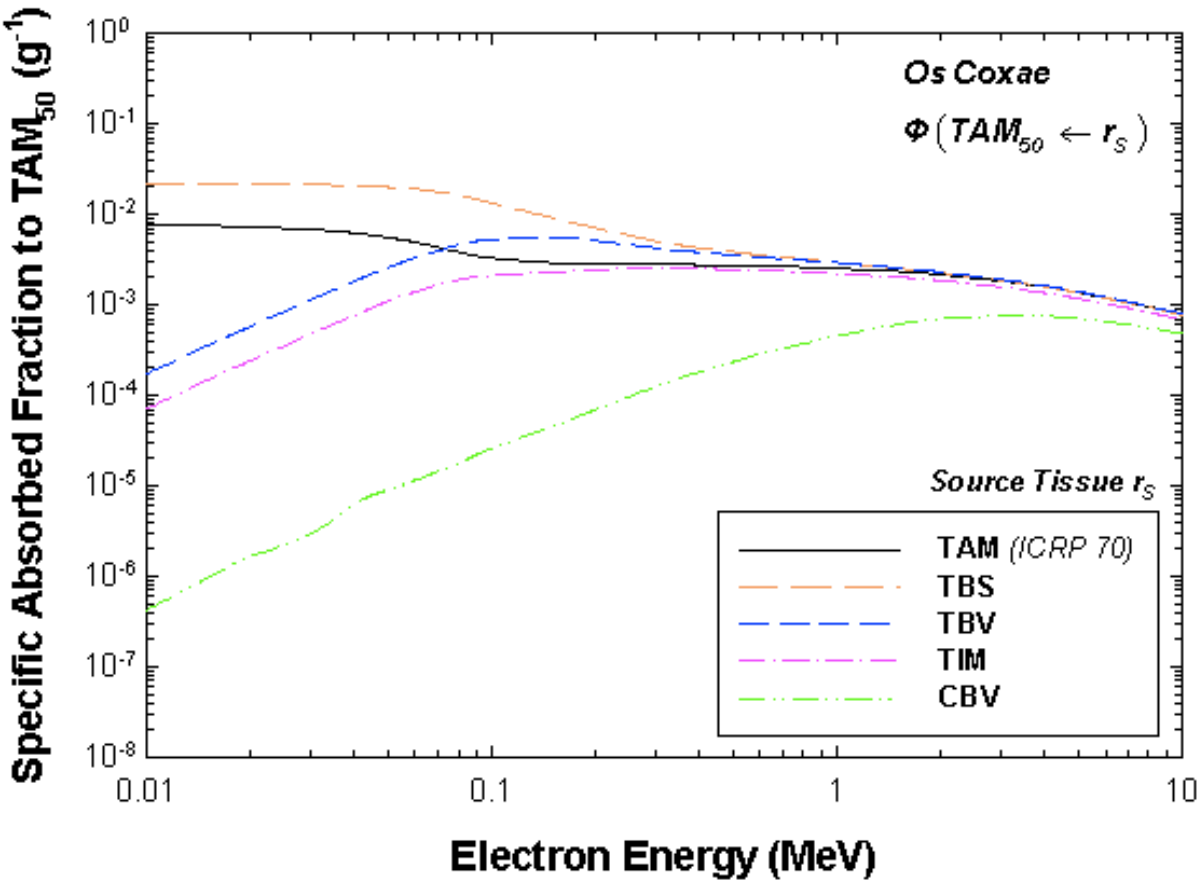

Figure B-44. Specific absorbed fraction for all sources irradiating the TAM_{50} for the os coxae.

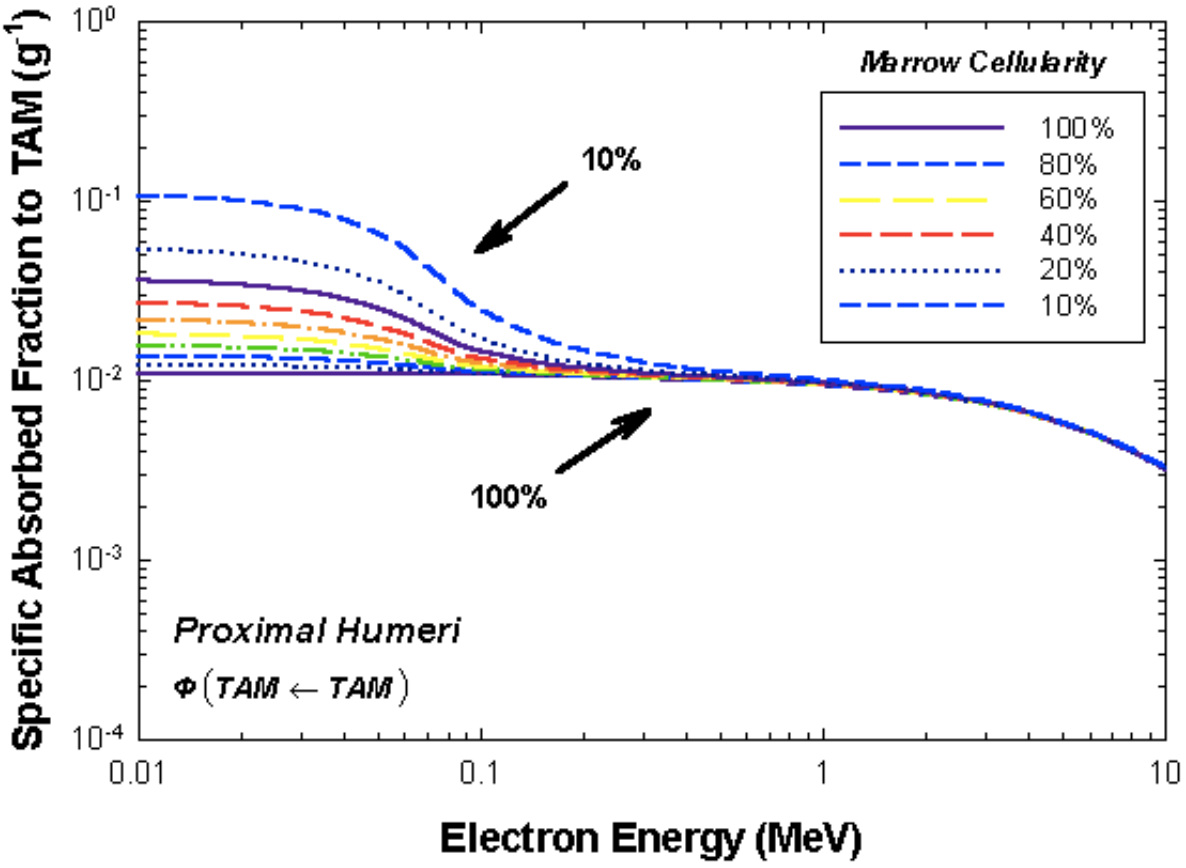

Figure B-45. Specific absorbed fraction for the TAM irradiating the TAM for the proximal humeri.

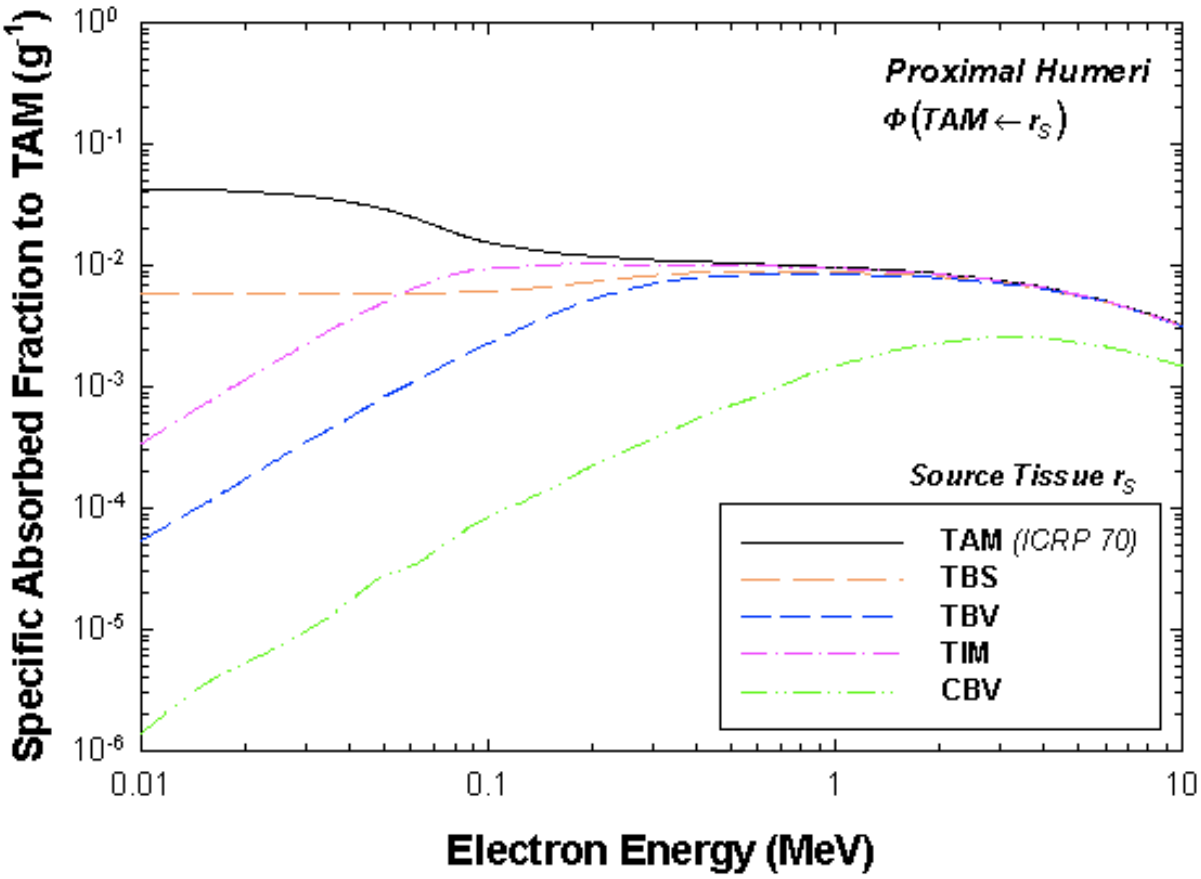

Figure B-46. Specific absorbed fraction for all sources irradiating the TAM for the proximal humeri.

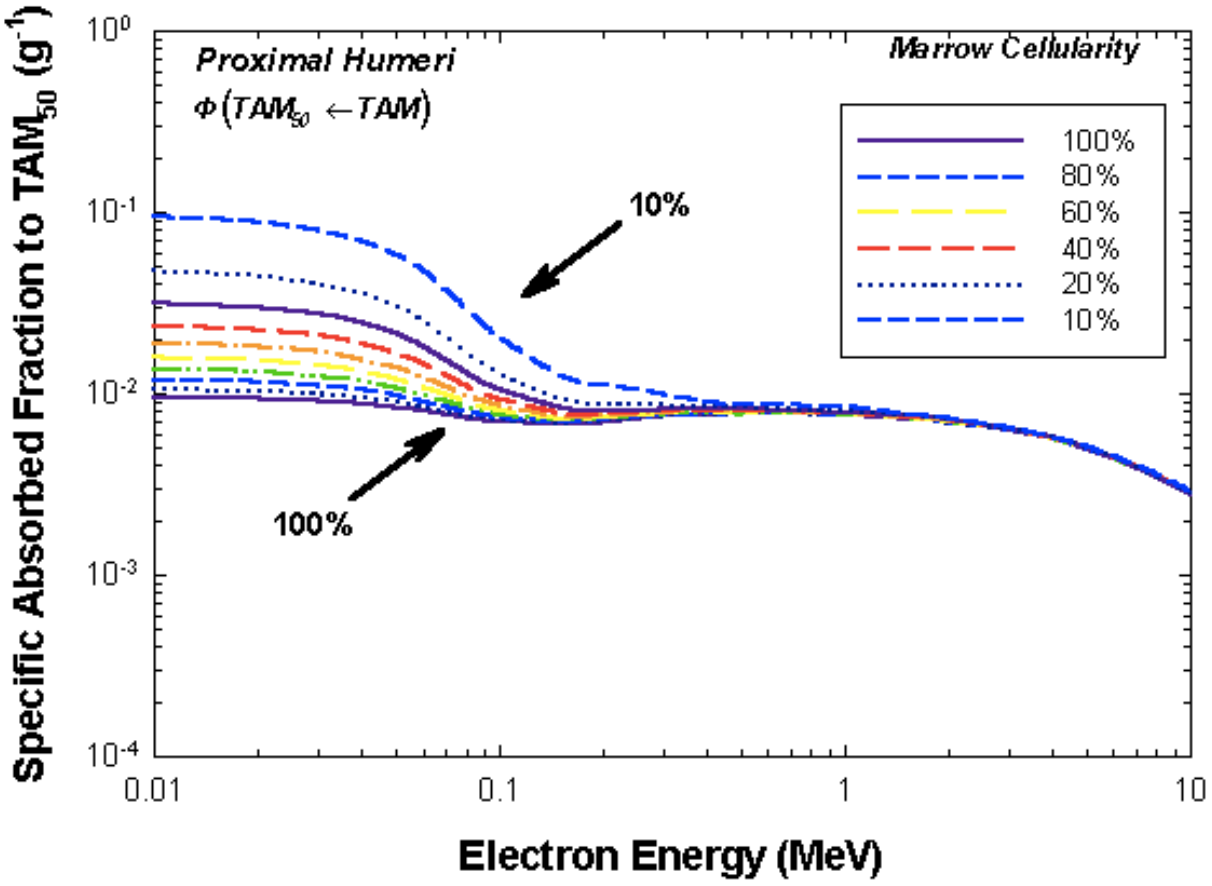

Figure B-47. Specific absorbed fraction for the TAM irradiating the TAM_{50} for the proximal humeri.

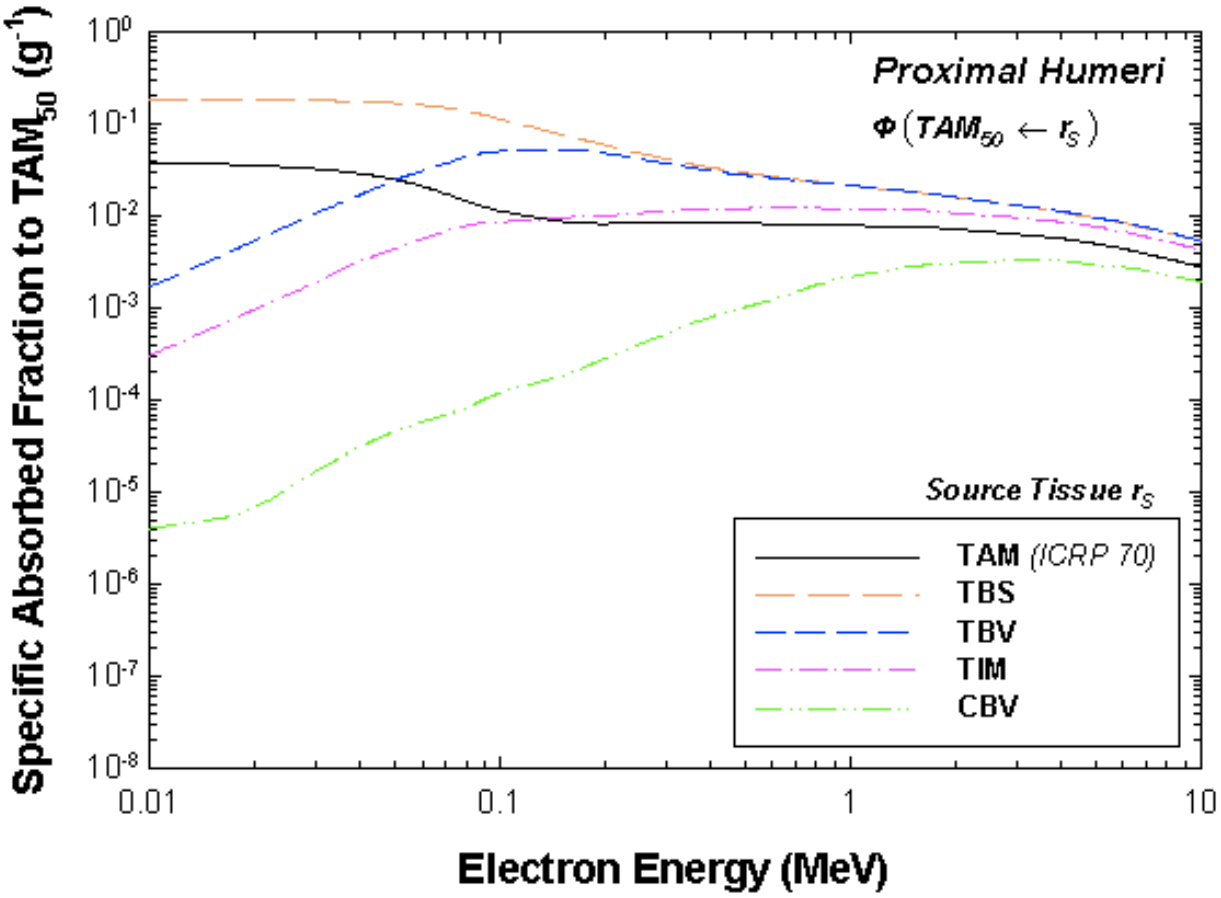

Figure B-48. Specific absorbed fraction for all sources irradiating the TAM_{50} for the proximal humeri.

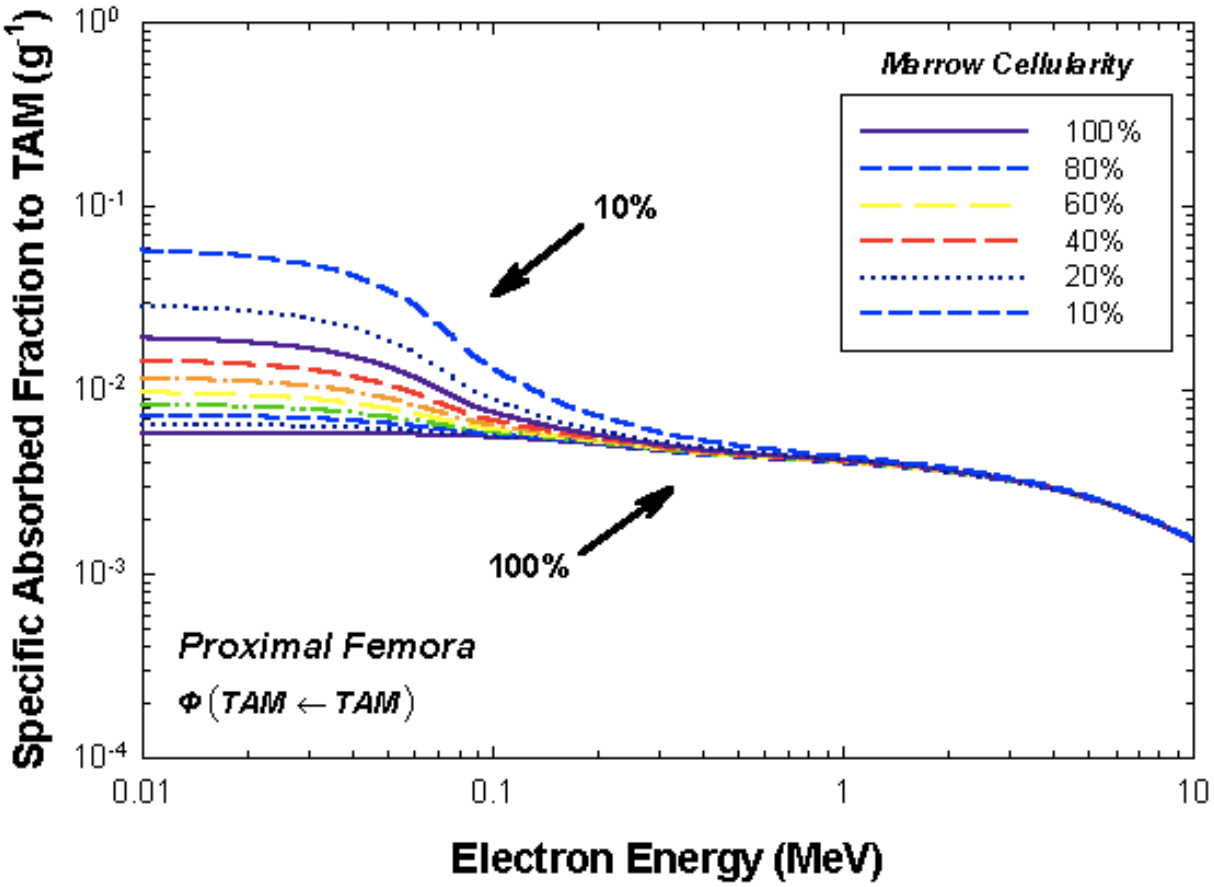

Figure B-49. Specific absorbed fraction for the TAM irradiating the TAM for the proximal femora.

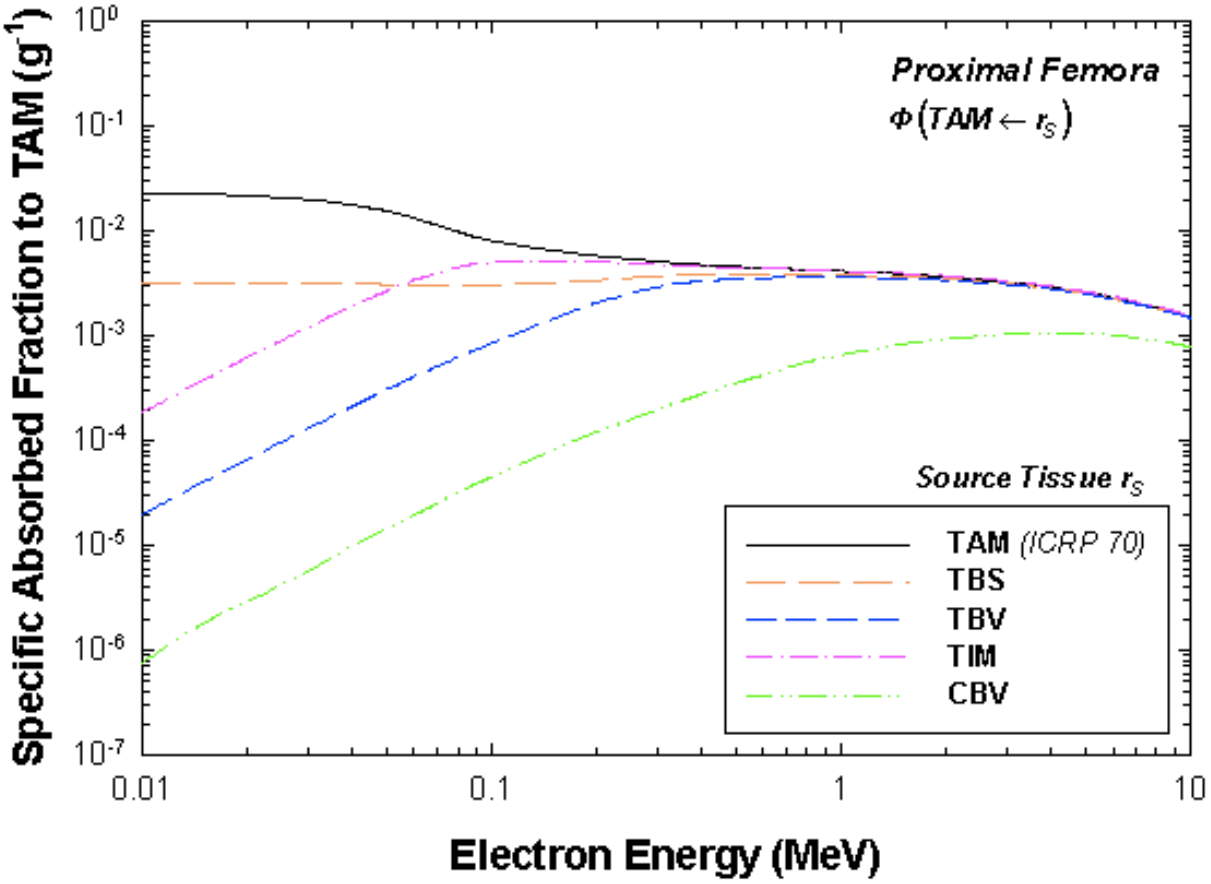

Figure B-50. Specific absorbed fraction for all sources irradiating the TAM for the proximal femora.

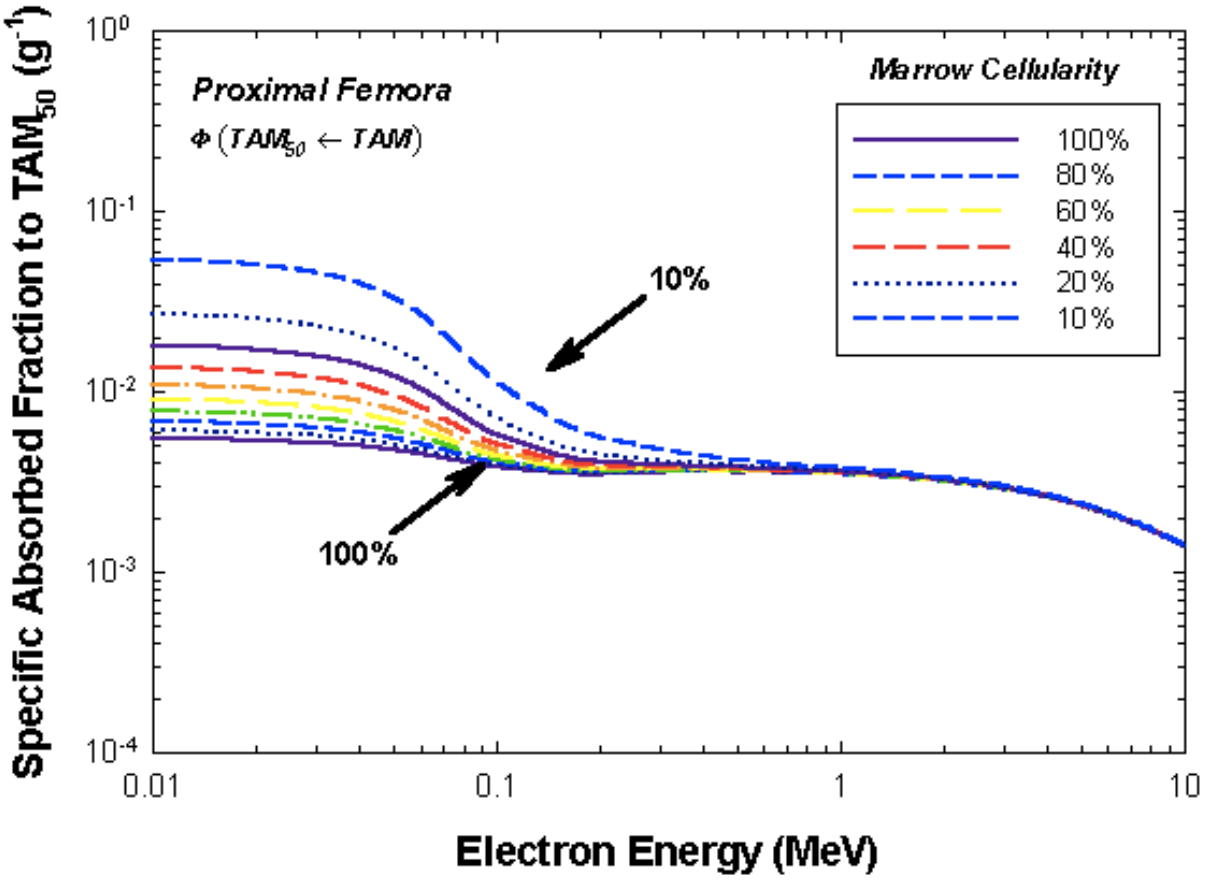

Figure B-51. Specific absorbed fraction for the TAM irradiating the TAM_{50} for the proximal femora.

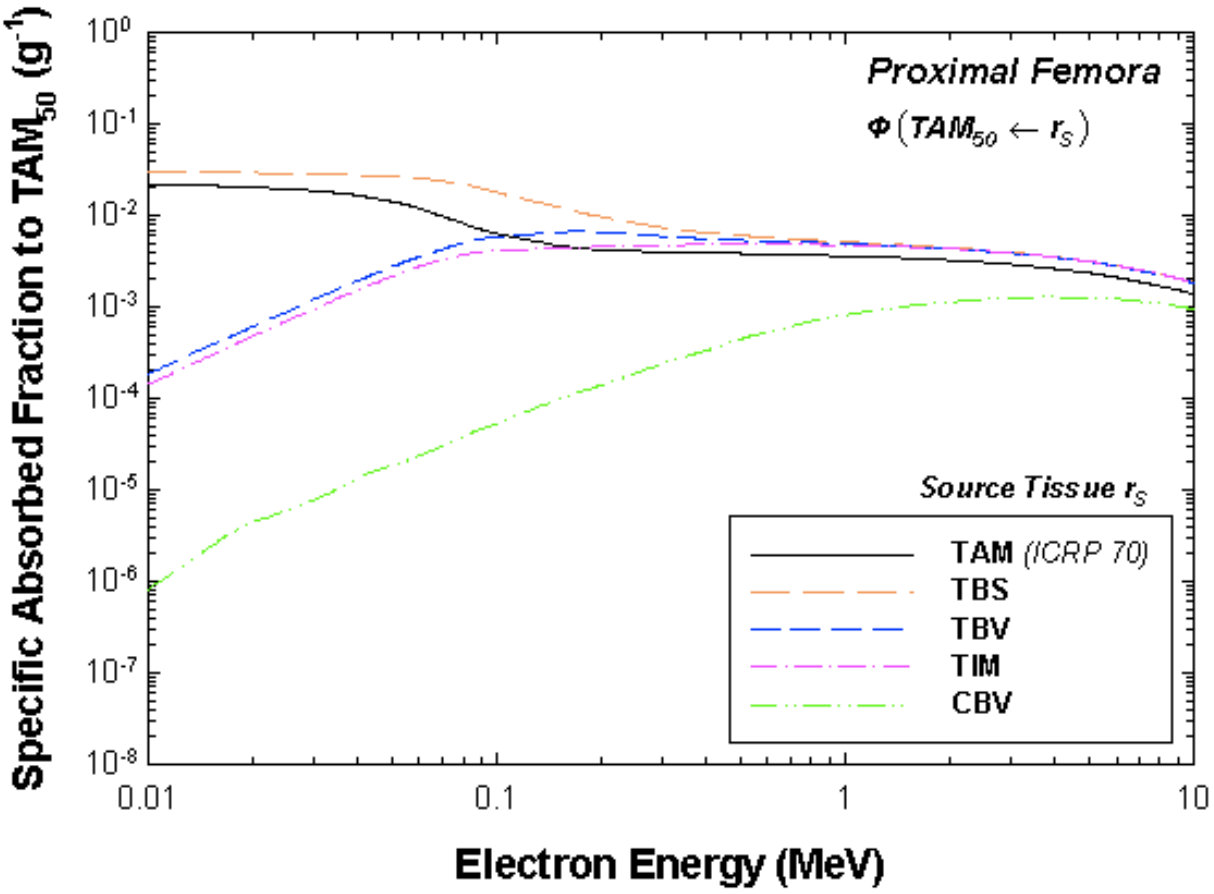

Figure B-52. Specific absorbed fraction for all sources irradiating the TAM_{50} for the proximal femora.

APPENDIX C
SPECIFIC ABSORBED FRACTIONS FOR ALL BONE SITES

Specific Absorbed Fraction (SAF) data for UFRF is given for any combination of source (TAM, TBS, TBV, TAM_{50}, TIM) and target (TAM, TAM_{50}) regions in the entire skeleton containing active marrow. ICRP reference cellularity for each bone site was used.

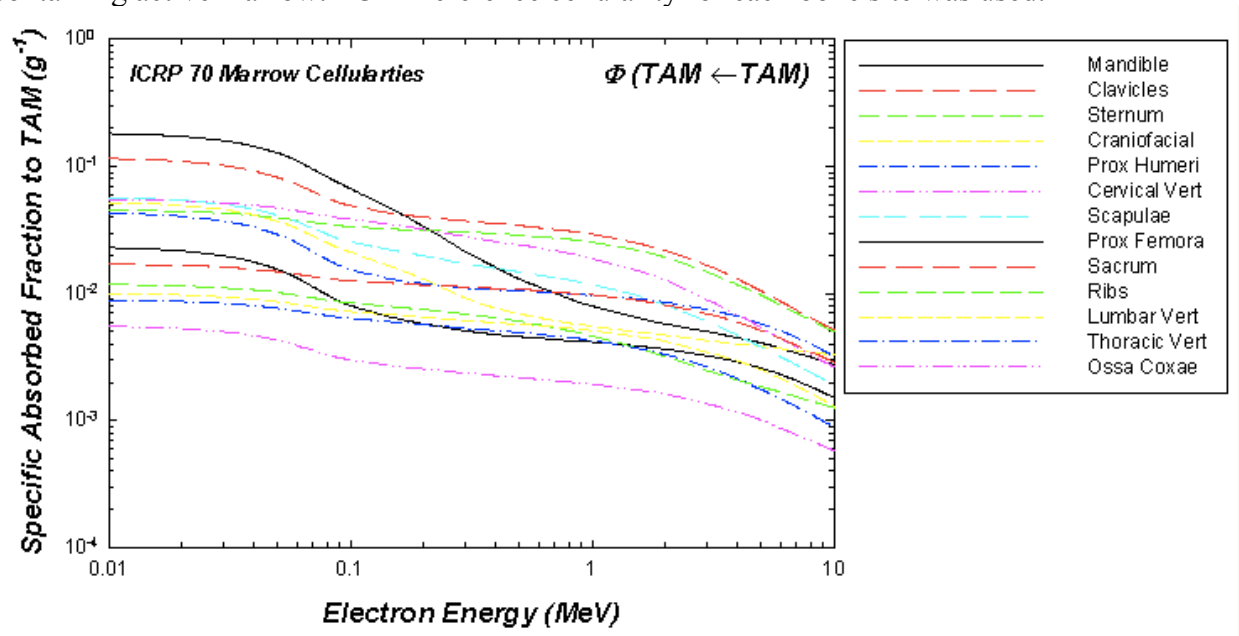

Figure C-1. Specific absorbed fraction for the TAM irradiating the TAM for all bone sites.

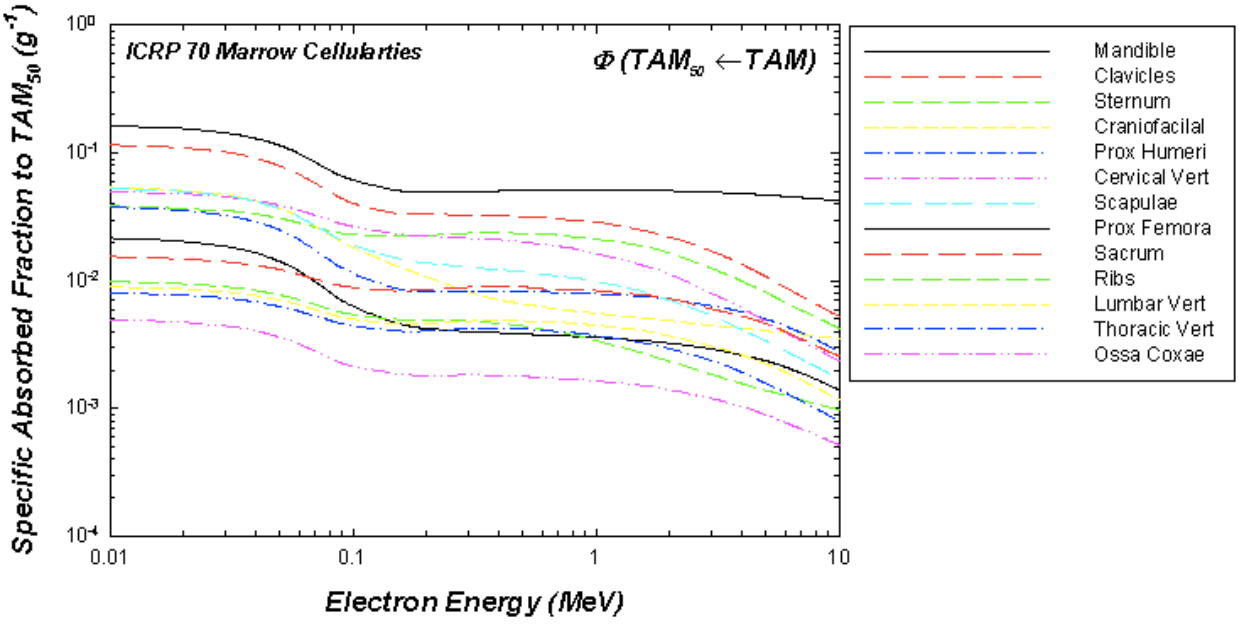

Figure C-2. Specific absorbed fraction for the TAM irradiating the TAM_{50} for all bone sites.

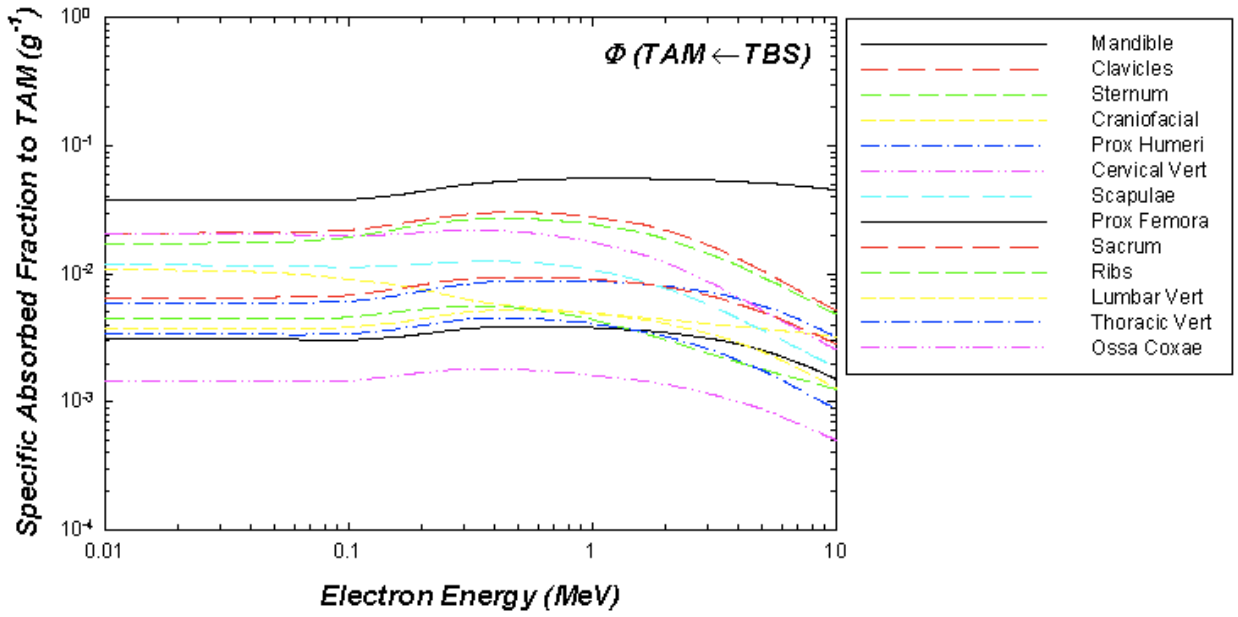

Figure C-3. Specific absorbed fraction for the TBS irradiating the TAM for all bone sites.

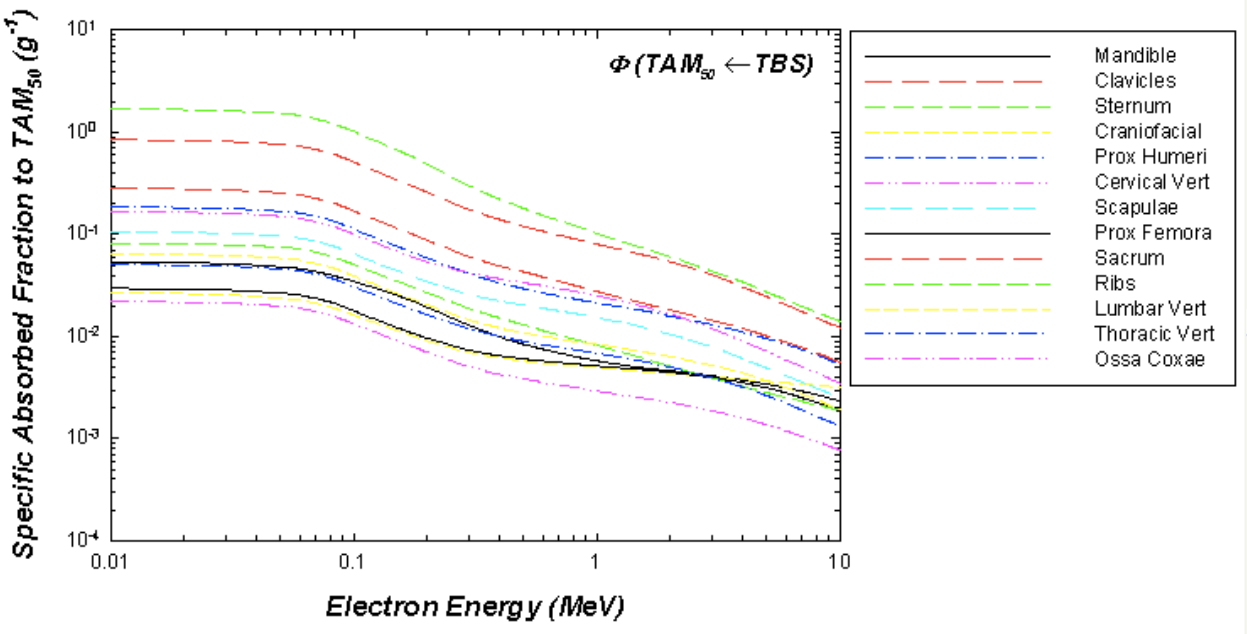

Figure C-4. Specific absorbed fraction for the TBS irradiating the TAM_{50} for all bone sites.

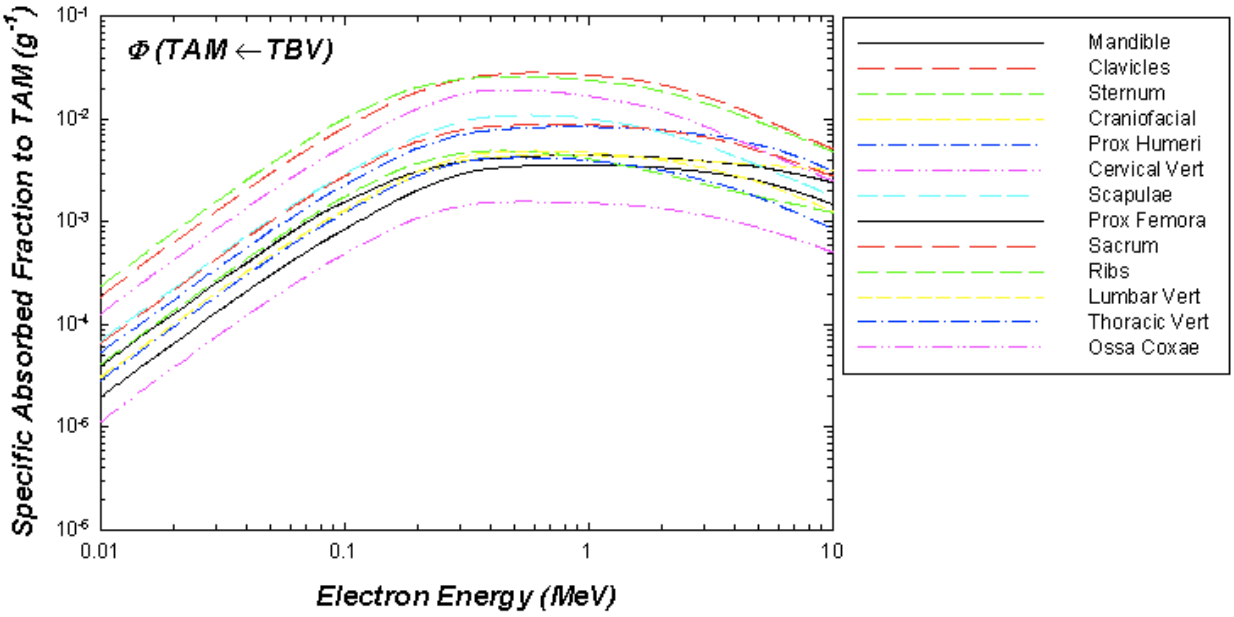

Figure C-5. Specific absorbed fraction for the TBV irradiating the TAM for all bone sites.

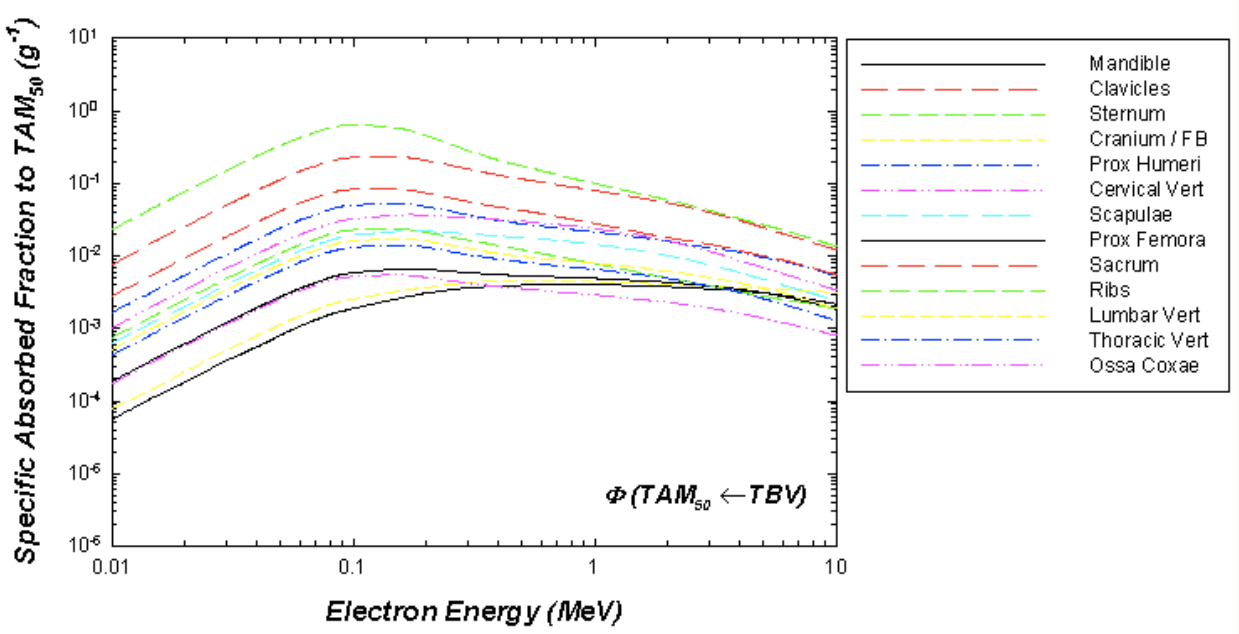

Figure C-6. Specific absorbed fraction for the TBV irradiating the TAM_{50} for all bone sites.

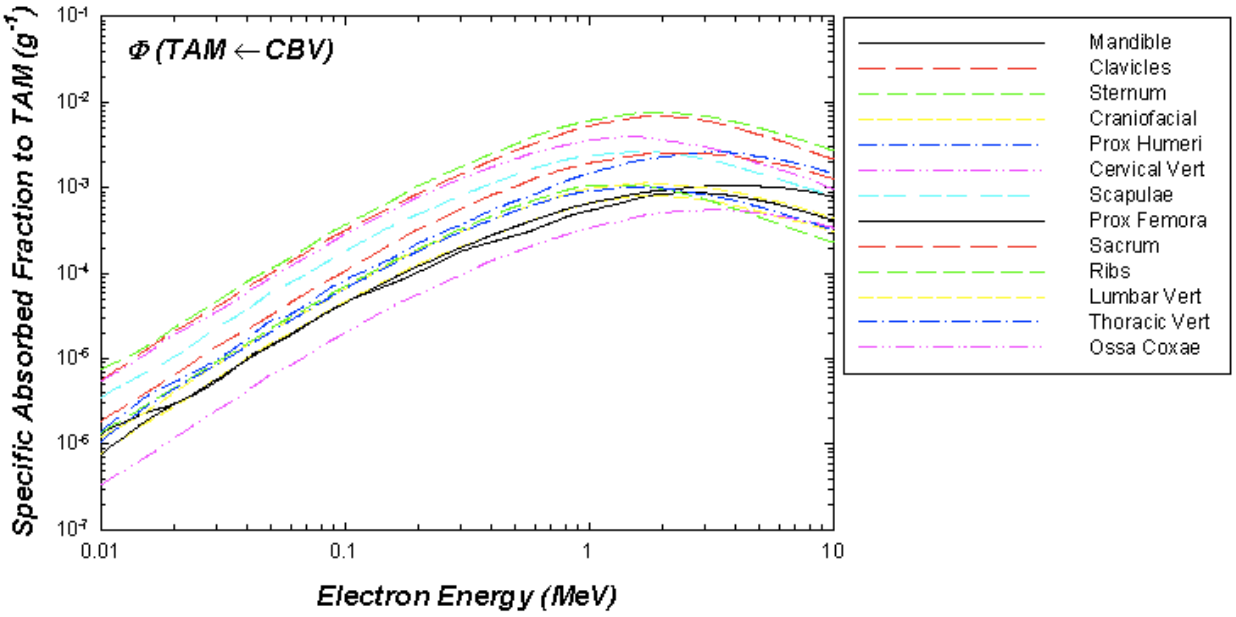

Figure C-7. Specific absorbed fraction for the CBV irradiating the TAM for all bone sites.

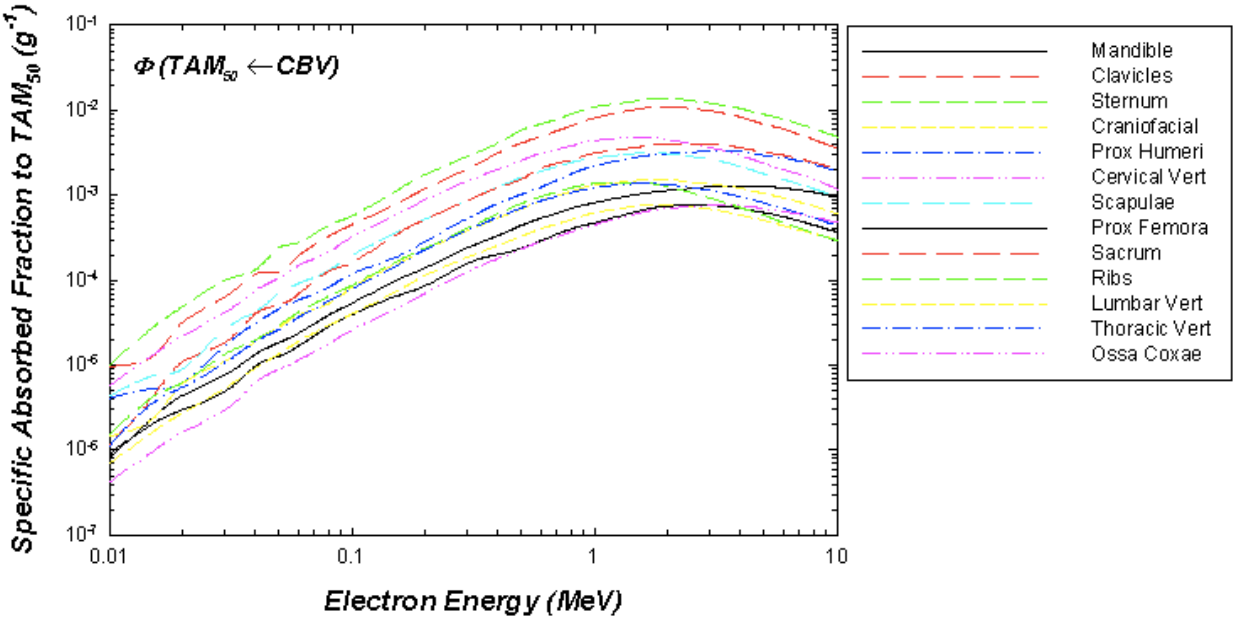

Figure C-8. Specific absorbed fraction for the CBV irradiating the TAM_{50} for all bone sites.

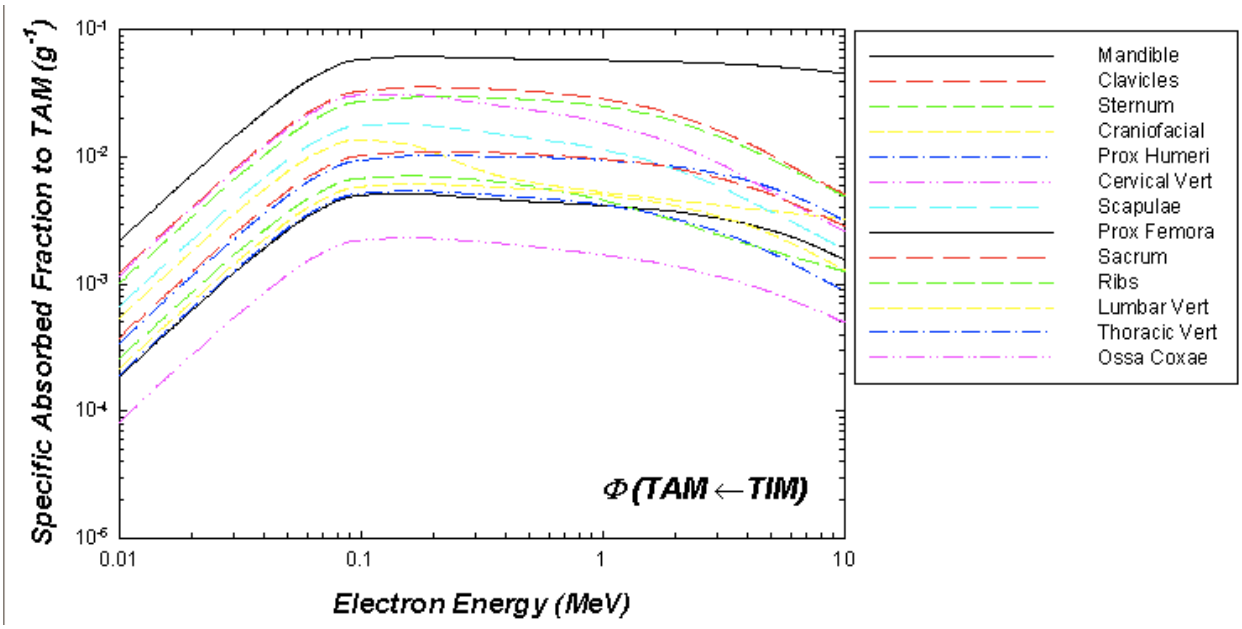

Figure C-9. Specific absorbed fraction for the TIM irradiating the TAM for all bone sites.

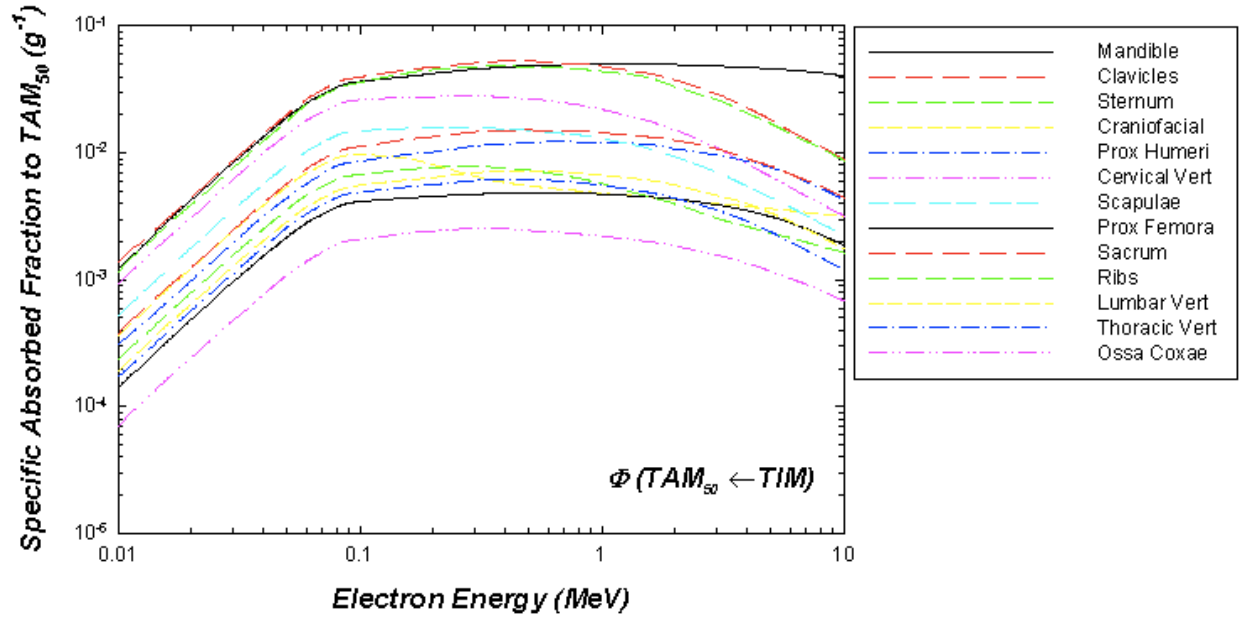

Figure C-10. Specific absorbed fraction for the TIM irradiating the TAM_{50} for all bone sites.

APPENDIX D
SPECIFIC ABSORBED FRACTIONS FOR LONG BONES

This appendix provides Specific Absorbed Fraction (SAF) data in bone sites not containing active marrow for combinations of sources (CBV, CIM, CBS_{MC}) and target (CIM_{50}) regions. For the shafts of the long bones of the adult, cellularity is 0%. Absorbed fractions are divided by the mass of the shaft of the long bones to report SAF.

Table D-1. Specific absorbed fractions in the shafts of the leg bones.

Distal Femora			
ϕ ($TAM_{50} \leftarrow r_S$)			
Source Tissue r_S			
Energy (MeV)	CBV	CIM	CBS_{MC}
0.010	4.76E-04	6.50E-03	7.29E-03
0.015	7.15E-04	6.47E-03	7.24E-03
0.020	9.53E-04	6.44E-03	7.17E-03
0.030	1.43E-03	6.34E-03	6.99E-03
0.040	1.91E-03	6.23E-03	6.79E-03
0.050	2.38E-03	6.12E-03	6.57E-03
0.060	2.86E-03	6.00E-03	6.35E-03
0.080	3.81E-03	5.79E-03	5.98E-03
0.10	4.76E-03	5.64E-03	5.76E-03
0.15	7.15E-03	5.34E-03	5.40E-03
0.20	9.53E-03	5.08E-03	5.12E-03
0.30	1.43E-02	4.67E-03	4.70E-03
0.40	1.91E-02	4.45E-03	4.47E-03
0.50	2.38E-02	4.33E-03	4.34E-03
0.60	2.86E-02	4.25E-03	4.27E-03
0.80	3.81E-02	4.12E-03	4.13E-03
1.0	4.76E-02	4.01E-03	4.03E-03
1.5	7.15E-02	3.78E-03	3.79E-03
2.0	9.53E-02	3.56E-03	3.57E-03
3.0	1.43E-01	3.18E-03	3.19E-03
4.0	1.91E-01	2.84E-03	2.85E-03
5.0	2.38E-01	2.56E-03	2.56E-03
6.0	2.86E-01	2.29E-03	2.29E-03
8.0	3.81E-01	1.85E-03	1.85E-03
10.0	4.76E-01	1.51E-03	1.51E-03

Fibulae			
ϕ ($TAM_{50} \leftarrow r_S$)			
Source Tissue r_S			
Energy (MeV)	CBV	CIM	CBS_{MC}
0.010	1.20E-03	1.43E-04	1.71E-05
0.015	1.80E-03	2.15E-04	2.57E-05
0.020	2.39E-03	2.87E-04	3.43E-05
0.030	3.59E-03	4.30E-04	5.14E-05
0.040	4.79E-03	5.73E-04	6.86E-05
0.050	5.98E-03	7.16E-04	8.57E-05
0.060	7.18E-03	8.60E-04	1.03E-04
0.080	9.58E-03	1.15E-03	1.37E-04
0.10	1.20E-02	1.43E-03	1.71E-04
0.15	1.80E-02	2.15E-03	2.57E-04
0.20	2.39E-02	2.87E-03	3.43E-04
0.30	3.59E-02	4.30E-03	5.14E-04
0.40	4.79E-02	5.73E-03	6.86E-04
0.50	5.98E-02	7.16E-03	8.57E-04
0.60	7.18E-02	8.60E-03	1.03E-03
0.80	9.58E-02	1.15E-02	1.37E-03
1.0	1.20E-01	1.43E-02	1.71E-03
1.5	1.80E-01	2.15E-02	2.57E-03
2.0	2.39E-01	2.87E-02	3.43E-03
3.0	3.59E-01	4.30E-02	5.14E-03
4.0	4.79E-01	5.73E-02	6.86E-03
5.0	5.98E-01	7.16E-02	8.57E-03
6.0	7.18E-01	8.60E-02	1.03E-02
8.0	9.58E-01	1.15E-01	1.37E-02
10.0	1.20E+00	1.43E-01	1.71E-02

Tibiae			
ϕ ($TAM_{50} \leftarrow r_S$)			
Source Tissue r_S			
Energy (MeV)	CBV	CIM	CBS_{MC}
0.010	1.11E-03	1.24E-04	1.38E-05
0.015	1.67E-03	1.86E-04	2.08E-05
0.020	2.23E-03	2.48E-04	2.77E-05
0.030	3.34E-03	3.73E-04	4.15E-05
0.040	4.46E-03	4.97E-04	5.54E-05
0.050	5.57E-03	6.21E-04	6.92E-05
0.060	6.69E-03	7.45E-04	8.31E-05
0.080	8.92E-03	9.94E-04	1.11E-04
0.10	1.11E-02	1.24E-03	1.38E-04
0.15	1.67E-02	1.86E-03	2.08E-04
0.20	2.23E-02	2.48E-03	2.77E-04
0.30	3.34E-02	3.73E-03	4.15E-04
0.40	4.46E-02	4.97E-03	5.54E-04
0.50	5.57E-02	6.21E-03	6.92E-04
0.60	6.69E-02	7.45E-03	8.31E-04
0.80	8.92E-02	9.94E-03	1.11E-03
1.0	1.11E-01	1.24E-02	1.38E-03
1.5	1.67E-01	1.86E-02	2.08E-03
2.0	2.23E-01	2.48E-02	2.77E-03
3.0	3.34E-01	3.73E-02	4.15E-03
4.0	4.46E-01	4.97E-02	5.54E-03
5.0	5.57E-01	6.21E-02	6.92E-03
6.0	6.69E-01	7.45E-02	8.31E-03
8.0	8.92E-01	9.94E-02	1.11E-02
10.0	1.11E+00	1.24E-01	1.38E-02

Table D-2. Specific absorbed fractions in the shafts of the arm bones.

Distal Humeri			
$\phi\ (TAM_{50} \leftarrow r_S)$			
Source Tissue r_s			
Energy (MeV)	CBV	CIM	CBS_{MC}
0.010	7.63E-04	5.83E-05	4.45E-06
0.015	1.15E-03	8.74E-05	6.68E-06
0.020	1.53E-03	1.17E-04	8.90E-06
0.030	2.29E-03	1.75E-04	1.34E-05
0.040	3.05E-03	2.33E-04	1.78E-05
0.050	3.82E-03	2.91E-04	2.23E-05
0.060	4.58E-03	3.50E-04	2.67E-05
0.080	6.11E-03	4.66E-04	3.56E-05
0.10	7.63E-03	5.83E-04	4.45E-05
0.15	1.15E-02	8.74E-04	6.68E-05
0.20	1.53E-02	1.17E-03	8.90E-05
0.30	2.29E-02	1.75E-03	1.34E-04
0.40	3.05E-02	2.33E-03	1.78E-04
0.50	3.82E-02	2.91E-03	2.23E-04
0.60	4.58E-02	3.50E-03	2.67E-04
0.80	6.11E-02	4.66E-03	3.56E-04
1.0	7.63E-02	5.83E-03	4.45E-04
1.5	1.15E-01	8.74E-03	6.68E-04
2.0	1.53E-01	1.17E-02	8.90E-04
3.0	2.29E-01	1.75E-02	1.34E-03
4.0	3.05E-01	2.33E-02	1.78E-03
5.0	3.82E-01	2.91E-02	2.23E-03
6.0	4.58E-01	3.50E-02	2.67E-03
8.0	6.11E-01	4.66E-02	3.56E-03
10.0	7.63E-01	5.83E-02	4.45E-03

Radii			
$\phi\ (TAM_{50} \leftarrow r_S)$			
Source Tissue r_s			
Energy (MeV)	CBV	CIM	CBS_{MC}
0.010	5.13E-03	2.63E-03	1.35E-03
0.015	7.69E-03	3.94E-03	2.02E-03
0.020	1.03E-02	5.26E-03	2.70E-03
0.030	1.54E-02	7.89E-03	4.04E-03
0.040	2.05E-02	1.05E-02	5.39E-03
0.050	2.56E-02	1.31E-02	6.74E-03
0.060	3.08E-02	1.58E-02	8.09E-03
0.080	4.10E-02	2.10E-02	1.08E-02
0.10	5.13E-02	2.63E-02	1.35E-02
0.15	7.69E-02	3.94E-02	2.02E-02
0.20	1.03E-01	5.26E-02	2.70E-02
0.30	1.54E-01	7.89E-02	4.04E-02
0.40	2.05E-01	1.05E-01	5.39E-02
0.50	2.56E-01	1.31E-01	6.74E-02
0.60	3.08E-01	1.58E-01	8.09E-02
0.80	4.10E-01	2.10E-01	1.08E-01
1.0	5.13E-01	2.63E-01	1.35E-01
1.5	7.69E-01	3.94E-01	2.02E-01
2.0	1.03E+00	5.26E-01	2.70E-01
3.0	1.54E+00	7.89E-01	4.04E-01
4.0	2.05E+00	1.05E+00	5.39E-01
5.0	2.56E+00	1.31E+00	6.74E-01
6.0	3.08E+00	1.58E+00	8.09E-01
8.0	4.10E+00	2.10E+00	1.08E+00
10.0	5.13E+00	2.63E+00	1.35E+00

Ulnae			
$\phi\ (TAM_{50} \leftarrow r_S)$			
Source Tissue r_s			
Energy (MeV)	CBV	CIM	CBS_{MC}
0.010	3.48E-03	1.21E-03	4.20E-04
0.015	5.22E-03	1.81E-03	6.30E-04
0.020	6.95E-03	2.42E-03	8.40E-04
0.030	1.04E-02	3.63E-03	1.26E-03
0.040	1.39E-02	4.83E-03	1.68E-03
0.050	1.74E-02	6.04E-03	2.10E-03
0.060	2.09E-02	7.25E-03	2.52E-03
0.080	2.78E-02	9.67E-03	3.36E-03
0.10	3.48E-02	1.21E-02	4.20E-03
0.15	5.22E-02	1.81E-02	6.30E-03
0.20	6.95E-02	2.42E-02	8.40E-03
0.30	1.04E-01	3.63E-02	1.26E-02
0.40	1.39E-01	4.83E-02	1.68E-02
0.50	1.74E-01	6.04E-02	2.10E-02
0.60	2.09E-01	7.25E-02	2.52E-02
0.80	2.78E-01	9.67E-02	3.36E-02
1.0	3.48E-01	1.21E-01	4.20E-02
1.5	5.22E-01	1.81E-01	6.30E-02
2.0	6.95E-01	2.42E-01	8.40E-02
3.0	1.04E+00	3.63E-01	1.26E-01
4.0	1.39E+00	4.83E-01	1.68E-01
5.0	1.74E+00	6.04E-01	2.10E-01
6.0	2.09E+00	7.25E-01	2.52E-01
8.0	2.78E+00	9.67E-01	3.36E-01
10.0	3.48E+00	1.21E+00	4.20E-01

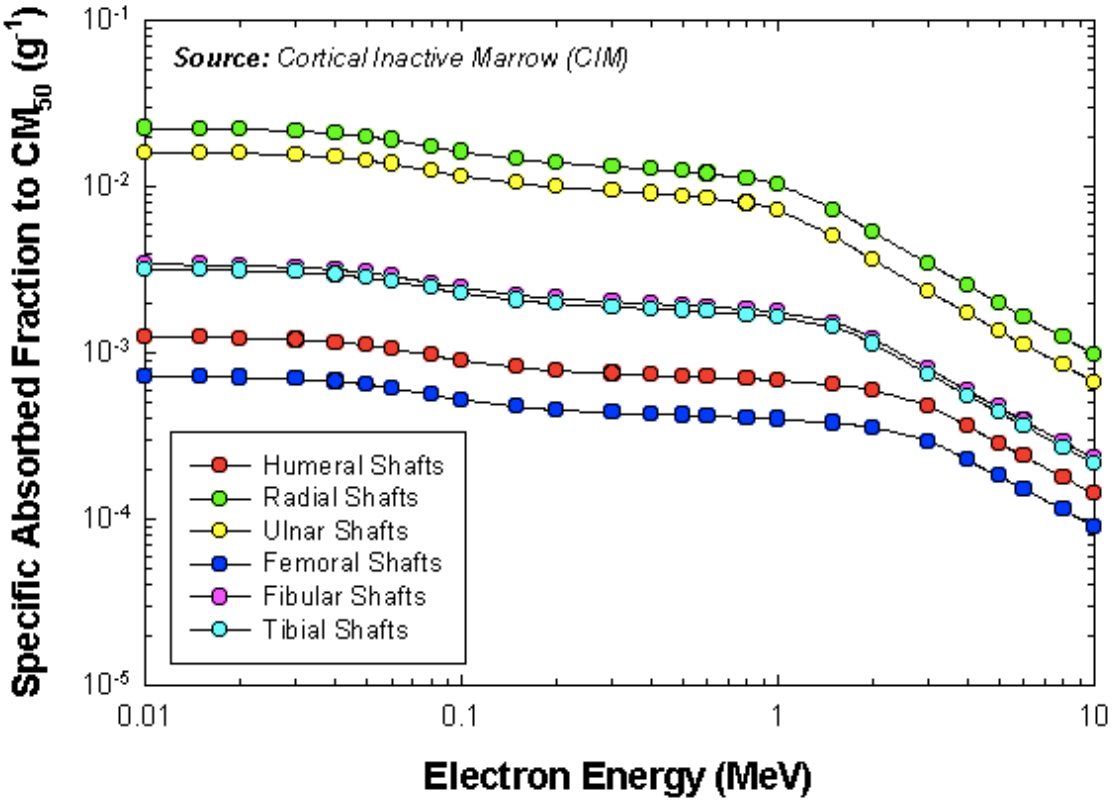

Figure D-1. Specific absorbed fraction for the CIM irradiating the CIM_{50} in the shafts of all long bones.

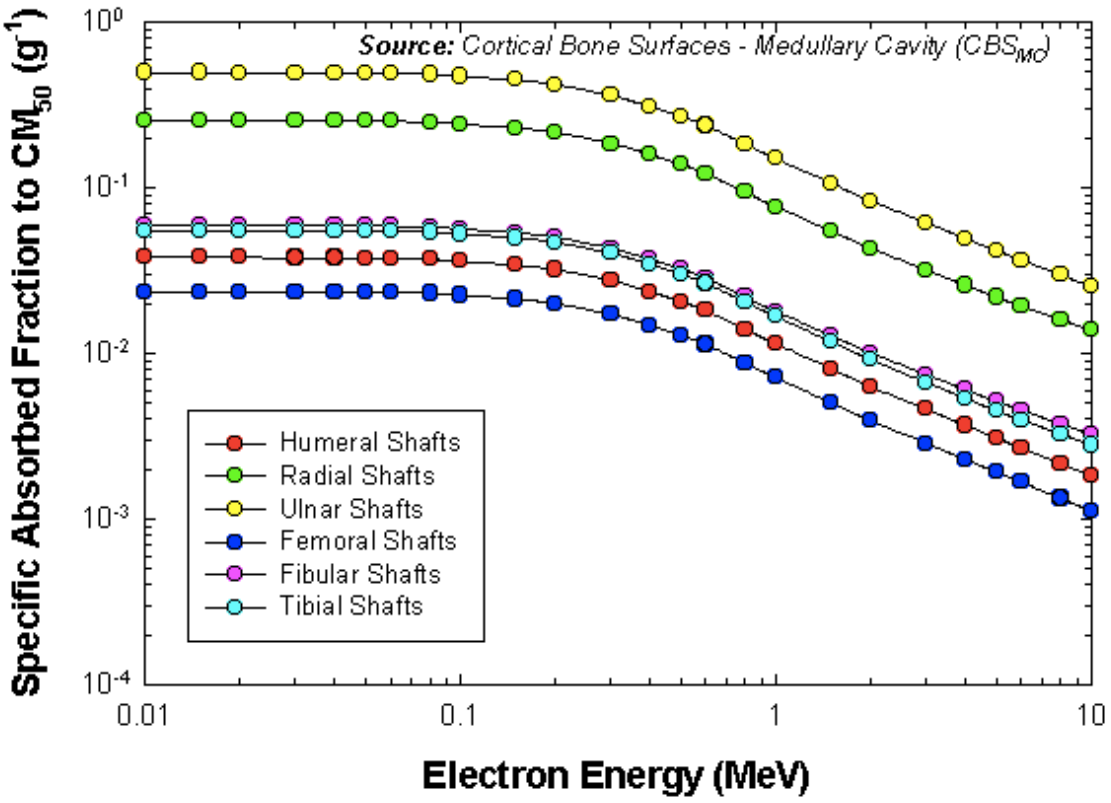

Figure D-2. Specific absorbed fraction for the CBS_{MC} irradiating the CIM_{50} in the shafts of all long bones.

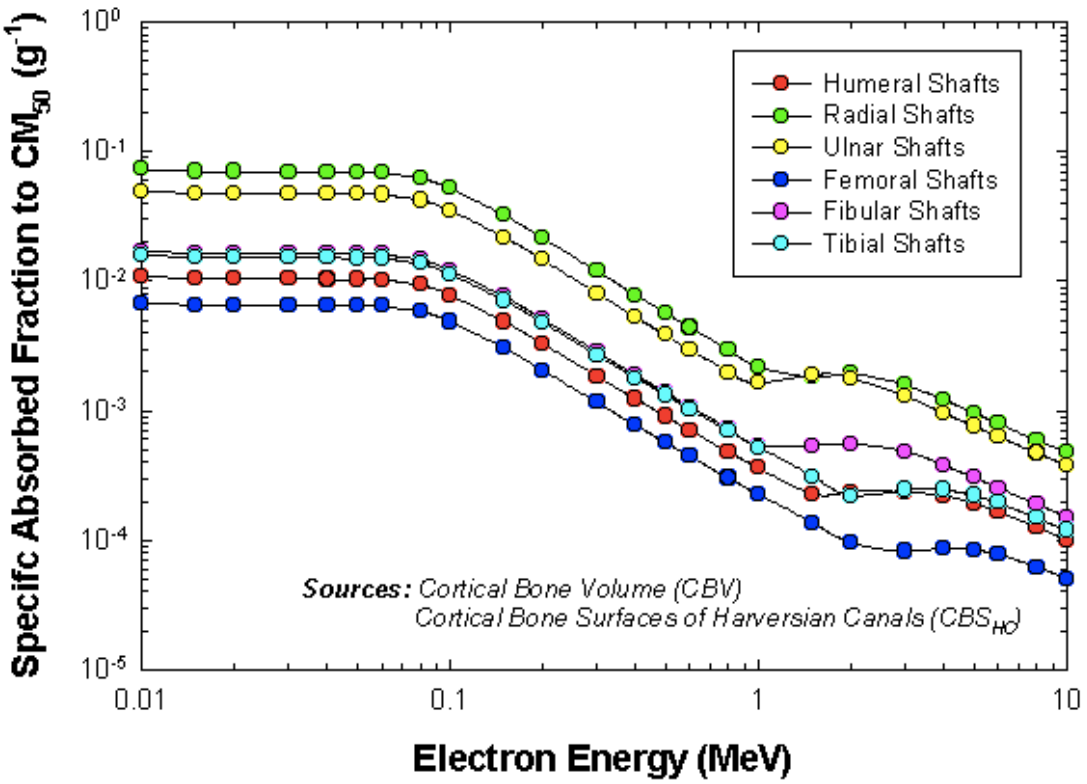

Figure D-3. Specific absorbed fraction for the CBV irradiating the CIM_{50} in the shafts of all long bones.

APPENDIX E
SKELETAL AVERAGED ABSORBED FRACTIONS

Skeletal averaged Absorbed Fraction (AF) data for UFRF is given for any combination of source (TAM, TBS, TBV, TAM_{50}, TIM) and target (TAM, TAM_{50}) regions in the entire skeleton containing active marrow. Bone site weighting factors were used to average AF for each skeletal site. Values of AF at ICRP reference cellularity were then compared to values from Stabin and Siegel (2003).

Table E-1. UFRF skeletal averaged absorbed fraction (AF) for various sources irradiating the trabecular active marrow.

Energy (MeV)	ϕ(TAM←TAM)	ϕ(TAM←TIM)	ϕ(TAM←TBS)	ϕ(TAM←CBV)	ϕ(TAM←TBV)
0.010	9.85E-01	1.76E-02	3.08E-01	8.90E-05	2.58E-03
0.015	9.71E-01	3.61E-02	3.08E-01	1.86E-04	5.29E-03
0.020	9.53E-01	5.93E-02	3.08E-01	3.17E-04	8.73E-03
0.030	9.08E-01	1.17E-01	3.08E-01	6.48E-04	1.75E-02
0.040	8.56E-01	1.85E-01	3.08E-01	1.08E-03	2.85E-02
0.050	8.00E-01	2.56E-01	3.08E-01	1.60E-03	4.09E-02
0.060	7.45E-01	3.24E-01	3.08E-01	2.15E-03	5.44E-02
0.080	6.57E-01	4.30E-01	3.09E-01	3.47E-03	8.30E-02
0.100	6.12E-01	4.75E-01	3.13E-01	5.05E-03	1.13E-01
0.150	5.61E-01	4.98E-01	3.37E-01	9.38E-03	1.87E-01
0.200	5.32E-01	4.91E-01	3.63E-01	1.42E-02	2.53E-01
0.300	4.95E-01	4.70E-01	3.94E-01	2.39E-02	3.33E-01
0.400	4.72E-01	4.52E-01	4.01E-01	3.39E-02	3.62E-01
0.500	4.54E-01	4.36E-01	3.98E-01	4.30E-02	3.69E-01
0.600	4.40E-01	4.23E-01	3.92E-01	5.17E-02	3.69E-01
0.800	4.15E-01	3.99E-01	3.77E-01	6.66E-02	3.63E-01
1.000	3.93E-01	3.78E-01	3.61E-01	7.71E-02	3.50E-01
1.500	3.49E-01	3.35E-01	3.24E-01	9.07E-02	3.19E-01
2.000	3.13E-01	2.99E-01	2.93E-01	9.38E-02	2.90E-01
3.000	2.57E-01	2.45E-01	2.42E-01	8.75E-02	2.42E-01
4.000	2.16E-01	2.06E-01	2.04E-01	7.95E-02	2.05E-01
5.000	1.85E-01	1.76E-01	1.75E-01	6.99E-02	1.76E-01
6.000	1.61E-01	1.53E-01	1.52E-01	6.32E-02	1.54E-01
8.000	1.27E-01	1.20E-01	1.20E-01	5.17E-02	1.21E-01
10.000	1.05E-01	9.92E-02	9.84E-02	4.29E-02	1.00E-01

Table E-2. UFRF skeletal averaged absorbed fraction (AF) for various sources irradiating the shallow trabecular active marrow.

Energy (MeV)	$\phi(TAM_{50} \leftarrow TAM)$	$\phi(TAM_{50} \leftarrow TIM)$	$\phi(TAM_{50} \leftarrow TBS)$	$\phi(TAM_{50} \leftarrow CBV)$	$\phi(TAM_{50} \leftarrow TBV)$
0.010	1.20E-01	1.20E-03	2.91E-01	6.29E-06	2.25E-03
0.015	1.17E-01	2.46E-03	2.89E-01	1.52E-05	4.57E-03
0.020	1.14E-01	4.04E-03	2.87E-01	2.64E-05	7.50E-03
0.030	1.07E-01	8.04E-03	2.81E-01	5.11E-05	1.49E-02
0.040	9.74E-02	1.29E-02	2.73E-01	9.12E-05	2.38E-02
0.050	8.72E-02	1.82E-02	2.63E-01	1.30E-04	3.34E-02
0.060	7.70E-02	2.34E-02	2.52E-01	1.78E-04	4.34E-02
0.080	6.00E-02	3.11E-02	2.16E-01	2.70E-04	6.03E-02
0.100	5.11E-02	3.41E-02	1.77E-01	3.86E-04	6.94E-02
0.150	4.30E-02	3.56E-02	1.21E-01	7.01E-04	7.39E-02
0.200	4.04E-02	3.59E-02	9.38E-02	1.07E-03	6.88E-02
0.300	3.87E-02	3.61E-02	6.79E-02	1.84E-03	5.69E-02
0.400	3.75E-02	3.55E-02	5.68E-02	2.61E-03	5.02E-02
0.500	3.66E-02	3.47E-02	5.10E-02	3.36E-03	4.64E-02
0.600	3.55E-02	3.39E-02	4.70E-02	4.10E-03	4.36E-02
0.800	3.39E-02	3.23E-02	4.20E-02	5.21E-03	3.96E-02
1.000	3.22E-02	3.08E-02	3.84E-02	6.13E-03	3.69E-02
1.500	2.90E-02	2.76E-02	3.25E-02	7.22E-03	3.17E-02
2.000	2.61E-02	2.49E-02	2.87E-02	7.43E-03	2.81E-02
3.000	2.19E-02	2.08E-02	2.34E-02	6.93E-03	2.31E-02
4.000	1.88E-02	1.78E-02	1.98E-02	6.29E-03	1.96E-02
5.000	1.64E-02	1.55E-02	1.71E-02	5.58E-03	1.71E-02
6.000	1.45E-02	1.38E-02	1.51E-02	5.01E-03	1.50E-02
8.000	1.18E-02	1.13E-02	1.22E-02	4.14E-03	1.22E-02
10.000	1.01E-02	9.59E-03	1.04E-02	3.45E-03	1.03E-02

Table E-3. UFRF skeletal averaged specific absorbed fraction (SAF) for various sources irradiating the trabecular active marrow.

Energy (MeV)	$\phi(TAM \leftarrow TAM)$	$\phi(TAM \leftarrow TIM)$	$\phi(TAM \leftarrow TBS)$	$\phi(TAM \leftarrow CBV)$	$\phi(TAM \leftarrow TBV)$
0.010	1.87E-02	2.97E-04	5.19E-03	1.43E-06	4.35E-05
0.015	1.84E-02	6.06E-04	5.19E-03	2.91E-06	8.87E-05
0.020	1.80E-02	9.95E-04	5.20E-03	4.93E-06	1.46E-04
0.030	1.70E-02	1.97E-03	5.20E-03	9.99E-06	2.93E-04
0.040	1.58E-02	3.10E-03	5.19E-03	1.68E-05	4.77E-04
0.050	1.46E-02	4.29E-03	5.19E-03	2.48E-05	6.84E-04
0.060	1.34E-02	5.44E-03	5.18E-03	3.33E-05	9.10E-04
0.080	1.15E-02	7.22E-03	5.19E-03	5.39E-05	1.39E-03
0.100	1.06E-02	7.97E-03	5.25E-03	7.84E-05	1.88E-03
0.150	9.51E-03	8.33E-03	5.64E-03	1.44E-04	3.11E-03
0.200	8.93E-03	8.20E-03	6.04E-03	2.20E-04	4.19E-03
0.300	8.22E-03	7.81E-03	6.53E-03	3.68E-04	5.50E-03
0.400	7.80E-03	7.51E-03	6.65E-03	5.21E-04	5.98E-03
0.500	7.50E-03	7.27E-03	6.62E-03	6.62E-04	6.13E-03
0.600	7.26E-03	7.06E-03	6.54E-03	8.02E-04	6.15E-03
0.800	6.84E-03	6.68E-03	6.32E-03	1.03E-03	6.05E-03
1.000	6.49E-03	6.35E-03	6.06E-03	1.20E-03	5.86E-03
1.500	5.75E-03	5.64E-03	5.46E-03	1.41E-03	5.34E-03
2.000	5.15E-03	5.05E-03	4.93E-03	1.44E-03	4.86E-03
3.000	4.23E-03	4.16E-03	4.09E-03	1.33E-03	4.05E-03
4.000	3.59E-03	3.52E-03	3.48E-03	1.18E-03	3.46E-03
5.000	3.11E-03	3.05E-03	3.01E-03	1.02E-03	3.01E-03
6.000	2.74E-03	2.69E-03	2.66E-03	9.19E-04	2.66E-03
8.000	2.22E-03	2.18E-03	2.16E-03	7.42E-04	2.18E-03
10.000	1.88E-03	1.84E-03	1.83E-03	6.09E-04	1.86E-03

Table E-4. UFRF skeletal specific averaged absorbed fraction (SAF) for various sources irradiating the shallow trabecular active marrow.

Energy (MeV)	$\phi(TAM_{50} \leftarrow TAM)$	$\phi(TAM_{50} \leftarrow TIM)$	$\phi(TAM_{50} \leftarrow TBS)$	$\phi(TAM_{50} \leftarrow CBV)$	$\phi(TAM_{50} \leftarrow TBV)$
0.010	1.97E-02	1.85E-04	5.16E-02	9.70E-07	4.32E-04
0.015	1.93E-02	3.79E-04	5.13E-02	2.36E-06	8.78E-04
0.020	1.88E-02	6.21E-04	5.09E-02	3.96E-06	1.44E-03
0.030	1.75E-02	1.24E-03	4.98E-02	7.99E-06	2.85E-03
0.040	1.59E-02	1.99E-03	4.83E-02	1.40E-05	4.56E-03
0.050	1.42E-02	2.81E-03	4.67E-02	2.01E-05	6.40E-03
0.060	1.25E-02	3.61E-03	4.47E-02	2.73E-05	8.29E-03
0.080	9.67E-03	4.80E-03	3.82E-02	4.16E-05	1.15E-02
0.100	8.18E-03	5.26E-03	3.13E-02	5.94E-05	1.31E-02
0.150	6.82E-03	5.53E-03	2.14E-02	1.08E-04	1.36E-02
0.200	6.40E-03	5.60E-03	1.65E-02	1.64E-04	1.25E-02
0.300	6.10E-03	5.65E-03	1.18E-02	2.78E-04	1.01E-02
0.400	5.92E-03	5.60E-03	9.79E-03	3.94E-04	8.75E-03
0.500	5.76E-03	5.51E-03	8.73E-03	5.07E-04	8.02E-03
0.600	5.60E-03	5.40E-03	8.01E-03	6.19E-04	7.48E-03
0.800	5.34E-03	5.18E-03	7.07E-03	7.87E-04	6.70E-03
1.000	5.08E-03	4.93E-03	6.43E-03	9.23E-04	6.18E-03
1.500	4.56E-03	4.45E-03	5.39E-03	1.08E-03	5.24E-03
2.000	4.11E-03	4.01E-03	4.72E-03	1.10E-03	4.62E-03
3.000	3.44E-03	3.37E-03	3.84E-03	1.00E-03	3.78E-03
4.000	2.97E-03	2.90E-03	3.25E-03	8.86E-04	3.21E-03
5.000	2.62E-03	2.55E-03	2.84E-03	7.73E-04	2.82E-03
6.000	2.34E-03	2.29E-03	2.53E-03	6.92E-04	2.52E-03
8.000	1.96E-03	1.92E-03	2.09E-03	5.62E-04	2.10E-03
10.000	1.71E-03	1.66E-03	1.81E-03	4.64E-04	1.83E-03

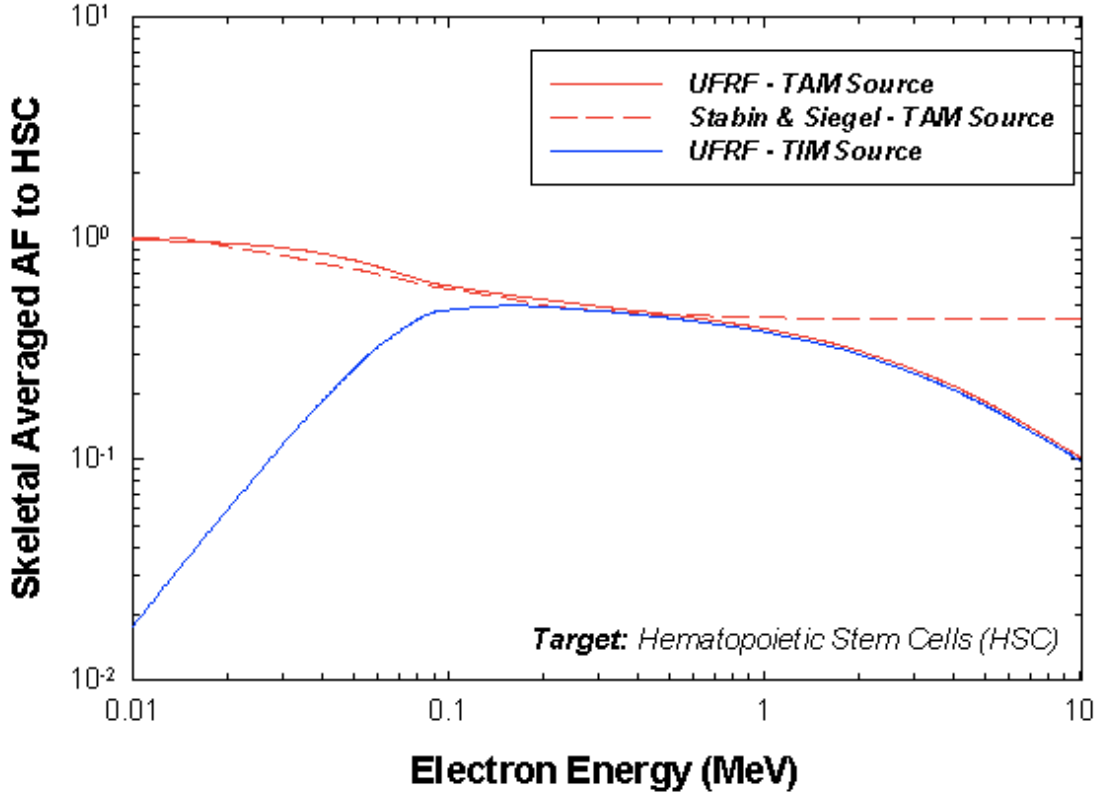

Figure E-1. Skeletal averaged AF for marrow sources irradiating the TAM for both UFRF and Stabin and Siegel (2003).

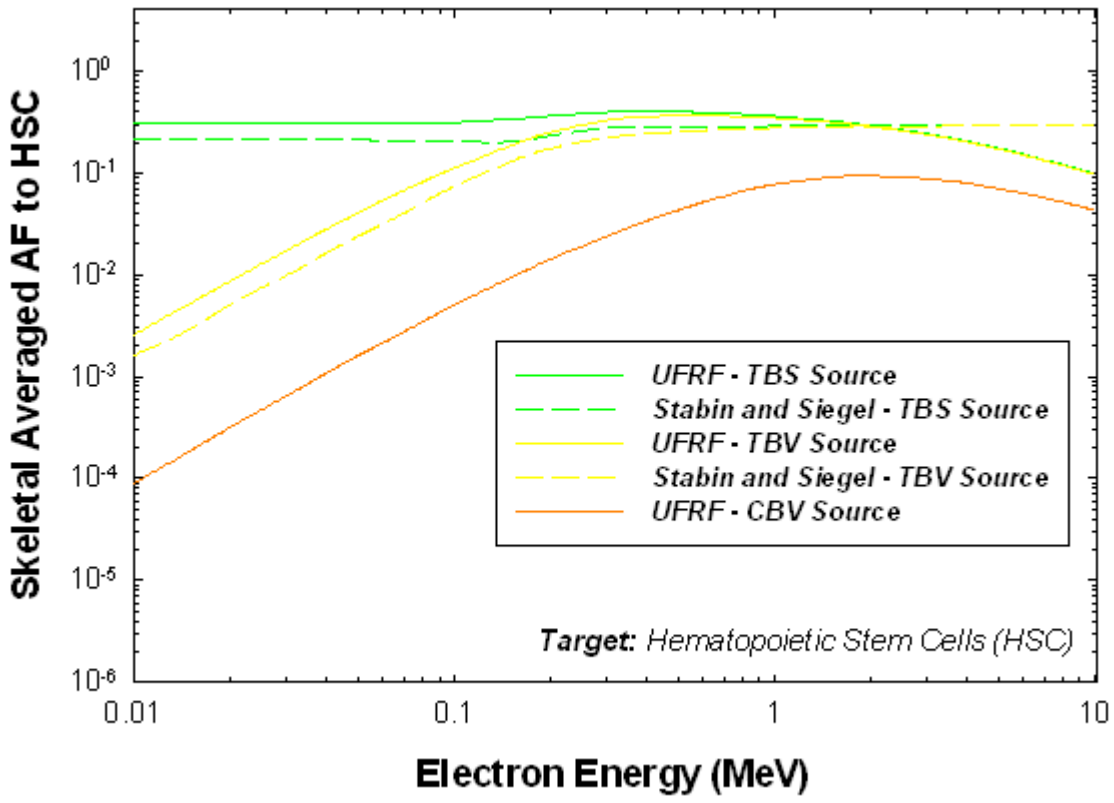

Figure E-2. Skeletal averaged AF for trabecular bone sources irradiating the TAM for both UFRF and Stabin and Siegel (2003).

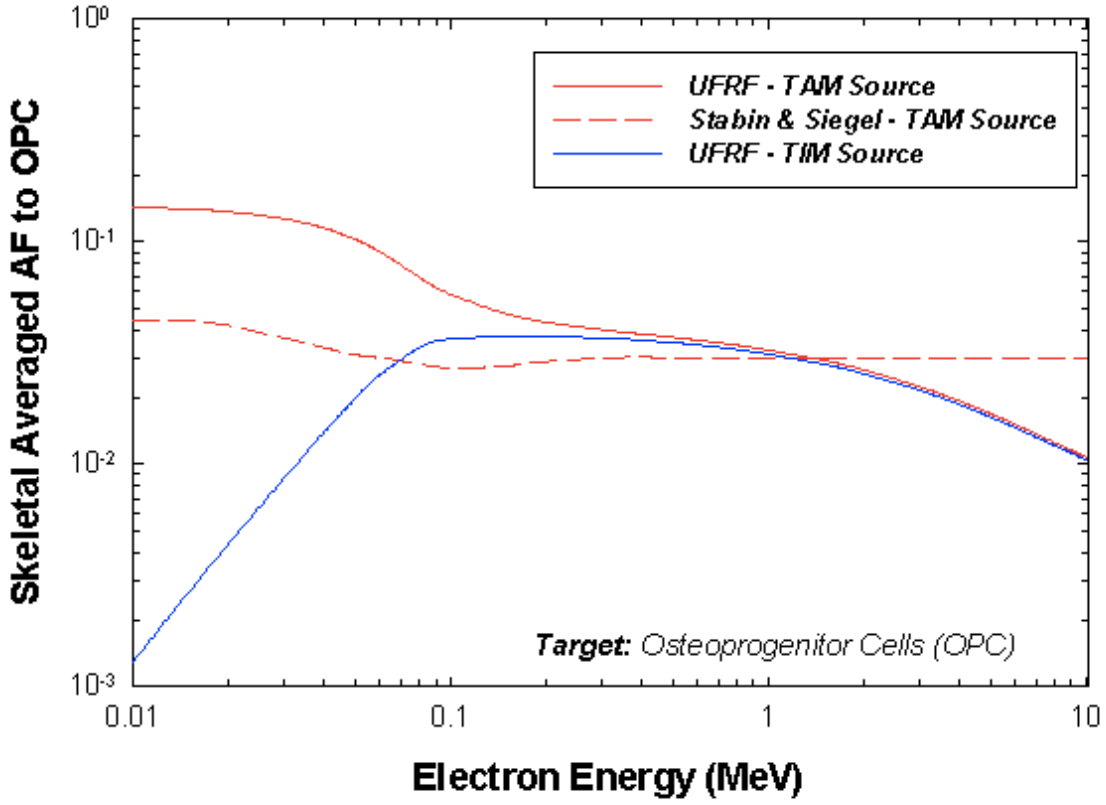

Figure E-3. Skeletal averaged AF for marrow sources irradiating the TAM_{50} for both UFRF and Stabin and Siegel (2003).

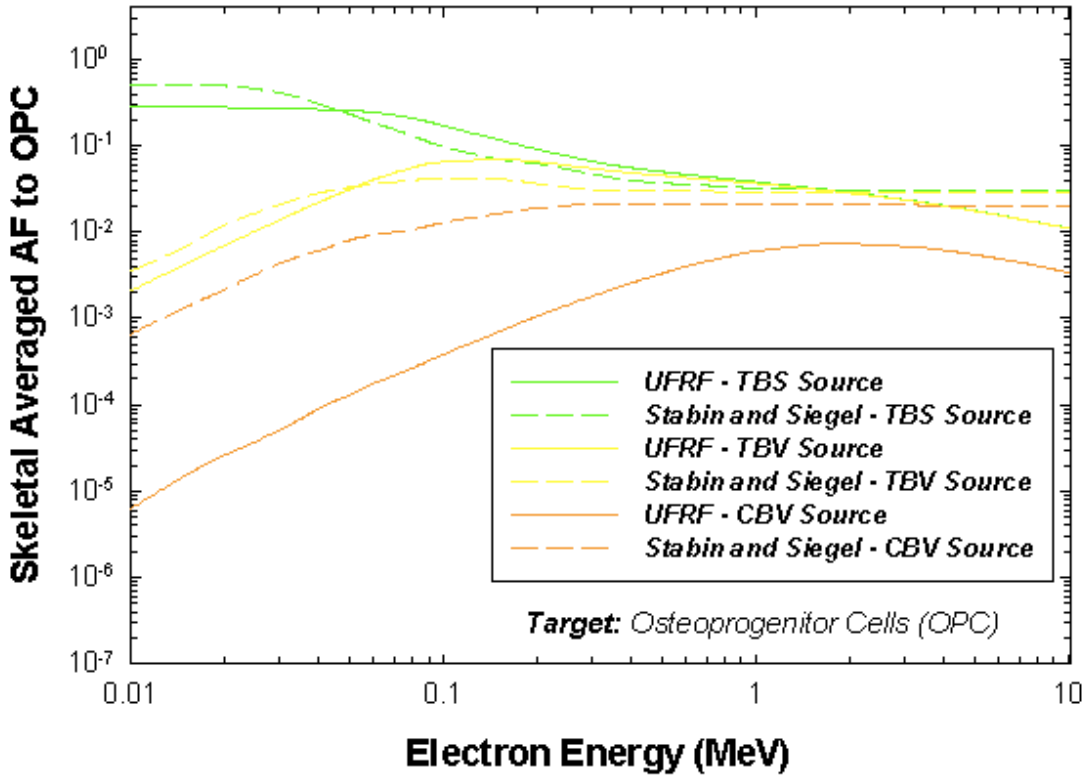

Figure E-4. Skeletal averaged AF for trabecular bone sources irradiating the TAM_{50} for both UFRF and Stabin and Siegel (2003).

LIST OF REFERENCES

Armitage J O 2005 Staging Non-Hodgkin Lymphoma *CA Cancer J Clin* **55** 368-76

Atkinson P J 1965 Changes in resorption spaces in femoral cortical bone with age. *J. of Pathol. and Bacteriol.* **89** 173-8

Beddoe A H, Darley P J and Spiers F W 1976 Measurements of trabecular bone structure in man *Phys. Med. Biol.* **21** 589-607

Berne R M 1993 *Physiology* (St. Louis: Mosby)

Bolch W, Jokisch D, Patton P, Bouchet L, Rajon D, Inglis B and Myers S 1998 NMR microimaging of trabecular bone: a new tool for the development of bone dosimetry models *Health Phys.* **74** S13

Bolch W E, Shah A P, Watchman C J, Jokisch D W, Patton P W, Rajon D A, Zankl M, Petoussi-Henss N and Eckerman K F 2007 Skeletal absorbed fractions for electrons in the adult male: Considerations of a revised 50-micron definition of the bone endosteum *Radiat Prot Dosimetry*

Bouchet L G and Bolch W E 1999 A three-dimensional transport model for determining absorbed fractions of energy for electrons in cortical bone *J. Nucl. Med.* **40** 2115-24

Bouchet L G, Bolch W E, Howell R W and Rao D V 2000 S values for radionuclides localized within the skeleton *J. Nucl. Med.* **41** 189-212

Bourke V A, Watchman C J, Reith J D, Jorgensen M L, Dieudonne A and Bolch W in press Spatial gradient of blood vessels and hematopoietic stem and progenitor cells within the marrow cavities of the human skeleton *Blood*

Brindle J, Trindade A, Pichardo J, Myers S, Shah A and Bolch W 2006a CT volumetry of the skeletal tissues *Med Phys* **33** 3796-803

Brindle J M, Myers S L and Bolch W E 2006b Correlations of total pelvic spongiosa volume with both anthropometric parameters and CT-based skeletal size measurements *Cancer Biother Radiopharm* **21** 352-63

Brindle J M, Trindade A A, Shah A P, Jokisch D W, Patton P W and Bolch W E 2006c Linear regression model for predicting patient-specific total skeletal spongiosa volume for use in molecular radiotherapy dosimetry *J Nucl Med* **47** 1875-83

Calvi L M, Adams G B, Weibrecht K W, Weber J M, Olson D P, Knight M C, Martin R P, Schipani E, Divieti P, Bringhurst F R, Milner L A, Kronenberg H M and Scadden D T 2003 Osteoblastic cells regulate the haematopoietic stem cell niche *Nature* **425** 841-6

Charlton D E, Utteridge T D and Beddoe A H 1996 Microdosimetry of haemopoietic stem cells irradiated by alpha particles from the short-lived products of 222Rn decays in fat cells and haemopoietic tissue *Int J Radiat Biol* **69** 585-92

Chavez-Gonzalez A, Rosas-Cabral A, Vela-Ojeda J, Gonzalez J and Mayani H 2004 Severe functional alterations in vitro in CD34+ cell subpopulations from patients with chronic myeloid leukemia *Leukemia research* **28** 639-47

Cristy M 1981 Active bone marrow distribution as a function of age in humans *Phys Med Biol* **26** 389-400.

Cui Y F, Lord B I, Woolford L B and Testa N G 1996 The relative spatial distribution of in vitro-CFCs in the bone marrow, responding to specific growth factors *Cell Prolif* **29** 243-57

Custer R 1974 *An atlas of the blood and bone marrow* (Philadelphia, PA: W.B. Saunders)

DOH 2001 Stem Cells: Scientific Progress and Future Research Directions. Department of Health and Human Services)

DOH 2006 Regenerative Medicine. Department of Health and Human Services)

Eckerman K F 1985 Aspects of the dosimetry of radionuclides within the skeleton with particular emphasis on the active marrow. In: *Proceedings of the Fourth International Radiopharmaceutical Dosimetry Symposium,* ed A T Schlafke-Stelson and E E Watson (Oak Ridge, Tennessee: Oak Ridge Associated Universities) pp 514-34

Eckerman K F, Ryman J C, Taner A C and Kerr G D 1985 Traversal of cells by radiation and absorbed fraction estimates for electrons and alpha particles. In: *Proceedings of the Fourth International Radiopharmaceutical Dosimetry Symposium,* ed A T Schlafke-Stelson and E E Watson (Oak Ridge, Tennessee: ORAU) pp 67-81

Eckerman K F and Stabin M G 2000 Electron absorbed fractions and dose conversion factors for marrow and bone by skeletal regions *Health Phys.* **78** 199-214

Forero A and Lobuglio A F 2003 History of antibody therapy for non-Hodgkin's lymphoma *Semin Oncol* **30** 1-5

Foucar K 2001 *Bone marrow pathology* (Chicago, IL: American Society of Clinicial Pathologists)

Frassoni F, Testa N G and Lord B I 1982 The relative spatial distribution of erythroid progenitor cells (BFUe and CFUe) in the normal mouse femur *Cell Tissue Kinet* **15** 447-55

Gossner W 2003 Target cells in internal dosimetry *Radiat Prot Dosimetry* **105** 39-42

Gossner W, Masse R and Stather J W 2000 Cells at risk for dosimetric modeling relevant to bone tumour induction *Radiat Prot Dosimetry* **92** 209-13

Harris N, Jaffe E, Stein H, Banks P, Chan J, Cleary M, Delsol G, De Wolf-Peeters C, Falini B and Gatter K 1994 A revised European-American classification of lymphoid neoplasms: a proposal from the International Lymphoma Study Group [see comments] *Blood* **84** 1361

Heddy Z and Swart B 2005 The human leucocyte differentiation antigens (HLDA) workshops: the evolving role of antibodies in research, diagnosis and therapy *Cell Research* **15** 691-4

Hoffman R, Benz Jr E, Shattil S, Furie B and Cohen H 1991 Hematology: basic principles and practice *Blood* **235**

Huerta-Zepeda A, Talavera A, AvilŽs A, Neri N and Mayani H 2000 In vitro hematopoiesis in patients with malignant lymphoma during active disease and at complete clinical remission after chemotherapy *Leukemia & lymphoma* **39** 613

ICRP 1977 Recommendations of the International Commission on Radiological Protection. Pergamon, Oxford)

ICRP 1995 Basic anatomical and physiological data for use in radiological protection: the skeleton. (Oxford, UK: International Commission on Radiological Protection)

ICRP 2002 Basic anatomical and physiological data for use in radiological protection: reference values. (Oxford; Pergamon Press: International Commission on Radiological Protection)

Jensen K, Jensen M, Grundtvig P, Thomsen C, Karle H and Henriksen O 1990 Localized in vivo proton spectroscopy of the bone marrow in patients with leukemia *Magnetic resonance imaging* **8** 779

Jokisch D 1999 Beta particle dosimetry of the trabecular region of a thoracic vertebra utilizing NMR microscopy. In: *Nuclear and Radiological Engineering,* (Gainesville, Florida: University of Florida) p 235

Juweid M, Sharkey R M, Siegel J A, Behr T and Goldenberg D M 1995 Estimates of red marrow dose by sacral scintigraphy in radioimmunotherapy patients having non-Hodgkin's lymphoma and diffuse bone marrow uptake *Cancer Res* **55** 5827s-31s.

Juweid M E, Zhang C H, Blumenthal R D, Hajjar G, Sharkey R M and Goldenberg D M 1999 Prediction of hematologic toxicity after radioimmunotherapy with (131)I- labeled anticarcinoembryonic antigen monoclonal antibodies *J Nucl Med* **40** 1609-16.

Kaminski M, Tuck M, Estes J, Kolstad A, Ross C, Zasadny K, Regan D, Kison P, Fisher S and Kroll S 2005 131I-tositumomab therapy as initial treatment for follicular lymphoma *The New England journal of medicine* **352** 441

Kuppers R, Klein U, Hansmann M and Rajewsky K 1999 Cellular origin of human B-cell lymphomas *New England Journal of Medicine* **341** 1520-9

Kuznetsov S A, Mankani M H, Gronthos S, Satomura K, Bianco P and Robey P G 2001 Circulating skeletal stem cells *J Cell Biol* **153** 1133-40

Kuznetsov S A, Riminucci M, Ziran N, Tsutsui T W, Corsi A, Calvi L, Kronenberg H M, Schipani E, Robey P G and Bianco P 2004 The interplay of osteogenesis and hematopoiesis: expression of a constitutively active PTH/PTHrP receptor in osteogenic cells perturbs the establishment of hematopoiesis in bone and of skeletal stem cells in the bone marrow *J Cell Biol* **167** 1113-22

Kvinnsland Y, Skretting A and Bruland O S 2001 Radionuclide therapy with bone-seeking compounds: Monte Carlo calculations of dose-volume histograms for bone marrow in trabecular bone *Phys Med Biol* **46** 1149-61

Lim S M, DeNardo G L, DeNardo D A, Shen S, Yuan A, O'Donnell R T and DeNardo S J 1997a Prediction of myelotoxicity using radiation doses to marrow from body, blood and marrow sources *J Nucl Med* **38** 1374-8.

Lim S M L, DeNardo G L, DeNardo D A, Shen S, Yuan A, O'Donnell R T and DeNardo S J 1997b Prediction of myelotoxicity using radiation doses to marrow from body, blood, and marrow sources *J. Nucl. Med.* **38** 1374-8

Liu T, Meredith R F, Saleh M N, Wheeler R H, Khazaeli M B, Plott W E, Schlom J and LoBuglio A F 1997 Correlation of toxicity with treatment parameters for 131I-CC49 radioimmunotherapy in three phase II clinical trials *Cancer Biother Radiopharm* **12** 79-87.

Loevinger R, Budinger T F and Watson E E 1991 *MIRD primer for absorbed dose calculations* (New York: The Society of Nuclear Medicine)

Lombardi M H 2006 *Radiation safety in nuclear medicine*: CRC Press)

Lord B I and Hendry J H 1972 The distribution of hematopoietic colony forming units in the mouse femur and its modification by x-rays *Br. J. Radiol.* **45** 110-5

Macey D J, DeNardo S J, DeNardo G L, DeNardo D A and Shen S 1995 Estimation of radiation absorbed doses to the red marrow in radioimmunotherapy *Clin Nucl Med* **20** 117-25

Madrigal-Velazquez M, Avilas A, Neri N, Huerta J, Martinez-Jaramillo G and Mayani H 2006 Expression of ice, bcl-2, c-myc and p53 in different bone marrow cell populations from patients with diffuse large B-cell lymphoma *Leukemia and Lymphoma* **47** 665-73

Marieb E N 2006 *Human anatomy and physiology* (San Francisco, CA: Pearson Education, Inc.)

Martinez-Jaramillo G, Aviles A, Neri N, Huerta J, Madrigal-Velazquez M, Flores-Guzman P and Mayani H 2004 In vitro proliferation and expansion of hematopoietic progenitors from patients with diffuse large B-cell lymphoma before and after chemotherapy *Leukemia and Lymphoma* **45** 1247-54

McPherson R and Pincus M 2007 *Henry's clinical diagnosis and management by laboratory methods*: Saunders Elsevier)

Mechanik N 1926 Studies of the weight of bone marrow in man *Zeitschrift fur die Gest. Anatomy* **79** 58-99

Mosekilde L 1989 Sex differences in age-related loss of vertebral trabecular bone mass and structure - biomechanical consequences *Bone* **10** 425-32

Moulopoulos L A and Dimopoulos M A 1997 Magnetic Resonance Imaging of the Bone Marrow in Hematologic Malignancies *Blood* **90** 2127-47

Muller A, Ihorst G, Mertelsmann R and Engelhardt M 2005 Epidemiology of non-Hodgkin's lymphoma (NHL): trends, geographic distribution, and etiology *Annals of Hematology* **84** 1-12

O'Donoghue J A, Baidoo N, Deland D, Welt S, Divgi C R and Sgouros G 2002 Hematologic toxicity in radioimmunotherapy: dose-response relationships for I-131 labeled antibody therapy *Cancer Biother Radiopharm* **17** 435-43

Orazi A, Cattoretti G, Schiro R, Siena S, Bregni M, Di Nicola M and Gianni A 1992 Recombinant human interleukin-3 and recombinant human granulocyte- macrophage colony-stimulating factor administered in vivo after high- dose cyclophosphamide cancer chemotherapy: effect on hematopoiesis and microenvironment in human bone marrow *Blood* **79** 2610-9

Patton P W 2000 NMR microscopy for skeletal dosimetry: an investigation of marrow cellularity on dose estimates. In: *Nuclear and Radiological Engineering,* (Gainesville, FL: University of Florida) p 426

Patton P W, Jokisch D W, Rajon D A, Shah A P, Myers S L and Bolch W E 2002a Skeletal dosimetry via NMR microscopy: investigations of sample reproducibility and signal source *Health Phys* **82** 316-26

Patton P W, Rajon D A, Shah A P, Jokisch D W, Inglis B and Bolch W E 2002b Site-specific variability in trabecular bone dosimetry: considerations of energy loss to cortical bone *Med Phys* **29** 6-14

Pichardo J C, Trindade A A, Brindle J M and Bolch W E 2007 Method for estimating skeletal spongiosa volume and active marrow mass in the adult male and adult female *J Nucl Med* **48** 1880-8

Rafii S, Shapiro F, Rimarachin J, Nachman R L, Ferris B, Weksler B, Moore M A and Asch A S 1994 Isolation and characterization of human bone marrow microvascular endothelial cells: hematopoietic progenitor cell adhesion *Blood* **84** 10-9

Rajon D, Pichardo J, Brindle J, Kielar K, Jokisch D, Patton P and Bolch W 2006 Image segmentation of trabecular spongiosa by visual inspection of the gradient magnitude *Phys Med Biol* **51** 4447-67

Rajon D A, Jokisch D W, Patton P W, Shah A P and Bolch W E 2000 Voxel size effects in three-dimensional nuclear magnetic resonance microscopy performed for trabecular bone dosimetry *Med Phys* **27** 2624-35

Schick F, Weiss B and Einsele H 1995 Magnetic resonance imaging reveals a markedly inhomogeneous distribution of marrow cellularity in a patient with myelodysplasia *Annals of Hematology* **71** 143-6

Sgouros G 1993 Bone marrow dosimetry for radioimmunotherapy: Theoretical considerations *J. Nucl. Med.* **34** 689-94

Sgouros G, Chiu S, Pentlow K S, Brewster L J, Kalaigian H, Baldwin B, Daghighian F, Graham M C, Larson S M and Mohan R 1993 Three-dimensional dosimetry for radioimmunotherapy treatment planning *J. Nucl. Med.* **34** 1595-601

Sgouros G, Deland D, Loh A C, Divgi C R and Larson S M 1997 Marrow and whole-body absorbed dose versus marrow toxicity folling 131-I-G250 antibody therapy in patients with renal-cell carcinoma *J. Nucl. Med.* **38** 252P

Sgouros G, Divgi C R, Scott A M, Willams J and Larson S M 1996a Hematologic toxicity in radioimmunotherapy: An evaluation of different predictive measures *J. Nucl. Med.* **37** 43P

Sgouros G, Howell R, Bolch W and Fisher D 2009 MIRD Commentary: Proposed Name for a Dosimetry Unit Applicable to Deterministic Biological Effects--The Barendsen (Bd) *Journal of Nuclear Medicine* **50** 485

Sgouros G, Jureidini I M, Scott A M, Graham M C, Larson S M and Scheinberg D A 1996b Bone marrow dosimetry: regional variability of marrow-localizing antibody *J. Nucl. Med.* **37** 695-8

Shah A 2004 Reference skeletal dosimetry model for an adult male radionuclide therapy patient based on 3D imaging and paired-image radiation transport. In: *Department of Biomedical Engineering,* (Gainesville, FL: University of Florida) p 488

Shah A, Jokisch D, Watchman C, Rajon D, Patton P and Bolch W 2005a Chord-based versus voxel-based methods of electron transport in the skeletal tissues *Med Phys* **32** 3151-9

Shah A P, Bolch W E, Rajon D A, Patton P W and Jokisch D W 2005b A paired-image radiation transport model for skeletal dosimetry *J Nucl Med* **46** 344-53

Shah A P, Patton P W, Rajon D A and Bolch W E 2003 Adipocyte spatial distributions in bone marrow: Implications for skeletal dosimetry models *J Nucl Med* **44** 774-83

Shen S, Meredith R F, Duan J, Macey D J, Khazaeli M B, Robert F and LoBuglio A F 2002 Improved prediction of myelotoxicity using a patient-specific imaging dose estimate for non-marrow-targeting (90)y-antibody therapy *J Nucl Med* **43** 1245-53

Siegel J A, Goldenberg D M and Badger C C 1993 Radioimmunotherapy dose estimates in patients with B-cell lymphoma *Med. Phys.* **20** 579-82

Siegel J A, Pawlyk D A, Lee R E, Sasso N L, Horowitz J A, Sharkey R M and Goldenberg D M 1990a Tumor, red marrow, and organ dosimetry for ^{131}I-labeled anti-carcinoembryonic antigen monoclonal antibody *Cancer Res. (Suppl.)* **50** 1039s-42s

Siegel J A, Stabin M G and Sparks R B 2003 Total-body and red marrow dose estimates *J Nucl Med* **44** 320-1; author reply 1-3

Siegel J A, Wessels B W and Watson E E 1990b Bone marrow dosimetry and toxicity for radioimmunotherapy *Antibody Immunoconjugates Radiopharm.* **3** 213-33

Snyder B D, Piazza S, Edwards W T and Hayes W C 1993 Role of trabecular morphology in the etiology of age-related vertebral fractures *Calcified Tissue International* **53 (Suppl 1)** S14-S22

Soligo D, Lambertenghi Delilieris G, Servida F, Quirici N, Campiglio S and E T 1998 Hematopoietic abnormalities after autologous stem cell transplantation in lymphoma patients *Bone Marrow Transplantation* **21** 15-22

Spiers F W, Whitwell J R and Beddoe A H 1978 Calculated dose factors for the radiosensitive tissues in bone irradiated by surface-deposited radionuclides *Phys Med Biol* **23** 481-94.

Stabin M 2004 The OLINDA/EXM Personal Computer Code. Vanderbilt University)

Stabin M G 1994 MIRDOSE3. (Oak Ridge: Oak Ridge Institute for Science and Education)

Stabin M G 1996 MIRDOSE: personal computer software for internal dose assessment in nuclear medicine *J. Nucl. Med.* **37** 538-46

Stabin M G, Sparks R B and Crowe E 2005 OLINDA/EXM: the second-generation personal computer software for internal dose assessment in nuclear medicine *J Nucl Med* **46** 1023-7

Sugiyama T, Kohara H, Noda M and Nagasawa T 2006 Maintenance of the hematopoietic stem cell pool by CXCL12-CXCR4 chemokine signaling in bone marrow stromal cell niches *Immunity* **25** 977-88

Swerdlow S, Campo E, Harris N, Jaffe E, Pileri S, Stein H, Thiele J and Vardiman J 2008 *WHO Classification of tumours of Haematopoietic and Lymphoid Tissues*: International Agency for Research on Cancer (IARC))

Taichman R S 2005 Blood and bone: two tissues whose fates are intertwined to create the hematopoietic stem-cell niche *Blood* **105** 2631-9

Trotter M and Hixon B 1974 Sequential changes in weight, density, and percentage ash weight of human skeletons from an early fetal period through old age *Anat. Rec.* **179** 1-18

U. S. National Institutes of Health N C I SEER Training Modules.

US Department of Health and Human Services O o t S G

Vogler J 1988 Bone marrow imaging *Radiology* **168** 679

Watchman C, Jokisch D W, Patton P, Rajon D, Sgouros G and Bolch W 2005 Absorbed fractions for alpha-particles in tissues of trabecular bone: Considerations of marrow cellularity within the ICRP reference male *J Nucl Med* **46** 1171-85

Watchman C J 2005 Skeletal dosimetry models for alpha-particles for use in molecular radiotherapy. In: *Nuclear and Radiological Engineering,* (Gainesville, FL: University of Florida)

Watchman C J, Bourke V A, Lyon J R, Knowlton A E, Butler S L, Grier D D, Wingard J R, Braylan R C and Bolch W E 2007 Spatial distribution of blood vessels and CD34+ hematopoietic stem and progenitor cells within the marrow cavities of human cancellous bone *J Nucl Med* **48** 645-54

Whitwell J R 1973 Theoretical investigations of energy loss by ionizing particles in bone. In: *Department of Medical Physics,* (Leeds, UK: University of Leeds) p 268

Whitwell J R and Spiers F W 1976 Calculated beta-ray dose factors for trabecular bone *Phys. Med. Biol.* **21** 16-38

Wiseman G, White C, Sparks R, Erwin W, Podoloff D, Lamonica D, Bartlett N, Anthony Parker J, Dunn W and Spies S 2001 Biodistribution and dosimetry results from a phase III prospectively randomized controlled trial of Zevalin[a] radioimmunotherapy for low-grade, follicular, or transformed B-cell non-Hodgkin's lymphoma *Critical Reviews in Oncology and Hematology* **39** 181-94

Yao M, Fouillard L, Lemoine F, Bouchet S, Firat H, Andreu G, Gorin N, Douay L and Lopez M 2000 Ex vivo expansion of CD34-positive peripheral blood progenitor cells from patients with non-Hodgkin's lymphoma: no evidence of concomitant expansion of contaminating bcl2/JH-positive lymphoma cells *Bone Marrow Transplantation* **26** 497

Yao W, Wu C, Wang S, Chang C, Chiu N and Yu C 2001 Differential changes in regional bone mineral density in healthy Chinese: age-related and sex-dependent *Calcified Tissue International* **68** 330-6

Yoffey J and Courtice F 1970 *Lymphatics, lymph and the lymphomyeloid complex*: Academic Press)

Zhang J, Niu C, Ye L, Huang H, He X, Tong W, Ross J, Haug J, Johnson T and Feng J 2003 Identification of the haematopoietic stem cell niche and control of the niche size *Nature* **425** 836-41

BIOGRAPHICAL SKETCH

Kayla N. Kielar was born in Pittsburgh, Pennsylvania, but grew up in Palm Beach, FL. Kayla is the daughter of David and Susan Kielar and the sister of Karla. Kayla graduated from the Medical Magnet program at Lake Worth High School in 2001 and her career as a Gator at the University of Florida began. She went on to receive a Bachelor of Science in Nuclear Engineering, graduating Summa Cum Laude in 2004. In 2006, Kayla earned a Master of Science in Nuclear Engineering Sciences. While engaged in doctoral research, Kayla pursued an M.S. in Business Management from the Warrington College of Business, which she earned in May 2009. She also finished a full Ironman triathlon the same year. Upon completion of her Doctorate in Philosophy, Kayla will be joining the Department of Radiation Oncology at the Stanford Cancer Center as a radiation oncology physics resident.